DEVELOPMENT OF LOW-FREQUENCY REPETITIVE TRANSCRANIAL MAGNETIC STIMULATION AS A TOOL TO MODULATE VISUAL DISORDERS: INSIGHTS FROM NEUROIMAGING

SARA RAFIQUE

A DISSERTATION SUBMITTED TO
THE FACULTY OF GRADUATE STUDIES
IN PARTIAL FULFILLMENT OF THE REQUIREMENTS
FOR THE DEGREE OF
DOCTOR OF PHILOSOPHY

GRADUATE PROGRAM IN PSYCHOLOGY
YORK UNIVERSITY
TORONTO, ONTARIO

August 2018

Abstract

Repetitive transcranial magnetic stimulation (rTMS) has become a popular neuromodulation technique, increasingly employed to manage several neurological and psychological conditions. Despite its popular use, the underlying mechanisms of rTMS remain largely unknown, particularly at the visual cortex. Moreover, the application of rTMS to modulate visual-related disorders is under-investigated. The goal of the present research was to address these issues. I employ a multitude of neuroimaging techniques to gain further insight into neural mechanisms underlying low-frequency (1 Hz) rTMS to the visual cortex. In addition, I begin to develop and refine clinical low-frequency rTMS protocols applicable to visual disorders as an alternative therapy where other treatment options are unsuccessful or where there are simply no existing therapies. One such visual disorder that can benefit from rTMS treatment is the perception of visual hallucinations that can occur following visual pathway damage in otherwise cognitively healthy individuals. In Chapters 2–3, I investigate the potential of multiday low-frequency rTMS to the visual cortex to alleviate continuous and disruptive visual hallucinations consequent to occipital injury. Combining rTMS with magnetic resonance imaging techniques reveals functional and structural cortical changes that lead to the perception of visual hallucinations; and rTMS successfully attenuates these anomalous visual perceptions. In Chapters 4–5, I compare the effects of alternative doses of low-frequency rTMS to the visual cortex on neurotransmitter levels and intrinsic functional connectivity to gain insight into rTMS mechanisms and establish the most effective protocol. Differential dose-dependent effects are observed on neurotransmitter levels and functional connectivity that suggest the choice of protocol critically depends on the neurophysiological target. Collectively, this work provides a basic framework for the use of low-frequency rTMS and neuroimaging in clinical application for visual disorders.

Acknowledgments

This research would not have been possible without the support and guidance of mentors, friends, and family, and of course, all of those who participated in the studies.

First, my deep gratitude to my supervisor, Dr. Jennifer Steeves, for taking me under your wing. Thank you for the opportunity to pursue new research paths and your continued support. Your patience, mentoring, and steering me in the right the direction along the way has been invaluable. But perhaps, most importantly, your motivation and faith in my abilities has been a great encouragement. This experience has been a period of intense learning, and your unwavering efforts to further our research development and provide opportunities has been considerable to my development as a researcher.

I thank my committee members, Dr. Dale Stevens and Dr. Gary Turner, for their guidance and reviewing my work. I would like to thank Dr. Dale Stevens for always making time to answer my frequent research design questions throughout the years and guiding my experimental design. Thank you both for your advice and insightful comments that has improved this work.

I extend my thanks to Dr. Georg Oeltzschner (Johns Hopkins Medicine) for his technical magnetic resonance spectroscopy support and modification of Gannet scripts to suit my requirements. Without this support, I'm not sure where that research would be!

I thank my fellow labmates in the Perceptual Neuroscience Lab, Stefania Moro and Nikita Wong—discussing our work and concepts, the conferences, the adventures, the laughs, and the combined efforts to keep each other sane, have all been memorable.

My thanks to all the participants, for their time, patience, and enduring the lengthy experiments.

I owe much thanks to friends and family for their patience, understanding, support, and acceptance of my continued absences over the years.

This research was made possible by funding from the Natural Sciences and Engineering Research Council of Canada, and Canada Foundation for Innovation.

Table of Contents

List of Tables

List of Figures

List of Abbreviations

^{1}H	Proton
2D	Two-dimensional
3D	Three-dimensional
3T	3 Tesla
AD	Axial diffusivity
ANOVA	Analysis of variance
BDNF	Brain-derived neurotrophic factor
BEDPOSTX	FMRIB's Bayesian estimation of diffusion parameters obtained using sampling techniques for modelling crossing fibres
BET	FMRIB's brain extraction tool
BOLD	Blood oxygen level-dependent
CHESS	Chemical shift selective suppression
CompCor	Component-based noise correction
Cr	Creatine
CT	Computed tomography
DMN	Default mode network
DTI	Diffusion tensor imaging
DTIFIT	FMRIB's diffusion tensor fitting program
EEG	Electroencephalography/electroencephalogram
ES_{YW}	Effect size for Yuen's *t*-tests
ETDRS	Early treatment diabetic retinopathy study
FA	Fractional anisotropy

FDR	False discovery rate
FDT	FMRIB's diffusion toolbox
FLAIR	Fluid attenuated inversion recovery
FLIRT	FMRIB's linear image registration tool
fMRI	Functional magnetic resonance imaging
FNIRT	FMRIB's non-linear image registration tool
FoV	Field of view
GABA	γ-Aminobutyric acid
GABA+	γ-Aminobutyric acid and macromolecules composite
GLM	General linear model
Glx	Glutamate and glutamine composite
HARDI	High angular resolution diffusion imaging
HDFIT	High definition fiber tracking
Hz	Hertz
IC	Independent component
ICA	Independent component analysis
i.u.	Institutional units
IV	Intravenous
JHU	John Hopkins University
LSHS	Launay-Slade Hallucination Scale
LTD	Long-term depression
LTP	Long-term potentiation
M	Mean

MD	Mean diffusivity
ME	Multi-echo
MEGA-PRESS	Mescher-Garwood point resolved spectroscopy
ME-ICA	Multi-echo independent components analysis
MNI	Montreal Neurological Institute
MoCA	Montreal Cognitive Assessment
MPRAGE	Magnetisation-prepared rapid gradient echo
MR	Magnetic resonance
MRI	Magnetic resonance imaging
mRNA	Messenger ribonucleic acid
MRS	Magnetic resonance spectroscopy
MT	Motor threshold
NMDA	*N*-methyl-D-aspartate
PCA	Principal component analysis
PET	Positron emission tomography
ppm	Parts per million
PROBTRACKX	FMRIB's probabilistic tracking with crossing fibres
PT	Phosphene threshold
RD	Radial diffusivity
ROI	Region-of-interest
rsFC	Resting-state functional connectivity
rsfMRI	Resting-state functional magnetic resonance imaging
rTMS	Repetitive transcranial magnetic stimulation

SEM	Standard error of the mean
SNR	Signal-to-noise ratio
TBS	Theta burst repetitive transcranial magnetic stimulation
TBSS	Tract-based spatial statistics
tDCS	Transcranial direct current stimulation
TE	Echo time
TI	Inversion time
TMS	Transcranial magnetic stimulation
TR	Repetition time
V1	Primary visual cortex/striate cortex
V2	Visual association area/extrastriate cortex
VOI	Volume-of-interest
VVIQ	Vividness of Visual Imagery Questionnaire
WIP	Work-in-progress
YW	Yuen's *t*-tests
Z_{CC}	Effect size ($Z_{case\text{-}controls}$) for modified *t*-test for single-case studies

CHAPTER 1

GENERAL INTRODUCTION

Methods of noninvasive human brain stimulation are increasingly used to study neural function/processes, pathophysiology, and as treatment alternatives or adjunct neuromodulatory therapy in a number of psychological and neurological conditions (for reviews, see Dayan, Censor, Buch, Sandrini, & Cohen, 2013; Fregni & Pascual-Leone, 2007). Transcranial magnetic stimulation (TMS) and transcranial direct stimulation (tDCS) are popular examples of noninvasive brain stimulation techniques. Different neuromodulatory stimulation techniques do not however induce the same physiological or behavioural effects. Repetitive TMS (rTMS) is capable of producing long-lasting plasticity, thus, it has important clinical applications in treatment-resistant conditions. Specifically, low-frequency rTMS is widely used as an inhibitory (suppressive) intervention to regulate neural activity, e.g., in stroke, and schizophrenia (Chen et al., 1997; Lee et al., 2005; Mansur et al., 2005). Despite its popular use, the underlying neural mechanisms of noninvasive brain stimulation remain largely unknown, and its application to manage visual-related disorders has received considerably less interest. The advancement of neuroimaging techniques permits noninvasive investigation of stimulation on a variety of neural mechanisms in humans. This dissertation explores the application of low-frequency rTMS to the visual cortex as a therapeutic alternative in visual-related disorders for which there are currently no effective interventions. I combine low-frequency rTMS investigation with neuroimaging techniques to gain understanding of local rTMS effects at the visual cortex and distal effects across the brain.

Transcranial Magnetic Stimulation

TMS is an effective neuroscientific stimulation tool to modulate cortical activity and plasticity, evaluate connectivity, map brain function, and assess the impact of pharmacological or other interventions in healthy control individuals and clinical populations. TMS was first

introduced by Barker, Jalinous, and Freeston (1985) as a noninvasive and painless neuromodulatory technique based on Faraday's law of electromagnetic induction (Faraday, 1832). A rapid pulse of electric current is sent through a conductive TMS wire coil that generates a fluctuating magnetic field. Short, rapidly changing magnetic field pulses pass through the coil on an individual's scalp to induce secondary electrical currents in underlying neural tissue perpendicular to the current passing through the coil. The rate of change of the magnetic field determines the induction of the secondary current in nearby conductors (neural tissue). Electromagnetic induction adheres to the inverse cube law—the power of the magnetic field decreases exponentially as the distance from the original current increases. Accordingly, the induced current in the brain also decreases rapidly with distance from the coil. Because of this, the majority of direct TMS stimulation is restricted to superficial layers on the surface of the brain, e.g., 1–2 cm deep with a figure-of-eight coil (Zangen, Roth, Voller, & Hallett, 2005). However, single TMS pulses induce the perception of phosphenes (visual sensations of unformed lights) by activating the visual cortex (V1) approximately 4 cm deep to the scalp with a figure-of-eight coil (Marg & Rudiak, 1994), therefore, direct stimulation of the visual cortex may be deeper. TMS coils exist that allow for deeper stimulation (4–6 cm), such as the H and double cone coil; however, these coils produce greater diffuse disruption in underlying tissue compared with a figure-of-eight coil that has much more focussed stimulation, and they are generally less tolerated as they are more painful with deeper stimulation. In addition, coils allowing for deeper and more widespread stimulation have potential for a greater range of side effects, and their safety or efficacy in high doses of TMS in clinical applications is not well studied compared with the figure-of-eight coil. Regardless, superficial areas of the brain closer to the plane of the coil will always be exposed to greater induced currents than deeper brain regions

(Roth, Amir, Levkovitz, & Zangen, 2007). Effects are local to the area of stimulation and reach distal regions from the site of stimulation through axonal projections to functionally and/or anatomically connected regions (Lee et al., 2003; Rafique, Solomon-Harris, & Steeves, 2015; Reithler, Peters, & Sack, 2011). Thus, the area of the brain stimulated by TMS will affect activity in specific brain networks in which the stimulated area is involved and potentially between functionally connected networks (Fox et al., 2014).

Precise neural mechanisms of TMS are yet to be determined. Numerous studies suggest that TMS exerts its effect in the gyrus, lip of the gyrus, or in the wall of a sulcus because of their proximity to the coil (Day et al., 1989, 1987; Fox et al., 2004; Silva, Basser, & Miranda, 2008). The magnetic field strength is found to be largest at the gyral crown; while in white matter, field strength has been found to be largest in deeper fibres and is positively related to white matter anisotropy (degree of directionality) (Opitz, Windhoff, Heidemann, Turner, & Thielscher, 2011). However, since neurons in the gyral crown are perpendicular to the cortical surface, it has been suggested that the activation of cortical columns must be achieved indirectly via synaptic inputs through an initial activation of horizontally oriented excitatory interneurons (Day et al., 1989, 1987). The induced electrical current activates a mixture of inhibitory and excitatory neurons beneath the coil (for reviews, see Hallett, 2007; Kobayashi & Pascual-Leone, 2003; Wagner, Valero-Cabre, & Pascual-Leone 2007). TMS may also actively initiate action potentials in the axons of neurons in the cortex and subcortical white matter rather than the cell bodies of cortical neurons (which have a much higher threshold). Changes in action potentials may occur via changes in membrane resting potentials and thresholds, channel properties with subsequent modifications in spontaneous activity through changes in synaptic connectivity, and timing dynamics of cellular gating components (Wagner, Rushmore, Eden, & Valero-Cabre, 2009).

Modification of cell membranes by TMS leads to depolarisation or hyperpolarisation of neurons (Amassian, Eberle, Maccabee, & Cracco, 1992; Nagarajan, Durand, & Warman, 1993). Sites where current amplitudes are highest (Wagner et al., 2009) and neuronal thresholds are lowest (Ridding & Rothwell, 2007) within the fastest conducting fibres, typically pyramidal tracts (Corthout, Barker, & Cowey, 2001; Day et al., 1989, 1987), are considered more susceptible to TMS effects. Due to the uncertainty of precise underlying cellular mechanisms, TMS has been proposed as exerting its effects by altering noise amongst neurons via the introduction of random neural events. Random neural events will bring about a reduction in the strength of the relevant neural signal relative to irrelevant background neural noise (Allen et al., 2007). In addition, TMS alters the level of neural excitability during (online) and after (offline) stimulation. More specifically, with regards to offline TMS, effects are thought to arise from an alteration of longer-term excitability of neural cells and networks following stimulation (Thickbroom, 2007). Longer-term effects are considered a form of facilitated synaptic plasticity (i.e., long-term potentiation [LTP] or long-term depression [LTD] like effects) depending on the stimulation parameters (Hallett, 2007; Hoogendam, Ramakers, & Di Lazzaro, 2010; Pell, Roth, & Zangen, 2010).

A variety of TMS paradigms are currently available that explore causal relations between brain activity and behaviour that are briefly worth mentioning due to their distinguishable effects. TMS can be administered in isolated pulses (single-pulse TMS), in pairs of pulses a few milliseconds apart (paired-pulse TMS), or repeatedly in a sequence lasting seconds to minutes (rTMS). In addition, online TMS protocols refer to cognitive tasks undertaken while TMS is being administered. For instance, generating pulses during a language task to disrupt speech production (Stewart, Walsh, Frith, & Rothwell, 2001a). Offline TMS protocols refer to studies

with or without a task undertaken after TMS has been administered. For instance, assessing visual processing after rTMS at rest is an "offline" paradigm (Mullin & Steeves, 2013; Rafique et al., 2015; Solomon-Harris, Rafique, & Steeves, 2016).

Single- and paired-pulse paradigms. Single-pulse paradigms can be used to briefly disrupt or excite underlying neural tissue, and are useful for diagnostic and exploratory measurements of cortical response (for a review, see Chen et al., 1998) or to determine cortical excitability to each pulse, e.g., motor threshold (MT; excitability measure of the motor cortex) and phosphene threshold (PT; excitability measure of the visual cortex) (Ray, Meador, Epstein, Loring, & Day, 1998; Rossini et al., 1994). Paired-pulse paradigms utilise two isolated pulses delivered in close succession and have been used to induce a form of Hebbian learning, where the first pulse has a conditioning effect and the effect of the second pulse is dependent on the intensity and inter-pulse interval duration. Paired-pulse TMS is therefore useful for examining cortical excitation/inhibition ratios and functional connectivity in healthy subjects and in patients (for reviews, see Rotenberg, Horvath, & Pascual-Leone, 2014; Udupa & Chen, 2010).

Repetitive transcranial magnetic stimulation paradigms. rTMS paradigms utilise repeated trains of pulses lasting seconds to minutes to induce neural effects that outlast stimulation duration. With offline rTMS, we can assess underlying neural mechanisms of longer-lasting rTMS effects with a variety of neurotechniques, e.g., behavioural tasks, magnetic resonance imaging (MRI) (Ridding & Rothwell, 2007; Rossi & Rossini, 2004; Thut & Pascual-Leone, 2010). rTMS is widely used to transiently disrupt neural activity, enabling researchers to modify cortical function during task performance that can reveal causal relations between brain regions/activity and behaviour in neurologically intact subjects (e.g., Ganaden, Mullin, & Steeves, 2013; Mullin & Steeves, 2011; Pascual-Leone et al., 1998; Wagner et al., 2007). Due to

its longer-term effects, rTMS also has valuable therapeutic potential in higher doses in clinical applications and will be the protocol of focus in this dissertation. rTMS has important implications as a safe and effective means to treat and manage a number of disorders where pharmaceutical intervention is ineffective, as well as to evaluate effects on neuroplasticity, for example in Parkinson's disease, mood disorders, schizophrenia, and stoke rehabilitation (e.g., Cassidy, Gillick, & Carey, 2014; Freitas, Fregni, & Pascual-Leone, 2009). The effects of rTMS and desired manipulation of neural mechanisms are highly dependent on the brain region of stimulation, state of neurons prior to stimulation (e.g., potentiated, depotentiated), and rTMS parameters.

Parameters. The magnitude and direction of rTMS effects depends on a variety of parameters including the inter-pulse interval, total number of pulses delivered in the stimulation session (train length), frequency, and stimulation intensity of pulses. Safety guidelines on recommended values of stimulus parameters are provided in a number of reports (Rossi, Hallett, Rossini, Pascual-Leone, & The Safety of TMS Consensus Group, 2009; Wassermann, 1998). Moreover, the coil configuration, current direction, pulse waveform, and position of the coil with respect to the cortex influence rTMS effects (Kozel et al., 2000).

In rTMS protocols, stimulation pulses are delivered in trains separated by time intervals termed the inter-pulse interval. The effect of rTMS pulses is cumulative in the brain as it shows dose-dependent effects (Hallett, 2007; Ridding & Rothwell, 2007; Rossi & Rossini, 2004). The number of sessions of rTMS used in clinical applications is considerably variable, ranging from 5–10 sessions (e.g., Manes et al., 2001; Miniussi et al., 2005) to more than 30 sessions (e.g., Fitzgerald et al., 2003; O'Reardon et al., 2007; Rumi et al., 2005). Greater cumulative effects are associated with a greater number of sessions. A greater number of sessions (> 10) is therefore

associated with greater therapeutic effect and continuing improvement in symptoms (Goldsworthy, Müller-Dahlhaus, Ridding, & Ziemann, 2014; Holtzheimer et al., 2010; Spronk, Arns, & Fitzgerald, 2011). Further, rTMS effects vary with the choice of interval time between multiple stimulations (Goldsworthy, Pitcher, & Ridding, 2015; Monte-Silva, Kuo, Liebetanz, Paulus, & Nitsche, 2010).

The stimulation frequency refers to the number of pulses delivered per second and are usually between 1 hertz (Hz) (one pulse per second) and 50 Hz (50 pulses per second). Low-frequency refers to protocols employing < 5 Hz, while high-frequency refers to protocols ≥ 5 Hz. Lower frequencies are usually applied continuously for periods up to 30 min. Higher frequency paradigms are typically applied in a patterned fashion (bursts interrupted by pauses, e.g., 1 s stimulation with 20 s inter-pulse interval) for seconds to a few minutes. Traditionally, low-frequency rTMS is considered "inhibitory" in its effects, whereas high-frequency stimulation is viewed as "excitatory". This traditional view largely arises from animal studies and human electrophysiology recordings from motor and frontal cortices (for reviews, see Hallett, 2007; Thut & Pascual-Leone, 2010), and from behavioural aftereffects (e.g., Rafique et al., 2016; Rumi et al., 2005). Neurophysiological measures (e.g., changes in motor evoked potentials) suggest that low-frequency rTMS suppresses excitability of the motor cortico-spinal tract (e.g., Chen et al., 1997; Gerschlager, Siebner, & Rothwell, 2001; Houdayer et al., 2008; Touge, Gerschlager, Brown, & Rothwell, 2001), while higher frequency stimulation facilitates excitability (e.g., Huang, Edwards, Rounis, Bhatia, & Rothwell, 2005; Pascual-Leone, Valls-Solé, Wassermann, & Hallett, 1994; Peinemann et al., 2004). However, these frequency-dependent effects are far too simplistic and have become a misinformed generalisation for aftereffect predictability (Allen, Pasley, Duong, & Freeman, 2007). Both low- and high-frequency rTMS are observed to produce

an elevating antidepressant effect in medication-resistant major depression (Fitzgerald et al., 2003). Similarly, both high- and low-frequency paradigms have been used to disrupt cognitive function (Brückner, Kiefer, & Kammer, 2013; Ko et al., 2008; Mullin & Steeves, 2011; Rafique et al., 2015). Several studies have demonstrated that the inter-pulse interval also plays a role in the direction of rTMS effects. For example, theta burst stimulation (TBS), a variant of high-frequency rTMS, applied intermittently (e.g., 2 s of stimulation every 10 s) leads to facilitated excitability; and when it is applied continuously (e.g., 40 s), it leads to a suppression in excitability (Huang et al., 2005). The influence these inter-pulse intervals exert is likely a result of metaplasticity (i.e., ability of the synapse to undergo a secondary plastic change following the recent induction of plasticity). Moreover, findings on rTMS aftereffects from animal studies have been relatively inconsistent with those in human studies because of differences in techniques (e.g., invasive methods used in animals compared to noninvasive methods in humans) and heterogeneity among species (for a review, see Goldsworthy et al., 2015). Further, TMS effects are considered to be activity dependent (state-dependency), suppressing the most active neurons and changing the balance between excitation and inhibition (Pasley, Allen, & Freeman, 2009; Perini, Cattaneo, Carrasco, & Schwarzbach, 2012).

For TMS to be effective, the stimulation intensity determines the potential of the magnetic field that induces electrical currents in neurons of underlying neural tissue. This intensity is expressed as a percentage of the maximal output percentage, and the choice of intensity depends on the stimulation site. For most cortical regions (excluding the visual cortex), the MT is commonly used (Pridmore, Filho, Nahas, Liberatos, & George, 1998; Rossini et al., 1994). The MT is obtained by applying single-pulses to the motor cortex in a stepwise variation of the output intensity of the device and is defined as the minimal output intensity which yields a

motor response (e.g., produce muscle contraction in small muscles of the hand) in at least half of the applied trials. Stimulation intensity for the visual cortex is largely based on the PT. Pulses are applied to the visual cortex in a similar manner to the motor cortex until phosphenes are perceived. The PT is the minimum intensity of TMS to the visual cortex that elicits the perception of phosphenes (transient perception of unformed lights) in at least half of delivered pulses (Elkin-Frankston, Fried, Pascual-Leone, Rushmore III, & Valero-Cabré, 2010). Both MT and PT provide indirect measures of neural excitability, and are considered established methods to calibrate and normalise TMS coil output for individual neurophysiological variability. These threshold measures determine dose and safety limits with regards to adverse effects and its efficacy in stimulating neurons (Rossi et al., 2009; Wassermann, 1998). Lower intensities of low-frequency may induce inhibition and higher intensities may produce facilitation (Classen & Stefan, 2008; Fox et al., 1997; Nahas et al., 2001), whereas lower intensities of high-frequency rTMS reduce excitability (Paus et al., 1998; Siebner, Rossmeier, Mentschel, Peinemann, & Conrad, 2000b).

Neurobiochemical effects. Ultimately, parameter-dependent TMS effects arise via neurobiochemical responses to the pulse(s). Neurobiochemical responses to stimulation drive the overall effect to form the basis of therapeutic intervention (for a review, see Hoogendam et al., 2010). Much of our knowledge of biochemical effects of low- and high-frequency rTMS stem from invasive animal studies, thereby limiting translation of results. In general, high-frequency protocols have received greater attention due to their desired aftereffects in a variety of neurological and psychological disorders (e.g., stroke, schizophrenia) and approved application in mood disorders (e.g., depression). A brief overview of known high- and low-frequency biochemical aftereffects is provided here.

In vitro rat and cat studies show high-frequency rTMS to the hippocampus and visual neocortex induces *N*-methyl-D-aspartate (NMDA) glutamate receptor-mediated LTP (long-lasting strengthening of synaptic efficiency), while low-frequency protocols induce LTD (long-lasting decrease in the strength of synapses) (Dudek & Bear, 1992; Kirkwood, Dudek, Gold, Aizenman, & Bear, 1993). Long trains of low-frequency stimulation are capable of inducing LTD lasting for hours (Dudek & Bear, 1992; Mulkey & Malenka, 1992). Long-lasting effects are also observed in human studies, where stimulation to the prefrontal cortex and motor cortex is shown to induce effects lasting up to a year (e.g., Dunner et al., 2014; Liepert, Bauder, Miltner, Taub, & Weiller, 2000). However, the effects are not consistent across cortical/subcortical sites or even in subregions, e.g., in layers of the cat visual cortex (Bear & Kirkwood, 1993; Komatsu, Fujii, Maeda, Sakaguchi, Toyama, 1988). Similar inconsistent effects are observed between different low-frequency protocols in the rat and cat hippocampus and visual neocortex (e.g., 1 Hz versus 3 Hz; Kirkwood et al., 1993). The amino acid neurotransmitters glutamate and γ-Aminobutyric acid (GABA) modify the membrane potential of the receptive neuron. Glutamate and GABA have opposing excitatory and inhibitory effects, respectively, and modulate the induction of LTP and LTD (for a review, see Lüscher & Malenka, 2012). Electrical stimulation can exert excitatory or inhibitory cortical effects at the stimulated area via glutamate (NMDA) and GABA receptor activity (for a review, see Bear & Malenka, 1994). These effects on GABAergic and glutamatergic systems are additionally relatively inconsistent between high- and low-frequency protocols, and duration of stimulation. However, human and rat studies of the subcortex, motor and prefrontal cortices suggest that low-frequency is thought to act on GABAergic mechanisms and high-frequency on glutamate systems (Michael et al., 2003; Stagg et al., 2009b; Yue, Xiao-Lin, & Tao, 2009).

High-frequency rTMS protocols (e.g., 25 Hz versus 15 Hz) to frontal brain regions also have variable effects on monoamines (e.g., serotonin, norepinephrine, dopamine, and associated metabolites) in the rat brain (Ben-Shachar et al., 1997, 1999; Keck et al., 2002) and humans (Strafella et al., 2001), as well as on messenger ribonucleic acid (mRNA) expression of monoamine transporter genes (Ikeda, Kurosawa, Uchikawa, Kitayama, & Nukina 2005). The rTMS-induced modulation of dopamine in humans may be a consequence of direct stimulation via glutamate (Strafella, Paus, Fraraccio, & Dagher, 2003), or indirectly via GABA-mediated activity (for a review, see Pascual-Leone et al., 1998). An increase in dopaminergic neurotransmission with high-frequency rTMS is in line with the therapeutic effects of rTMS in the treatment of conditions implicating dopamine including affective disorders (e.g., Schutter & van Honk, 2005) and Parkinson's disease (e.g., Lomarev et al., 2006).

Chronic high-frequency rTMS in the rat brain is observed to increase brain-derived neurotrophic factor (BDNF) mRNA and BDNF-like immunoreactivity across the brain, as well as protect against oxidative stressors (e.g., high glutamate concentrations) that cause neuronal damage and neurotoxic effects (Müller, Toschi, Kresse, Post, & Keck, 2000; Post, Müller, Engelmann, & Keck, 1999). High-frequency rTMS demonstrates gene expression of glial fibrillary acidic protein in the murine central nervous system in mice (Fujiki & Steward, 1997) that is associated with recovery such as synaptic reorganisation (Steward, Torre, Phillips, & Trimmer, 1990). In contrast, low-frequency rTMS to the rat motor cortex and hippocampus demonstrates no significant differences in glial fibrillary acidic protein (Liebetanz et al., 2003).

Associations between regional cerebral blood flow and local cerebral glucose metabolism are well established. Increased glucose levels correlate with greater energy consumption and accordingly greater neuronal (mainly synaptic) activity (for reviews, see Heeger & Ress, 2002;

Jueptner & Weiller, 1995). During high- and low-frequency rTMS to the visuoparietal cortex in anaesthetised cats, (^{14}C)2-deoxyglucose uptake is significantly reduced in the stimulated cortex and in remote cortical and subcortical networks compared with the contralateral hemisphere (Valero-Cabré, Payne, & Pascual-Leone, 2007). (^{14}C)2-deoxyglucose is considered a close correlate of neuronal presynaptic activity (Kennedy et al., 1975). A greater effect is observed for high- than low-frequency rTMS. However, immediately following cessation of high-frequency rTMS, (^{14}C)2-deoxyglucose uptake is increased in the stimulated cortex only. Conversely, (^{14}C)2-deoxyglucose uptake remains attenuated following cessation of low-frequency rTMS in the stimulated cortex with mild effects in subcortical regions compared with the contralateral hemisphere. These findings suggest that during rTMS (high- and low-frequency) neuronal firing may be suppressed, with a greater suppressive effect with high-frequency rTMS. Yet, local and distal effects are highly dependent on the stimulation parameters in that suppression versus facilitation of neuronal firing is frequency-dependent (1 Hz versus 20 Hz, respectively). Magnetic resonance spectroscopy (MRS) measures of glucose however show no change in glucose at the stimulation site following 1 Hz low-frequency rTMS in rats (Liebetanz et al., 2003). In human subjects, ^{18}fluoro-deoxyglucose positron emission tomography (PET) provides a noninvasive alternative and shows an increase in normalised regional cerebral metabolic rate for glucose following 2 Hz low-frequency rTMS to the sensorimotor cortex (Siebner et al., 2001).

In summary, rTMS can induce changes in neuromodulator (neurotransmitters and metabolites) release, synaptic efficiency, signalling pathways, and in gene transcription. Effects of rTMS are specific to brain regions and/or networks and stimulation parameters. Variability between study methods including rTMS parameters, stimulation schedules, stimulation sites,

stimulation coils, differences in technique sensitivity of rTMS effects, and the use of different animal models limits comparability of rTMS effects. Moreover, a larger proportion of studies investigate high-frequency rTMS to frontal and motor cortices for therapeutic treatment in several psychological and neurological disorders. Further research is needed on low-frequency rTMS across the bran in human studies. Noninvasive in vivo investigation of neurobiochemical effects in humans has also been limited post-rTMS. However, with advancing noninvasive neuroimaging techniques in humans and a growing number of studies, a greater variety of rTMS parameters have been exploited with more detailed probing of effects, revealing complex effects that are not simply predicted by frequency of stimulation. This increasing number of techniques and parameter choices have also added to the variety of inconsistent effects that vary across brain regions within humans. rTMS effects on the visual cortex are even less investigated, and thus the application of TMS in visual disorders has received little attention. Knowledge of biochemical mechanisms of rTMS has important implications for predicting effects in humans, predominantly for validating causal inferences of brain function/regions and developing therapeutic applications. Depending on the disorder in question and its associated altered mechanisms, the desired neurobiochemical response will be highly dependent on the rTMS protocol.

Magnetic Resonance Imaging

MRI provides a method of noninvasive investigation of cortical and subcortical structure and activity. Brain regions form a complex integrative network in which information is continuously processed and transported between structurally and/or functionally linked brain regions. Due to the complexity, a number of neuroimaging techniques sensitive to a variety of measures are necessary to gain better overall understanding of neuroarchitecture. Identifying group differences between healthy control subjects and those with impairments using MRI can

segregate functional and structural abnormalities underlying different disease states from which we can infer changes. This knowledge could in turn lead to identification of diagnostic/prognostic markers, new treatments, or drug targets. For instance, a lesion will not only affect the implicated region and nearby regions, but it will also affect the functional and structural network architecture of areas in both hemispheres distant from the lesion (Hummel et al., 2005; Murase, Duque, Mazzocchio, & Cohen, 2004; Nomura et al., 2010; Rafique, Richards, & Steeves, 2016, 2018). The combination of noninvasive brain stimulation with neuroimaging offers a valuable means to explore how rTMS impacts the human brain, providing new insights into the changeability of functional and structural brain networks, and efficacy of rTMS as a therapeutic tool in clinical populations. Neuroimaging highlights the neurophysiological response to stimulation at the targeted cortex, whether it be disruptive or facilitative. For instance, functional MRI (fMRI) demonstrates that stimulation to a given brain region typically induces significant inhibitory or excitatory changes in the activity of regions distal from the coil, but which are anatomically and/or functionally connected to the targeted stimulation region (e.g., Lee et al., 2003; Rafique et al., 2015; Solomon-Harris et al., 2016). In this dissertation, I use a number of neuroimaging techniques (fMRI, MRS, diffusion imaging) to identify neural mechanisms of low-frequency rTMS to the visual cortex and determine its efficacy for development of therapeutic protocols in visual-related disorders. The techniques employed are also well suited to longitudinal studies and for monitoring treatment effects. For example, we can examine the effect of clinical intervention (e.g., rTMS) by comparing pre- and post-treatment data (e.g., Inzitari et al., 2009; Kunimatsu et al., 2003).

Functional magnetic resonance imaging. fMRI is a noninvasive technique for measuring brain activity and understanding function of brain regions. fMRI assesses changes in

blood oxygen level-dependent (BOLD) signal to identify areas of increased or decreased neuronal activity (Logothetis, 2003; Raichle & Mintun, 2006). BOLD signal arises from the magnetic properties of haemoglobin that are dependent on brain metabolism, blood flow, and essential changes in neuronal excitability (Logothetis & Wandell, 2004; Raichle & Mintun, 2006). Regional changes in brain activity can be inferred throughout the brain by assessing changes in the BOLD signal that indicate the direction (increase or decrease) of neuronal activity, and allowing the researcher to make inferences about the contribution of a cortical area or its interconnected region to a distinct brain function. As the brain consists of functionally interconnected nodes within a network, fMRI offers insights into the overall organisation of functional communication in the brain network and how regions with different functions communicate.

Task-based functional magnetic resonance imaging. Typical fMRI research focusses on the change in BOLD signal caused by the neural response to an externally controlled stimulus (i.e., neural response to a task). The fMRI signal during processing of a task is contrasted with fMRI acquisition during a baseline or control condition, resulting in the relative signal change because of the specific process being studied. Task-based fMRI provides information about regions that are engaged/disengaged in different functions (i.e., tasks), for example, visual processing of scenes compared to objects.

Resting-state functional magnetic resonance imaging. At rest, in the absence of explicit input or output demands (i.e., task engagement), the brain remains functionally and metabolically active. One index of this intrinsic activity is the spontaneous fluctuations of low-frequency oscillations (∼0.01–0.1 Hz; Biswal et al., 1995, 1997) in the BOLD signal of fMRI (for reviews, see Fox & Raichle, 2007; van den Heuvel & Hulshoff Pol, 2010). Identification and correlation

of patterns in these spontaneous fluctuations between functionally and/or anatomically distinct regions is termed resting-state functional connectivity (rsFC). rsFC therefore highlights intrinsic functional connectivity among cortical and subcortical networks (Aertsen, Gerstein, Habib, & Palm, 1989; Friston, Frith, Liddle, & Frackoqiak, 1993; Friston, Jezzard, & Turner, 1994). Support for the neural basis of resting-state fMRI (rsfMRI) comes from the observation that most resting-state patterns occur between brain regions that overlap in both function and neuroanatomy, for example, regions of the motor, visual, and auditory networks (Biswal et al., 1995; Damoiseaux et al., 2006; Lowe, Dzemidzic, Lurito, Mathews, & Phillips, 2000; van den Heuvel, Mandl, & Hulshoff Pol, 2008).

rsfMRI holds tremendous potential to greatly increase the translation of fMRI into clinical care and improve the clinical applicability of fMRI (Fox & Greicius, 2010; Fox & Raichle, 2007). During resting conditions, the brain consumes ~20% of the body's energy, of which a considerable amount supports ongoing neuronal signalling (Ames III, 2000; Attwell & Laughlin, 2001; Shulman, Rothman, Behar, & Hyder, 2004). Task-related increases in neuronal metabolism are considerably small (< 5%) compared to the larger resting-state energy consumption (Raichle & Mintun, 2006). Fox and Greicius (2010) report that differences in task-related changes between normal and pathological populations are even smaller (< 1%). Therefore, studying resting-state conditions to investigate pathophysiology can be much more valuable as focus is on a greater proportion of neural brain activity than studying task-related changes (Fox & Greicius, 2010).

Although task-based fMRI remains extremely valuable to determine function of brain regions, rsfMRI also minimises limitations associated with task-based fMRI. We undertake a wide array of tasks on a daily basis incorporating multiple interchanging brain networks that

would be extremely difficult to fully assess and account for in pathophysiology given that it would require a countless number of diverse task manipulations. The incorporation of numerous task-based fMRI experiments is additionally time consuming and a considerable expense due to high MRI costs. Further difficulties arise in interpreting results between different task data sets and after treatment due to a number of confounds (Fox & Greicius, 2010). For example, a single task involves a variety of cognitive processes and it can be difficult to discern changes between different brain regions with overlapping function if task demands are not precisely controlled for. rsfMRI also avoids task performance confounds between individuals and groups because there is a reduced need for participant compliance (e.g., task engagement and responsiveness). In cognitive dysfunction, physical, or visual impairment, many patients cannot accurately perform tasks in the MRI scanner. Resting-state removes task performance confounds that may occur in these patients if undertaking a task and places only minimal demands on the patient (Fox & Greicius, 2010). Specifically, in the case of visual disorders, for example visual pathway damage, there is potential for extensive visual loss which may reduce accuracy of fixation and impair simple viewing. As intrinsic neural activity provides insight into neural processing that encompasses the majority of the brain's resources, it not only provides a richer source of disease-related signal changes but also a means of studying multiple cortical systems at once.

Diffusion tensor imaging. White matter tracts enable connectivity between spatially separate regions. Diffusion imaging is currently the only noninvasive technique available to reconstruct, visualise, and characterise the architecture of white matter fibre tracts. Diffusion tensor imaging (DTI) measures the diffusion profile of water molecules through fibres that are influenced by underlying microstructure rather than directly capturing anatomical structures of axons. DTI relies on the principle that water molecules diffuse differently along tissues

depending on their type, integrity, architecture, and barriers (e.g., cell membranes, myelin sheaths, and microtubules), providing information about their orientation and quantitative anisotropy (Beaulieu, 2002; Chenevert, Brunberg, & Pipe, 1990; Moseley et al., 1990). A number of images, each sensitised to diffusion in a different direction, are used to determine the rate and orientation of water diffusion in a given voxel that is summarised in a diffusion tensor model (Mori & Zhang, 2006). Faster diffusion will occur along a fibre tract rather than perpendicular to it, giving rise to diffusion anisotropy (directionally-dependent). The particular orientation of axons leads to the segregation of specific fibre tracts in order to map axonal orientations, thereby enabling measurement of white matter properties and microstructure in vivo. Accordingly, anisotropy in cerebral organisation for white matter tracts corresponds to the main axonal fibres connecting cortical areas. Direct association is determined between functional and structural connectivity in the human brain by combining fMRI with DTI (e.g., Hagmann et al., 2008; Koch, Norris, & Hund-Georgiadis, 2002). Microstructural organisation of white matter tracts is found to be directly related to the level of functional connectivity between regions (van den Heuvel et al., 2008). Regions with a higher level of structural connectivity show a higher level of functional connectivity (Hagmann et al., 2008; Honey et al., 2008). Pathological processes can alter structural organisation either by injury, regeneration of cell membranes, or via change in cellularity (e.g., scarring, inflammation, cell infiltration) that impact diffusivity (Bammer, 2003). DTI can therefore provide insight in damaged nerve fibres that connect an area of the brain affected by injury and regions that are distant from it. Moreover, DTI can provide information on the presence of abnormal or new aberrant connections resulting from damage (e.g., Arfanakis et al., 2002; Rafique et al., 2018; Wong et al., 2018).

Identified pathways can be interpreted quantitatively using indices inferring diffusion properties in each voxel. Diffusion tensor indices combine contributions from the different sub-compartments of white matter into a single metric that characterises different aspects of diffusion and is useful in making implications regarding white matter connectivity and structure (Jones, Knösche, & Turner, 2013). Fractional anisotropy (FA) represents the directional preference of diffusion and describes the degree of directionality (anisotropy) of diffusion using a scalar value between zero and one. FA values close to zero represent isotropic regions, that is, unrestricted water movement that will diffuse in all directions. FA values approaching one represent anisotropy, that is, restricted water diffusion in one direction (Mori & Zhang, 2006). Mean diffusivity (MD) is a measure of the average rate of diffusion per voxel or the molecular diffusion rate. Axial diffusivity (AD) represents the degree of diffusion parallel to the main axis of diffusion. Lastly, radial diffusivity (RD) is a measure of diffusion perpendicular to the axon (Mori & Zhang, 2006). Diffusion in white matter is more restricted along the axon and tends to be anisotropic, whereas in grey matter diffusion is less anisotropic, and in cerebrospinal fluid diffusion is unrestricted in all directions and is therefore isotropic (Hagmann et al., 2006; Pierpaoli & Basser, 1996; Pierpaoli, Jezzard, Basser, Barnett, & Di Chiro, 1996).

Diffusion pathways can also be interpreted qualitatively to infer the extent and the general course of certain fibre bundles. Tractography is a three-dimensional (3D) modelling technique that enables qualitative visualisation and quantification of fibre tracts based on statistical inferences as true anatomy of nerve fibres cannot be directly reconstructed. Computed trajectories or pathways in tractography are determined by following from voxel to voxel the direction of maximum diffusion coherence. Tractography results are considered to run reasonably parallel to a large portion of the nerve fibres (for a review, see Soares, Marques,

Alves, & Sousa, 2013) and correspond well with post-mortem dissection studies (Lawes et al., 2008).

Magnetic resonance spectroscopy. Proton (^{1}H) MRS enables noninvasive in vivo quantification of neurotransmitter concentrations and of other neurometabolites (molecules involved in a neuronal metabolic process) within a localised region (voxel). ^{1}H MRS measures the magnetic properties and energies of protons in nuclei of various chemical compounds (e.g., metabolites). MRI pulse sequences consist of a combination of radiofrequency and gradient pulses arranged in a specific order to excite, detect, and encode resonance signals. Nuclei found in matter (e.g., brain tissue) in a magnetic field (e.g., MRI) absorb the executed MR pulse and emit electromagnetic radiation in the radiofrequency range. Nuclei from the same chemical compound will absorb and emit radiofrequency energy at different frequencies depending on the chemical environment surrounding the nuclei (Dickinson, 1950a, 1950b; Protor & Yu, 1950). Therefore, metabolites will emit signals of a chemically specific frequency based on their molecular structure. ^{1}H MRS detects the radiofrequency signals that arise from tissue metabolites within the localised region of interest. Resonance signals are then processed into images or spectra that reflect properties of the metabolite of interest (Puts & Edden, 2012). MRS identifies a number of metabolites by their discrete peak or a set of peaks in the frequency spectrum (Pfeuffer, Tkáč, Provencher, & Gruetter, 1999). Change in neurotransmitter and neurometabolite concentrations provides insight into neurobiochemical processes underlying pathological processes or following treatment (e.g., neuromodulation with noninvasive brain stimulation).

Clinical Application of Noninvasive Brain Stimulation

Noninvasive brain stimulation induces plasticity allowing modification of cortical networks. Thus, noninvasive brain stimulation provides a valuable tool to investigate and

manipulate neural mechanisms to promote recovery of brain function in neurological and psychological disorders. In higher doses for therapeutic application, it can elicit significant neurophysiological and behavioural aftereffects outlasting stimulation itself (for a review, see Wassermann & Lisanby, 2001). Plasticity is retained throughout life and enables modification of function and structure in response to environmental demands via strengthening, weakening, pruning, recruitment of synaptic connections, and by promoting neurogenesis (for a review, see Pascual-Leone, Amedi, Fregni, & Merabet, 2005). Plasticity is essential to forming and maintaining brain circuitry in the absence of pathophysiology, yet it is also necessary to enable acquisition of new skills and adaptation after injury via compensatory recruitment of healthy circuitry and networks (e.g., Carmichael, 2003; Cramer, 2008). However, maladaptive plasticity processes can give rise to disability and symptoms of pathophysiology. Local pathophysiological changes cause maladaptive network dynamics through interconnected regions leading to widespread dysfunction in networks and remote regions (for a review, see Fox & Greicius, 2010). Noninvasive brain stimulation can manipulate mechanisms involved in deficits and promote recovery of brain functionality. Clinical therapeutic protocols of targeted stimulation to a brain region typically fall under three distinct categories (Horvath, Najib, & Press, 2014): (1) directly target the specific area of dysfunction that is considered to be a critical functional node in a network driving the dysfunctional behaviour of interest. The aim is to modulate cortical excitability and normalise aberrant activity by either up-regulating pathologically under-excited tissue (e.g., Avery et al., 2006; Ward & Cohen, 2004) or down-regulating pathologically over-excited tissue (e.g., Hummel & Cohen, 2006; Fregni & Pascual-Leone, 2007; Rafique et al., 2016). (2) Target a distal area functionally connected to the area of dysfunction and normalise aberrant activity via excitation or inhibition, for instance, if the dysfunctional region is too deep

to reach directly with noninvasive brain stimulation. (3) Modulate distributed brain activity via network-specific release of neurotransmitters to normalise aberrant activity.

The number and type of neurological and psychological conditions being treated with noninvasive brain stimulation, particularly rTMS, is ever increasing. rTMS is accepted as a safe and effective method with minimal adverse effects, if used within safety limits (Rossi et al., 2009; Wassermann, 1998), for rehabilitation and therapeutic intent long-term in a number of disorders where pharmaceutical intervention is ineffective (e.g., Hallet, 2007; Kobayashi & Pascual-Leone, 2003; Ridding & Rothwell, 2007; Rossi & Rossini, 2004). In addition, stimulation parameters employed to treat these conditions are continuously evolving. In cases where rTMS is applied for therapeutic purposes, the classic approach involves a stimulation session provided daily over consecutive days usually for a period of 2–6 weeks. Aftereffects of these longer doses of stimulation have been reported to last months (Bortolomasi et al., 2007; Liepert et al., 2000a; Triggs et al., 1999) and even up to one year (Dunner et al., 2014). Repeated daily applications of stimulation have cumulative effects on the induction/maintenance of neuroplastic changes (e.g., Bäumer et al., 2003; Dunner et al., 2014). More recently, accelerated (or within-session) stimulation has been proposed as an alternative to the classical approach, where multiple spaced stimulation sessions are provided in a single day over consecutive days, but for fewer days/weeks than the classical approach. The interval at which spaced stimulation is applied critically influences the neuroplastic response (Monte-Silva et al., 2013, 2010). Spaced intervals of stimulation produce more long-lasting effects than simply extending the length of stimulation protocols (Gamboa, Antal, Moliadze, & Paulus, 2010; Monte-Silva et al., 2013, 2010). Increasing the number of spaced stimulation sessions disproportionately extends the duration of induced neuroplastic changes. Additionally, spaced noninvasive brain stimulation

aftereffects in human studies are found to be more stable, possibly owing to a consolidation of longer-term plasticity effects (e.g., Cazzoli et al., 2012; Nyffeler, Cazzoli, Hess, & Müri, 2009).

The application of noninvasive brain stimulation in disorders with known disease mechanisms has advanced our understanding by measuring biochemical and behavioural changes that occur following stimulation. However, despite established protocols and effects, mechanisms and evidence of efficacy are lacking, mainly due to the inconsistency of stimulation parameters and absence of long-term follow-up with neuroimaging. As mentioned previously, different stimulation paradigms have substantially different effects on plasticity. This is of considerable importance in clinical contexts as the choice of paradigm will depend on its underlying effect and the pathological mechanism one intends to modulate.

Non-visual disorders. TMS devices and protocols have received United States Food and Drug Administration, and European Union approval for the treatment of medication-resistant depression, and presurgical motor and speech mapping. In Europe, several devices have been awarded European CE Mark approval and are increasingly used for diagnostic and therapeutic indications in clinical practice. Clinical trials of TMS are currently underway in a number of countries exploring the effects in diverse conditions including autism, epilepsy, migraine, tinnitus, stroke recovery, schizophrenia, obsessive compulsive disorder, Parkinson's and Alzheimer's disease (Cassidy et al., 2014; Freitas et al., 2009; George, Lisanby, & Sackeim, 1999; Ridding & Rothwell, 2007; Wassermann & Lisanby, 2001).

For instance, in stroke, neuroimaging studies demonstrate hyperactivity in the contralesional motor cortex and interhemispheric inhibition between motor cortices that is greater in those with a poorer prognosis (Murase et al., 2004; Ward, Brown, Thompson, & Frackowiak, 2003). rTMS restores imbalanced cortical activity across hemispheres leading to

functional improvement in the paretic limb either by facilitating the lesioned hemisphere using high-frequency protocols (10 Hz rTMS or intermittent TBS; Kim et al., 2006; Talelli, Greenwood, & Rothwell, 2007), or by down-regulating the contralesional hemisphere using low-frequency protocols (1 Hz rTMS; Fregni et al., 2006; Mansur et al., 2005; Takeuchi et al., 2008). Most rTMS studies in depression to date have been performed by means of applying high-frequency (5–20 Hz) stimulation to the left prefrontal cortex to produce an antidepressant/elevating effect by exciting the depressed activity (e.g., Avery et al., 2006; O'Reardon et al., 2007). However, low-frequency (1 Hz) rTMS to the right prefrontal cortex elicits a similar reduction in depressive symptoms (Fitzgerald et al., 2003). Both treatment modalities in depression appear to be equally efficacious (Fitzgerald, Hoy, Daskalakis, & Kulkarni, 2009). Based on a meta-analysis of randomised controlled rTMS studies in depression, it is suggested that low-frequency rTMS might even be more beneficial than high-frequency rTMS as low-frequency is better tolerated, e.g., patients reported fewer headaches. Low-frequency protocols may also minimise the risk of inducing adverse events like seizures (Schutter, 2010).

Visual disorders. The visual system comprises the most complex circuitry of all the sensory systems and possesses the ability to undergo induced and spontaneous neuroplastic changes. Numerous distinct unimodal areas are involved in visual processing in the macaque and human brain (Felleman & Van Essen, 1991; Tootel, Dale, Sereno, & Malach, 1996). Different levels of visual processing are coded in different regions—such as oriented lines and edges, colour, to more complex movement and form—and each visual processing region presents with distinct anatomical properties and functional connectivity patterns. Very few studies so far have investigated the effects of noninvasive brain stimulation in visual disorders.

In amblyopia, low- and high-frequency rTMS to the visual cortex significantly improves contrast sensitivity (Clavagnier, Thompson, & Hess, 2013; Thompson, Mansouri, Koski, & Hess, 2008) with long-lasting effects > 2 months (Clavagnier et al., 2013). Similarly, tDCS to the visual cortex also shows improvement in contrast sensitivity in amblyopia, but this effect is only transient (Spiegel, Byblow, Hess, & Thompson, 2013). tDCS has been explored as potential treatment in visual field loss related to cerebral stroke. tDCS applied over the visual cortex in combination with vision restoration training is shown to facilitate regaining parts of the visual field and accelerating recovery time following stroke (Gall et al., 2015; Plow et al., 2011). These results are consistent with findings from stroke-related motor and speech rehabilitation demonstrating improved performance with adjunct therapies of noninvasive brain stimulation (e.g., Seniów et al., 2013; Takeuchi et al., 2008). Similarly, tDCS to parieto-occipital cortex combined with blindsight rehabilitation in homonymous hemianopia shows better functional outcome than rehabilitation on its own (Alber, Moser, Gall, & Sabel, 2017; Halko et al., 2011; Matteo et al., 2017).

Aftereffects of tDCS are thought to be relatively short-lasting compared to rTMS, and more so in visual areas compared to the motor cortex using equivalent stimulation parameters (Antal, Paulus, & Nitsche, 2011). Visual and motor cortices vary in factors influencing neuroplasticity and excitatory/inhibitory systems. There are differences in cortical connections and neuronal membrane properties (e.g., receptor expression), and these may account for the dissimilar responses of tDCS in the motor and visual cortices (Creutzfeldt, Fromm, & Kapp, 1962). Moreover, rTMS allows for more focal and therefore targeted stimulation compared to tDCS (Woods et al., 2016). Therefore, rTMS may provide a better neuromodulatory tool for clinical applications, particularly in visual-related disorders.

Visual hallucinations. A secondary consequence of vision loss that has received limited investigation into therapeutic intervention, and would benefit from noninvasive brain stimulation, is visual hallucinations that occur in otherwise cognitively healthy individuals (Kölmel, 1985; Lepore, 1990). Visual hallucinations are involuntary visual perceptions in the absence of an external stimulus. This perception is considered to arise from widespread miscommunication within neural circuitry, for example, disturbance of input or processing (Adachi, Watanabe, Matsuda, & Onuma, 2000; Anderson & Rizzo, 1994; Behrendt, 2003; ffytche et al., 1998). Dysfunction of part of the network involved in processing visual information has downstream effects on perception and is considered to give rise to the visual hallucinations (ffytche & Howard, 1999). However, underlying mechanisms are yet to be confirmed as there is little evidence from neuroimaging in cases of hallucinations following visual pathway damage. Visual hallucinations can be differentiated into two main categories (Baier et al., 2010; Santhouse, Howard, & ffytche, 2000): simple hallucinations/phosphenes, and complex hallucinations otherwise referred to as Charles Bonnet syndrome. The type of hallucinatory image is related to the site of damage along the visual pathway, and/or the visual processing function of the implicated region(s). Phosphenes consist of unstructured lights—such as flashes and unformed images—and are thought to relate to pathology of the primary visual cortex and optic radiations (Anderson & Rizzo, 1994), but also arise in certain eye diseases (e.g., optic neuritis; Davis, Bergen, Schauf, McDonald, & Deutsch, 1976). Complex visual hallucinations are structured images—such as objects, scenes, people, and animals—and are thought to have underlying pathology in visual associative cortices and temporo-parieto-occipital regions, but can also occur following degenerative eye disease (e.g., glaucoma, age-related macular degeneration) (Manford & Andermann, 1998; Santhouse et al., 2000; Vaphiades,

Celesia, & Brigell, 1996). The type of hallucinatory image seen by an individual can be variable and change over time.

Patients with hallucinations in the absence of hallucinogenic agents (e.g., alcohol, recreational drugs, antipsychotics) or underlying neuropsychiatric disease (e.g., Alzheimer's disease, Parkinson's disease, dementia with Lewy bodies, schizophrenia) are aware that the hallucinations are fictitious. Visual hallucinations associated with vision loss are more prevalent than commonly thought, with the most common occurrence among acute cases. Studies report a prevalence of 10–50% depending on the site of damage (e.g., Baier et al., 2010; Gordon, 2016). In many cases the phenomena dissipate with time (Kölmel, 1985; Manford & Andermann, 1998), but for others the hallucinations persist chronically and may worsen rather than improve over time. Persistent visual hallucinations lasting for more than five years are reported in 75% of patients with Charles Bonnet syndrome; and 32% report adverse outcomes including fear, negative impacts on daily activities, and contribution to the onset of psychological illness such as anxiety and depression (Cox & ffytche, 2014). In persistent hallucinations, the experience of the abnormal percept is both mentally and physically exhausting. For instance, patients have trouble discerning real stimuli from overlapping hallucinatory images despite being fully aware the hallucinatory images are not real. The presence of a hallucinatory image requires constant cognitive effort in continuously trying to ignore the hallucination resulting in exhaustion. In some cases, the hallucinations can be frightening for the individual and commonly include disturbing experiences such as seeing crawling insects or disfigured people. Ultimately, pervasive visual hallucinations lead to further psychological consequences that interfere with quality of life in addition to the vision loss, which in turn results in further social and economic burden (Cox & ffytche, 2014).

In general, reports of hallucinations following visual pathway damage are frequently dismissed by clinicians or simply not reported due to poor understanding of pathogenesis. Patients are often reassured that hallucinations will subside, or it may be incorrectly implied that these perceptions stem from a psychological basis. Patients may also not report the phenomena despite being very aware they are fictitious due to the misconceived associations made with psychological illness, or their own fear of these associations. Attention in vision loss primarily focusses on aetiology, prevention, and treatment, rather than secondary consequences such as visual hallucinations. As such, hallucinations following vision loss are typically deemed less significant due to poor understanding of the phenomenon and its implications, yet they are also an important factor to consider in rehabilitation due to their impact on psychological health.

At present there are no standard pharmacological protocols or alternative therapies to alleviate visual hallucinations subsequent to vision loss. Pharmacological intervention in the absence of neurological or psychological disorders (e.g., schizophrenia, Parkinson's disease) have generally been ineffective long-term and show inconsistency in responsiveness across patients (e.g., Hughes, 2013; Paulig & Mentrup, 2001). However, there is one previous published case study of a patient with Charles Bonnet syndrome following bilateral ischaemic damage to occipital cortex in which a single 30 min application of low-frequency (1 Hz) rTMS was sufficient to cease visual hallucinations for two weeks (Merabet, Kobayashi, Barton, & Pascual-Leone, 2003). Unfortunately, there was no long-term follow-up or neuroimaging measures post-rTMS. Multiday low-frequency rTMS to the temporoparietal cortex is also observed to significantly decrease auditory hallucinations in schizophrenia (Lee et al., 2005; Vercammen, Knegtering, Liemburg, den Boer, & Aleman, 2010). A complex array of processes occur giving rise to hallucinations that will not be consistent among cases depending on underlying disease

processes and site of damage. However, the potential for low-frequency rTMS to modulate hallucinations requires further investigation. It has been suggested that the content of the visual hallucinations likely reflects the functional specialisation of the region(s) involved (ffytche et al., 2008) that can help in identifying stimulation target regions. Regions can be targeted directly with rTMS or indirectly via remote interconnected nodes.

Purpose of the Current Work

In the present work, I begin to develop and refine low-frequency (1 Hz) rTMS protocols applicable to visual-related disorders. To effectively translate this work to therapeutic protocols, I investigate underlying neural mechanisms of 1 Hz rTMS at the stimulation site (visual cortex) as well as local and distal rTMS effects using MRI. The choice of 1 Hz rTMS paradigm is based on work described previously demonstrating that it may have an overall suppressive effect on symptoms and neural activity. The chosen neuromodulation regime was further based on evidence that 1 Hz rTMS to the visual cortex induces dishabituation of electrophysiological responses (visual evoked potentials), whereas 10 Hz (high-frequency) rTMS of comparable pulses has no significant effect (Bohotin et al., 2002; Fumal et al., 2003). Moreover, multiday sessions of 1 Hz rTMS to the visual cortex produce a cumulative effect in dishabituation (Fumal et al., 2006).

A focal point of the research was to develop rTMS treatment for disruptive chronic visual hallucinations, a frequent and dismissed consequence of visual pathway damage. In Chapter 2–3, I begin by investigating the efficacy of 1 Hz rTMS in mitigating these visual hallucinations. As mechanisms of both rTMS to the visual cortex and visual hallucinations in cases of visual pathway damage are still relatively unknown, I address this by investigating functional and structural correlates of visual hallucinations and rTMS effects using task-based fMRI and DTI.

For rTMS paradigms to be effective, it was necessary to not only understand the neural mechanisms of therapy but also the pathophysiology as this provides insight into the pathological mechanisms to target. Investigation of these aspects can provide valuable information in determining the appropriate therapeutic tool, prognosis, as well as longer-term post-treatment efficacy.

A major problem when applying rTMS in clinical populations is that pre-existing abnormalities in function and excitability can alter the responsiveness of the targeted area to rTMS (e.g., Bohotin et al., 2002; Siebner et al., 1999a, 1999b). Inevitable heterogeneity in patient groups due to pathological processes also makes interpretation and generalisability of results more difficult. Because of limited combined MRI and TMS studies of the visual cortex, it was difficult to determine whether the rTMS findings in Chapter 2 were because of aberrant functional and structural processes following visual cortical damage. It became clear that it was crucial to take a step back and begin to investigate rTMS effects using consecutive MRI in healthy control participants to guide development of therapeutic interventions that would be relevant to visual disorders and not just cases of visual hallucinations. Investigating rTMS effects in healthy individuals would determine neural substrates and aid predictability of effects. It was desirable to determine underlying neurochemical mechanisms of rTMS prior to translation to clinical protocols targeted at altering plasticity and to minimise adverse effects. Moreover, typical rTMS effects in controls and deviations from the expected response in clinical populations can provide more information regarding underlying pathophysiology and which mechanisms to target. In Chapter 4, I investigate the potential of 1 Hz rTMS to the visual cortex on altering GABA and glutamate neurotransmitters that are key in plasticity. In addition, in pathophysiology, network communication becomes destabilised from disturbances; therefore, an

effective protocol must sufficiently target networks in the appropriate direction. In Chapter 5, I address this by investigating the effects of rTMS to the visual cortex on global functional connectivity across brain regions. Chapter 5 investigates which nodes, and correspondingly which networks become altered following 1 Hz rTMS to the visual cortex, as well as the magnitude of rTMS effects on network communication.

Further, before rTMS can be considered as a therapeutic tool in visual disorders, it was necessary to refine parameters that would induce sufficiently long plasticity to modify neuronal activity in visual and associated cortices with minimal stimulation application. The current combination of stimulation parameters used in experimental research involving visual cortices would not provide optimal clinical effects due to insufficient aftereffect duration (for a review, see Thut & Pascual-Leone, 2010). Therefore, the effects of prolonged and/or repeated exposures to noninvasive brain stimulation, as well as dose-dependent effects needed to be explored in the visual cortex. Longer-term follow-up of rTMS effects and its potential for adverse effects is also lacking, particularly within the domain of neuroimaging studies. In Chapters 4–5, I additionally address these unknown aspects using two different regimes of 1 Hz rTMS and investigate their differential effects on GABA and glutamate concentrations, global functional connectivity, and their potential for adverse effects to determine the most efficient protocol. Constant stimulation is less than ideal; thus, it was important to develop methodologies of optimal stimulation parameters and performance to transition brain stimulation technologies into operational clinical practice. Ultimately the suitability of 1 Hz rTMS in visual disorders depends on its neurophysiological aftereffects.

In summary, this novel research aims to develop and refine 1 Hz rTMS protocols for widespread clinical use in visual-related disorders that are non-responsive to alternative

treatment modalities or for which there is currently no treatment. Due to the investigation of different 1 Hz rTMS regimes in healthy control participants, this research also advances non-clinical investigations of rTMS to determine function and processes associated with the visual cortex. Overall, this work aims to carry out more detailed studies to better characterise low-frequency rTMS effects on the visual cortex that would inform therapeutic protocols.

CHAPTER 2

MITIGATING VISUAL HALLUCINATIONS ASSOCIATED WITH OCCIPITAL STROKE USING LOW-FREQUENCY REPETITIVE TRANSCRANIAL MAGNETIC STIMULATION[1]

[1]Adapted version published as: Rafique, S. A., Richards, J. R., & Steeves, J. K. E. (2016). *Neurology*, *87*(14), 1493–1500.

Preface

We investigated the efficacy of multiday rTMS to the visual cortex in mitigating chronic and continuous phosphene hallucinations in a patient who suffered occipital stroke. Low-frequency (1 Hz) rTMS was applied to the lesion site for 30 min daily over five consecutive days. fMRI was performed before and after rTMS treatment. Pre-rTMS fMRI revealed focal excitatory discharges at the border of the lesion highlighting the origin of phosphenes, and an imbalance of functional activity across hemispheres. Increased application of rTMS resulted in a cumulative reduction in intensity of phosphene hallucinations that was reflected in altered BOLD signal. rTMS did not simply suppress the disorganised activity at the lesion site in the patient, but rather, it redistributed the previously imbalanced cortical activity at the lesion site and remote regions so that it more closely resembled the balanced functional activity across hemispheres observed in controls. This case is rare in its presentation of continuous visual hallucinations. We provide neuroimaging insight into neural mechanisms of visual hallucinations following occipital injury; and demonstrate that multiday 1 Hz rTMS to the visual cortex provides a valuable therapeutic intervention for mitigating visual hallucinations.

Posterior circulation stroke involving the posterior and middle cerebral arteries accounts for 17–40% of ischaemic strokes (87% of all strokes; Benjamin et al., 2017). Posterior and middle cerebral artery stroke affects cortical regions involving the visual pathway (occipital, temporal, parietal, and frontal cortices; Marinković, Milisavljević, Lolić-Draganić, & Kovacević, 1987). It is estimated that 30–70% of stroke patients have deficits in vision or visual perception (Brandt, Thie, Caplan, & Hacke 1995; Pambakian & Kennard, 1997). Injury to these visual pathway cortical regions following stroke can cause a variety of visual and perceptual deficits including visual agnosia, visual field loss, and achromatopsia (Damasio et al., 1982, 1980; Marinković et al., 1987). In addition, visual hallucinations are frequently reported subsequent to stroke injury to the occipital cortex, and are attributed with the more frequent consequence of hemianopia (Anderson & Rizzo, 1994; De Haan, Nys, van Zandvoort, & Ramsey, 2007; Kishi, Ishino, & Naganuma, 1998; Kölmel, 1985; Lance, 1976; Vaphiades et al., 1996). Visual hallucinations following stroke are frequently localised to the affected part of the visual field (Kölmel, 1985; Manford, & Andermann, 1998). Visual field defects in themselves have significant implications on functional prognosis of daily activities such as driving, reading, and navigating within an environment. The presence of abnormal visual experiences in addition to the visual field loss causes further psychological distress (Cox & ffytche, 2014; De Haan et al., 2007). Depending on the location and severity of the occipital stroke lesion, many patients demonstrate partial functional recovery over time. Prognosis is worse with primary visual cortex (V1) involvement and greater extent of damage (Çelebisoy, Çelebisoy, Bayam, & Köse, 2010; Tiel And & Kölmel, 1991). Recovery in visual field loss following stroke is dependent on the return of V1 activity and is unlikely beyond 3–6 months (Ajina & Kennard, 2012; Sabel, 1997; Zhang, Kedar, Lynn, Newman, & Biousse, 2006). While much focus is paid to stroke prevention

and treatment/rehabilitation of motor, speech, and visual field deficits, little work has been done to alleviate visual hallucinations despite historical reports in patients with occipital lobe stroke (De Haan et al., 2007).

Typically following stroke, the interhemispheric balance of neural activity becomes modified between ipsilesional and contralesional hemispheres that normalise over time. Hyperexcitability is observed in the contralesional hemisphere as result of decreased interhemispheric inhibition and hypoexcitability is observed in the lesioned hemisphere (Liepert et al., 2000a). Interhemispheric inhibition induces diaschisis following stroke in brain areas that are spatially distinct but functionally related to the stroke site (Feeney & Baron, 1986). This process is correlated with functional progress and reflects brain plasticity induced by spontaneous recovery and rehabilitation (Traversa et al., 2000). Neurons with absolute damage from stroke are not salvageable, but those affected as a result of diaschisis remain viable (Cassidy et al., 2014). With greater alteration in interhemispheric inhibition after stroke, the prognosis for recovery is poorer (Murase et al., 2004). TMS has been popularly applied to promote motor recovery in stroke and is shown to disinhibit interhemispheric transcallosal interactions that are essential for rehabilitation (Bäumer et al., 2006; Meyer, Röricht, Von Einsiedel, Kruggel, & Weindl, 1995). Therefore, TMS may also have valuable application to visual deficits subsequent to stroke.

Occipital lesions from stroke causing hemianopia with visual hallucinations are significantly smaller than those that cause hemianopia without hallucinations, suggesting that involved regions with intact visual processing are required to yield hallucinations (Manford & Andermann, 1998). However, visual hallucinations do not only occur following stroke but are frequently observed in other causes of vision loss (retinal, subcortical, or cortical damage), e.g.,

age-related macular degeneration, and optic neuropathy (Baier et al., 2010; Gordon, 2016). Several theories are posited as to why visual hallucinations occur following visual pathway damage. In short, (1) the “irritative” process is described as spontaneous excitatory discharges at the border of the ischaemic area, or an imbalance of resting potentials within the lesion that stimulate neighbouring associative cortical areas, which are falsely interpreted as sensory input (Cogan, 1973; Seguin, 1886). (2) The “perceptual release” phenomenon is described as the withdrawal of inhibition within the lesioned area that normally inhibits irrelevant impulses from conscious perception. The interference of normal inhibitory circuitry results in abnormal cortical excitation and processing. Disinhibition of previously subconscious perceptions or memories is consequently viewed as visual hallucinations (Cogan, 1973; Manford & Andermann, 1998; Santhouse et al., 2000). (3) The “deafferentation” theory argues that surviving neurons within the lesion continue to receive input from intact cortical visual areas and remaining visual processing capacity is expressed as hallucinations. Hallucinatory phenomena arise from pathological feedback of neuronal clusters in regions bordering the lesion that presumably contain records of “visual feature fragments” (Anderson & Rizzo, 1994; Manford & Andermann, 1998). However, there is little evidence from neuroimaging studies to confirm that these neural mechanisms underlie visual hallucinations in visual pathway damage. In addition, mechanisms that differentiate acute and chronic visual hallucinations have not been investigated. Visual hallucinations in the absence of dementia, delusions, or confusion, e.g., dementia with Lewy bodies, schizophrenia, Parkinson’s disease (Aarsland et al., 2009; Oishi et al., 2005; Yoon et al., 2010), provide isolated evidence for underlying neural substrates and cognitive mechanisms. fMRI can reveal injury-induced neural processes and plasticity within localised and remote regions principal to visual hallucinations in order to ascertain treatment modalities.

We describe the case of a 31-year-old patient presenting with continuous and disruptive phosphene hallucinations within an incomplete left homonymous hemianopia following right occipital stroke that remained unchanged for over two years. Although visual hallucinations can occur long-term in large number of patients with visual pathway damage (Cox & ffytche, 2014), the experience is intermittent, and cases of continuous hallucinations are extremely rare. The patient was treated with rTMS to the visual cortex for 30 min daily over five consecutive days. We demonstrate that rTMS can be successfully applied to mitigate these abnormal percepts following occipital lobe damage. Combining rTMS with fMRI, we assess the underlying neural correlates of hallucinations secondary to occipital injury, as well as rTMS-modulated alterations in functional activity. We performed fMRI on an age-matched healthy controls to enable statistical comparison of the patient to a neurologically intact group. This study presents the first case of multiday rTMS to the visual cortex to mitigate visual hallucinations subsequent to visual pathway damage.

Methods

This study was approved by York University's Office of Research Ethics. All individuals gave informed written consent.

Participants

Patient. We evaluated a 31-year-old female experiencing continuous phosphene hallucinations within an incomplete congruous left homonymous hemianopia for 2.5 years after the onset of right subacute occipital lobe stroke. Symptoms initially began as a severe right occipital headache followed by an incomplete left homonymous hemianopia (Figure 2.1a). Her visual deficit initially appeared as a dark grey scotoma with irregular borders and within two hours evolved into phosphene hallucinations. Her past medical history was notable only for

migraine headache with visual aura since age 18 years occurring 1–2 times per week. MRI revealed a right subacute ischaemic occipital lobe stroke within the calcarine artery distribution (Figure 2.1b) and a benign subarachnoid cyst. Possible vasospasm of the calcarine artery was noted on computed tomography (CT) angiogram performed immediately after MRI. Other initial investigations included an echocardiogram with bubble study that revealed a patent foramen ovale. Electroencephalogram (EEG) recordings were normal, ruling out epileptiform excitatory activity as a cause of the hallucinations. After two weeks, her headache resolved but the phosphene hallucinations remained unchanged and were present all times of the day and night. Several pharmacological approaches were attempted during this period to eliminate or suppress the phosphene hallucinations. Initially, intravenous (IV) infusion of magnesium sulfate was administered and had no effect. Subsequent trials of IV diazepam (Valium®), IV phenobarbital (Luminal®), and IV levetiracetam (Keppra®) were also ineffective. Oral levetiracetam was taken for one week without effect. Oral topiramate (Topamax®) was then attempted but also failed to mitigate the phosphene hallucinations. She was then started on daily aspirin for future stroke prevention and verapamil for migraine prophylaxis. Her patent foramen ovale was closed endovascularly with an Amplatzer™ septal occluder. Visual field rehabilitation was attempted next over a period of six months with Vision Restoration Therapy (NovaVision, Boca Raton, Florida) and had no significant improvement in visual field loss nor the perception of phosphene hallucinations. Lastly, noninvasive brain stimulation in the form of tDCS was attempted with no noticeable effect. Over the next two years, the phosphene hallucinations persisted, but with a slight overall decrease in intensity. The phosphene hallucinations were described as moving white/grey vibrating images of shattered glass and small–medium circular lights within the scotoma. Occasional high-frequency lightning bolts and irregular zigzag shapes were perceived

migrating inferolateral within the scotoma into the normal visual field. Phosphenes were more intense at the relative (incomplete damage) field defect, accompanied with macropsia and general distortion. The hallucinations were perceived at all times; however, intensity increased with stress, lack of sleep or increasing light intensity, and intensity decreased in the dark or with eyes closed. The patient found the constant need to differentiate real percepts and phosphene hallucinations confusing and exhausting despite full awareness the hallucinations were not real. The hallucinations were debilitating, interfering with sleep, vision, and quality of life. At the time of our investigation, the calcarine artery vasospasm and occipital ischaemia had resolved. The patient had normal foveal vision (> 0.2 logMAR; stereoacuity ≥ 50”; previous Lasik refractive surgery) and all other ophthalmic findings were unremarkable. The patient was right-handed and there were no known contraindications to MRI and TMS.

Healthy controls. Eight healthy female controls ($M_{age} \pm SEM = 29 \pm 0.79$ years) were recruited with no history of neurological disorders and no known contraindications to MRI. All controls were right-handed, had normal or corrected-to-normal vision (> 0.2 logMAR; stereoacuity ≥ 50”) and otherwise normal visual assessment findings.

Vision Assessments

Standard clinical vision testing was performed to ensure otherwise normal visual status in the patient and controls. Monocular and binocular visual acuity and contrast sensitivity were measured using the standardised early treatment diabetic retinopathy study (ETDRS) vision chart (Precision Vision, La Salle, IL). Stereoacuity was measured using the Titmus circles test (Stereo Optical Company Inc., Chicago, IL), and colour vision was assessed using the Ishihara test (Kanehara Trading Inc., Tokyo, Japan). Ocular muscle status involved assessment with the cover test (distance and near), near point of convergence, and ocular motility. Visual field perimetry

was performed using the Octopus 900 (Haag-Streit, Mason, OH). Vision testing was repeated in the patient following cessation of rTMS to determine any adverse effects on basic visual status.

Experimental Design Overview

The patient underwent the following: (1) pre-rTMS (baseline) clinical vision testing and MRI, (2) sham and vertex rTMS, (3) five consecutive days of rTMS, and (4) post-rTMS MRI and vision testing. Healthy controls underwent (1) only.

Magnetic Resonance Imaging

Stimuli and procedure. We performed two fMRI experiments. The patient self-reported increases in phosphene hallucinations with increasing brightness of visual input and a corresponding decrease in phosphene hallucinations under reduced or dark visual environments. Based on these reports, a phosphene localiser was used to delineate cortical and subcortical origins of the hallucinations. The phosphene localiser consisted of five full screen 30 s blocks of a bright white stimulus interleaved with five full screen 30 s blocks of black stimulus, with a continuous central fixation (Figure 2.2a). A grey screen with central fixation appeared for 30 s at the start and finish of the run. Each run lasted 6 min and was repeated twice. During the phosphene localiser, the patient was asked to indicate a change in intensity (increase or decrease) of perceived phosphene hallucinations using a MRI compatible response button box. Control participants were also given the same button response instructions when undergoing the phosphene localiser to minimise cognitive differences, although visual hallucinations were not expected. The phosphene localiser was performed first in the patient to prevent any confounding manipulations in phosphene hallucinations from viewing previous experimental visual stimuli and to ensure maximal effect. For consistency, the phosphene localiser was also performed first in control participants.

Since the lesion was located in the occipital cortex (involving the parahippocampal and lingual gyri, cuneus, and sub-lobar regions), we expected network changes in visual processing regions connected to the lesion site and peri-infarct regions. Much of this network contributes to the processing of specialised visual stimuli, mainly faces, scenes, and objects, that are also implicated in complex visual hallucinations (ffytche et al., 1998). A face-scene-object localiser was therefore performed to delineate regions involved in processing these visual stimuli, and to measure alterations in activity induced by the lesion and/or with rTMS in the patient. The face-scene-object localiser consisted of three different blocks (Figure 2.2b), each with sixteen images: (1) faces (males and females of different ethnicities), (2) scenes (natural and non-natural scenes), (3) objects (natural and man-made). Digitised colour images of objects were obtained from a bank of standardised stimuli (Brodeur, Dionne-Dostie, Montreuil, & Lepage, 2010), and coloured images of faces and scenes were obtained from a compact disc photo image library. Epochs containing three blocks of the three categories of stimuli were repeated 6 times in a counterbalanced order to minimise first-order carry over effects. Each image was presented for 900 ms with a 100 ms inter-stimulus interval, and images were presented without repetition. A central fixation cross appeared for 16 s at the start and finish of the run and between epochs. Each run lasted 6 min 52 s and was repeated twice.

Localisers were performed prior to and immediately after rTMS treatment ceased in the patient to assess stimulation-induced changes. Control participants underwent both localisers to enable comparison that would highlight deviations of functional activity in the patient, and hence determine contributions to the perception of hallucinations. Stimuli were viewed in a dark room.

Apparatus. Stimuli were presented with VPixx software (VPixx Technologies Inc., Montreal, QC, Canada; www.vpixx.com). Images were viewed on a screen (resolution: 1024 x

768) ~40 cm from the participant's eyes via a rear-projector system of the same resolution (Avotec SV6011; Avotec Inc., Stuart, FL, USA) while in the scanner. Refractive errors were corrected where necessary during acquisition using fMRI compatible goggles.

Image acquisition. Functional and anatomical images were acquired with a 3 Tesla (3T) Siemens Magnetom® Tim Trio magnetic resonance scanner (Siemens, Erlanger, Germany) using BOLD fMRI imaging. Head motion was minimised with the placement of soft pads holding the participant's head in place. Functional volumes were acquired using a Siemens 32-channel high-resolution brain array coil and echo-planar imaging with a T1-weighted sequence (number of contiguous axial slices = 32; in-plane resolution = 2.5 x 2.5 mm; slice thickness = 3 mm; imaging matrix = 96 x 96; repetition time (TR) = 2000 ms; echo time (TE) = 30 ms; flip angle = 90°; field of view (FoV) = 240 mm). Anatomical images were acquired after functional scans with a T1 magnetisation-prepared rapid gradient echo (MPRAGE) imaging sequence (number of slices = 192; in-plane resolution = 1 x 1 mm; slice thickness = 1 mm; imaging matrix = 256 x 256; TR = 1900 ms; TE = 2.5 ms; TI = 900 ms; flip angle = 9°; FoV = 256 mm).

Repetitive Transcranial Magnetic Stimulation

Only the patient underwent rTMS treatment. The demarcation between the absolute (complete) and relative (incomplete) visual field defect (Figure 2.1a) is a functional representation of intact or partially intact neurons with residual recovery of function. This suggested disorganised activity from surviving or partially damaged neurons within or around the lesion and was confirmed from the restricted disorganisation of hyperexcitability at the lesion border evident from fMRI analysis compared with controls. Therefore, we chose the lesion as the target site for rTMS in order to reach the partially damaged neurons considered responsible for the perception of visual hallucinations. The lesion was mapped onto the patient's anatomical MR

images that were reconstructed to 3D cortical surfaces in Brainsight software (Rogue Research, Montreal, QC, Canada). Reference points were mapped onto the patient's head (tip of nose, nasion, right and left tragus) using infrared tracking balls. The spatial relationship between reference points from the lesion site (MR images) and those on the patient's head were co-registered using a Polaris infrared tracking system (Northern Digital Instruments, Kitchener, ON, Canada) to enable targeted rTMS to the disorganised activity at the border of the lesion. The image-guided stereotaxic system enables accurate coil position over the target stimulation site and tracking of the coil with respect to the patient's head during stimulation that can be continuously monitored and corrected in real time.

A Magstim Rapid^2 Stimulator and a 70 mm diameter figure-of-eight coil (Magstim, Whitland, Wales, UK) were used to deliver the stimulation pulses to the targeted stimulation site. The figure-of-eight coil provides more focal stimulation and allows detailed mapping of cortical representation (Kobayashi & Pascual-Leone, 2003). The patient was seated in a comfortable position with an adjustable chin rest to limit head movement and provided with earplugs to prevent changes in auditory thresholds during rTMS (Rossi et al., 2009). The TMS coil was held tangential to the surface of the skull to minimise coil-to-cortex distance, and to maximise the TMS effect (Ulmer & Jansen, 2010). A low-frequency pulse (1 Hz) was delivered at 85% of maximum stimulator output (110% visible twitch MT; Bohotin et al., 2002; Pridmore et al., 1998) for 30 min (1800 pulses) at rest. Due to the continuous and variable perception of phosphene hallucinations, MT instead of PT was chosen. We chose a low-frequency rTMS protocol since is typically considered to be suppressive (for a review, see Hallet, 2007) in an attempt to reduce disorganised activity. Prior to stimulation of the target site, two separate placebo control conditions were performed in a single day: rTMS to vertex and sham rTMS (coil

held orthogonal to the skull and no pulses enter the brain), during which the patient reported no effect on hallucinations. rTMS treatment was then performed daily over five consecutive days to the target stimulation site at the posterior tip of the lesion (Talairach coordinates: x = 14, y = -75, z = 9; ~14 mm deep), which was within TMS penetration limits of the figure-of-eight coil (1–2 cm; Zangen et al., 2005).

A subjective log of rTMS effects on intensity of phosphene hallucinations was recorded during and after vertex and sham rTMS, and for each active rTMS session. We recorded the length of time the effects persisted and any changes in perception throughout the day. Subjective changes were reported as a percentage decrease in the self-reported average baseline intensity of phosphene hallucinations that were perceived prior to beginning rTMS treatment. The patient reported this daily average baseline intensity to be 70% (relative to worst intensity previously experienced).

Data Analyses

MRI analyses were performed using BrainVoyager QX (v2.8; Brain Innovation, Maastricht, The Netherlands).

Preprocessing. Functional data underwent a series of preprocessing steps to minimise noise in the data, including temporal high-pass filtering to remove temporal frequencies (lower than 3 cycles/run), and linear trend removal to exclude scanner-related signal drift. The 3D motion correction algorithm using linear and sinc interpolation was applied to evaluate and correct small inter-scan head movements. Outputs from the motion correction algorithm were assessed to ensure motion did not exceed the recommended 1–2 voxels (Huettal, Song, & McCarthy, 2004). Functional data were not subjected to spatial smoothing. Undesirable effects of smoothing include shifting of activation and merging of adjacent peaks of activation (Mikl et

al., 2008). The precise localisation of activation and any shifts in location were important to the study because of changes with rTMS. Each participant's functional images were analysed using a multiple regression general linear model (GLM) in order to determine the magnitude of activity in each scan. Z-transformation was applied to normalise time courses. All brains were skull-stripped and standardised with Talairach standard space transformation (Talairach & Tournoux, 1988). Functional images were then co-registered with their anatomical images.

Phosphene localiser. A whole-brain fixed effects analysis was performed using a linear balanced contrast (white < > black stimuli), cluster threshold of 6 voxels, false discovery rate (FDR) multiple comparison corrected single-voxel threshold of $q < .05$, to compare: (1) patient (pre- and post-rTMS, separately) and control activation for white and black event predictors. Further, subtraction analysis (beta-difference maps) was performed for the following comparisons (2) patient's pre- versus post-rTMS phosphene localiser activity, (3) patient (pre- and post-rTMS, separately) versus control phosphene localiser activity. Subtraction of maps was performed for white and black event predictors independently for voxels above selected beta thresholds of $b > 0.5$, where beta values quantify the level of cortical activity.

The patient's subjective button responses (indicating an increase or decrease in perception of phosphene hallucinations) were compared with event (white and black stimuli) predictors to assess any differences between subjective and neuronal processes. A reported intensity increase in phosphene hallucinations during the localiser corresponded with the onset of white stimuli, while a decrease in phosphene hallucinations intensity corresponded with the onset of black stimuli (i.e., no significant differences between comparisons). No button responses were pressed by control participants. Therefore, only event predictor activity was used to compare patient and control data. This ensured more comparable perceptual or cognitive processes across

individuals, and that a perceptual delay in the patient while discerning an increase/decrease in hallucinations for button responses did not result in added confounds between comparisons.

Face-scene-object localiser. A priori regions known to be involved in the processing of faces, scenes, and objects were defined in all individuals independently. The a priori face preferential regions included the fusiform and occipital face areas. The scene preferential regions included the transverse occipital sulcus (also known as the occipital place area), parahippocampal place area, and lingual gyrus. The object preferential region involved the lateral occipital area. A priori regions were defined using a linear balanced contrast and were identified by determining the peak selective activation for the region in question, using a cluster threshold of 6, and FDR corrected single-voxel threshold of $q < .05$. The scene preferential regions were defined as the set of voxels in the transverse occipital sulcus and collateral sulcus/posterior parahippocampal gyrus that responded more strongly to scenes than to objects and faces (contrast: scenes > objects + faces). The lingual gyrus also showed preferential activation to scenes and was defined as the region between the calcarine sulcus and the posterior part of the collateral sulcus in the visual cortex using the same contrast (scenes > objects + faces). The object preferential lateral occipital area was defined as the region of lateral/dorsal occipitotemporal cortex that responded more strongly to objects than to faces and scenes (contrast: objects > scenes + faces). The face preferential regions were defined as regions maximally responsive to faces compared to objects and scenes in the fusiform gyrus (fusiform face area) and inferior occipital gyrus (occipital face area) (contrasts: faces > scenes + objects). Locations were consistent with those identified previously (Ewbank, Schluppeck, & Andrews, 2005; Grill-Spector et al., 1999). Activity within a priori regions was quantified from the event-related time course as beta-weights. We used the modified *t*-test (two-tailed tests) developed for

single-case studies (Crawford & Garthwaite, 2002; Crawford, Garthwaite, Azzalini, Howell, & Laws, 2006) to compare the patient's level of functional activation to controls. We report significant differences at $p < .05$, and results trending significance are reported at $p < .1$.

Results

Subjective Perception of Phosphene Hallucinations and Visual Testing

The patient reported a gradual reduction in phosphene hallucinations with increased application of rTMS. Effects summated with increased time of rTMS application during each session. With each new day of rTMS treatment, hallucinations were mitigated faster and effects continued to summate and last longer. As a result, with each new day, the patient also reported an overall improvement in well-being described as being less mentally and physically exhausted. Effects of rTMS were maintained for a few days after discontinuation of stimulation with a gradual linear return to baseline intensity by 1-week (Figure 2.3). The perception of phosphene hallucinations did not completely cease during the treatment, however, they were reduced to less than 15% subjective intensity (Figure 2.3). In addition, the patient reported minimal distortion and macropsia after rTMS treatment, however, this reduction was not quantified. There was no change in visual status measured using clinical vision testing during or after rTMS cessation, and no adverse effects of rTMS were reported.

Phosphene Localiser

The anatomical regions with significant differences in activation between bright (white > black stimuli) and dark (black > white stimuli) viewing conditions for the patient (pre- and post-rTMS) and controls are detailed in Tables 2.1–2.2, respectively.

Figure 2.4 highlights the most notable difference in patterns of functional cortical activity at the lingual gyrus and cuneus, not only between the patient and controls, but a remarkable

difference is seen between the patient pre- and post-rTMS. Pre-rTMS, a greater concentration of diffuse activity is observed in the contralesional hemisphere at the lingual gyrus and cuneus, while ipsilesional activity was focal to the calcarine sulcus and anterior to the lesion in the patient in both bright (white > black stimuli) and dark (black > white stimuli) viewing conditions. Post-rTMS cortical activity appeared balanced across hemispheres resembling that of controls. Unlike the patient, controls did not show greater activation at the lingual gyrus in dark viewing conditions (Table 2.2).

Subtraction analysis of the phosphene localiser providing beta-difference maps for the patient pre-rTMS and controls, and for the patient post-rTMS and controls are shown in Tables 2.3–2.4, respectively. Beta-difference maps for the patient pre- and post-rTMS showed greater activation pre-rTMS in the left superior frontal gyrus (Brodmann area 9; Talairach coordinates: x = -24, y = 57, z = 28) and greater activation post-rTMS in the left lingual gyrus (Brodmann area 17, Talairach coordinates: x = -7, y = -93, z = -7).

Face-Scene-Object Localiser

Results of the a priori analysis and significant differences between the patient and controls (using modified *t*-tests) are shown in Figure 2.5. Differences are observed in processing resources allocated within regions for preferential and non-preferential task-specific processing between the patient and controls. Compared with controls, pre-rTMS, the patient displayed greater selectivity to scenes (and minimal object and face processing) in the left scene preferential region transverse occipital sulcus, but reduced scene selectivity (i.e., greater non-preferential processing) in the right transverse occipital sulcus and right lingual gyrus. Within the left lateral occipital area, typically an object preferential region, the patient showed greater non-preferential processing of faces and reduced non-preferential processing of scenes pre-rTMS

compared with controls. Greater face selectivity (and minimal object and scene processing) was observed in the bilateral face preferential occipital face area pre-rTMS compared with controls.

Post-rTMS, in some cases, there was redistribution of activity in preferential and non-preferential processing towards a similar level of activation to that of controls. For example, post-rTMS in the left parahippocampal place area, the patient showed reduced selectivity to faces and scenes, and increased selectivity to objects, similar to control selectivity. However, post-rTMS in the right parahippocampal place area, the patient showed reduced face, object, and scene selectivity (as opposed to increased selectivity pre-rTMS) compared with controls.

Discussion

Using low-frequency (1 Hz) rTMS, we greatly reduced the perception of continuous phosphene hallucinations following occipital stroke in our patient who had been unresponsive to alternative therapies (e.g., tDCS, pharmacological approaches). These rTMS effects summated daily and outlasted stimulation. rTMS did not simply reduce activity in regions with previously disorganised functional activity contributing to the perception of phosphene hallucinations, but rather, it redistributed imbalanced activity throughout the brain to a level similar to that of controls. The reorganisation of imbalanced functional activity presumably occurs through disinhibition of intra- and interhemispheric interactions via rTMS mechanisms.

Regions Associated with Visual Hallucinations

Several differences in functional activity were observed between the patient pre-rTMS and controls (Tables 2.1–2.3; Figure 2.4) that implicate these regions in the patient's perception of phosphene hallucinations. MRI studies in occipital ischaemic stroke with phosphene hallucinations demonstrate a common involvement of visual association areas, e.g., lingual gyrus and cuneus (Baier et al., 2010; Missimer, Seitz, & Kleiser, 2010; Vaphiades et al., 1996), as in

our patient. Electrical stimulation to V1, the calcarine fissure, and the visual association Brodmann area 18 induces the perception of phosphenes (Foerester, 1931; Lance, 1976), which further supports the involvement of these regions in the genesis of phosphene hallucinations. Whereas, stimulation of Brodmann area 19 instead induces complex organised images (Foerester, 1931; Lance, 1976).

The patient showed greater activation in regions of the middle occipital gyrus in both bright and dark viewing conditions pre-rTMS, and only in bright viewing conditions post-rTMS. Conversely, controls showed greater activation at the middle occipital gyrus under darker viewing conditions (Tables 2.1–2.2). The middle occipital gyrus is involved in shape analysis operations (Gauthier, Tarr, Anderson, Skudlarski, & Gore, 1999; Sergent, Ohta, & MacDonald, 1992). Differences between the patient and controls in the middle occipital gyrus may therefore be attributed to the perceptual processing of phosphene hallucinations consisting of unformed shapes. In addition, differences of activation were observed in the middle temporal gyrus between the patient pre-rTMS and controls (Tables 2.1–2.2). A possible theory that has been put forward to explain visual hallucinations is that areas involved in memory retrieval (including category-specific visual areas) may release percepts from memory when sensory impulses that are excluded from consciousness are no longer inhibited following damage (Lance, 1976; Weinberger & Grant, 1940). Both the middle occipital and middle temporal gyri demonstrate involvement in object memory (Yonelinas, Hopfinger, Buonocore, Kroll, & Baynes, 2001), and their involvement may contribute to the validity of this theory. Consistent with the notion that inappropriate functional recruitment of these regions may contribute to the perception of visual hallucinations, lesions in the middle temporal gyrus instead produce the extreme opposite and

cause visual agnosia (Chao, Haxby, & Martin, 1999; Gross, 1994; Puce, Allison, Asgari, Gore, & McCarthy, 1996).

Only the patient showed activation in the anterior vermis of the cerebellum (pre-rTMS only; Table 2.1). The anterior vermis is frequently reported in studies of visual and even auditory hallucinations (Caparelli et al., 2010; Kenny, Blamire, Firbank, & O'Brien, 2012; van Lutterveld, Diederen, Koops, Begemann, & Sommer, 2013). While the precise function of the anterior vermis remains unknown, the cerebellum plays a significant role in mental imagery (Grealy & Lee, 2011). Greater vivid imagery and a weak ability to distinguish real perception from mental imagery has been linked to hallucinations (Mintz & Alpert, 1972). The cerebellum also shows connectivity to the dorsal visual stream, visual cortices, and is involved in visual attention to moving stimuli (Kellermann et al., 2012). Further, the cerebellum, together with extensive cortical networks, yields higher activation when receiving incongruent sensory information presumably to cope with increasing cortical computational demands (Shih et al., 2009). Therefore, the functional recruitment of the cerebellum in the absence of task-specific engagement is also consistent with the irregular afferent sensory input of moving and consistently changing perception of phosphenes in the patient.

The claustrum regulates communication across the brain via cholinergic mechanisms. Acetylcholine is concentrated in both visual thalamic and visual cortex regions (Fitzpatrick, Diamond, & Raczkowski, 1989; Smith, Pare, Deschenes, Parent, & Steriade, 1988). Cholinergic input inhibits GABAergic inhibitory input from the reticular nucleus (Wilson, 1993). Release of visual association cortex with loss of cortico-cortical inputs after stroke (Jones & Powell, 1970) alters cortical activity via the reticular activating system by decreasing cholinergic input that is linked to hallucinations (Manford & Andermann, 1998). The involvement of the claustrum in the

patient pre-rTMS (Table 2.3) is consistent with evidence of its involvement in visual hallucinations.

The face-scene-object localiser enables assessment of category-specific visual processing regions connected to the lesion and peri-infarct regions. In the patient, prior to rTMS, a redistribution of category-specific responses was observed from the impaired attenuation of non-preferential processing within these regions. Analysis following rTMS revealed reconfiguration of preferential and non-preferential selectivity of regions to some level matching that of controls. The a priori regions investigated in this study (e.g., lingual, parahippocampal, and fusiform gyri) are key structures for object representation in the ventral stream of visual information processing (Haxby et al., 2001; Kanwisher, 2000). Damage to these regions leads to the disruption in normal flow of shape and contour information processing and results in visual form agnosia (Karnath, Rüter, Mandler, & Himmelbach, 2009). Conversely, hyperexcitability or imbalanced activity of these regions, as in the present study, has been linked to the onset of visual hallucinations (ffytche et al., 1998). Although controls did not undergo rTMS in this study, our previous studies show no change to stimulus category selectivity in the same regions following rTMS to the visual cortex in healthy controls (Mullin & Steeves, 2013; Rafique et al., 2015).

Mechanisms of Visual Hallucinations

The regions discussed may be directly involved in the origin of hallucinations (the cause) or are connected to the primary origin through direct or indirect connections. Alternatively, the regions might be recruited as a function-specific response to the continuous perception or subjective interpretation of recurrent phosphene hallucinations (the effect). The occurrence of hallucinations with a visual field defect implies that the visual association cortex is more likely to discharge spontaneously once deprived of normal afferent inflow from the calcarine cortex or

once its afferent connections with V1 are severed (Lance, 1976). Moreover, given that the phosphenes were mainly constrained to the area of visual field loss in our patient, in line with retinotopic organisation, this suggests that the primary origin of hallucinations arises close to the lesion site. The concept of spontaneous discharge of neuronal circuits in ischaemic regions is attractive in this patient since hallucinations were reported to continue (less distinctly) in dark viewing conditions or with eyes closed, and therefore were not triggered by external visual stimuli. When the majority of the calcarine fissure is intact, suggesting V1 and visual association area V2 are mostly intact, pathways between preserved portions provide a means for continued relay of signals (Kölmel, 1984). Partially damaged neurons retain the ability to process but relay dysfunctional signals to nearby lesioned or intact regions (Kasten, Wüst, Behrens-Baumann, & Sabel, 1998). Alternatively, neural signals that cannot be relayed beyond lesioned borders may result in a build-up of signal (excitatory discharges), and an overall disruption in flow of communication. Relatively consistent activation at the posterior rim of a lesion, as observed in this case, is observed in other non-visual cortical regions following stroke damage (Rijntjes et al., 1994), and this activation poses a popular theory for neural mechanisms of hallucinations (Anderson & Rizzo, 1994; De Haan et al., 2007). Neural systems surrounding the lesion that receive input from the now lesioned area will have altered activity and deficiencies in modulating activity through feedback connections (Braun, Dumont, Duval, Hamel-Hébert, & Godbout, 2003; Manford & Andermann, 1998).

Changes in Functional Activity with Repetitive Transcranial Magnetic Stimulation

Following five consecutive days of rTMS application to the visual cortex in the patient, some rebalance of previously aberrant functional activation was observed inter- and intrahemispherically post-rTMS (Figures 2.4–2.5). This included deactivation of regions

observed in the patient pre-rTMS that were not observed in controls, or conversely activation of regions that were observed in controls but not in the patient pre-rTMS (Tables 2.1–2.4). Thus, post-rTMS activation in the patient became similar to neural processes in controls within these regions. The redistribution of activation across the brain with rTMS demonstrates that rTMS was not restricted in its effects to the targeted region in the occipital lobe, but rather, it led to a more global redistribution of activity in remotely interconnected regions. Nonetheless, the patient continued to demonstrate some differences post-rTMS compared with controls (Table 2.4). The ipsilesional lingual gyrus continued to demonstrate greater activation at the posterior border of the lesion post-TMS compared with controls. This residual activity, particularly at the border of the lesion, demonstrates persistent neuronal firing, which corresponds to the continued, yet greatly reduced, perception of phosphene hallucinations after rTMS treatment. Notably, we did not observe a typical response to 1 Hz rTMS in the patient, in that we do not see the typical "inhibition" of activity at the stimulation site following low-frequency rTMS as is observed in healthy controls (Caparelli et al., 2010; Rafique et al., 2015). In the deafferented cortex, there is an increase of membrane resistance that can cause excitability of involved regions (Prince & Tseng, 1993), therefore, reducing the susceptibility to inhibition. It is likely that remote stimulation effects and restoration to normal function were limited due to impaired inhibitory mechanisms in the patient. Underlying mechanisms of rTMS remain largely unknown, and effects are less predictable in pathophysiology (e.g., Siebner et al., 1999a, 199b). Despite the absence of predicted suppression in functional activity at the target stimulation site, 1 Hz rTMS instead, to an extent, normalised the previous aberrant activity that had suppressive effects on the patient's symptoms.

Limitations

In order to overcome limitations of a single-case study, future work requires a larger patient sample size, refinement of rTMS parameters, and further neuroimaging to probe a variety of neural mechanisms (e.g., rsfMRI, MRS). It is our experience during patient recruitment that complex hallucinations following visual pathway damage (i.e., Charles Bonnet syndrome) are more common. Charles Bonnet syndrome more frequently occurs following age-related retinal disease (e.g., age-related macular degeneration, glaucoma, diabetic retinopathy). A frequent problem we encountered with these patients due to age-related consequences is that they co-occur with underlying systemic or psychological conditions that present contraindications to TMS or MRI (e.g., pace makers, drug interactions; Najib & Horvarth, 2014). As the effects of chronic low-frequency rTMS on the visual cortex are still relatively unknown, we cannot predict adverse effects in patients taking medications such as those altering seizure-thresholds. We were correct to exert caution as we saw an increase in neural activity at the rTMS target site with an "inhibitory" 1 Hz protocol. Unfortunately, due to our limited time with this patient, we were unable to further refine stimulation parameters (e.g., intensity and duration) in order to achieve maximal phosphene suppression. Our future work will refine these stimulation parameters.

Conclusion

This study provides the first report of therapy-induced multiday rTMS to the visual cortex to mitigate abnormal visual percepts following cortical injury. We demonstrate that a therapeutic intervention with 1 Hz rTMS interferes with abnormal cortical and subcortical activity that give rise to visual hallucinations. rTMS alters deficient functional activity at the stimulation site and remote nodes of interconnected networks to greatly reduce the perception of hallucinations. These effects were maintained and outlasted the stimulation itself. A number of

neurodegenerative conditions present with secondary visual hallucinations, e.g., Parkinson's disease (Manford & Anderson, 1998), schizophrenia (Yoon et al., 2010), and Alzheimer's disease (Palop & Mucke, 2010), as well as degenerative eye disease leading to Charles Bonnet syndrome (Burke, 2002; ffytche et al., 1998). These conditions share analogous mechanisms of dysfunction involving mutually implicated neurotransmitters and brain regions, and interhemispheric imbalance of neural activity. Neuromodulation with rTMS could provide a valuable tool for effective treatment of visual hallucinations in these populations.

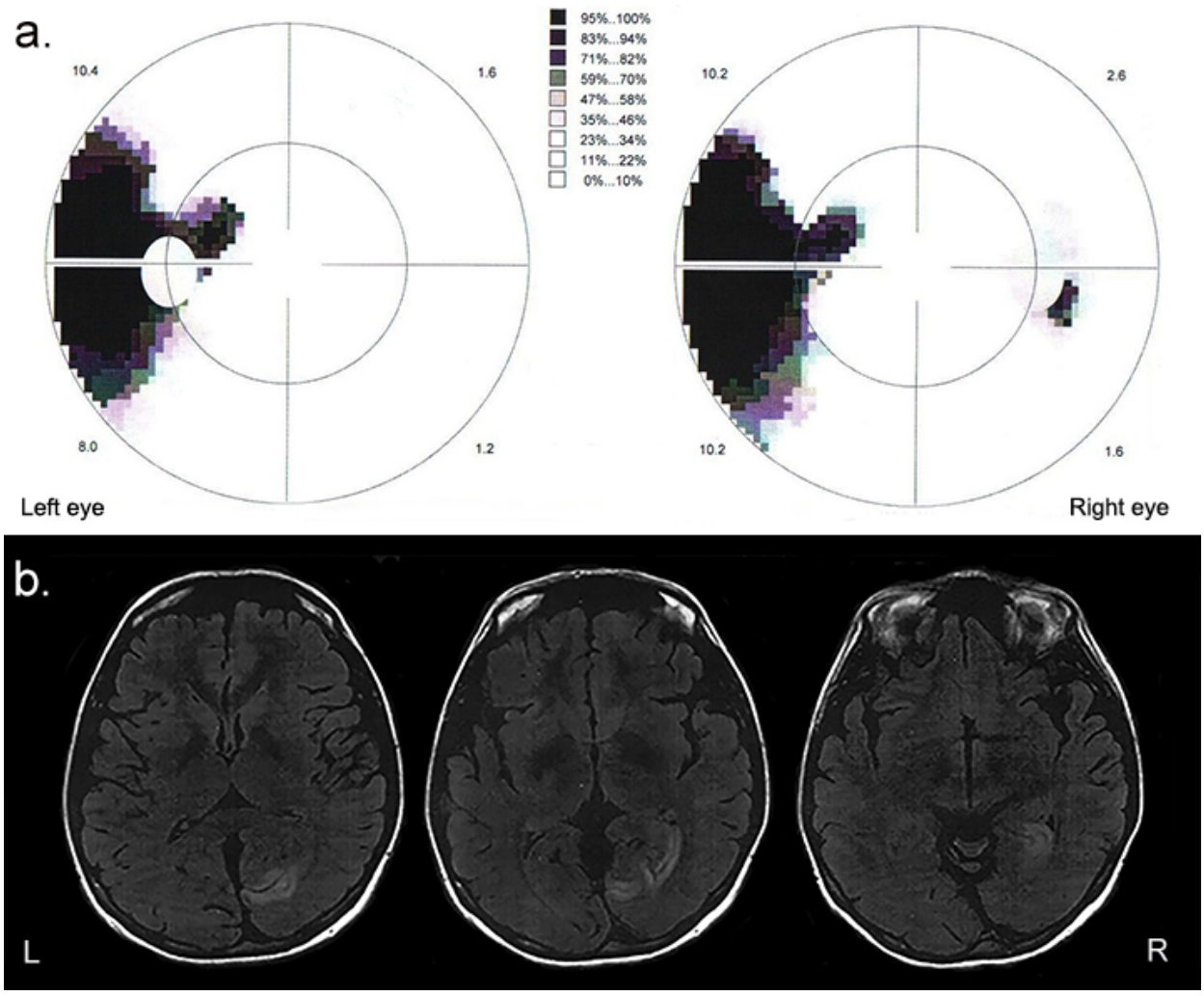

Figure 2.1. Images of the patient's visual field plot and ischaemic occipital stroke lesion. (a) Patient's visual field plots show an incomplete contralateral (left) congruent homonymous hemianopia. (b) T2-weighted MRI images taken at the time of stroke showing the location of the ischaemic occipital lesion in the right hemisphere at different slices. L = left; R = right.

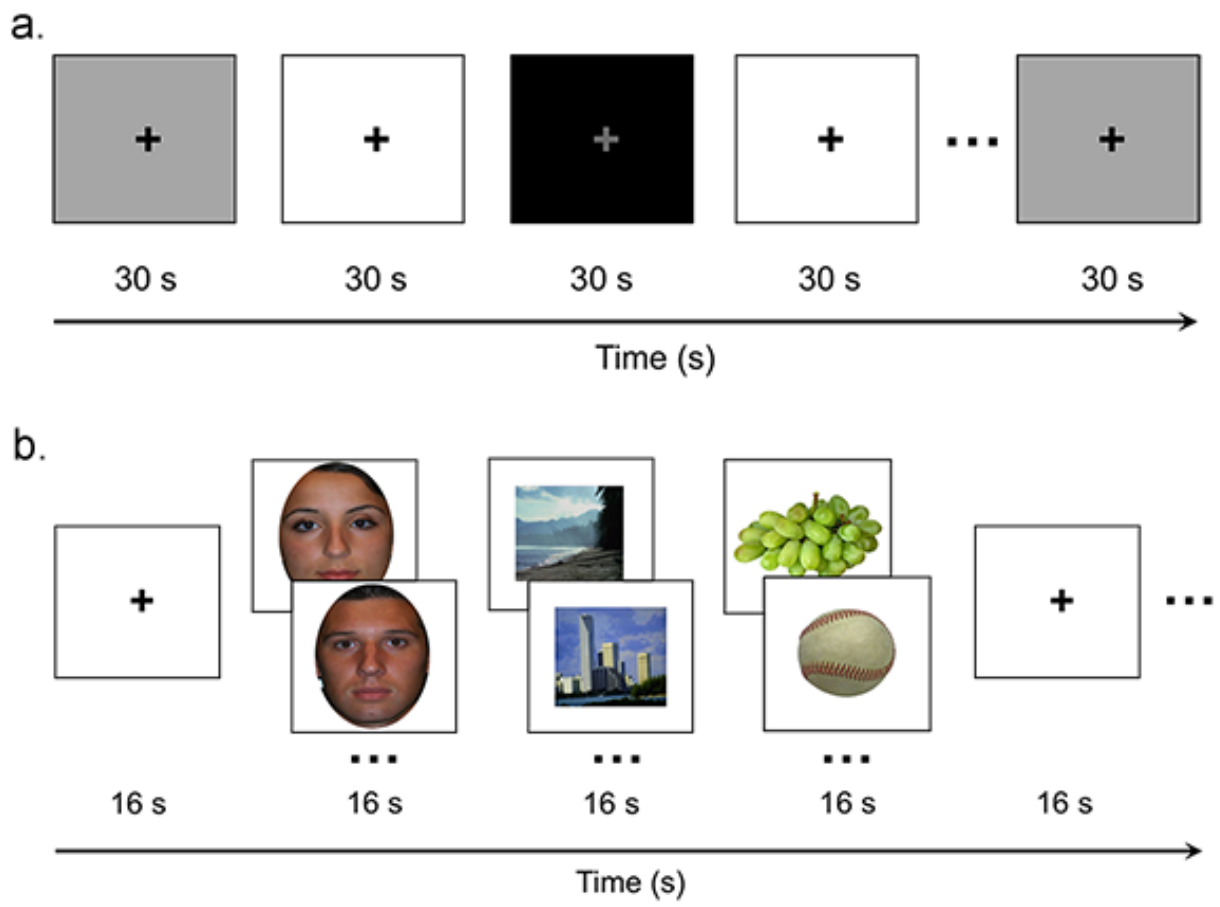

Figure 2.2. Schematic images of the localisers. (a) Phosphene localiser—each epoch contained a block of white and black stimuli (each shown for 30 s). (b) Face-scene-object localiser showing one epoch with sample stimuli—each epoch contained three blocks of each stimulus category with 16 images (each image shown for 900 ms with a 100 ms inter-stimulus interval) in each block.

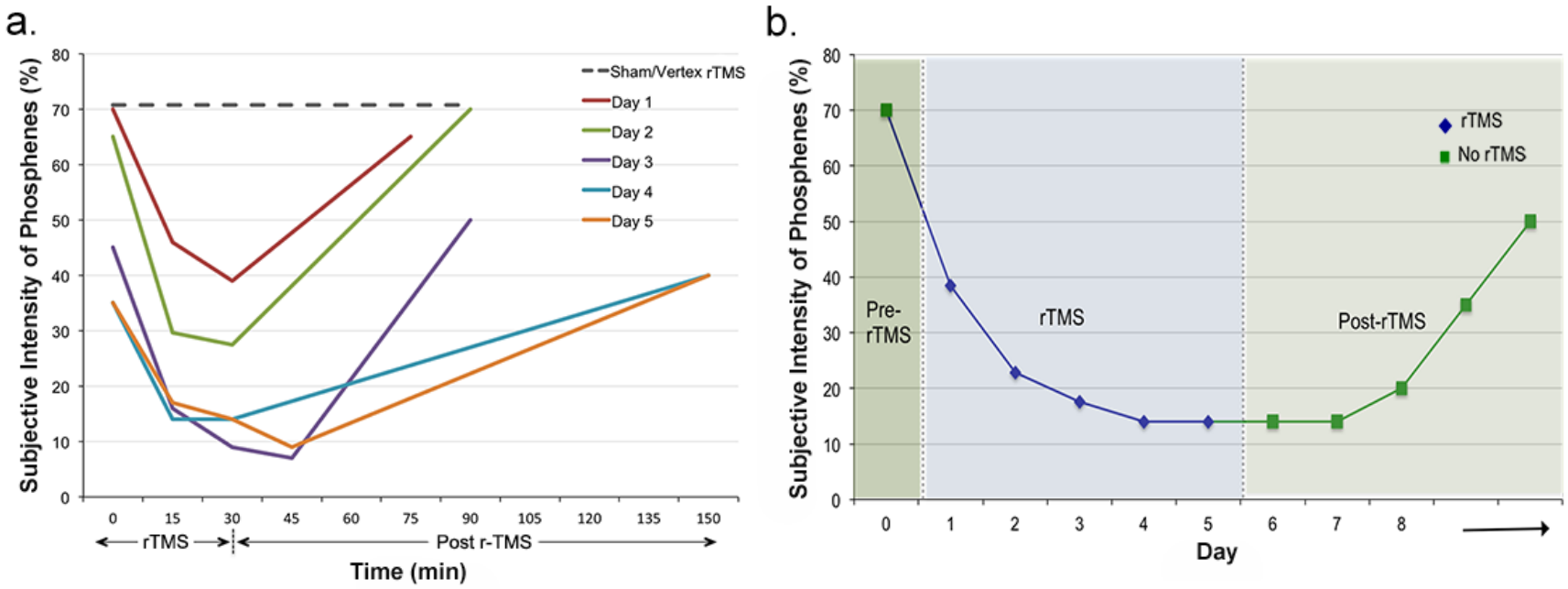

Figure 2.3. Patient subjective changes in perception of phosphene hallucinations with rTMS. (a) Daily subjective reduction in phosphenes assessed at 15 min intervals. (b) Average daily subjective reduction in phosphenes. Improvement is reported as a reduction in severity of hallucinations compared with average baseline intensity of phosphene hallucinations (~70%) experienced prior to commencing rTMS treatment.

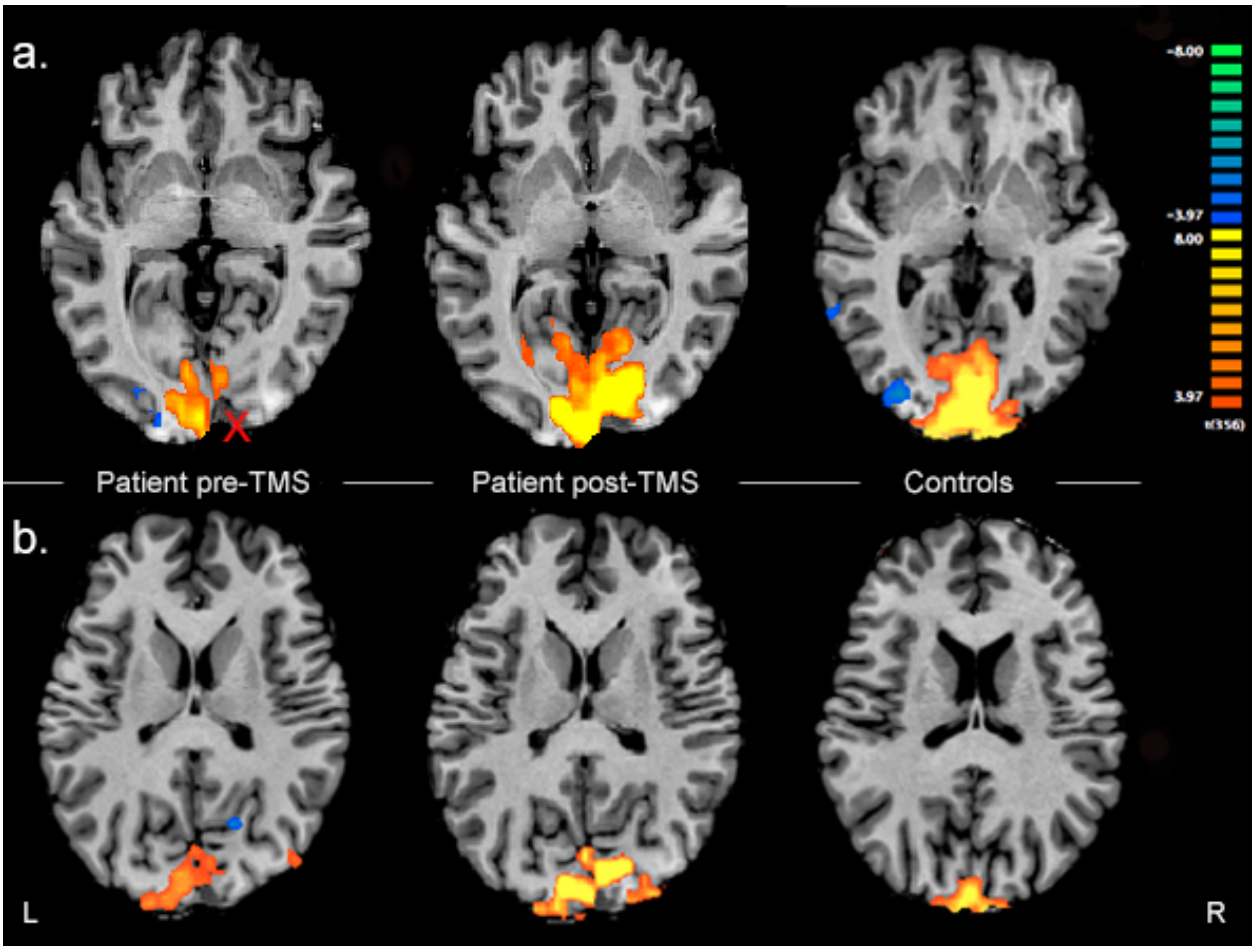

Figure 2.4. Phosphene localiser (white < > black stimuli) activity for the patient and control average. (a) Cortical activity at the lingual gyrus. 'X' marks the approximate location of the rTMS target site. A benign subarachnoid cyst is visible under the 'X' and is not to be confused with the lesion. (b) Cortical activity at the cuneus. Activation to white stimuli is indicated in orange/yellow and activation to black stimuli is indicated in blue/green; $q < .05$. L = left (contralesional in the patient); R = right (ipsilesional in the patient).

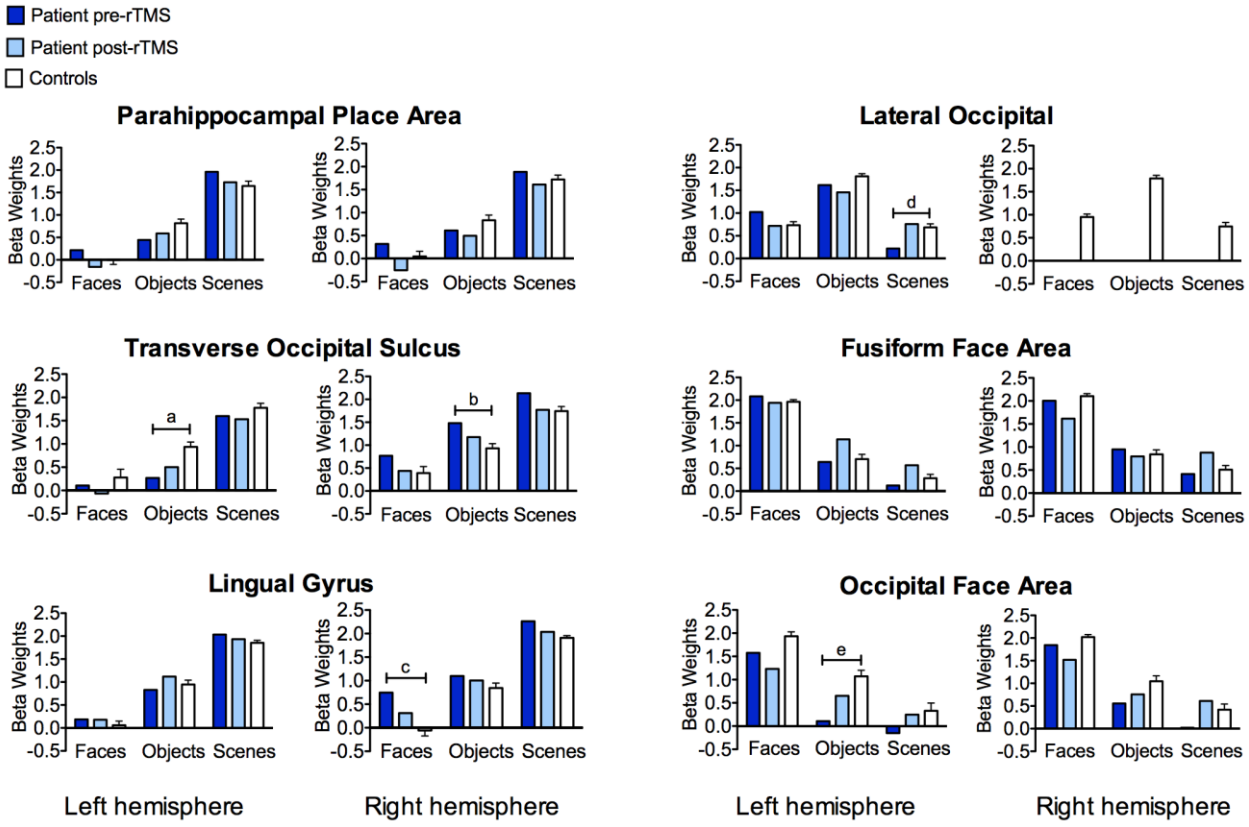

Figure 2.5. A priori analysis of the face-scene-object localiser. Right lateral occipital activation was not observed for the patient. Data are presented as mean ± *SEM* for controls. Significant differences in cortical activation for preferential and non-preferential processing are observed between the patient and controls. [a]t = -2.654, p = .033, effect size ($Z_{case\text{-}controls\ [cc]}$) = -2.815; [b]t = 2.095, p = .074, Z_{CC} = 2.222; [c]t = 2.386, p = .048, Z_{CC} = 2.531; [d]t = -2.183, p = .065, Z_{CC} = -2.315; [e]t = -2.525, p = .039, Z_{CC} = -2.678. Scene processing preferential regions: parahippocampal place area, transverse occipital sulcus, lingual gyrus. Object processing preferential region: lateral occipital area. Face processing preferential regions: fusiform face area, occipital face area.

Table 2.1.

Phosphene Localiser Results for the Patient

Region	Brodmann area	Talairach coordinates: White > black stimuli x	y	z	Black > white stimuli x	y	z
Patient pre-rTMS							
R lingual gyrus	17				23	-82	3
R lingual gyrus	18	12	-76	4			
L lingual gyrus	17	-7	-89	4			
L lingual gyrus	18	-21	-71	-9			
R cuneus	18	1	-80	16			
L cuneus	18	-6	-87	12			
L middle occipital gyrus	18				-27	-82	-8
R middle temporal gyrus	19	35	-80	22			
L fusiform gyrus	19				-25	-84	-13
R anterior vermis (culmen)		16	-55	-10			
L anterior vermis (culmen)					35	-51	-15
Patient post-rTMS							
R lingual gyrus	18	13	-68	1			
L lingual gyrus		-17	-76	3			
R middle occipital gyrus	19	27	-83	14			
R cuneus	19	10	-83	26			
L cuneus	18	-8	-86	14			
R sub-gyral	37	49	-48	-5			
R superior parietal lobule	7	19	-66	52			
L superior parietal lobule	7	19	-66	54			
L inferior parietal lobule	40	-37	-43	45			
R precentral gyrus	6	51	-12	28			
L precentral gyrus	6	-55	-4	34			
L postcentral gyrus	3	-49	-15	50			
R posterior lobe		28	-52	-13			

Note. The columns list (from left to right) the anatomical regions showing significant differences in functional activation between white and black stimuli ($q < .05$) for the patient in pre- and post-rTMS conditions, the Brodmann area, and (mean) Talairach coordinates of the cluster for the associated contrast. R = right (ipsilesional); L = left (contralesional).

Table 2.2.

Phosphene Localiser Results for Controls

		Talairach coordinates					
		White > black stimuli			Black > white stimuli		
Region	Brodmann area	x	y	z	x	y	z
R lingual gyrus	17	14	-92	-2			
R lingual gyrus	18	13	-71	-3			
L lingual gyrus	17	-7	-87	-2			
L lingual gyrus	18	-3	-68	-2			
R cuneus	18	4	-85	22			
L cuneus	19	-4	-87	26			
R middle occipital gyrus	18				32	-79	2
L middle occipital gyrus	19				-44	-71	4
R inferior occipital gyrus	18				34	-80	-1
L inferior occipital gyrus	18				-28	-88	-12
R middle temporal gyrus	22				60	-45	5
R fusiform gyrus	19				34	-78	-12
R fusiform gyrus	37				42	-59	-7
L superior parietal lobule	7	-33	-70	43			
R inferior parietal lobule	7	40	-60	44			
R inferior parietal lobule	39	40	-64	42			
R precentral gyrus	6	43	-8	52			
L precentral gyrus	6	-40	-12	36			
L precentral gyrus	4	-43	-11	45			
L postcentral gyrus	3	-51	-15	45			
R superior frontal gyrus	10	26	55	18			
R middle frontal gyrus	8	41	26	46			
R middle frontal gyrus	9	47	34	32			
L middle frontal gyrus	10	-37	54	9			
R inferior frontal gyrus	44	50	13	19			
R posterior lobe		15	-79	-17	28	-79	-20
L posterior lobe		-12	-75	-20			

Note. The columns list (from left to right) the anatomical regions showing significant differences in functional activation between white and black stimuli ($q < .05$) for age-matched controls, the Brodmann area, and (mean) Talairach coordinates of the cluster for the associated contrast. R = right; L = left.

Table 2.3.

Subtraction Analysis of the Phosphene Localiser Between the Patient Pre-rTMS and Controls

Region	Brodmann area	Talairach coordinates					
		White stimuli			Black stimuli		
		x	y	z	x	y	z
Patient pre-rTMS							
R lingual gyrus	17				24	-78	-1
R lingual gyrus	18				27	-83	4
R precuneus	31				19	-62	22
R cuneus	18	5	-71	21			
L cuneus	19				-25	-78	24
L cuneus	18	-4	-71	18	-25	-78	23
L middle occipital gyrus	18				-23	-86	0
R inferior occipital gyrus	19				32	-75	0
L inferior occipital gyrus	18				-25	-86	-7
L sub-gyral	20	-47	-18	-16			
R middle temporal gyrus	38	-48	5	-20			
R middle temporal gyrus	21	58	-18	-10			
L middle temporal gyrus	21	-50	-14	-16			
R inferior parietal lobule	40	35	-38	44	50	-37	35
R precentral gyrus	9	-34	12	39			
R superior frontal gyrus	10	33	51	19	16	61	24
R superior frontal gyrus	8	15	26	44			
R middle frontal gyrus	46	49	37	14			
R middle frontal gyrus	10				24	56	21
R middle frontal gyrus	9	43	20	32			
R middle frontal gyrus	8				37	29	45
R middle frontal gyrus	6	36	3	44			
L middle frontal gyrus	46	-47	19	20			
L middle frontal gyrus	9	-36	18	28			
L medial frontal gyrus	32	-17	12	47			
R inferior frontal gyrus	47	30	29	-3			
R inferior frontal gyrus	45	63	22	12			
R inferior frontal gyrus	10	43	49	3			
L inferior frontal gyrus	47	-34	30	-6			
L inferior frontal gyrus	46	-45	41	10	-43	43	9
L inferior frontal gyrus	9				-54	14	27
L anterior cingulate	32	-8	33	20			
R posterior cingulate	30	5	-58	6			
L posterior cingulate	30	-23	-65	5			
L anterior lobe (culmen)		-32	-38	-23			
L posterior lobe		-40	-67	-25	-30	-82	-20
R claustrum		31	6	-3			

Table 2.3. (continued)

Region	Brodmann area	Talairach coordinates					
		White stimuli			Black stimuli		
		x	y	z	x	y	z
Controls							
R lingual gyrus	17	13	-93	-2			
R lingual gyrus	18	2	-80	-5			
R precuneus	18	4	-90	15			
R cuneus	23				1	-72	11
R cuneus	18				22	-89	16
R cuneus	17	13	-93	3	15	-90	8
L cuneus	18				-4	-82	22
L cuneus	19	-6	-84	30			
L middle occipital gyrus	18				-20	-90	12
L superior temporal gyrus	13	-47	-20	7			
R middle temporal gyrus	19				38	-78	20
L middle temporal gyrus	21	-50	-41	11			
R inferior temporal gyrus	37				-47	-50	0
L precentral gyrus	6	-56	1	38			
R superior frontal gyrus	6				12	13	60
L superior frontal gyrus	9	-31	48	34			
R middle frontal gyrus	46	46	44	27			
R middle frontal gyrus	6	32	23	54			
R medial frontal gyrus	10	15	57	12			
L anterior cingulate	32	-21	41	2			
R posterior lobe		1	-81	-16			
L posterior lobe		-7	-83	-20			

Note. Beta-difference maps (b > 0.5) between the patient pre-rTMS and age-matched controls. The columns list (from left to right) the anatomical regions showing differences in functional activation for the patient and controls, the Brodmann area, and (mean) Talairach coordinates of the cluster for the associated stimuli. R = right (ipsilesional in the patient); L = left (contralesional in the patient).

Table 2.4.

Subtraction Analysis of the Phosphene Localiser Between the Patient Post-rTMS and Controls

		Talairach coordinates					
	Brodmann	White stimuli			Black stimuli		
Region	area	x	y	z	x	y	z
Patient post-rTMS							
R lingual gyrus	18	13	-75	4	3	-87	-13
R lingual gyrus	17				12	-93	-4
L lingual gyrus	18				-9	-90	-10
L lingual gyrus	17	-11	-85	4			
R precuneus	19	32	-74	31			
R precuneus	7	15	-63	47			
L precuneus	31	-1	-74	27			
L precuneus	19	-28	-75	31			
L precuneus	7	-24	-55	47			
R cuneus	18	9	-80	20			
R cuneus	17	11	-78	12			
L cuneus	23	-1	-72	11			
L cuneus	18	-4	-87	11			
R middle occipital gyrus	19	32	-79	10			
L middle occipital gyrus	19	-33	-82	10			
L fusiform gyrus	18				-26	-86	-17
R middle temporal gyrus	37	52	-58	-8			
L middle temporal gyrus	37	-58	-50	-6			
L precentral gyrus	6	-50	2	28			
R inferior frontal gyrus	9	48	8	30			
R posterior cingulate	30	26	-55	13			
R posterior lobe		27	-58	-13			

Note. Beta-difference maps ($b > 0.5$) between the patient post-rTMS and age-matched controls. The columns list (from left to right) the anatomical regions showing differences in functional activation for the patient and controls, the Brodmann area, and (mean) Talairach coordinates of the cluster for the associated stimuli. No clusters of activity were observed to be greater in controls for both white and black stimuli ($b < 0.5$). R = right (ipsilesional); L = left (contralesional).

CHAPTER 3

ALTERED WHITE MATTER CONNECTIVITY ASSOCIATED WITH VISUAL HALLUCINATIONS FOLLOWING OCCIPITAL STROKE[2]

[2]Adapted version published as: Rafique, S. A., Richards, J. R., & Steeves, J. K. E. (2018). *Brain and Behaviour*, e01010.

Preface

We sought to determine if structural changes in white matter connectivity play a role in the aberrant functional activity that is observed in cases of chronic visual hallucinations associated with visual pathway damage. We performed DTI and probabilistic fibre tractography to assess white matter connectivity in a patient suffering from continuous and disruptive phosphene hallucinations for more than two years following right occipital stroke. Data were compared to that of healthy age-matched controls. Probabilistic tractography to reconstruct white matter tracts suggested regeneration of terminal fibres of the ipsilesional optic radiations in the patient. However, arrangement of the converse reconstruction of these tracts, which were seeded from the ipsilesional visual cortex to the intrahemispheric lateral geniculate body, remained disrupted. We further observed compromised structural characteristics and changes in diffusion (measured using diffusion tensor indices) of white matter tracts in the patient connecting the visual cortex with frontal, parietal, and temporal regions, and also in interhemispheric connectivity between visual cortices. Cortical remapping and the disruption of connectivity between visual cortices and remote regions are consistent with our previous fMRI data showing imbalanced functional activity in the same regions in this patient (Chapter 2; Rafique et al., 2016). Long-term adaptive and disruptive changes in white matter connectivity may account for cases presenting with chronic visual hallucinations, particularly in the rare nature of continuous hallucinations. Investigation of structural white matter connectivity can be valuable for providing prognostic information and resistance to therapeutic interventions (e.g., neuromodulation).

Previous fMRI studies have shown that visual hallucinations following vision loss are associated with disorganised functional activity in visual cortices across both hemispheres, and in interconnected cortical and subcortical networks (ffytche et al., 1998; Rafique et al., 2016). We sought to determine if structural changes in white matter connectivity are also present in cases of chronic visual hallucinations following visual pathway damage. Cortical injury induces a process of remapping and reconnection within the adult brain through changes in neuronal activity. Lesions can induce axonal sprouting within local intra- and interhemispheric projections to establish substantially new patterns of cortical connections with deafferented or partially damaged brain areas (for a review, see Carmichael, 2003; Darian-Smith & Gilbert, 1995). Investigation of structural connectivity can provide valuable information for determining the appropriate therapeutic protocol and prognosis, as well as longer-term post-treatment efficacy (Inzitari et al., 2009; Kunimatsu et al., 2003). We employed DTI and probabilistic fibre tractography to enable noninvasive investigation of white matter structure. To gain information about the integrity of white matter, the diffusion of water in white matter tracts that is influenced by underlying microstructure and orientation of axonal fibres was characterised using diffusion tensor indices: FA (directionality of diffusion parallel to fibre tracts), MD (directionally averaged measure of diffusion), AD (measure of diffusion parallel to axonal fibres), and RD (measure of diffusion perpendicular to axonal fibres). Probabilistic fibre tracking algorithms use directions of greatest diffusion to estimate white matter fibre orientation and employ Bayesian modelling to infer these fibre directions and generate 3D depictions of white matter tracts (Behrens, Berg, Jbabdi, Rushworth, & Woolworth, 2003; Ciccarelli, Catani, Johansen-Berg, Clark, & Thompson, 2008).

We investigated a patient experiencing chronic and continuous phosphene hallucinations following occipital stroke. In a previous study (Chapter 2; Rafique et al., 2016), the patient underwent fMRI and therapeutic treatment with rTMS to the lesion site to provide relief from hallucinations that were interfering with quality of life. fMRI showed aberrant functional activity in visual cortices, and an imbalance of activity across frontal, parietal, temporal, and cerebellar regions prior to rTMS treatment. In the present study, we investigated whether the previously documented aberrant functional activity and persistent nature of hallucinations in the patient (Chapter 2; Rafique et al., 2016) were a reflection of compromised structural characteristics in white matter connectivity. We used DTI and probabilistic tractography to examine white matter connectivity between cortical regions implicated in our previous fMRI study. Moreover, in our previous fMRI study, we observed some restoration of functional activity in the patient following treatment with rTMS. However, this redistribution of functional activity post-rTMS in the patient did not completely match that of controls; and despite a significant reduction in intensity of visual hallucination with rTMS treatment, the hallucinations persisted, albeit to a lesser extent (Chapter 2; Rafique et al., 2016). We further expected that this incomplete functional restoration and failure to fully suppress the hallucinations with rTMS would in part, if not wholly, be due to white matter connectivity changes. There are presently no cases in the literature that have investigated white matter in cases of visual hallucinations following visual pathway damage.

Methods

This study was approved by York University's Office of Research Ethics. All individuals gave informed written consent.

Participants

We evaluated a 31-year-old female experiencing persistent and disruptive phosphene hallucinations within an incomplete congruous left homonymous hemianopia for 2.5 years following right subacute occipital stroke. A detailed patient history and description of visual hallucinations is provided in Chapter 2 (see Methods: Participants, pp. 39–41).

Seven age-matched healthy female control participants ($M_{age} \pm SEM = 29 \pm 0.79$ years) with no history of neurological disorders, and normal or corrected-to-normal vision (> 0.2 logMAR; stereoacuity ≥ 50") were recruited. All participants (patient included) had taken part in a previous fMRI study (Chapter 2; Rafique et al., 2016).

Magnetic Resonance Imaging

Whole-brain imaging was acquired with a 3T Siemens Magnetom® Tim Trio magnetic resonance scanner and a Siemens 32-channel high-resolution brain array coil (Siemens, Erlanger, Germany). Head motion was minimised with the placement of soft pads holding the participant's head in place. DTI was obtained with diffusion-weighted scanning using two-dimensional (2D) gradient echo echo-planar sequencing (number of contiguous axial slices = 56; in-plane resolution = 1.5 x 1.5 mm; slice thickness = 2 mm with no interslice gap; imaging matrix = 128 x 128; TR = 6900 ms; TE = 86 ms; FoV = 192 mm) with 64 isotropically distributed orientations for the diffusion-sensitising gradients at a *b*-value of 1000 s/mm^2, and $b = 0$ s/mm^2 for T2-weighted images. Anatomical images were acquired with a T1-weighted sequence using 3D MPRAGE (number of slices = 192; in-plane resolution = 1 x 1 mm; slice thickness = 1 mm; imaging matrix = 256 x 256; TR = 1900 ms; TE = 2.5 ms; inversion time (TI) = 900 ms; flip angle = 9°; FoV = 256 mm). A T2-weighted turbo spin echo fluid attenuated inversion recovery (FLAIR) imaging sequence was obtained in the patient to localise the lesion site (number of

slices = 25; in-plane resolution = 0.9 x 0.9 mm; slice thickness = 4 mm; imaging matrix = 256 x 256; TR = 900 ms; TE = 93 ms; TI = 2500 ms; flip angle = 130°; FoV = 220 mm).

Data Analyses

All DTI analyses were performed using FSL's DTI processing pipeline (FMRIB, Oxford, UK; www.fmrib.ox.ac.uk/fsl).

Image processing and normalisation. Diffusion images underwent preprocessing. Diffusion images were corrected for eddy current-induced spatial distortions and head motion using affine registration to the reference (*b*0) volume (Andersson & Sotiropoulos, 2016) within FSL's diffusion toolbox (FDT), and brain-extracted using the brain extraction tool (BET) to remove skull and head tissue (Smith, 2002). T1-weighted images also underwent brain-extraction using BET. Diffusion tensor models were fitted at each voxel of the eddy current corrected diffusion data using standard linear regression with the diffusion tensor fitting program (DTIFIT) of the FDT toolbox. The brain-extracted T1-weighted images underwent linear registration to diffusion space and also to standardised Montreal Neurological Institute (MNI) space (MNI152, 1 x 1 x 1 mm) using the linear image registration tool (FLIRT; Jenkinson, Bannister, Brady, & Smith, 2002) with default parameters (affine 12 degrees of freedom; correlation ratio cost function; tri-linear interpolation). Diffusion images were non-linearly registered to T1-weighted anatomical and standard MNI spaces (MNI152, 1 x 1 x 1 mm) to derive transformation matrices using the non-linear image registration tool (FNIRT) of FDT (Andersson, Jenkinson, & Smith, 2007) with default parameters (normal search; correlation ratio cost function; 6 and 12 degrees of freedom for anatomical and standard space, respectively). T1-weighted images were also registered to standard MNI space (MNI152, 1 x 1 x 1 mm).

Diffusion tensor indices. The diffusion tensor indices FA, MD, AD, and RD were extracted from 11 major white matter tracts of John Hopkins University (JHU) white-matter tractography atlas provided with FSL (Wakana et al., 2007). Accordingly, diffusion tensor indices were extracted from the following bilateral tracts: anterior thalamic radiations, corticospinal tracts, cingulum (cingulate gyrus and hippocampus), inferior fronto-occipital fasciculi, inferior longitudinal fasciculi, superior longitudinal fasciculi, temporal aspects of superior longitudinal fasciculi, and uncinate fasciculi. Diffusion tensor indices were also extracted from the forceps major and minor. Indices were extracted using tract-based spatial statistics (TBSS; Smith et al., 2006). Using the diffusion-weighted brain images computed from DTIFIT, each participant's FA image underwent preprocessing to remove outliers from the diffusion tensor fitting. The FA image was then aligned to standard MNI space using affine non-linear registration, and thinned to create a binary skeleton image using a threshold of FA > 0.2. Tracts from the JHU atlas were thresholded at a 15% probability to allow for inter-subject variation and binarised. Each binarised tract was then co-registered (masked) to each participant's binary skeleton diffusion image using *fslmaths*. The fit of the white matters tracts was manually assessed to ensure accurate overlap with skeleton images. White matter tract values were then extracted from skeletonised diffusion images for each participant and each tract separately using *fslmeants*. To obtain the non-FA diffusion indices, the FA-derived non-linear transformations were applied to the MD, AD, and RD images, and projected onto the FA binary skeleton to estimate projection vectors from the same voxels as in the FA analysis. AD was defined as the principal diffusion eigenvalue ($\lambda 1$), and RD as the mean of the second and third eigenvalues ($\lambda 2 + \lambda 3/2$). The extracted diffusion tensor indices underwent statistical analyses to compare the patient with controls using the modified independent *t*-test (one-tailed) for single-

case studies (Crawford & Garthwaite, 2002). We report significant differences in diffusion tensor indices at $p < .05$, and trending significance at $p < .1$.

Probabilistic fibre tractography. Our main interests were tracts connected with the visual cortex (primary and association cortices) consistent with the location of the patient's lesion site. Tracts of interest were generated to cortical regions of interest based on our previous fMRI findings, which showed functional differences in BOLD signal between the patient (prior to rTMS, consistent with visual system status at time of DTI acquisition) and controls (Chapter 2; Rafique et al., 2016). To reconstruct tracts of interest, we used FDT's Bayesian estimation of diffusion parameters obtained using sampling techniques for modelling crossing fibres (BEDPOSTX), which uses Markov Chain Monte Carlo sampling to estimate diffusion parameters at each voxel and model crossing fibres within each voxel of the corrected diffusion data (Behrens et al., 2007). We then used FDT's probabilistic tracking with crossing fibres (PROBTRACKX) to generate fibre tractography in MNI space (Behrens et al., 2007). A two-region of interest approach was used to isolate streamlines (tracts). A seed mask was placed at the visual cortex (to include primary and association cortices, i.e., Brodmann areas 17, 18, 19) to waypoint (identifies tracts passing through this point only) and terminate (end point) in intrahemispheric sub-regions of frontal lobe gyri (superior, middle, and inferior), temporal lobe gyri (superior, and middle temporo-occipital), parietal lobules (superior and inferior), and precentral and postcentral gyri, independently. We further reconstructed the optic radiations by placing a seed mask at the lateral geniculate body, and waypoint and termination masks at the ipsilateral primary visual cortex. A converse intrahemispheric reconstruction was generated from the primary visual cortex (seed mask) to the lateral geniculate body (waypoint and termination masks) as these are shown to differ from feedforward connections (Shipp, 2007; Sillito, Cudeiro,

& Jones, 2006). A cerebral white matter exclusion mask of the opposite hemisphere was used to limit tracts within the ipsilateral hemisphere and minimise false positive tracts. Tracts were reconstructed for all participants and both hemispheres. To investigate interhemispheric connectivity between the visual cortices, a seed mask was placed at one hemisphere of the visual cortex with waypoint and termination masks placed at the contralateral visual cortex (with no exclusion mask). This was reversed to generate interhemispheric connections between the visual cortices for the opposite direction. Interhemispheric visual cortex connectivity was also reconstructed for all participants separately. Fibre tracking involved 5000 streamlines drawn from each voxel in the seed mask through the probability distribution in the principle fibre direction. Streamlines ended at a pathway curvature threshold of 0.2 (~80°) and a maximum number of 2000 steps (step length of 0.5 mm) (default parameters). Reference to seed and termination points does not imply tract directionality, but strictly refers to the generation of tracts from every point in the seed to only enter and end at the target termination point. Tracts were visually inspected for changes in size and orientation compared with the contralateral hemisphere, and comparing the patient with controls.

Results

Diffusion Tensor Indices

A T2-weighted image and colour-coded FA map for the patient indicating the lesion site are shown in Figure 3.1. Table 3.1 contains values for diffusion tensor indices obtained from the 11 major white matter tracts and demonstrates significant differences in diffusivity between the patient and controls.

Probabilistic Fibre Tractography

Reconstruction of intrahemispheric tracts seeded from the visual cortex to the inferior frontal gyrus showed greater tracts for the patient within the ipsilesional visual cortex compared with the contralesional hemisphere and controls (Figure 3.2a). Similarly, for intrahemispheric tracts seeded from the ipsilesional visual cortex to the precentral gyrus, the patient showed greater tracts close to the precentral gyrus relative to the contralesional hemisphere and controls (Figure 3.2b).

Probabilistic tractography for the patient further showed incomplete intrahemispheric tracts seeded from the ipsilesional visual cortex to superior temporal and middle temporo-occipital gyri, and the lateral geniculate body, compared with the contralesional hemisphere and controls (Figure 3.3a-c, respectively). This is observed from the absence of intrahemispheric tracts within the ipsilesional visual cortex in the patient—instead the tracts originate further anteriorly, closer to anterior temporo-occipital regions.

Reconstruction of the optic radiations in the patient shows a marked displacement of ipsilesional optic radiations relative to the contralesional hemisphere and controls. The terminal fibres of the patient's ipsilesional optic radiations are seen to deviate anterior to the lesion site (Figure 3.4).

Altered interhemispheric connectivity between visual cortices is observed in the patient. Tracts seeded from the ipsilesional visual cortex fail to terminate in the contralesional visual cortex, and instead discontinue at the midline. However, the converse is spared as tracts seeded from the contralesional visual cortex continue past the midline and terminate in the ipsilesional visual cortex (Figure 3.5). In comparison, control participants demonstrate overlapping interhemispheric connections (Figure 3.5).

Given that directionality cannot be inferred from probabilistic tractography, it is important to note that tracts seeded from the lateral geniculate body to the visual cortex are intermingled with and cannot be differentiated from the converse reconstruction of these tracts (i.e., seeded from the visual cortex to the lateral geniculate body) using this method. The same applies to interhemispheric visual cortex tracts.

For ease of comparison of probabilistic fibre tractography between the patient and controls, we only present data of one control example in Figures 3.2–3.5. The results of probabilistic tractography for all other controls are presented in Appendix A (Figures A1–A7). Despite inter-individual variation in tracts, the patient consistently showed these differences compared with all control participants.

No differences were observed between the patient and controls for intrahemispheric tracts seeded from the visual cortex to superior and middle frontal gyri, and postcentral gyrus. Probabilistic tractography did not reveal tracts from the visual cortex to the middle temporal gyrus or parietal lobules in the patient or controls based on our seed and termination masks.

Discussion

Diffusion imaging highlights changes in diffusion indices of major white matter tracts associated with the patient's lesion site compared with controls. Moreover, probabilistic fibre tractography demonstrates changes in white matter tracts between the visual cortex and remote regions in the patient that are consistent with previously observed alterations in functional activity between the patient and controls. Overall, these results suggest that altered global structural connectivity contributes to chronic cases of visual hallucinations in visual pathway damage.

White Matter Changes with Occipital Stroke and Associated Vision Loss

In the patient, we observed incomplete intrahemispheric tracts from the ipsilesional visual cortex to superior temporal and middle temporo-occipital gyri (Figure 3.3a-b, respectively). This finding is consistent with observed differences in functional activation within these regions between the patient and controls during a basic visual task (Chapter 2, Tables 2.1–2.3). Although we only observed greater intrahemispheric tracts from the ipsilesional visual cortex to the inferior frontal gyrus (Figure 3.2a), the patient has shown significantly greater functional activation in bilateral inferior frontal gyri compared with controls (Chapter 2, Table 2.3). These regions are connected via the major white matter tracts superior longitudinal and inferior fronto-occipital fasciculi. The superior longitudinal fasciculus connects frontal, parietal, temporal, and occipital lobes (Catani, Howard, Pajevic, & Jones, 2002), while the inferior fronto-occipital fasciculus connects the frontal lobe with posterior aspects of parietal, temporal, and occipital lobes (Martino, Brogna, Robles, Vergani, & Duffau, 2010). The inferior fronto-occipital fasciculus further passes through the lateral geniculate body and claustrum (Kier, Staib, Davis, & Bronen, 2004). Not only did the patient show incomplete tracts from the ipsilesional visual cortex to the intrahemispheric lateral geniculate body (Figure 3.3c), our previous fMRI findings implicate the ipsilesional claustrum in the genesis of visual hallucinations in this patient (Chapter 2, Table 2.3).

The inferior longitudinal fasciculus connects anterior temporal and posterior occipito-temporal regions of the occipital lobe, including visual association areas, fusiform and parahippocampal gyri (Catani, Jones, & Donato, 2003; Wakana, Jiang, Nagae-Poetscher, van Zijl, & Mori, 2004). Given that the lesion site involved the right visual association areas (Chapter 2, Figure 2.1b), it did indeed compromise the structural integrity of the right inferior longitudinal

fasciculus (Figure 3.1b; Table 3.1). Additionally, the visual association areas (e.g., lingual gyrus and cuneus) showed the most obvious alterations in functional activity in our patient and were considered the primary regions contributing to the perception of visual hallucinations (Chapter 2, Figure 2.4).

Changes in FA and/or AD of the superior (including temporal aspects) and inferior longitudinal fasciculi in the patient (Table 3.1) are therefore not surprising given the disruption to diffusivity at the stroke site (Figure 3.1), and consequent changes in tractography between regions concerned with these fasciculi (Figures 3.2–3.3). Altered FA suggests changes to white matter microstructure (Jones et al., 1999) indicative of change in aspects of connectivity (Jones, Simmons, Williams, & Horsefield, 2013). AD measures are considered variable in white matter changes and pathology; however, a decrease is observed in axonal injury/damage (Song et al., 2002). Despite involvement of intrahemispheric ipsilesional tracts in the patient (Figures 3.2a, 3.3b-c) implicating the ipsilesional inferior fronto-occipital fasciculus, it was the contralesional inferior fronto-occipital fasciculus that showed significantly lower AD (Table 3.1). A possible explanation for contralesional inferior fronto-occipital fasciculus involvement may be from sharing of axons with the ipsilesional fasciculus or axons originating from the lesion site.

Alterations in interhemispheric white matter connectivity between visual cortices in the patient (Figure 3.5) offer further explanation to the disorganised and imbalanced functional activity in visual processing regions previously observed across both hemispheres, for example, greater functional activity in the contralesional hemisphere (Chapter 2, Figure 2.4).

Compensatory White Matter Changes with Occipital Stroke and Associated Vision Loss

The marked displacement of the ipsilesional optic radiations in the patient (Figure 3.4) suggests recovery of function with new connections via recruitment of peri-infarct regions that adapt to new roles after stroke (Carmichael, 2003; Cramer, 2008). The optic radiations carry visual information from the retina via the lateral geniculate body to the primary visual cortex. Damage to the optic radiation pathway is consistent with the presence of hemianopia in the patient (Chapter 2, Figure 2.1a). Quite notably, the location of terminal fibres of the ipsilesional optic radiations is consistent with the location of disorganised functional activity anterior to the patient's lesion at the lingual gyrus (Chapter 2, Figure 2.4). In this patient, it appears that input from the retina to ipsilesional visual cortex, via remapping of optic radiations, produces sustained sensory responses in new structural circuits in peri-infarct regions; and this aberrant neuronal firing may produce the perception of phosphene hallucinations in the area of hemianopia. Indeed, in vivo cortical recordings of mice show an effect of prolonged depolarisation at remapped peri-infarct regions and in regions with greater connectivity post-stroke (Brown, Aminoltejari, Erb, Winship, & Murphy, 2009). A DTI study in an infant with perinatal temporo-parieto-occipital stroke shows the same pattern of regeneration of ipsilesional optic radiations (Seghier et al., 2005) as in our patient. In both cases, the location of terminal fibres of the regenerated optic radiations are consistent with the location of disorganised ipsilesional functional activity. Moreover, ipsilesional functional activation in the infant was localised anterior to the lesion at the lingual gyrus in the same manner as our patient. No follow-up was reported in the infant past 20 months of age; therefore, we cannot ascertain whether visual hallucinations manifested in the infant.

Despite the pattern of regeneration of ipsilesional optic radiations, we do not see such a recovery in the converse reconstruction of these tracts (seeded from the visual cortex to the lateral geniculate body) that remain disrupted in the patient (Figure 3.3c) and may suggest retrograde degeneration. Post-mortem studies of occipital lobotomies in primates have shown retrograde degeneration persists back to the retina corresponding to the visual field representation of the damaged occipital cortex (Cowey, 1974; Johnson & Cowey, 2000).

Lower FA and increased RD were observed in the contralesional corticospinal tract of the patient (Table 3.1). An increase in RD suggests white matter pathology (Song et al., 2002) in this motor pathway. Although motor deficits were not a consequence of stroke in our patient, corticospinal tract plasticity following early vision loss is thought to arise from overcoming difficulty with eye-hand coordination from loss of vision (Yu et al., 2007). Many corticospinal neurons originate in the precentral gyrus (Dum & Strick, 1991), and accordingly, we observed greater tracts from the ipsilesional visual cortex to the intrahemispheric precentral gyrus (Figure 3.2b). These combined findings may indicate compensation for the need for increased left eye-hand coordination following left homonymous hemianopia in the patient. Consistent with these structural white matter changes, subtraction analysis of fMRI responses during a basic visual task between the patient and controls has shown greater patient activation in the ipsilesional (right) precentral gyrus, while controls showed greater activation in the left precentral gyrus (Chapter 2, Tables 2.2–2.3).

Changes in white matter tracts in the patient at both ipsi- and contralesional hemispheres stem from altered intra- and interhemispheric communication, e.g., major forceps, or commissural tracts. Early studies of occipital lobe lesions in animals show retinotopic reorganisation and changes of neuronal response properties in the ipsilesional hemisphere, and

aberrant distribution of callosal connections in both ipsi- and contralesional hemispheres (Payne & Lomber, 2001; Restrepo, Manger, Spenger, & Innocenti, 2003). Greater ipsilesional tracts in the patient (Figure 3.2) suggest recruitment of redundant neurons/interneurons. Global over-connectivity is observed in patients with hemianopia following occipital stroke, with greater node strength in ipsilesional temporal and orbitofrontal areas as well as the contralesional visual association cortex (Guo, Jin, Feng, & Tong, 2014). Reduced contralesional tracts (Figure 3.2) may occur to compensate for changes in ipsilesional tracts (e.g., greater tracts), or from pruning that occurs from loss of interhemispheric communication following stroke (Grefkes et al., 2008).

White Matter Changes Associated with Persistent Visual Hallucinations

Reduced FA of the contralesional anterior thalamic radiation in the patient (Table 3.1), which connects the anterior and dorsomedial thalamic nuclei with the prefrontal cortex (Wakana et al., 2004), suggests changes to white matter microstructure and connectivity of this tract (Jones et al., 2013, 1999). Thalamic degeneration is previously implicated in visual hallucinations (Manford & Andermann, 1998), consistent with its involvement in this patient. Additionally, reduced FA in the anterior thalamic radiation is observed in cases of auditory hallucinations in schizophrenia (Ćurčić-Blake et al., 2015). The uncoupling of processes underlying perception from sensory input are linked to the emergence of hallucinations via dysregulation of thalamic sensory transmission (Behrendt, 2006).

The inferior longitudinal and inferior fronto-occipital fasciculi are involved in visual perception (ffytche, 2008) and visual processing (Fox, Iaria, & Barton, 2008). As in our patient, visual hallucinations have been linked to lower FA in the inferior longitudinal fasciculus in individuals with schizophrenia (Ashtari et al., 2007) and dementia with Lewy bodies (Kantarci et al., 2010), suggesting an association of visual hallucinations with temporo-occipital projections.

Furthermore, frontal lesions can produce visual hallucinations in the temporal and occipital lobes thought to arise through the spread of increased activity from one area to another (Schneider, Crosby, Bagchi, & Calhoun, 1961). Consistent with this notion, direct electrical stimulation of the inferior frontal gyrus evokes visual hallucinations of faces considered to originate from activity propagated in the prefrontal cortex along white matter pathways to face processing regions (Vignal, Chauvel, & Halgren, 2000), for example, via the inferior longitudinal fasciculus. In addition to frontal stimulation, stimulation of the temporal lobe (Lee, Hong, Seo, Tae, & Hong, 2000; Penfield & Perot, 1963) and visual cortices (Lee et al., 2000) also evokes visual hallucinations. This suggests that it is not simply an increase and/or disorganisation of activity in visual associated cortices that produce visual hallucinations (ffytche et al., 1998; Rafique et al., 2016), but rather, the additional involvement of these white matter tracts (and accordingly specific networks) that differentiates these patients from those with similar disorders who do not experience visual hallucinations.

Limitations

Given the single-case study approach of the present research, we appreciate that the data may be insufficient to generalise specific plasticity effects following occipital stroke associated with chronic visual hallucinations. In addition, due to the number of independent *t*-tests, and the less conservative threshold for trending results ($p < .1$), some differences in diffusion tensor indices between the patient and controls (Table 3.1) may reflect statistical noise. Further diffusion imaging studies in patients with visual pathway damage who perceive visual hallucinations and those who do not are necessary in order to isolate factors predisposing individuals to visual hallucinations. To our knowledge, other than the case of perinatal stroke (Seghier et al., 2005), there are no other studies reported in the literature investigating white

matter structure in visual pathway damage with or without visual hallucinations. Knowledge of white matter structure is pivotal in elucidating underlying mechanisms of brain function associated with chronic and disruptive visual hallucinations in these patients. Evaluation of white matter connectivity in other leading causes of vision loss associated with visual hallucinations (e.g., age-related macular degeneration) is also needed to confirm or refute our hypotheses implicating specific structural networks and remapping in visual hallucinations.

The patient presents with a benign subarachnoid cyst at the occipital pole (Figure 3.1a). The cyst impinges on deeper occipital and cerebellar structures, and its location is sufficiently far removed that we would not expect it to directly affect the reconstruction of white matter tracts in this study. Therefore, the cyst would not account for the atypical anatomy of these tracts. Our results continue to show clear disturbance to white matter tracts in regions that are far from the cyst (e.g., Figure 3.2b).

Our tractography findings in the patient may also be influenced by diffusion properties of the lesion, for example, diffusion values within the lesion may be outside of the probabilistic tractography thresholds. A greater number of streamlines (tracts) can occur in probabilistic tractography in cases of Wallerian degeneration, where intact pathways with higher anisotropy will show a greater number of streamlines than the damaged pathways (Jones, 2010). However, the probabilistic tractography approaches used in this study (multi-fibre and a priori regions of interest) are shown to track reliably (Behrens et al., 2007; Dyrby et al., 2007), are fairly accurate in cases of crossing fibres, and can track through areas of low FA (Jones, 2010) such as degeneration of microstructure following stroke and in artefacts (Behrens et al., 2003; Jones, Travis, Eden, Pierpaoli, & Basser, 2005). It is important to clarify that probabilistic tractography does not indicate the strength of connectivity but only estimates the probability (Jones, 2010).

Tractography results compared with post-mortem dissection show DTI based tractography to be reliable (Lawes et al., 2008). Further, changes in diffusion tensor indices in our patient cannot simply be interpreted as compromised microstructure of white matter, e.g., specific to axonal changes or neurodegeneration, etc. Interpretation of diffusion indices is uncertain when other factors such as glial cells or crossing fibres of similar density may contribute to water diffusion (Jbabdi, Behrens, & Smith, 2010). However, we can be more certain that axonal loss has occurred from known Wallerian degeneration in stroke, and accordingly the degeneration of neurons.

Although we are cognisant that this is a single-case study and acknowledge that this case report using DTI is speculative, we have attempted to constrain the methods to the best of our ability by comparing to an age-matched healthy control group, as well as comparing intra-individual tracts between contralesional and ipsilesional hemispheres, and previous fMRI data to strengthen the validity of the current findings. Further, as we are unable to acquire longitudinal data in the patient, we can only speculate as to the nature of the tracts with respect to regeneration and reorganisation.

Conclusion

In short, our results point towards interruption of specific white matter tracts (networks) and cortical remapping as the root of disorganised functional activity in the patient that leads to the continued perception of visual hallucinations. Cortical reorganisation may offer explanation for chronic visual hallucinations differentiating this case from the more common reports of acute visual hallucinations (Manford & Andermann, 1998; Vaphiades et al., 1996). The extent of structural reorganisation in our patient likely explains why rTMS did not produce a more sustained mitigatory response in that long-term aberrant connectivity persists and is not easily

overcome with temporary neuromodulation. Diffusion imaging and fibre tractography combined with fMRI in future studies will provide a more accurate visualisation of plasticity following visual pathway damage associated with visual hallucinations in order to ascertain treatment modalities directed at improving functional outcome. To maximise functional recovery and prevent continued abnormal neural processing, it is likely that neuromodulatory intervention (e.g., rTMS) needs to be applied much earlier post-injury within the plasticity window for recovery (Kasten et al., 1998; Pinter & Brainin, 2013) before more permanent aberrant white matter connectivity changes occur.

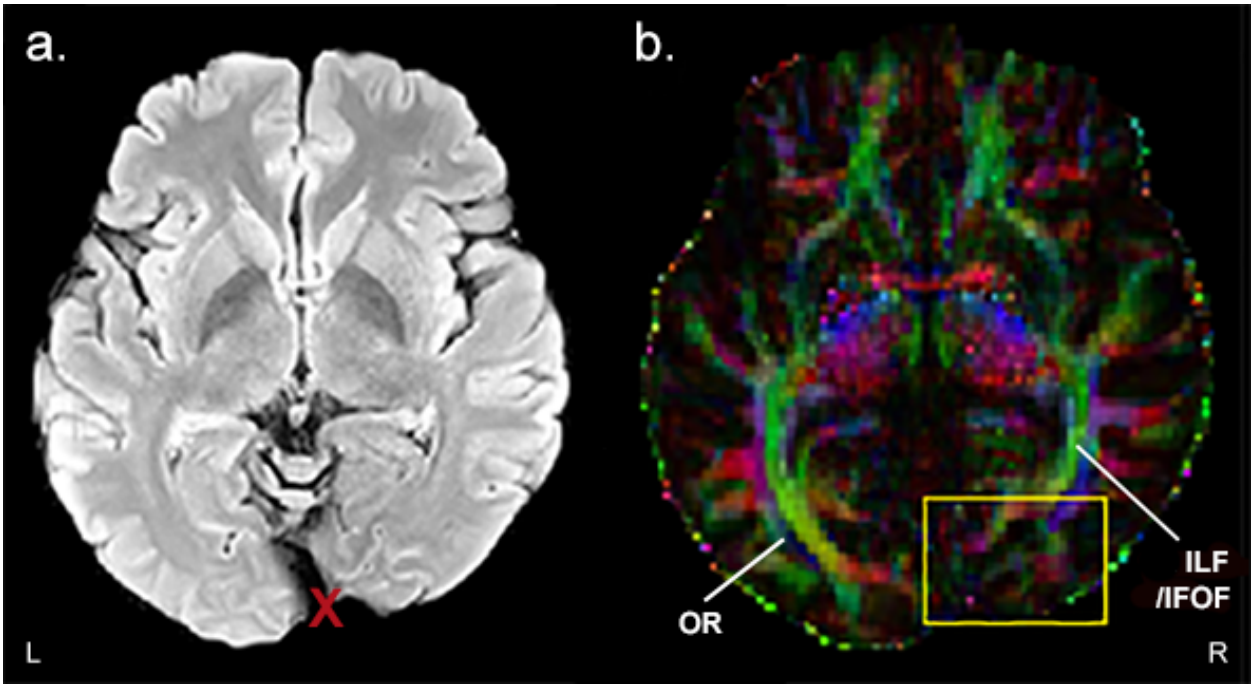

Figure 3.1. Diffusion images for the patient. (a) T2-weighted image shows no obvious lesion 2.5 years after occipital stroke. 'X' marks the location of a benign subarachnoid cyst. (b) Diffusion tensor image of a colour-coded FA map for the patient. Reduced anisotropy is observed at the lesion site (yellow box) and shows disruption in diffusivity at the right inferior longitudinal fasciculus (ILF)/inferior fronto-occipital fasciculus (IFOF), which merge with the optic radiations (OR) that are also disrupted. Red represents fibres crossing left–right, green represents fibres in the posterior–anterior direction, and blue represents fibres in the inferior–superior direction. Average MNI coordinates of lesion site: x = 15, y = -68, z = 5. L = left; R = right.

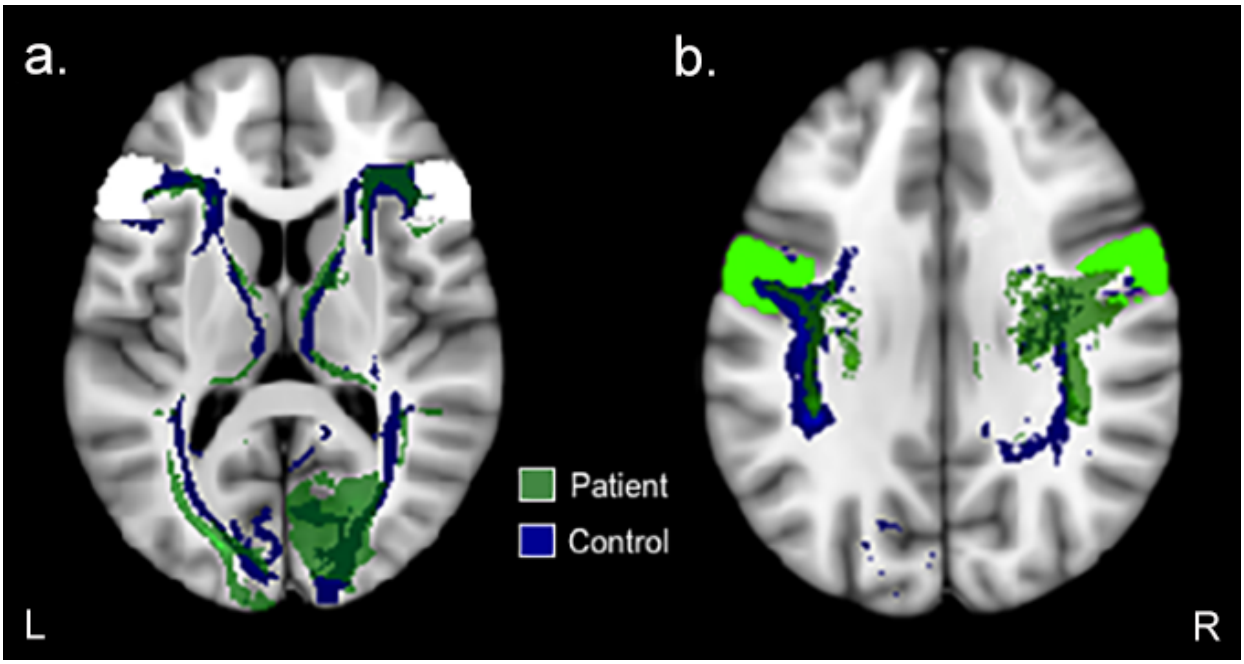

Figure 3.2. Probabilistic fibre tractography for intrahemispheric tracts seeded from the visual cortex to: (a) inferior frontal gyrus (white mask), and (b) precentral gyrus (lime green mask). Only one control example is presented here, all other controls are presented in Appendix A (Figures A1–A2, respectively). See Figure 3.5 for an example of the visual cortex mask (red mask). L = left (contralesional in the patient); R = right (ipsilesional in the patient).

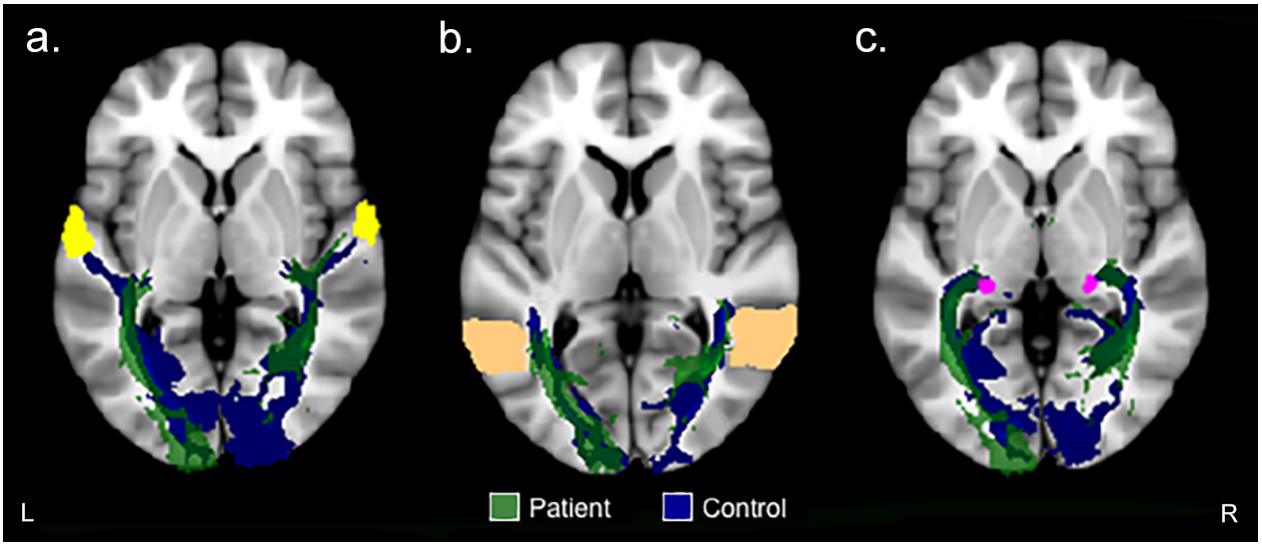

Figure 3.3. Probabilistic fibre tractography for intrahemispheric tracts seeded from the visual cortex to: (a) superior temporal gyrus (yellow mask), (b) middle temporo-occipital gyrus (peach mask), and (c) lateral geniculate body (pink mask). Only one control example is presented here, all other controls are presented in Appendix A (Figures A3–A5). See Figure 3.5 for an example of the visual cortex mask (red mask). L = left (contralesional in the patient); R = right (ipsilesional in the patient).

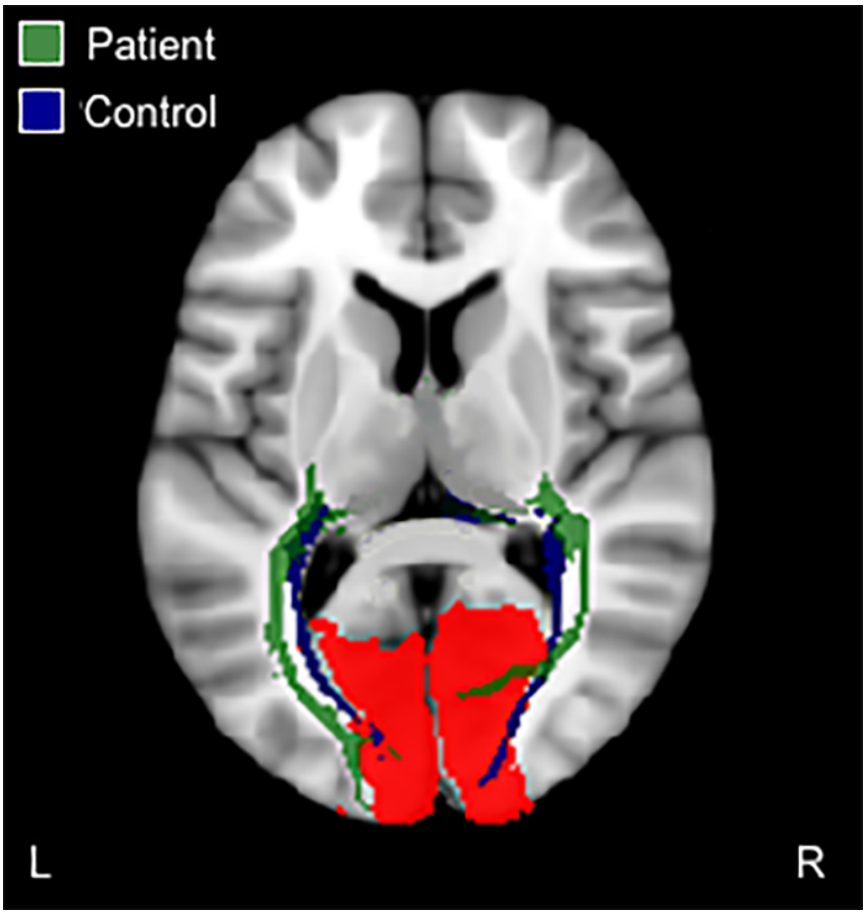

Figure 3.4. Probabilistic fibre tractography of the optic radiations. Tracts were seeded from the lateral geniculate body to the visual cortex (red mask). Only one control example is presented here, all other controls are presented in Appendix A (Figure A6). See Figure 3.3c for an example of the lateral geniculate body mask (pink mask). L = left (contralesional in the patient); R = right (ipsilesional in the patient).

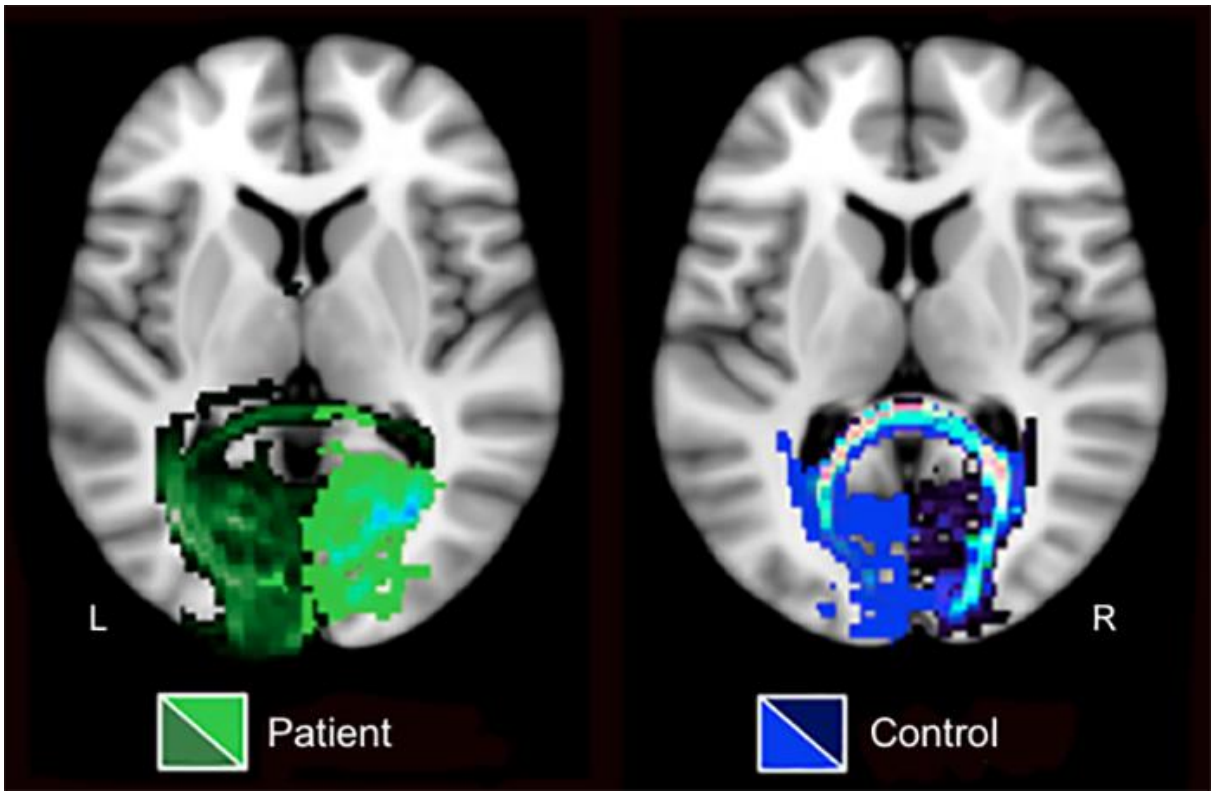

Figure 3.5. Probabilistic fibre tractography of interhemispheric connections between visual cortices. In the patient, tracts seeded from the ipsilesional (right) hemisphere (light green tracts) do not cross the midline to terminate in the contralesional (left) hemisphere, while contralesional to ipsilesional (dark green tracts) interhemispheric tracts do. In controls, tracts seeded from the right visual cortex (dark blue tracts) do cross the midline to connect with the left visual cortex, and vice versa (blue tracts), resulting in overlapping interhemispheric connections (light blue and pink tracts). Only one control example is presented here, all other controls are presented in Appendix A (Figure A7). L = left; R = right.

Table 3.1.

Diffusion Tensor Indices for Major White Matter Tracts

White matter tracts	FA		MD (x10^{-3})		AD (x10^{-3})		RD (x10^{-3})	
	Controls	Patient	Controls	Patient	Controls	Patient	Controls	Patient
R ATR	0.508 ± 0.008	0.501	0.692 ± 0.007	0.693	1.102 ± 0.008	1.099	0.487 ± 0.008	0.490
L ATR	0.513 ± 0.006	0.484 ↓	0.695 ± 0.008	0.689	1.108 ± 0.014	1.073	0.489 ± 0.006	0.497
R cCG	0.574 ± 0.014	0.625	0.671 ± 0.012	0.676	1.136 ± 0.023	1.221	0.438 ± 0.014	0.403
L cCG	0.607 ± 0.013	0.628	0.689 ± 0.011	0.688	1.221 ± 0.026	1.247	0.424 ± 0.012	0.409
R cH	0.588 ± 0.026	0.551	0.558 ± 0.024	0.637	0.928 ± 0.032	1.049	0.373 ± 0.025	0.432
L cH	0.588 ± 0.021	0.546	0.594 ± 0.021	0.593	1.014 ± 0.030	0.971	0.384 ± 0.022	0.404
R CT	0.626 ± 0.006	0.608	0.664 ± 0.008	0.670	1.197 ± 0.012	1.179	0.397 ± 0.007	0.415
L CT	0.633 ± 0.005	0.612 ↓	0.663 ± 0.009	0.673	1.202 ± 0.019	1.195	0.387 ± 0.004	0.412 ↑
FMa	0.685 ± 0.009	0.675	0.718 ± 0.008	0.726	1.423 ± 0.010	1.410	0.366 ± 0.011	0.383
FMi	0.570 ± 0.001	0.564	0.718 ± 0.008	0.729	1.249 ± 0.009	1.261	0.452 ± 0.010	0.463
R IFOF	0.562 ± 0.012	0.530	0.726 ± 0.008	0.751	1.236 ± 0.008	1.240	0.471 ± 0.013	0.506
L IFOF	0.561 ± 0.009	0.548	0.750 ± 0.007	0.735	1.280 ± 0.008	1.240 ↓	0.486 ± 0.010	0.482
R ILF	0.562 ± 0.011	0.517 ↓	0.724 ± 0.007	0.737	1.229 ± 0.009	1.240 ↑	0.471 ± 0.011	0.509
L ILF	0.549 ± 0.008	0.555	0.748 ± 0.008	0.727	1.265 ± 0.009	1.240	0.490 ± 0.009	0.471
R SLF	0.535 ± 0.008	0.497 ↓	0.686 ± 0.008	0.689	1.118 ± 0.011	1.080	0.468 ± 0.007	0.494
L SLF	0.516 ± 0.006	0.490 ↓	0.716 ± 0.007	0.714	1.146 ± 0.007	1.108 ↓	0.501 ± 0.008	0.518
R tSLF	0.586 ± 0.010	0.539 ↓	0.672 ± 0.009	0.683	1.149 ± 0.013	1.116	0.433 ± 0.011	0.467
L tSLF	0.557 ± 0.007	0.532	0.716 ± 0.007	0.719	1.193 ± 0.007	1.159 ↓	0.478 ± 0.009	0.499
R UF	0.518 ± 0.015	0.498	0.736 ± 0.011	0.734	1.206 ± 0.018	1.165	0.502 ± 0.015	0.519
L UF	0.514 ± 0.012	0.487	0.736 ± 0.008	0.730	1.192 ± 0.012	1.172	0.507 ± 0.011	0.508

Note. The columns list (from left to right) the major white matter tracts and their associated diffusion tensor indices for controls and the patient. Data are presented as mean (± S*EM*) control and single patient values. R = right; L = left; ATR = anterior thalamic radiation; cCG = cingulum - cingulate gyrus; cH = cingulum - hippocampus; CT = corticospinal tract; FMa = forceps major; FMi = forceps minor; IFOF = inferior fronto-occipital fasciculus; ILF = inferior longitudinal fasciculus; SLF = superior longitudinal fasciculus; tSLF = temporal part of superior longitudinal fasciculus; UF = uncinate fasciculus. Arrows indicate significant increase/decrease in patient's diffusion tensor index relative to controls (black arrows represent $p < .1$; red arrows represent $p < .05$).

CHAPTER 4

MODULATING VISUAL CORTEX γ-AMINOBUTYRIC ACID AND GLUTAMATE USING LOW-FREQUENCY REPETITIVE TRANSCRANIAL MAGNETIC STIMULATION

Preface

Neural plasticity is key in rehabilitation and recovery of function; thus, effective therapeutic strategies must be capable of modulating plasticity. Glutamate- and GABA-mediated changes in the balance between excitation and inhibition are prominent features in visual cortical plasticity. Particularly, reduced GABAergic inhibition facilitates synaptic plasticity. We investigated the effects of low-frequency (1 Hz) rTMS to the visual cortex on altering levels of neurotransmitters GABA and glutamate to determine the therapeutic potential of 1 Hz rTMS for visual-related disorders. Two rTMS regimes commonly used in clinical applications were investigated: participants received rTMS to the visual cortex either in a single 20 min session or five accelerated 20 min sessions. ^{1}H MRS for in vivo quantification of GABA (assessed via GABA+) and glutamate (assessed via Glx) concentrations was performed pre- and post-rTMS. GABA+ and Glx concentrations were unaltered following a single session of rTMS to the visual cortex. One day of accelerated rTMS significantly reduced GABA+ concentration lasting for up to 24 hr, with levels returning to baseline by 1-week post-rTMS. These findings demonstrate that accelerated rTMS to the visual cortex has greater potential for approaches targeting plasticity or in cases presenting with altered GABAergic responses with clinical translation for treatment in visual disorders. Notably, results provide preliminary insight into a critical window of plasticity with accelerated rTMS (e.g., 24 hr) in which adjunct therapies may offer better functional outcome.

A valuable therapeutic application of low-frequency rTMS to the visual cortex is to modulate disruptive visual hallucinations that are prevalent following visual pathway damage (Chapter 2; Merabet et al., 2003). Other forms of noninvasive brain stimulation (e.g., tDCS) have been used to promote vision restoration in visual field loss (for a review, see Alber, Cardoso, & Nafee, 2015). The desired neuromodulatory effect will largely depend on the stimulation technique and its underlying neural mechanisms (e.g., rTMS versus tDCS), altered mechanisms associated with the pathophysiology, and responsiveness of the cortical/subcortical structure in question. Despite the popular use of rTMS as a research and therapeutic tool (for reviews, see Chen et al., 2008; Thut & Pasucual-Leone, 2010; Wasserman & Lisanby, 2001), its potential to modulate neurobiochemical responses in the visual cortex, and hence its value as a therapeutic neuromodulation technique in visual-related disorders, is under-investigated.

Glutamate and GABA, key excitatory and inhibitory neurotransmitters in the mammalian brain, respectively, modulate the induction of LTP and LTD (for a review, see Lüscher & Malenka, 2012). Additionally, glutamine acts an important precursor in the glutamate/GABA-glutamine cycle (Bak, Schousboe, & Waagepetersen, 2006). rTMS can exert excitatory or inhibitory cortical effects at the stimulated area in non-visual cortical regions via glutamate and GABA receptor activity (Michael et al., 2003; Stagg et al., 2009b; Yue, Xiao-Lin, & Tao, 2009). Alterations in the delicate homeostatic balance between these neurotransmitters have significant implications in various disorders. For example, with relevance to visual disorders, a blockade of GABA and a resultant increase in neural firing is thought to underlie visual hallucinations (Manford & Andermann, 1998). Reduced GABA and unaffected glutamate levels have also been shown to promote visual cortical plasticity and improve visual function in amblyopia (Vetencourt et al., 2008). In order to advance the application of noninvasive brain stimulation to

target visual-related disorders, we sought to determine the ability of low-frequency (1 Hz) rTMS on altering visual cortical GABA (assessed via GABA+, the combined concentration of GABA and macromolecules) and glutamate (assessed via Glx, the combined concentration of glutamate and glutamine) levels in healthy control participants. Noninvasive in vivo quantification of visual cortex GABA+ and Glx concentrations were acquired using ^{1}H MRS. Knowledge of effects in healthy controls is desirable to determine underlying neurochemical mechanisms prior to translation for visual-related therapeutic application targeted at GABAergic and glutamatergic activity.

In addition, the most efficient stimulation protocol for different stimulation techniques is under question. In clinical applications, two alternative rTMS regimes are established: a single session or accelerated sessions applied in a single day over consecutive days. Accelerated (also termed within-session) stimulation consists of multiple sessions within a day, and significantly reduces the number of days/weeks of stimulation compared with single session rTMS. We tested a shorter schedule of these two regimes on the visual cortex. The first protocol consisted of a single 20 min session of 1 Hz rTMS to the visual cortex. Single sessions of rTMS have been applied over consecutive days for therapeutic application in visual-related disorders (e.g., Fumal et al., 2006; Rafique et al., 2016) and non-visual disorders (e.g., Dunner et al., 2014; Liepert et al., 2000a; Speer et al., 2000). The second accelerated protocol consisted of five consecutive 20 min sessions of 1 Hz rTMS separated by ~15 min in a single day. Intervals of 10–20 min in accelerated stimulation are considered to produce longer lasting effects (for a review, see Goldsworthy et al., 2015) compared with shorter intervals, e.g., 3 min (Monte-Silva et al., 2010) or 5 min (Bastani & Jaberzadeh, 2014). Advances in therapeutic use of rTMS in non-visual disorders demonstrate that accelerated rTMS produces more cumulative, stable, and longer-

lasting effects than single daily sessions over consecutive days/weeks (Goldsworthy et al., 2014; Holtzheimer et al., 2010). The effect of accelerated rTMS in visual disorders remains unknown. Accelerated rTMS additionally has better compliance in clinical settings due to the considerably reduced number of visits, for example, five accelerated sessions in a single day is comparable to a single daily session applied over five consecutive days. We have previously obtained a cumulative effect in modulating visual hallucinations following occipital stroke with a 30 min session of 1 Hz rTMS to the visual cortex repeated for 5 consecutive days (Chapter 2; Rafique et al., 2016). We considered five consecutive 30 min sessions taxing on participants in the accelerated protocol, thus, in the present study we opted for a minimum of 20 min of stimulation since it is more effective than shorter application times and reduces inter-individual variability (Aydin-Abidin, Moliadze, Eysel, & Funke, 2006).

Our focus was also to continue and refine our previous work using rTMS to modulate disruptive visual hallucinations (Chapter 2; Rafique et al., 2016, 2018) that prevalently occur following visual pathway damage (Baier et al., 2010; Gordon, 2016). Visual hallucinations are associated with increased vividness of visual imagery and a weak ability to distinguish real perception from mental imagery (Böker, Hijman, Kahn, & Haan, 2000; Mintz & Alpert, 1972). The neural substrates of visual imagery are similar to those of visual perception (Ishai & Sagi, 1995; Kosslyn, Thompson, & Alpert, 1997). Visual imagery critically depends on neural activity in V1 and is related to perception and memory that may facilitate cognitive performance (Kosslyn et al., 1999). Therefore, we also assessed the effects of the two alternative low-frequency rTMS regimes on vividness of visual imagery and predisposition to visual hallucinations, and their relationship with visual cortical excitability. Knowledge of rTMS effects on these aspects provides crucial information to inform recommended therapy in

disorders presenting with visual hallucinations (e.g., visual pathway damage, schizophrenia, Parkinson's disease; Burke, 2002; Manford & Anderson, 1998, Yoon et al., 2010). As far as we are aware, we are the first to investigate accelerated rTMS with a low-frequency protocol and its application to the visual cortex. To ensure safe and effective use of accelerated rTMS to the visual cortex, we also considered it necessary to assess adverse effects, including effects on basic cognitive function.

Methods

This study was approved by York University's Office of Research Ethics. All individuals gave informed written consent.

Participants

Sixteen healthy participants were recruited for the study ($M_{age} \pm SEM = 25.15 \pm 1.21$ years; 10 males/six females). All participants were right-handed, with normal or corrected-to-normal vision (> 0.04 logMAR; stereoacuity ≥ 50"), and no known contraindications to TMS and MRI. We recruited participants with no known underlying medical conditions, and no history of neurological or psychological disorders. Further, due to interactions with metabolite receptors and/or TMS mechanisms, we recruited participants that were not currently taking any medications (Stell, Brickley, Tang, Farrant, & Mody, 2003) including hormonal contraceptives (Kaore et al., 2012; Smith, Adams, Schmidt, Rubinow, & Wassermann, 2002b), with no history of frequent or chronic migraines (Bohotin et al., 2002; Russo et al., 2005), no history of alcohol/substance dependence, and were non-smokers (Epperson et al., 2005). We additionally asked that participants did not consume alcohol within 48 hr prior to each visit due to interactions with metabolites (Lobo & Harris, 2008). Participants received monetary compensation for their participation ($10 CAD/hr).

Experimental Design Overview

Participants underwent pre-rTMS (baseline) vision assessments and questionnaires, MRS, and PT measures. In a separate follow-up visit, participants received 1 Hz rTMS to the visual cortex (V1) at the individual PT, either in a (1) single 20 min session of rTMS, or (2) five accelerated 20 min sessions of rTMS (separated by intervals of ~15 min). MRS was repeated immediately following cessation of rTMS in both groups. MRS was further performed (1) 1 hr post-rTMS in the single rTMS group, and (2) 24 hr and 1-week post-rTMS in the accelerated rTMS group. Vision assessments and questionnaires were repeated at follow-up visits.

Vision Assessments, Cognitive and Imagery Questionnaires, and Adverse Effects

Standard visual testing was conducted to ensure normal visual status. Monocular and binocular visual acuities were measured using the standardised ETDRS vision chart (Precision Vision, La Salle, IL), stereoacuity was measured using the Titmus circles test (Stereo Optical Company Inc., Chicago, IL), and colour vision was assessed using the Ishihara test (Kanehara Trading Inc., Tokyo, Japan). Ocular muscle status involved assessment with the cover test (distance and near) and near point of convergence.

To ensure normal cognitive status, we administered the Montreal Cognitive Assessment (MoCA, v7.1–7.3; Appendix B), a brief 30-point cognitive screening test to detect mild cognitive impairment (Nasreddine et al., 2005). MoCA evaluates attention, concentration, working memory, short-term memory, delayed recall, language, visuospatial, orientation, and executive function. A different version of MoCA was administered at each follow-up visit.

Vividness of visual imagery was measured using the Vividness of Visual Imagery Questionnaire (VVIQ; Appendix C), a 15-item questionnaire (Marks, 1973). VVIQ was performed initially with eyes open and then repeated with eyes closed. We reversed the 5-point

rating scale, so that 1 = *no image at all, you only know that you are thinking of an object*, and 5 = *perfectly clear and as vivid as normal vision*, which provides a more intuitive scale.

Unusual positive perceptual experiences were assessed using a revised Launay-Slade Hallucination Scale (LSHS; Appendix D), a 16-item questionnaire. The LSHS measures predispositions to hallucinations in healthy and clinical populations (Launay & Slade, 1981; revised by Morrison, Wells, & Nothard, 2000). Questions were rated on a 4-point scale to measure frequency of the hallucinatory event (1 = *never*, 2 = *sometimes*, 3 = *often*, 4 = *almost always*).

Further, we asked participants to report changes in mood, concentration, cognition, sensory disruption (e.g., visual or hearing changes), as well as headaches, neck pain, or any other symptoms following rTMS. Adverse effects were reported on a five-point scale (1 = *no symptoms/change*, 2 = *minimal symptoms/change*, 3 = *slight symptoms/change*, 4 = *moderate symptoms/change*, 5 = *significant symptoms/change*).

We repeated all vision assessments and questionnaires at follow-up visits to assess any changes with rTMS, and for a more complete representation of longer-term effects of 1 Hz rTMS to the visual cortex.

Magnetic Resonance Imaging

Anatomical and ^{1}H MRS data were acquired with a 3T Siemens Magnetom® Tim Trio magnetic resonance scanner, with a 32-channel high-resolution brain array coil (Siemens, Erlangen, Germany). Head motion was minimised with the placement of soft pads holding the participant's head in place. Imaging was acquired at rest in a dark room, and participants were instructed to keep their eyes closed throughout.

Anatomical images were acquired first to allow placement of the MRS volume-of-interest (VOI) using a T1-weighted MPRAGE imaging sequence (number of slices = 192; in-plane resolution = 1 x 1 mm; slice thickness = 1 mm; imaging matrix = 256 x 256; TR = 2300 ms; TE = 2.62 ms; TI = 900 ms; flip angle = 9^{o}; FoV = 256 mm; acquisition time = ~5 min).

Using the anatomical images, MRS was acquired from a single 2.5 x 2.5 x 2.5 cm^3 VOI positioned medially in the visual cortex (V1). The VOI was positioned as far back within the posterior region of the occipital pole, centred on the calcarine sulcus, and avoided non-brain tissue (including cerebrospinal fluid and the sagittal sinus) to minimise macromolecule contamination. The lower edge followed the cortical surface and was aligned alongside the cerebellar tentorium (Figure 4.1a-b). The VOI position was recorded relative to anatomical landmarks in all three dimensions (sagittal, coronal, and transverse) using screenshots, and used as a reference for subsequent acquisitions. In two participants, because of a relatively small occipital lobe, the VOI had to be placed further supero-anteriorly, and may not have been constrained fully to the occipital lobe. The use of a smaller VOI was not desirable since it would reduce the signal-to-noise ratio (SNR) (for a review, see Mullins et al., 2014). ^{1}H MR spectra were obtained using Mescher-Garwood point resolved spectroscopy (MEGA-PRESS), a J-coupled difference editing technique (Mescher, Merkle, Kirsch, Garwood, & Gruetter, 1998), provided by Siemens as a work-in-progress (WIP) sequence (TR = 1500 ms; TE = 68 ms; spectral bandwidth = 1500 Hz; 1024 data points with water suppression yielding 512 averages; acquisition time = ~13 min). The MEGA-PRESS sequence provides reliable detection of GABA and other brain metabolites (Mullins et al., 2014; Puts & Edden, 2012). Siemens standard 3D automated shimming, followed by manual shimming were performed prior to each acquisition. During odd-numbered (‘ON resonance’) acquisitions, a frequency selective Gaussian inversion

pulse, and a chemical shift selective suppression (CHESS) water suppression band at 4.7 parts per million (ppm) of proton frequency were irradiated at 1.9 ppm. During even-numbered ('OFF resonance') acquisitions, the same pulse was applied symmetrically to the opposite side of the water spectrum at 7.5 ppm. The difference between the 'ON' and 'OFF' edited spectra provides a resulting spectrum retaining only peaks affected by the editing pulses: the GABA signal peak at 3.02 ppm, a combined glutamate and glutamine (Glx) signal peak at 3.75–3.8 ppm, and macromolecular peaks. The difference editing approach separates the GABA spectrum from overlapping spectra of more concentrated metabolites, in particular the creatine (Cr; an amino acid) peak at 3.0 ppm (Figure 4.1c, blue line). However, the GABA spectrum still contains contributions from other macromolecules (Aufhaus et al., 2014; Behar, Rothman, Spencer, & Petroff, 1994) and homocarnosine (a GABA derivative inhibitory neuromodulator; Rothman, Behar, Prichard, & Petroff, 1997), and is therefore referred to as GABA+ rather than GABA. Due to their similar chemical structure and overlapping spectra, glutamate (3.75 ppm) and its metabolic intermediate glutamine (3.76 ppm) cannot be differentiated using this method, and are therefore referred to as the composite measure Glx. An unsuppressed water reference was also acquired (16 averages, acquisition time = ~1 min).

Transcranial Magnetic Stimulation

A Magstim Rapid^2 Stimulator and a 70 mm diameter figure-of-eight coil (Magstim, Whitland, Wales, UK) were used to deliver stimulation pulses to the defined target site.

Phosphene threshold. Due to large inter-individual variability in visual cortical excitability thresholds (Stewart, Walsh, & Rothwell, 2001b), rTMS was delivered to the target stimulation site at the individual PT to minimise confounds in excitability and induce as consistent effects across participants. PT provides a well-established standard measure of visual

cortical excitability (Silvanto & Pascual-Leone, 2008). PT was measured using 1 Hz rTMS (7 s inter-pulse interval, 10 pulses) to the occipital lobe, and defined as the lowest stimulator output intensity (expressed as a percentage of maximal output) that evoked phosphenes in at least 50% of pulses (Elkin-Frankston et al., 2010). Participants were seated in a lit room wearing a blindfold with eyes closed and asked to report "yes/no/maybe" to phosphene elicitation following each TMS pulse. TMS was initially applied 2 cm lateral to the left of the inion, at an initial stimulator output intensity of 60%. The coil handle was held 90º to the left of the inion midline. If the participant reported a visual sensation, they were asked to describe the appearance (colour, shape, and size) and location to confirm phosphene perception. A "maybe" response was considered a negative response. If no visual sensation was reported, the TMS coil was repositioned in 1 cm steps above/below/lateral to the original site 2cm lateral to the inion, and pulses redelivered, to a maximum of 4 cm lateral and above/below the inion. If phosphenes were still not reported, the stimulator output intensity was increased by 5% and the process repeated. The process was repeated until a phosphene was perceived, and the stimulator output intensity was then refined in 1% steps. Blindfolds were removed every 10–15 min where necessary, for a minimum of 2 min, to prevent visual cortical excitability (Boroojerdi et al., 2000a).

Repetitive transcranial magnetic stimulation. Participants' anatomical MR images were reconstructed to 3D cortical surfaces using Brainsight software (Rogue Research, Montreal, QC, Canada). The target stimulation site corresponded to the centre of the MRS VOI ($M_{\text{depth}} \pm SEM = 38.631 \pm 0.74$ mm). The stimulation site was mapped on each participant's corresponding anatomical images in Brainsight by matching anatomical landmarks to the MRS VOI screenshots obtained at pre-rTMS MRS acquisition. The spatial relationship between the target stimulation site and reference points from the participant's head (tip of nose, nasion, right and left tragus)

were co-registered using a Polaris infrared tracking system (Northern Digital Instruments, Kitchener, ON, Canada). Movement of the coil with respect to the participant's head, and therefore the stimulation site, was visualised in real time using the infrared image-guided stereotaxy to ensure accurate positioning of the coil and targeted disruption of the stimulation site throughout rTMS. The TMS coil was held tangential to the surface of the skull to minimise coil-to-cortex distance, and to maximise the TMS effect (Ulmer & Jansen, 2010). Participants were seated in a comfortable position with an adjustable chin rest to limit head movement and provided with earplugs to prevent changes in auditory thresholds during rTMS (Rossi et al., 2009). Participants underwent 1 Hz rTMS (1 s inter-stimulus interval, 1200 pulses [20 min], 100% PT) at rest, either in a single 20 min session (n = 8, four male/four female) or five accelerated 20 min sessions separated by ~15 min intervals in a single day (n = 8, six male/two female). In the accelerated rTMS group, stereotaxic co-registration was assessed immediately prior to each new rTMS session and refined if necessary.

Experimental Procedure

To minimise diurnal variation of neuromodulators, including those implicated in TMS mechanisms (e.g., Ridding & Ziemann, 2010; Sale, Ridding, & Nordstrom, 2007), participants underwent testing at approximately the same time of day. We minimised the time difference between when the PT was obtained and rTMS was performed, while ensuring that MRI of different visits (pre- and post-rTMS) were also acquired at similar times irrespective of group allocation. Visit one (baseline/pre-rTMS): all participants initially underwent vision assessments and questionnaires to ensure inclusion criteria were met (including normal visual and cognitive status), followed by MRI, which commenced at ~13:00. PT was always obtained after pre-rTMS MRI, usually on the same day. Visit two (rTMS): offline 1 Hz rTMS was scheduled at least 4

days following pre-rTMS measures to prevent any lingering TMS effects from PT interacting with the rTMS protocol. rTMS commenced at ~13:40 for participants in the single rTMS session group, and at ~11:00 for participants in the accelerated rTMS sessions group. Participants were immediately transferred into the MRI scanner after rTMS ceased, and MRI acquisition commenced within 5 min of rTMS ending. In both groups, immediate post-rTMS MRI commenced at ~14:00. Participants in the single rTMS group underwent a further MRI 1 hr post-rTMS at ~15:00. We did not perform further follow-up visits in the single rTMS group based on previous research demonstrating that effects following ~15–20 min 1 Hz rTMS to the occipital cortex recover within 20–40 min (for a review, see Thut & Pasucal-Leone, 2010). We did not perform MRI 1 hr post-rTMS in the accelerated rTMS group because of fatigue following a long protocol (~5 hr), and since effects were expected to persist for > 24 hrs (for a review, see Goldsworthy et al., 2015). Visits three and four (follow-up for the accelerated rTMS group only): participants in the accelerated rTMS group were further followed-up at 24 hr, and 1-week post-rTMS, in both cases at ~1400.

MRI, vision assessments, and questionnaires were repeated at follow-up visits. Because participants were immediately transferred to the MRI following rTMS cessation, we could not perform vision assessments and questionnaires immediately post-rTMS in both groups; instead they were performed after immediate post-rTMS MRI acquisition. Therefore, for the single rTMS group, vision assessments and questionnaires were only followed up once, in-between immediate and 1 hr post-rTMS MRI acquisition. Figure 4.2 shows a diagram of the procedure for both rTMS groups.

Data Analyses

Magnetic resonance spectroscopy processing. MEGA-PRESS data were exported in RDA file format. Data were processed using the MATLAB-based tool Gannet (v3.0; http://www.gabamrs.com; Edden, Puts, Harris, Barker, & Evans, 2014). To filter out spectra of interest and improve the SNR, individual acquisitions underwent standard processing including frequency and phase correction, fast Fourier transform of time-domain acquired data to frequency-domain spectra, exponential line broadening, subtraction of the 'ON' and 'OFF' spectra resulting in the difference edited spectrum, and Gaussian model fitting of the GABA+ and Glx signal peaks. The amplitude of the peak for a given metabolite is related to the total number of molecules, and therefore represents the total concentration of that metabolite. GannetFit estimated the area under the edited GABA+, Glx, and Cr peaks, and the water signal from the unsuppressed water spectrum (Figure 4.1c). GannetCoRegister, which calls SPM8 (Statistical Parametric Mapping, Wellcome Centre for Human Neuroimaging, London, UK; http://www.fil.ion.ucl.ac.uk/spm), registered the MRS VOI to the corresponding anatomical images by creating a binary mask of the VOI with the same geometric parameters as the anatomical image. GannetSegment performed segmentation of the anatomical images, and determined tissue fractions (grey and white matter, and cerebrospinal fluid) within the VOI to provide cerebrospinal fluid-corrected GABA+ and Glx concentration estimates (in institutional units (i.u.)) using SPM8. Lastly, GannetQuantify accounted for tissue-related variance to provide tissue-corrected (relaxation- and alpha-corrected, voxel-average-normalised) GABA+ and Glx concentration estimates relative to water (i.u.) (Harris, Puts, & Edden, 2015). Gannet uses the standard deviation of the fitting residual, expressed as a percentage of the signal height, to

determine the fit error of the model, which reflects the SNR. All acquired spectra had a fit error < 5%.

Statistical analyses. All statistical analyses were performed using R statistical computing software (R Foundation for Statistical Computing, Vienna, Austria; www.R-project.org). Data were assessed for statistical assumptions and found to violate assumptions of parametric testing. We used multilevel (mixed) modelling and the maximum-likelihood estimation to analyse differences across multiple variables since it accounts for the repeated nature of the data, is highly flexible in dealing with varying intervals between measurements, and overcomes issues where assumptions of analysis of variance (ANOVA) are violated. Akaike's information criterion was used to measure the goodness of a fit of an estimated model, and the appropriate covariance structure. Where only two variables were compared, we conducted independent/dependent Yuen's *t*-tests (*YW*) for non-normally distributed data with 10% trimmed means. Effect sizes for Yuen (ES_{YW}) were calculated using 10% trimmed means, and additionally 500 bootstrapping samples for independent *t*-tests. Significance level was chosen as $p < .05$, and $p < .1$ for trending results, for all analyses. The rTMS groups were analysed separately due to different follow-up visit intervals (single rTMS group: pre-rTMS, immediate post-rTMS, 1 hr post-rTMS; accelerated rTMS group: pre-rTMS, immediate post-rTMS, 24 hr post-rTMS, 1-week post-rTMS).

To ensure consistent MRS VOI positioning in participants across visits, we assessed changes in tissue proportions within the VOI between visits using a multilevel model, with random effect for participant, and fixed effect for visit, for each rTMS group and for each tissue fraction (grey matter, white matter, cerebrospinal fluid) separately. To ensure tissue proportions

were consistent between rTMS groups, pre-rTMS tissue fractions were compared using Yuen's independent *t*-test.

The impact of single and accelerated rTMS sessions on visual cortex GABA+ and Glx concentrations were analysed using a multilevel model, with random effect for participant, and fixed effect for visits, for each metabolite and rTMS group separately. The effects of rTMS on all vision assessments and questionnaire responses (MoCA, VVIQ, and LSHS) were determined using Yuen's dependent *t*-test for the single rTMS group (pre-rTMS and immediate post-rTMS visits); and a multilevel model for the accelerated rTMS group (all visits), with random effect for participant and fixed effect for visits.

The relationship between PT (visual cortical excitability), pre-rTMS GABA+ and Glx concentrations, and pre-rTMS questionnaire responses was analysed using Kendall's tau (τ), a non-parametric correlation for non-normally distributed data.

Results

Tissue Fraction Analyses

Analyses of tissue fractions demonstrated consistent VOI positioning across visits. In the single rTMS group, there were no significant changes in tissue proportions across visits for white matter, $F(2, 14) = 2.61$, $p = .109$; and cerebrospinal fluid, $F(2, 14) = 1.839$, $p = .195$. Tissue proportions for grey matter trended significance across visits, $F(2, 14) = 3.147$, $p = .074$. In the accelerated rTMS group, there were no significant changes in tissue proportions across visits for grey matter, $F(3, 18) = .719$, $p = .554$; white matter, $F(3, 18) = .529$, $p = .668$; and cerebrospinal fluid, $F(3, 18) = .747$, $p = .538$. Based on pre-rTMS tissue proportions, there were no significant differences between the single and accelerated rTMS groups in grey matter, $YW(10.76) = .764$, p

= .462, ES_{YW} = .322; white matter, *YW*(10.9) = .442, *p* = .668, ES_{YW} = .223; and cerebrospinal fluid, *YW*(9.72) = .519, *p* = .615, ES_{YW} = .189.

Effect of Low-Frequency Repetitive Transcranial Magnetic Stimulation on GABA+ and Glx Concentrations

In the single rTMS group, there were no significant changes across visits in GABA+ concentration, *F*(2, 14) = .733, *p* = .498; and Glx concentration, *F*(2, 14) = .15, *p* = .862. In the accelerated rTMS group, there was a significant change in GABA+ concentration across visits, *F*(3, 21) = 5.446, *p* = .006. Pre-rTMS GABA+ concentration was significantly greater than immediate post-rTMS, *b* = - .285, *t*(21) = -2.203, *p* = .039; and showed a trend towards being significantly greater than 24 hr post-rTMS concentration, *b* = - .229, *t*(21) = -1.768, *p* = .092, in the accelerated rTMS group. Pre-rTMS GABA+ concentration was comparable with 1-week post-rTMS concentration, *b* = .178, *t*(21) = 1.372, *p* = .185. There were no significant changes across visits in the accelerated rTMS group for Glx concentration, *F*(3, 21) = .81, *p* = .503. Results for metabolite concentrations measured at each visit are presented in Figure 4.3.

Effect of Low-Frequency Repetitive Transcranial Magnetic Stimulation on Vision Assessments, Cognitive and Imagery Questionnaire Responses

For vision assessments, in the single rTMS group, there were no significant differences across visits for right eye visual acuity, *YW*(7) = - .424, *p* = .685, ES_{YW} = .009; left eye visual acuity, *YW*(7) = -1.286, *p* = .901, ES_{YW} = .002; and stereoacuity, *YW*(7) = 1, *p* = .351, ES_{YW} = .11. In the accelerated rTMS group, there were no significant differences across visits for right eye visual acuity, *F*(3, 21) = 1.629, *p* = .213; left eye visual acuity, *F*(3, 21) = .597, *p* = .624; and stereoacuity, *F*(3, 21) = 1.355, *p* = .284. In both rTMS groups, participants correctly identified all colour vision plates at all visits.

For questionnaire responses, in the single rTMS group, VVIQ with eyes closed was significantly greater at pre-rTMS compared with 1 hr post-rTMS, $YW(7) = 2.481$, $p = .042$, $ES_{YW} = .37$. There were no significant differences in the single rTMS group across visits for VVIQ with eyes open, $YW(7) = 0$, $p = 1$, $ES_{YW} = 0$; MoCA, $YW(7) = -.475$, $p = .649$, $ES_{YW} = .14$; and LSHS, $YW(7) = 1.764$, $p = .121$, $ES_{YW} = .16$. In the accelerated rTMS group, there was a significant difference in MoCA across visits, $F(3, 21) = 3.117$, $p = .048$; contrasts revealed a trend towards significance with a lower score pre-rTMS compared with 1-week post-rTMS, $b = .875$, $t(21) = 1.987$, $p = .06$. There were no significant differences in the accelerated rTMS group across visits for VVIQ with eyes open, $F(3, 21) = .944$, $p = .437$; VVIQ with eyes closed, $F(3, 21) = .232$, $p = .873$; and LSHS, $F(3, 21) = .684$, $p = .572$. Mean (± *SEM*) questionnaire measures are reported in Table 4.1. Participants' self-reported symptoms following rTMS are reported in Table 4.2.

Relationship Between Phosphene Threshold, GABA+, Glx, and Questionnaire Responses

There was a significant positive correlation between pre-rTMS GABA+ and Glx concentrations, $\tau = .68$, $p < .001$. PT was not significantly correlated with pre-rTMS measures of GABA+ concentration, $\tau = -.237$, $p = .206$; Glx concentration, $\tau = -.245$, $p = .19$; VVIQ with eyes open, $\tau = -.254$, $p = .175$; VVIQ with eyes closed, $\tau = -.017$, $p = .928$; or LSHS, $\tau = -.309$, $p = .109$. Pre-rTMS GABA+ concentration was not significantly correlated with corresponding visit measures of VVIQ with eyes open, $\tau = -.067$, $p = .718$; VVIQ with eyes closed, $\tau = -.136$, $p = .47$; and LSHS, $\tau = .219$, $p = .254$. Similarly, pre-rTMS Glx concentration was not significantly correlated with corresponding visit measures of VVIQ with eyes open, $\tau = -.092$, p

= .62; VVIQ with eyes closed, τ = - .093, p = .619; and LSHS, τ = .174, p = .362. Mean (± *SEM*) PT and questionnaire responses are reported in Table 4.1.

Discussion

A single 20 min session of low-frequency (1 Hz) rTMS (100% PT) to the visual cortex had no significant change on GABA+ or Glx concentrations compared with pre-rTMS levels. However, five accelerated sessions using the same stimulation parameters significantly reduced GABA+ concentration immediately following rTMS, with effects lasting up to 24 hr, and returning to baseline by 1-week post-rTMS. Despite a positive relationship between pre-rTMS GABA+ and Glx concentrations, there was no significant change in Glx concentration following accelerated rTMS compared with pre-rTMS levels, highlighting the differential effect of low-frequency rTMS.

Effect of Low-Frequency Repetitive Transcranial Magnetic Stimulation on Visual Cortical GABA+ and Glx Concentrations

According to traditional views on frequency-dependent rTMS effects, with a low-frequency (e.g., 1 Hz) rTMS protocol we may expect an "inhibitory" response (for reviews, see Hallett, 2007; Thut & Pascual-Leone, 2010), and accordingly an increase in GABA+ concentration following rTMS. We observed no change in GABA+ concentration following a single session of rTMS and instead a *decrease* in concentration following accelerated rTMS. In the motor cortex, sub-MT paired-pulse TMS suppresses motor cortex excitability by activating intracortical inhibitory circuits, while supra-MT intensity facilitates a response (Nakamura, Kitagawa, Kawaguchi, & Tsuji, 1997). Conversely, supra-MT low-frequency rTMS to the motor cortex does suppress motor evoked potentials (Chen et al., 1997). Therefore, in addition to the frequency, the intensity level relative to the excitability threshold (e.g., MT) influences excitation

or inhibition in the cortex. Our results are also in line with our previous patient study in which we used rTMS to ameliorate visual hallucinations that occurred as a consequence of occipital stroke (Chapter 2; Rafique et al., 2016). Although the rTMS protocol in our previous patient study used the classic multiday approach to rTMS, in which the patient underwent a single daily session of 1 Hz rTMS to the visual cortex over five consecutive days, we nonetheless observed an increase in functional activity at the stimulation site post-rTMS (and a corresponding decrease in hallucinations). Following the notion that low-frequency rTMS is simply inhibitory, we would expect a decrease in functional activity at the stimulation site in the patient. High doses of short trains of 1 Hz rTMS to the prefrontal cortex are reported to excite local and contralateral functional activity, with intensity-dependent increases with higher intensities, e g., ≥ 100% MT (Nahas et al., 2001). Consequently, sub-PT intensity rTMS in our study may have had the converse effect on GABA+ concentration. Similar intensity-dependent rTMS effects are also observed in regional cerebral blood flow. Low-frequency rTMS (1–2 Hz) at intensities above MT increases cerebral blood flow at the stimulation site in the motor cortex (Bohning et al., 1999; Fox et al., 1997), as well as modifying blood flow at local and distal regions with increasingly greater modulation observed for higher intensities (Speer et al., 2003). In converse, supra-MT high-frequency rTMS (5–10 Hz) decreases cerebral blood flow in the motor cortex (Paus et al., 1998; Siebner et al., 2000a).

We did not observe significant changes in Glx concentration in the visual cortex following low-frequency rTMS. Similarly, Stagg and colleagues (2009b) also report significant effects of inhibitory theta burst protocols of rTMS (continuous TBS) on MRS measured GABA but not Glx concentration in the motor cortex. Dose-dependent changes in Glx concentration are, however, seen with conventional high-frequency rTMS. A single 20 min session of 20 Hz rTMS

to the prefrontal cortex decreases Glx concentration. In contrast, single daily sessions of 20 Hz rTMS applied over five consecutive days does not affect Glx concentration at the stimulation site (prefrontal cortex), although a significant increase in Glx is observed in remote regions. These high-frequency rTMS effects are found to be dependent on pre-rTMS Glx levels, with lower concentrations pre-rTMS associated with a greater increase in Glx (Michael et al., 2003).

Relationship Between GABA+, Glx, and Visual Cortical Excitability

We observed no significant relationship between pre-rTMS GABA+/Glx concentrations and PT (visual cortical excitability) (Figure 4.4a), but a significant positive correlation between pre-rTMS GABA+ and Glx concentrations in the visual cortex. Terhune and colleagues (2015) report a strong negative correlation between PT and MRS measured glutamate concentration in the visual cortex, with lower PT associated with elevated glutamate concentration, and no correlation between GABA and glutamate. Although Terhune and colleagues report concentrations as ratios relative to Cr (to normalise data), we nonetheless fail to observe these relationships in our data using the same standard reference to Cr (Figure 4.4b). Variability in results between studies is likely attributed to differences in TMS parameters used to obtain PT, and MRS acquisition parameters. Furthermore, Terhune and colleagues measured PT following dark adaptation, which increases cortical excitability (Boroojerdi et al., 2000a). In the motor cortex at least, a significant positive correlation is also observed between MRS measured GABA and Glx relative to Cr (Tremblay et al., 2012). Additionally, as in the visual cortex, no direct relationship is observed between MRS measured GABA and TMS measures of cortical excitability ($GABA_A$ and $GABA_B$ receptor activity) in the motor cortex, suggesting that overall GABA concentration may not reflect specific synaptic activity, and hence excitability levels (Stagg et al., 2011c; Tremblay et al., 2012). Conversely, TMS measures of cortical excitability,

specifically $GABA_B$ receptor activity, in the motor cortex are positively correlated with MRS measured glutamate concentration (Tremblay et al., 2012). $GABA_B$ receptor mechanisms are instead mediated by glutamatergic activity (Chalifoux & Carter, 2011; Prout & Eisen, 1994), whereby a $GABA_B$ agonist has significant excitatory rather than inhibitory effects in the visual system (Luo, Wang, Su, Wu, & Chen, 2011). Moreover, a linear relationship is suggested between neuronal glucose oxidation and glutamate/glutamine cycling (Patel et al., 2004). These findings suggest that MRS metrics of glutamate relate to synaptic glutamatergic activity (Stagg & Nitsche, 2011). MRS measures of GABA instead are considered to represent the sum of inhibitory and excitatory activity ($GABA_A$ and $GABA_B$ receptor activity, respectively) across all cells affected by GABAergic modulation within the VOI (Rae, 2014). Therefore, an increase/decrease in MRS measured GABA concentration does not simply imply increased/deceased inhibition, respectively. Mechanisms underlying PT are not as well understood as MT, but GABAergic mechanisms are repeatedly implicated in PT (e.g., Boroojerdi, Prager, Muellbacher, & Cohen, 2000b; Mulleners et al., 2002). The use of a $GABA_A$ agonist is observed to increase PT, i.e., reduce cortical hyperexcitability in the visual cortex, in migraine patients with aura (Mulleners, Chronicle, Vredeveld, & Koehler, 2002). If phosphene induction via stimulation occurs via $GABA_A$ receptor activity, then collectively based on prior work, neither MRS measured GABA or glutamate levels would directly be associated with PT (visual cortical excitability).

Effect of Low-Frequency Repetitive Transcranial Magnetic Stimulation on Cognitive and Imagery Responses

Following accelerated rTMS, changes in cognitive scores measured with MoCA trended towards significance, with greater scores at 1-week post-rTMS compared with pre-rTMS.

Although GABA+ concentration did not show a significant change at 1-week post-rTMS, there was an increase relative to pre-rTMS, and this change in cognitive effect may be related. Or simply, the effect can be attributed to a learning effect—we employed all three MoCA versions, however, since there were four visits in the accelerated rTMS protocol, participants were tested on version one at pre-rTMS and 1-week post rTMS visits.

Following a single session of rTMS, VVIQ with eyes closed significantly decreased 1 hr post-rTMS compared with pre-rTMS, with no consistent change in GABA+/Glx concentration. It is possible that this effect is related to other mechanisms affected by a smaller dose of 1 Hz rTMS. Or perhaps, less likely, this effect may be due to mechanisms that only arise 1 hr post-rTMS since no change was detected immediately post-rTMS. Visual cortex activity and vividness of visual imagery show a trend for a positive correlation (Amedi, Malach, & Pascual-Leone, 2005), and 1 Hz rTMS to the occipital cortex impairs response time of visual imagery and perceptual versions of the same tasks (Kosslyn et al., 1999). Remarkably, there was no change in VVIQ following accelerated rTMS that may be due to adaptive processes or metaplasticity (Bocci et al., 2014; Lang et al., 2004). These findings on VVIQ may have important inferences for the differential effects of single and accelerated 1 Hz rTMS sessions.

Therapeutic Potential of Accelerated Low-Frequency Repetitive Transcranial Magnetic Stimulation to the Visual Cortex

The effect of accelerated 1 Hz rTMS to the visual cortex on reducing GABA+ concentration has valuable implications for cortical plasticity. Retinal and cortical lesions trigger visual cortical plasticity necessary for reorganisation and restitution of visual cortical function. Reorganisation is dependent on GABAergic modulation and associated LTP that enables nearby cells to adopt topographical representation of damaged cells and continued processing of the

involved region. There are major biochemical changes in adjacent deafferented synapses involving increased glutamatergic NMDA and decreased $GABA_A$ and $GABA_B$ response in the visual cortex (Eysel et al., 1999). Similarly, in stroke, during the acute phase of recovery, peri-infarct regions show diminished excitability associated with $GABA_B$ receptor activity (Clarkson, Huang, MacIsaac, Mody, & Carmichael, 2010). In the subacute stages of stroke, downregulation of GABA increases neuronal firing (Redecker, Wang, Fritschy, & Witte, 2002), thereby also increasing NMDA function that is integral to structural (Lee, Ueno, & Yamashita, 2011) and electrophysiological reorganisation, as well as reduced intracortical inhibition (Buchkremer-Ratzmann & Witte 1997; Liepert, Hamzei, Weiller, 2000b). Subacute GABA inhibition occurs not only in peri-infarct regions, but also in the contralesional hemisphere, and is related to improved motor skills in the nonparetic forelimb of stroke patients (Luke, Allred, & Jones, 2004). A continued widespread reduction of $GABA_A$ receptor activity, and associated excitability, persists for several months following cortical injury and is thought to facilitate plasticity changes via LTP and remapping of motor cortical representations (Carmichael, 2003; Neumann-Haefelin, Hagemann, & Witte, 1995). This rewiring underlies at least some recovery of function seen after stroke and is still maintained in the chronic stages of stroke recovery.

Pairing rTMS treatment with vision therapies (e.g., vision restoration therapy in visual field loss, patching treatment in amblyopia) within a critical window of plasticity (e.g., 24 hr for a single day of accelerated 1 Hz rTMS) may lead to more efficient recovery and requires further investigation. Adjunct therapies can provide a better method for improving connectivity of involved neuronal networks and for increasing synaptic efficiency, which permits changes in neuronal excitability and rewiring to restore function with longer-term effects (Liepert et al., 2000a; Pekna, Pekny, & Nilsson, 2012).

The use of 1 Hz rTMS may be preferable to other noninvasive brain stimulation techniques that have differing effects on MRS measured GABA/glutamate and likely plasticity. For example, continuous TBS (inhibitory TBS) to the motor cortex significantly increases MRS measured GABA, with no effect on Glx concentration, which is linked to LTD-like phenomena (Stagg et al., 2009b). Different stimulation techniques stimulate different populations or components of neurons to variable extents (e.g., Stagg et al., 2009a, 2011a). Further, metabolites are influenced by more than one biochemical pathway. Animal studies suggest that dopamine directly affects the excitability of GABAergic neurons, but also that modulation of dopamine occurs indirectly via GABA-mediated activity (for a review, see Pascual-Leone et al., 1998). These distinct effects have implications for the potential therapeutic use of stimulation paradigms where it may be clinically beneficial and more effective to use one paradigm over another. It is important to highlight that MRS quantifies overall local concentration of metabolites and does not provide insight into changes at the synapse/receptor level (for a review, see Stagg, Bachtiar, & Johansen-Berg, 2011b). As such, we can only speculate on the nature of changes in GABA+ concentration and take these factors into consideration when interpreting LTD/LTP like changes.

This study provides preliminary results for clinicians/researchers to determine appropriate responses to rTMS to the visual cortex on GABA and glutamate levels at the stimulation site by assessing any deviations in effects in patient populations compared with controls. Deviations in the expected response in patient populations can provide further valuable insight into underlying disease processes, the possibility to develop biomarkers for diagnosis, and information on whether the rTMS treatment is likely to be successful. Our results are from healthy control participants, and effects will indeed vary in patient populations, e.g., visual pathway damage, altered biochemical regulation in underlying medical conditions, interactions

with medications, etc. (Maeda, Keenan, Tormos, Topka, & Pasucal-Leone, 2000; Wassermann, 2002). We also do not expect the same results with accelerated rTMS applied over consecutive days as is used in protocols for therapeutic applications (e.g., 2–5 days). Instead, we would expect an augmented response in GABA+ concentration with higher doses of accelerated rTMS based on previous research (Goldsworthy et al., 2014; Holtzheimer et al., 2010), and perhaps a dissimilar effect on Glx concentration. Similarly, our differential results between single and accelerated rTMS sessions may be due to dose-dependent effects. It may be that single sessions over consecutive days can produce a similar effect, in which case one day of accelerated rTMS offers a more efficient protocol, or perhaps an opposite effect is observed with repeated doses of single sessions (e..g, Michael et al., 2003). The effect of single session and accelerated rTMS to the visual cortex over a greater number of days on GABA and glutamate mechanisms requires investigation. Knowledge of differential effects with a variety of protocols will enable modulation of a greater number of disorders presenting with variable pathophysiology. With longer applications of rTMS, there is greater potential of adverse effects on sensory and cognitive processing/responses, or self-reported effects. Adverse effects should be evaluated following repeated high doses of rTMS, and due to unpredictability of effects in disease states in patient populations.

Limitations

The sample size employed in this study is small; however, we minimised possible confounds (e.g., employing strict inclusion criteria to limit considerable inter-individual variability) to the best of our ability, and we observe significant changes despite a smaller sample size. The significant change in GABA+ concentration following accelerated rTMS is unlikely due to fluctuations as concentrations in the occipital cortex are consistent throughout the day

(Evans, McGonigle, & Edden, 2010), and stable for as much as 7 months (Near, Sandberg, Kumaragamage, & Blicher, 2014; O'Gorman, Michels, Edden, Murdoch, & Martin, 2011). It is important to note that we did not control for factors such as menstrual cycle effects (Harada, Kubo, Nose, Nishitani, & Matsuda, 2011) or cycle-linked disorders, which can cause changes in GABA receptors and neuronal function (for a review, see Bäckström et al., 2003; Epperson et al., 2002).

Due to MR set-up time, including VOI positioning and MRS shimming, and acquisition of anatomical images, there was a delay of ~20 min between the end of rTMS and the start of MRS acquisition that could not be avoided (MRS acquisition took an additional 13 min). Therefore, short-lived metabolite changes, especially following single session rTMS, may not be measurable. We did not consider the effect of rTMS on other metabolites as they were not supported by our acquisition protocols. Consequently, we cannot rule out effects of rTMS on other metabolites/biochemical pathways (Pascual-Leone et al., 1998) that may influence our results. Moreover, rTMS effects propagate from the stimulation site to remote regions (Rafique et al., 2015; Reithler et al., 2011), but because of the single voxel limit, we cannot effectively determine remote effects of rTMS on metabolite concentrations. Due to MRS technical constraints, acquisition of a second VOI would not commence for ~45 min following cessation of rTMS, and immediate or shorter-lasting measurable effects would be lost. Given that we cannot accurately localise rTMS effects, the MRS measured effect of rTMS may have been dampened by the spread of rTMS to regions outside of the VOI during acquisition, or the effect may be diluted from unaffected concentrations within the VOI.

The absence of significant rTMS effects on Glx concentration may be ascribed to the lower detection sensitivity compared with GABA using the MEGA-PRESS sequence (Henry,

Lauriat, Shanahan, Renshaw, & Jensen, 2011; Schubert, Gallinat, Seifert, & Rinneberg, 2004). The current sequence also cannot separate glutamate and glutamine spectra, thus, the composite value (Glx) may not accurately reflect sensitive changes in glutamate. Regardless, prior work suggests that Glx is primarily driven by the glutamate signal, as glutamate is found at ~10 times the concentration of glutamine in the brain (Stagg, 2014). There is potential for contamination of the edited signal with coedited macromolecular signals with the MEGA-PRESS sequence. Approaches to correct for macromolecules have their own significant limitations (Henry, Dautry, Hantraye, & Bloch, 2001; Rothman, Petroff, Behar, & Mattson, 1993), and we opted for the most common method to overcome macromolecule issues by reporting GABA+ concentrations. Nevertheless, variations in macromolecules between individuals are small compared with variations in GABA concentration (Hofmann, Slotboom, Boesch, & Kreis, 2001; Kreis, Slotboom, Hofmann, & Boesch, 2005; Mader et al., 2002), and so it is unlikely that this contamination affects interpretability of our observed effect in GABA+ concentration following accelerated rTMS. While GABA+ is also contaminated by homocarnosine, the in vivo concentration of homocarnosine is much lower than that of GABA (Govindaraju, Young, & Maudsley, 2000), thus, the effect on GABA+ concentration following accelerated rTMS is also less likely to be driven by homocarnosine.

Determining comparable tissue composition across visits is an indirect measure to demonstrate our consistent voxel positioning across visits. GABA concentrations are only weakly affected by voxel positioning in the occipital cortex, and as such, perfect voxel positioning is not critical (Near et al., 2014). Despite this reassurance, we remained critical in our voxel positioning to ensure as consistent positioning as possible between visits.

Conclusion

A single day of accelerated low-frequency (1 Hz) rTMS to the visual cortex at 100% PT significantly decreases GABA+ concentration in the visual cortex for at least 24 hours. The present approach and longer-term investigation of accelerated rTMS effects to the visual cortex has implications for developing treatment protocols in clinical vision applications involving altered GABAergic function. These findings have further significance for exploiting visual cortical plasticity and provide insight into a critical window of plasticity in which adjunct therapy would be most efficient for functional restoration and recovery. Future work should be directed at refining protocols and investigating accelerated 1 Hz rTMS protocols on the visual cortex in patients with visual-related disorders.

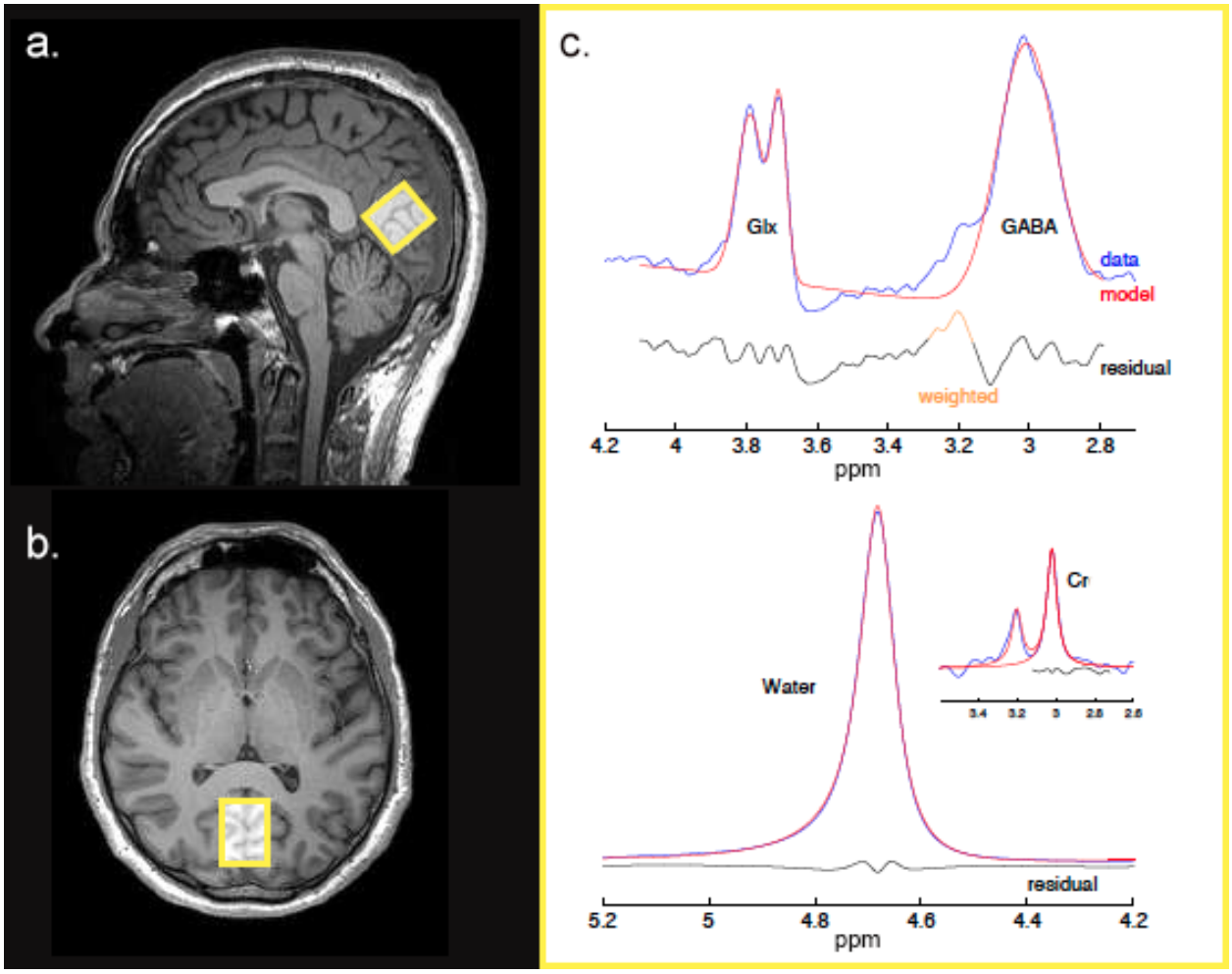

Figure 4.1. Proton (^{1}H) MR spectra acquired from the visual cortex. (a-b) Example of typical voxel placement in the occipital lobe on T1-weighted images for a single participant shown in sagittal and transverse planes, respectively. (c) Sample processing of the MEGA-PRESS difference edited spectrum (blue line) from the corresponding voxel using Gaussian fitting (red line) with Gannet (v3.0). Example shows typical signal peaks for GABA (3.02 ppm), Glx (3.75–3.8 ppm), Cr (3.0 ppm), and water (4.7 ppm) for a single participant.

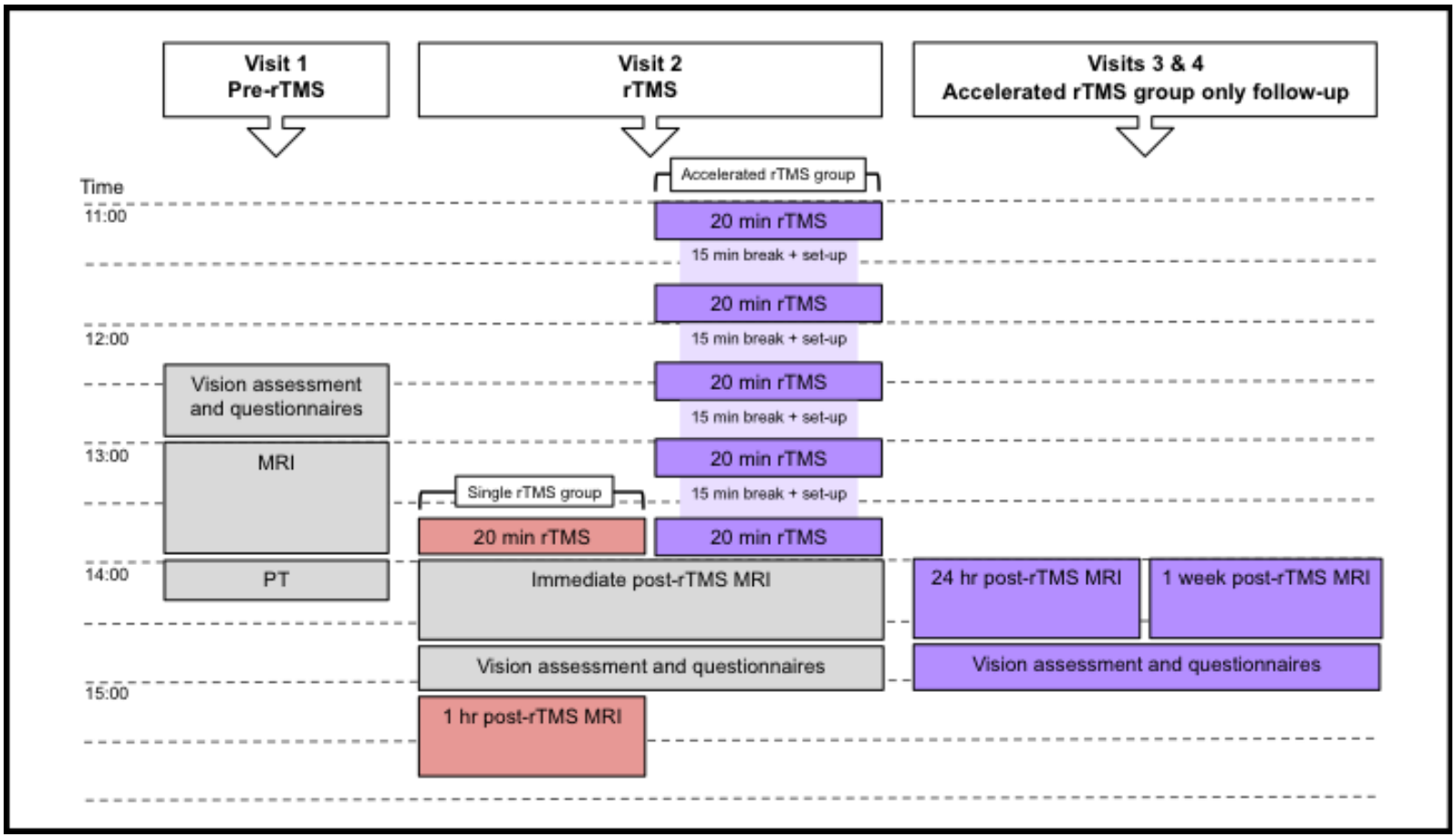

Figure 4.2. Diagram of the experimental procedure. All participants took part in procedures in grey, participants undergoing a single rTMS session took part in procedures in red, and participants who underwent accelerated rTMS took part in procedures in purple. Pre-rTMS (baseline) procedures took longer than follow-up visits as participants were provided with detailed instruction of procedures, and because of time involved in determining optimal positioning of the MRS voxel.

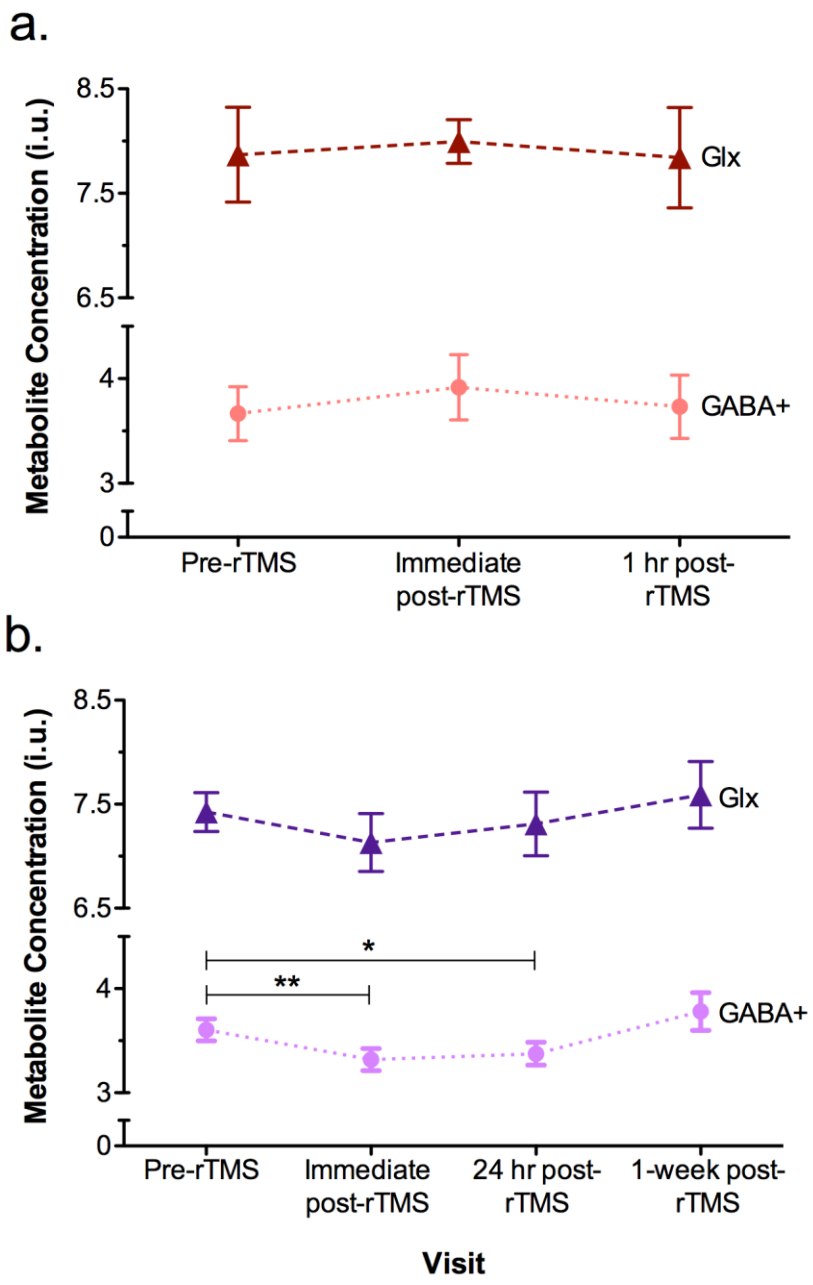

Figure 4.3. Mean GABA+ and Glx concentrations for all visits for the (a) single rTMS session group, and (b) accelerated rTMS sessions group. Error bars represent ± *SEM*. Triangle symbols represent Glx, and circles represent GABA+ concentrations.

* $p < .1$. ** $p < .05$.

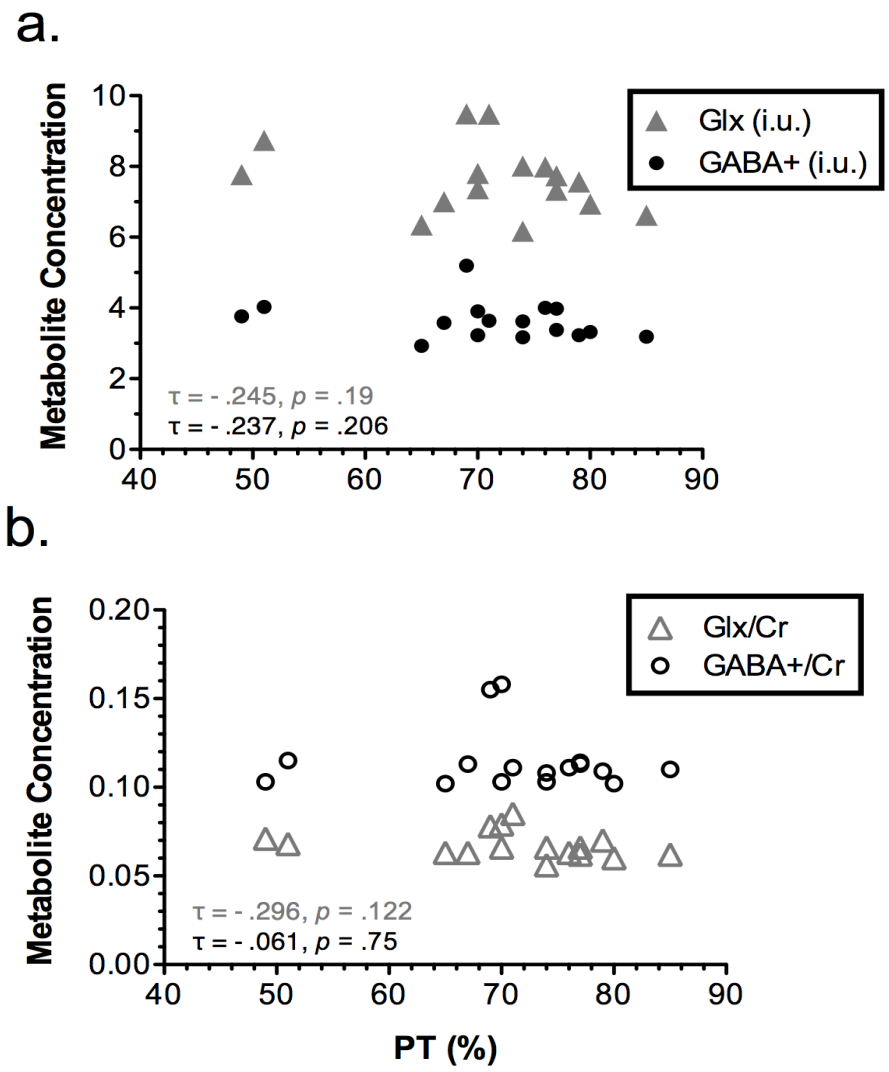

Figure 4.4. No significant relationship between visual cortical excitability (PT) and visual cortical GABA+/Glx expressed as (a) tissue-corrected concentrations (i.u.), and (b) normalised concentrations using integral ratios relative to Cr.

Table 4.1.

Group Characteristics and Questionnaire Responses Across Visits

Visit	Age (years)	PT (%)	MoCA	LSHS	VVIQ	
					eyes open	eyes closed
Single rTMS group	25.5 ± 2.25	68.625 ± 2.05				
Pre-rTMS			28.875 ± 0.55	22.38 ± 1.349	61.88 ± 3.34	65.875 ± 3.22
Immediate – 1 hr post-rTMS			29.13 ± 0.295	21.38 ± 1.36	61.88 ± 3.303	59.625 ± 4.63
Accelerated rTMS group	24.75 ± 1.07	73.13 ± 2.75				
Pre-rTMS			28.875 ± 0.52	21.63 ± 1.511	52.875 ± 2.955	54.625 ± 2.6
Immediate – 1 hr post-rTMS			29 ± 0.423	4.93 ± 1.742	50 ± 3.059	53.13 ± 4.147
24 hr post-rTMS			28.875 ± 0.61	22.875 ± 2.06	50.875 ± 3.55	54.429 ± 4.38
1-week post-rTMS			29.75 ± 0.16	22.875 ± 1.87	50.25 ± 3.56	52.75 ± 3.9

Note. The columns list (from left to right) rTMS group and visits for which measures are associated with, group age, PT, and questionnaire responses. Data are presented as mean (± *SEM*) values.

Table 4.2.

Adverse Effects Reported at Post-Stimulation Follow-Up Visits

	Visit	
Participant #	Immediate – 1 hr post-rTMS	24 hr post-rTMS
Single rTMS group		
2	Headache = 3	
3	Cognition = 2	
7	Headache = 2	
8	Concentration = 2	
Accelerated rTMS group		
10	Headache = 2	Headache = 4
11	Headache = 2	
12	Neck discomfort = 2	
13	Concentration = 3.5, hearing TMS tapping noises = 3	Hearing TMS tapping noises = 2

Note. The columns list (from left to right) participants (identified numerically) that experienced adverse effects following rTMS and their allocated rTMS group, and the post-rTMS follow-up visit at which symptoms were experienced. Symptoms were reported as: 1 = *no symptoms/change*, 2 = *minimal symptoms/change*, 3 = *slight symptoms/change*, 4 = *moderate symptoms/change*, 5 = *significant symptoms/change*. Participants reported no significant adverse effects (e.g., pain/discomfort) during or after rTMS, even at higher stimulation intensities. The side effects reported are transient and common with rTMS (Rossi et al., 2009).

CHAPTER 5

MODULATING INTRINSIC FUNCTIONAL NETWORK CONNECTIVITY WITH THE VISUAL CORTEX USING LOW-FREQUENCY REPETITIVE TRANSCRANIAL MAGNETIC STIMULATION

Preface

Intrinsic network connectivity between functionally interconnected nodes becomes altered in pathophysiology. Noninvasive brain stimulation can modulate pathological functional networks identified with rsFC and an attempt to restore the disease-driven response. The potential of stimulation protocols to target networks associated with the visual cortex for relevance in visual-related disorders requires investigation. Here we investigated the effects of alternative low-frequency (1 Hz) rTMS regimes to the visual cortex on modulating functional connectivity with the visual network and default mode network (DMN) in healthy controls using multi-echo (ME) rsfMRI. We further considered the influence of changes in visual cortex GABA (assessed via GABA+) and glutamate (assessed via Glx) concentrations on rsFC following rTMS. A single 20 min rTMS session to the visual cortex modulated rsFC with cortical and subcortical regions within and outside of the visual network and DMN. These rsFC changes were not evident immediately post-rTMS but were observed at 1 hr post-rTMS. In contrast, following five accelerated 20 min sessions to the visual cortex, absent or rather weak alterations in rsFC associated with the visual network and DMN were observed. Acute disruption with a single session of rTMS causes widespread reconfiguration of intrinsic rsFC in networks of interest, whereas accelerated sessions produce a relatively homeostatic response. GABA+ and Glx were differently associated with single and accelerated rTMS sessions and with the visual network and DMN. These findings offer insight into neural processes associated with intrinsic functional network connectivity with the visual cortex and the potential for 1 Hz rTMS to modulate interconnected regions. The differential effects associated with single and accelerated rTMS sessions are crucial for furthering the advancement of low-frequency rTMS in treatment modalities for visual-related disorders.

Examining the human brain as an integrative network of functionally interacting brain regions can provide new insights about large-scale neuronal communication in the human brain. It allows us to examine how connectivity and information integration relates to human behaviour, and how this organisation may be altered in pathophysiological processes or following neuromodulation (Bullmore & Sporns, 2009; Greicius, 2008). rsfMRI permits investigation of intrinsic connectivity between functionally related brain regions at rest. rsFC provides a measure of synchronous fluctuations in BOLD signal among regions to determine functional connectivity between interconnected nodes of networks. As such, rsFC provides insight into the brain's functional organisation of multiple systems and baseline neural processing (Fox & Raichle, 2007). Disturbances in rsFC are reported for a significant number of disease states (for a review, see Fox & Greicius, 2010) and potential biomarkers have been identified that show variability in the strength of functional coupling within distinct networks, for example, in Alzheimer's disease (Li et al., 2002), depression (Greicius et al., 2007), schizophrenia (Liang et al., 2006), and in cases of visual impairment (Dai et al., 2013; Liu et al., 2007; Yu et al., 2008). In addition, in cortical lesions, abnormal communication between the lesion site and remote interconnected regions causes pathophysiological changes locally and distal to the site of damage (Chapters 2–3; Guo et al., 2014; Rafique et al., 2016, 2018).

Noninvasive brain stimulation influences neuronal properties of the stimulated region, an accessible network node, which propagates the response transsynaptically to functionally interconnected nodes (Fox et al., 2014). A variety of rTMS protocols are capable of modulating functional network connectivity associated with the stimulation site (van der Werf, Sanz-Arigita, Menning, & van den Heuvel, 2010; Watanabe et al., 2014). The combination of rTMS and rsFC offers a promising technique to both diagnose and modulate pathological network interactions

for perceptual, behavioural and/or neurochemical gains in conditions associated with altered network connectivity (Fox, Halko, Eldaief, & Pascual-Leone, 2012; Grefkes et al., 2010; Strafella et al., 2003). The combined application of rsFC and rTMS in visual disorders has received little attention. For example, visual hallucinations associated with vision loss are a frequent and under-investigated consequence stemming from disorganised functional activity in interconnected cortical and subcortical networks (Chapter 2; ffytche et al., 1998; Rafique et al., 2016). Similarly, widespread alterations in rsFC are observed in amblyopia, suggesting that deficits are related to abnormal neural connections across networks (Wang et al., 2014). While rTMS can alter functional network connectivity, the effects can be unpredictable, unstable, and short lasting, particularly in pathophysiology (Maeda et al., 2000; Ridding & Ziemann, 2010), thus, limiting its usefulness. If we wish to selectively increase or decrease functional connectivity between specific brain regions in a controlled manner in visual disorders, knowledge of effects for different stimulation protocols is necessary in healthy individuals. A reference model of expected effects in healthy controls can provide knowledge of underlying mechanisms of rTMS, from which therapeutic protocols for visual-related disorders can be developed, and patient data can be compared.

The purpose of the present study was to explore the efficacy of low-frequency (1 Hz) rTMS to the visual cortex on modulating intrinsic functional network connectivity. Two alternative rTMS regimes are established in clinical applications (in non-visual disorders): a single session of rTMS applied over consecutive days for weeks/months or accelerated sessions (multiple sessions within one day) applied over consecutive days for a shorter period than single session rTMS. Previous research using accelerated rTMS in patient populations suggests that despite the reduced number of days of stimulation compared with single session rTMS, the

increased stimulation doses within a single day produce augmented effects (for a review, see Goldsworthy et al., 2015). Thus, we explored the effect of these alternative rTMS protocols by employing a shorter schedule consisting of a single 20 min session or five accelerated 20 min sessions of 1 Hz rTMS to the visual cortex. Further, we assessed whether longer-term changes persisted beyond the immediate post-rTMS measured effects. Further details of the two regimes are provided in Chapter 4 (pp. 98–99).

The effect of these rTMS protocols was investigated on two networks of interest using ME rsfMRI. We considered the direct effect of 1 Hz rTMS on nodes of the visual processing network interconnected to the stimulation site in the visual cortex (V1) (Beckmann, DeLuca, Devlin, & Smith, 2005; Yeo et al., 2011). Additionally, we explored the indirect effect of rTMS to the visual cortex on the DMN. The DMN consists of brain regions that show increased levels of activity during rest and are engaged in spontaneous and self-generated mental activity in the absence of external attentional demands (Gusnard, Akbudak, Shulman, & Raichle, 2001). The DMN is functionally and structurally interconnected with a considerable number of cortical and subcortical regions (Buckner, Krienen, Castellanos, Diaz, & Yeo, 2011; Hagmann et al., 2008; Margulies et al., 2009). We chose to investigate effects on the DMN since it has been suggested that dysfunction may arise in the DMN in disorders affecting visual processing (Lewis et al., 2014). In addition, significant disruption of the DMN, e.g., via stimulation to the visual cortex, may also have substantial implications for cognitive and behavioural performance. Data were analysed using ME-independent components analysis (ICA) and a whole-brain exploratory seed-based analysis approach. ME-ICA uses ME fMRI acquisition and TE dependency of resting-state BOLD signal to denoise artefactual fluctuations more effectively than other approaches (e.g., physiological noise modelling, band-pass filtering) and improves temporal SNR (Kundu, Inati,

Evans, Luh, & Bandettini, 2012). ME-ICA addresses the problem of low statistical power in fMRI studies by attenuating non-BOLD-related noise, leading to improvement in sensitivity and statistical power of fMRI (Kundu et al., 2012). The enhanced sensitivity facilitates detection of smaller and more subtle effects in brain regions that are methodologically fraught by other denoising methods (for a review, see Kundu et al., 2017; Lombardo et al., 2016).

We have previously assessed changes in visual cortical GABA (assessed via GABA+) and glutamate (assessed via Glx) concentrations following stimulation of the visual cortex using identical rTMS protocols (Chapter 4). The coordination between GABAergic interneurons and glutamatergic neurons directly impacts BOLD signal (Logothetis, 2008; Magistretti & Pellerin, 1999; Smith et al., 2002a). However, the neurochemical basis for variability in rsFC remains poorly understood and is to some extent related to GABAergic and glutamatergic systems; therefore, we explored the influence of these metabolites on changes in rsFC following rTMS. The neurochemical underpinnings of network connectivity will provide a better understanding of normal neurophysiological responses and alterations with rTMS associated with GABAergic/glutamatergic systems, with translation to therapeutic protocols of noninvasive brain stimulation.

Methods

This study was approved by York University's Office of Research Ethics. All individuals gave informed written consent.

Participants

Sixteen participants took part in the study ($M_{age} \pm SEM = 25.15 \pm 1.21$ years; 10 males/six females). All participants were right-handed, with normal or corrected-to-normal vision (> 0.04 logMAR; stereoacuity ≥ 50"), and no known contraindications to TMS and MRI.

Participants presented with no underlying medical conditions, were not taking any medications at the time of the study, and had no history of neurological or psychological disorders. All participants had also taken part in an MRS study to quantify changes in visual cortex GABA+ and Glx concentrations (Chapter 4) following the same experimental procedure as the present study. Participant history is provided in more detail in Chapter 4 (see Methods: Participants, p. 97). Participants received monetary compensation for their participation ($10 CAD/hr).

Experimental Design Overview

Participants initially underwent pre-rTMS (baseline) ME rsfMRI. In a separate follow-up visit, participants received offline 1 Hz rTMS to the visual cortex (V1) at the individual PT, either in a (1) single 20 min session of rTMS, or (2) five accelerated 20 min sessions of rTMS (separated by intervals of ~15 min). ME rsfMRI was repeated immediately following cessation of rTMS in both groups. ME rsfMRI was further performed (1) 1 hr post-rTMS in the single rTMS group, and (2) 24 hr and 1-week post-rTMS in the accelerated rTMS group.

Magnetic Resonance Imaging

ME rsfMRI and anatomical data were acquired with a 3T Siemens Magnetom® Tim Trio magnetic resonance scanner, with a 32-channel high-resolution brain array coil (Siemens, Erlangen, Germany). Head motion was minimised using soft pads surrounding participants' heads. Imaging was acquired in a dark room, and participants were instructed to keep their eyes closed and to not think of anything in particular throughout.

ME rsfMRI data were acquired first to capture immediate post-rTMS effects using whole-brain ME echo-planar imaging with a T2*-weighted sequence (number of contiguous axial slices = 43; in-plane resolution = 3.4 x 3.4 mm; slice thickness = 3 mm; imaging matrix = 64 x 64; TR = 3000 ms; TE = 14, 30, 46 ms; flip angle = 83°; FoV = 216 mm; acquisition time =

~10 min). Anatomical images were acquired with a T1-weighted MPRAGE imaging sequence (number of slices = 192; in-plane resolution = 1 x 1 mm; slice thickness = 1 mm; imaging matrix = 256 x 256; TR = 2300 ms; TE = 2.62 ms; TI = 900 ms; flip angle = 9°; FoV = 256 mm; acquisition time = ~5 min).

Repetitive Transcranial Magnetic Stimulation

Anatomical MR images were reconstructed to 3D cortical surfaces, and individual stimulation sites were mapped to their corresponding reconstructed cortical surface using Brainsight software (Rogue Research, Montreal, QC, Canada). Participant target stimulation sites in the visual cortex were based on our MRS study (Chapter 4, Methods, pp. 103, 105) from which GABA+ and Glx concentrations were extracted. Therefore, target sites in the present study and the MRS study were identical to enable a direct relationship between changes in metabolites and rsFC following the two rTMS protocols. Anatomical images in native space were manually co-registered to MNI coordinate space (see Table 5.1 for individual stimulation site MNI coordinates) within Brainsight using a linear transformation (translation, rotation, and scaling). Positioning of the coil with respect to the participant's head and the stimulation site was visualised in real time using a Polaris infrared image-guided tracking system (Northern Digital Instruments, Kitchener, ON, Canada) to ensure accurate and targeted disruption of the stimulation site throughout. Participants were seated in a comfortable position with an adjustable chin rest to limit head movement and provided with earplugs to prevent changes in auditory thresholds during rTMS (Rossi et al., 2009). A Magstim Rapid^2 Stimulator and a 70 mm diameter figure-of-eight coil (Magstim, Whitland, Wales, UK) were used to deliver the stimulation pulses to the stimulation site. The TMS coil was held tangential to the surface of the skull to minimise coil-to-cortex distance and to maximise the TMS effect (Ulmer & Jansen,

2010). rTMS was delivered to the stimulation site at the participant's PT to minimise inter-individual variability in visual cortical excitability thresholds (Stewart et al., 2001b). Details in obtaining the PT are described in Chapter 4 (Methods: Phosphene Threshold, pp. 104–105). Participants underwent 1 Hz rTMS (100% PT) at rest either in a single 20 min session (n = 8, four male/four female) or five accelerated 20 min sessions separated by ~15 min (n = 8, six male/two female) within a single day. Each rTMS session consisted of 1200 pulses (20 min). Stereotaxic co-registration was assessed immediately prior to each new rTMS session for accelerated sessions and refined where necessary. Details on the choice of rTMS protocols can be found in Chapter 4 (pp. 98–99).

Experimental Procedure

Participants initially underwent ME rsfMRI which commenced at ~13:00. On a different day, participants underwent rTMS to the visual cortex, which commenced at ~13:40 for participants in the single rTMS group, and commenced at ~11:00 for participants in the accelerated rTMS group. These times for rTMS commencement were chosen so that rTMS would cease at the time same of day irrespective of group, and accordingly immediate post-rTMS rsfMRI would be performed at ~14:00 in both groups to minimise diurnal confounds. Following cessation of rTMS, participants were immediately transferred into the MRI scanner and acquisition commenced within 5 min of rTMS ending. Participants in the single rTMS group underwent further rsfMRI 1 hr post-rTMS at ~15:00. Participants in the accelerated rTMS group received further rsfMRI at 24 hr and 1-week post-rTMS, both at ~1400. The procedure was identical to that of our MRS study in order to support any correlation between changes in rsFC with our previous data on GABA+ and Glx concentrations following rTMS. Full details on MRS methods and scheduling choice of follow-up visits is found in Chapter 4 (Methods: Magnetic

Resonance Imaging, pp. 102–104; Methods: Experimental Procedure, pp. 106–107). ME rsfMRI and MRS were performed in participants within a time period of 1 month.

Data Analyses

Preprocessing and denoising. MRI data were manually assessed and showed minimal participant movement in the scanner; therefore, all participants and acquisition runs were included in subsequent analyses. ME rsfMRI data were initially preprocessed and denoised using the AFNI integrated ME-ICA pipeline (v3.2.2; http://afni.nimh.nih.gov; Kundu et al., 2013, 2012). The first five TRs were removed to achieve steady-state equilibration. MR images were skull-stripped and intensity-normalised. Images were deobliqued, slice-timing corrected, axialised, and despiked. Motion correction parameters were estimated for each time point by aligning the middle TE (30 ms) images to the corresponding first time point image using a rigid body (six parameters) alignment procedure. Functional and anatomical images were co-registered by registering the skull-stripped middle TE image from the first time point to the skull-stripped anatomical image using an affine (12 parameters) alignment procedure with the local Pearson correlation and T2* weights. Motion correction and anatomical co-registration parameters were then applied in one step. Functional and anatomical images additionally underwent non-linear warping to standard MNI space (MNI Colin27, 1 x 1 x 1 mm). The three TEs provide different BOLD contrasts and are combined to create an optimal combination of contrast specific to each voxel therefore, producing a more homogenous contrast-to-noise ratio compared with single-echo fMRI (Kundu et al., 2015). The concatenated optimally combined functional data underwent principal component analysis (PCA) to distinguish BOLD signal of high and low variance components from noise. Denoising in ME-ICA is achieved with spatial FastICA, which decomposes and classifies the retained components from PCA into BOLD signal

and non-BOLD noise, and effectively removes noise components using linear regression, including motion, physiological and scanner artefacts (e.g., draining veins, and in-plane acceleration) (Evans, Kundu, Horovitz, & Bandettini, 2015; Kundu et al., 2017). Using non-BOLD component time courses as noise regressors greatly improves seed-based correlation mapping by minimising the influence of high- and low-frequency non-BOLD fluctuations (Kundu et al., 2012). ME-ICA denoising retains thermal noise and low variance ICs with high degrees of freedom, therefore, increasing sensitivity for determining significant effects (Kundu et al., 2015, 2017) and temporal SNR (Kundu et al., 2015).

In CONN: functional connectivity toolbox (v17.f; http://www.nitrc.org/projects/conn; Whitfield-Gabrieli & Nieto-Castanon, 2012), a Matlab-based cross-platform, ME-ICA denoised time series were spatially smoothed using a 6 mm full width at half maximum Gaussian kernel. Each participant's anatomical scan from each visit was segmented into cerebrospinal fluid, grey and white matter. These preprocessing steps within the CONN toolbox were implemented using SPM8 (Statistical Parametric Mapping, Wellcome Centre for Human Neuroimaging, London, UK; http://www.fil.ion.ucl.ac.uk/spm). BOLD signal from white matter and cerebrospinal fluid masks were identified using a component-based noise correction (CompCor; Behzadi, Restom, Liau, & Liu, 2007) and associated residual confounding effects were linearly regressed with PCA (five components each with no additional temporal expansion derivative terms; Chai, Castañón, Öngür, & Whitfield-Gabrieli, 2012) to improve (centre) the distribution of connectivity values of the data. The CompCor method addresses confounding effects without affecting intrinsic functional connectivity (Chai et al., 2012), while improving specificity, sensitivity, and validity of subsequent functional connectivity analyses such as false positive anticorrelated activity (Whitfield-Gabrieli & Nieto-Castanon, 2012). Data were not band-pass

filtered or detrended since they underestimate the effect of non-BOLD fluctuations, remove BOLD-related fluctuations, and discard low-frequency components (Evans et al., 2015; Kundu et al., 2012) that mediate rsFC and are necessary for the detection of functionally relevant networks (Biswal et al., 1995; Fransson, 2005; Greicius, Krasnow, Reiss, & Menon, 2003).

Functional connectivity. We used exploratory whole-brain seed-based analyses to determine the effects of the two rTMS regimes on rsFC using the CONN toolbox. Temporal correlations of BOLD signal during rest were computed between a seed region-of-interest (ROI) (from which the reference time series were extracted) and all other voxels in the brain, yielding seed ROI-specific spatial functional maps (seed-to-voxel analysis; Biswal et al., 1995). Two networks were explored: the visual network associated with the stimulation site at the visual cortex (V1) and the DMN. A 10 mm radius sphere ROI was centred at the stimulation site and positioned closest to the posterior surface of the occipital pole (Brodmann area 17), which received the strongest stimulation (i.e., region closest to the TMS coil), and was specific to each participant (average MNI coordinates: x = 1, y = -81, z = 15; see Table 5.1 for individual MNI coordinates). The DMN seed ROI was selected from the CONN DMN atlas. For the DMN, a 10 mm radius sphere ROI was placed in the posterior cingulate cortex/precuneus (Brodmann area 23/31; MNI coordinates: x = -6, y = -52, z = 40; Whitfield-Gabrieli & Nieto-Castanon, 2012) in all participants. Overlapping posterior cingulate cortex/precuneus regions are considered a critical node in the DMN (Damoiseaux et al., 2006; Grecius et al., 2003; Gusnard et al., 2001) and are shown to extract reliable patterns of DMN functional connectivity using seed-based analyses (e.g., Fox et al., 2005; Fransson, 2005; Greicius et al., 2003). First-level analyses correlated the average BOLD time course between each seed ROI to whole-brain voxels (one dimension, no temporal expansion of derivatives, no frequency decomposition) to create rsFC

maps for each visit and participant separately using a weighted GLM and bivariate Pearson's correlations (with no haemodynamic response function weighting). The correlation coefficients represent the level of association between two time series that reflects the relative degree of functional connectivity of each seed and each voxel in the brain. The resulting weighted correlation coefficients were converted to normally distributed *z*-scores using Fisher's transformation. The first-level individual rsFC maps were subsequently used for second-level GLM analyses to investigate significant changes in seed-to-voxel rsFC between pre-rTMS and follow-up visits for each rTMS group and seed ROI, separately. The rTMS groups were analysed independently due to different follow-up visit intervals. Paired *t*-tests were calculated to investigate whole-brain differences in rsFC between pre-rTMS and each follow-up visit. The number of degrees of freedom from ME-ICA denoised data for each participant and visit were entered as a covariate of no interest for subject- and group-level analyses to control for and avoid inflated test statistics and false positive results (Kundu et al., 2017). Nonparametric statistics (1000 permutations; Pernet, Latinus, Nichols, & Rousselet, 2015) were chosen to control for false positive rates and to provide added protection against potential violations of parametric assumptions with small sample sizes (Eklund, Nichols, & Knutsson, 2016). Significant clusters were investigated with post-hoc simple effects analyses to identify the direction of rsFC effects (i.e., increase or decrease) between the pre-rTMS visit and each post-rTMS follow-up visit. The resulting rsFC maps were thresholded at a whole-brain uncorrected voxel-level (height) threshold of $p < .001$, cluster-mass (extent) threshold of $p < .05$ corrected with FDR for multiple comparisons, with a minimum cluster size of 25 voxels. These a priori thresholds were chosen in accordance with CONN toolbox guidelines for supporting strong focal effects as opposed to weaker diffuse effects (e.g., uncorrected voxel-level threshold of $p < .01$), and to further

constrain false positive effects. Positive and negative correlations (two-sided) were examined. Regions showing significant changes in rsFC associated with the seed ROIs between pre-rTMS and follow-up visits were identified using the Harvard-Oxford cortical and subcortical probabilistic (25% probability) anatomical atlases (Desikan et al., 2006), the Automated Anatomical Labeling atlas to parcellate cerebellar areas (Tzourio-Mazoyer et al., 2002), and the Brodmann Area atlas (Brodmann, 1909, 1910), all implemented within the CONN toolbox.

To investigate how changes in rsFC within these networks are influenced by GABA+ and Glx concentrations following the two rTMS protocols, we repeated the above procedure with multiple regression analyses. The metabolite concentrations obtained from our MRS study (Chapter 4) were acquired from the same stimulation site seed ROI used for rsFC and were included as a covariate of interest in second-level analyses. We still controlled for the number of degrees of freedom from ME-ICA denoised data (covariate of no interest). These analyses evaluated the correlation between change in rsFC (difference in connectivity pre- and post-rTMS) and change in metabolite concentration (difference in GABA+/Glx concentration pre- and post-rTMS) in the networks of interest. Analyses compared pre- and post-rTMS for each metabolite, seed ROI, and rTMS group, separately.

Results

Effect of Low-Frequency Repetitive Transcranial Magnetic Stimulation on Resting-State Functional Connectivity

Regions demonstrating significant changes in rsFC with the stimulation site (V1) and posterior cingulate cortex/precuneus seed ROIs following a single rTMS session are provided in Tables 5.2–5.3, respectively. For both seed ROIs, there were no significant changes in rsFC with correlated regions immediately following cessation of rTMS compared with pre-rTMS.

However, significant changes in rsFC were detected 1 hr after rTMS had ceased compared with pre-rTMS. The stimulation site showed significant changes in rsFC with frontal, parietal, temporal, and occipital lobe regions, as well as the brainstem, thalamus, and cerebellum (Table 5.2; Fig 5.1a). The posterior cingulate cortex/precuneus showed significant changes in rsFC with frontal and temporal lobe regions, as well as the cingulate gyrus, cerebellum, and basal ganglia (putamen, pallidus, accumbens) (Table 5.3; Fig 5.1b).

There were no significant changes in rsFC between the stimulation site and correlated regions following accelerated rTMS compared with pre-rTMS. Only the middle temporo-occipital region showed a significant decrease in rsFC with the posterior cingulate cortex/precuneus at 1-week post-rTMS compared with pre-rTMS (Brodmann area 22; MNI coordinates: x = 54, y = -41, z = 1; voxels = 411 mm; effect size = .21). However, using a less conservative voxel-level threshold of $p < .01$ revealed diffuse weak changes in rsFC between the stimulation site and correlated regions only at 24 hr post-rTMS (Table 5.4), and only at 1-week post-rTMS for regions correlated with the posterior cingulate cortex/precuneus (Table 5.5).

The average difference in connectivity strength between pre- and post-rTMS visits across participants for each seed ROI and correlated regions are represented by effect size values in Tables 5.2–5.5.

Influence of GABA+ and Glx on Resting-State Functional Connectivity

Multiple regression analyses demonstrated a significant correlation between pre- and post-rTMS differences in rsFC and metabolite concentrations in networks associated with our seed ROIs. These findings suggest that changes in rsFC are related to GABA+ and/or Glx changes following 1 Hz rTMS to the visual cortex.

Significant changes in rsFC following a single rTMS session for both seed ROIs, the stimulation site (V1) and posterior cingulate cortex/precuneus, are provided in Tables 5.6–5.7, respectively. Significant changes in rsFC between the stimulation site and correlated regions associated with GABA+/Glx were only apparent 1 hr after rTMS ceased. The stimulation site showed significant changes in rsFC with frontal, parietal, and occipital lobe regions, and the cerebellum (Table 5.6). However, in the case of the posterior cingulate cortex/precuneus seed, significant changes in rsFC with correlated regions were only associated with GABA+ and not Glx. Effects with the posterior cingulate cortex/precuneus were detected immediately after rTMS ceased and continued until 1 hr post-rTMS. The posterior cingulate cortex/precuneus showed significant changes in rsFC with frontal, parietal, occipital, and temporal lobe regions, as well as the cingulate gyrus, basal ganglia (caudate), thalamus, and cerebellum (Table 5.7). Notably, the effects associated with the posterior cingulate cortex/precuneus were more widespread and not stable, showing variable changes in network connectivity at 1 hr compared with immediately post-rTMS.

Tables 5.8–5.9 show significant changes in rsFC following accelerated rTMS sessions for the stimulation site and posterior cingulate cortex/precuneus seed ROIs, respectively. With accelerated rTMS, significant changes in rsFC between the seed ROIs and correlated regions associated with GABA+ and Glx were apparent immediately after rTMS and continued to 1-week post-rTMS. Widespread changes in rsFC associated with GABA+/Glx were observed in frontal, parietal, occipital, and temporal lobe regions, as well as the cingulate gyrus, basal ganglia, thalamus, amygdala, brainstem, and cerebellum. These effects were additionally not stable in that they continued to change even at 1-week post-rTMS, as observed from the inconsistent involvement of interconnected regions and/or changes in connectivity at the

different follow-visits. For example, the left superior lateral occipital cortex shows a decrease in rsFC with the stimulation site associated with a change in GABA+ immediately post-rTMS; while, an increase in rsFC is observed between these regions at 24 hr post-rTMS (Table 5.8).

The effect size values in Tables 5.6–5.9 represent connectivity strength as a ratio of change in rsFC between the seed and correlated cluster per unit change in metabolite concentration. The average change in metabolite concentration at the stimulation site (average pre-rTMS concentration minus post-rTMS concentration) relative to the rTMS protocol is provided in the corresponding Table captions.

Discussion

We report unexpected differential rsFC changes in nodes associated with the stimulation site in the visual cortex and the DMN following two different low-frequency (1 Hz) rTMS (100% PT) protocols. A single 20 min session produced delayed strong changes in rsFC across cortical and subcortical regions compared with pre-rTMS. Surprisingly, five accelerated 20 min sessions of rTMS produced weak and relatively insignificant changes in rsFC. We further observed that rsFC was associated with changes in GABA+ and Glx concentrations in both rTMS protocols, and these changes to rsFC fluctuated between post-rTMS visits. This study demonstrates that 1 Hz rTMS modulates rsFC with regions distal to the site of stimulation and with regions that are not usually functionally connected to the seed ROIs pre-rTMS.

Effect of Low-Frequency Repetitive Transcranial Magnetic Stimulation on Intrinsic Visual Cortex Functional Connectivity

The resting-state visual network consists of primary visual and extrastriate cortices, with additional functional connectivity with the motor network (van den Heuvel, Mandl, Kahn, Hulshoff Pol, & Hilleke, 2009). A single 20 min session of 1 Hz rTMS to the visual cortex

modulated rsFC (correlated and anticorrelated) to cortical regions outside the usual visual network (Table 5.2), including nodes of the DMN (e.g., precuneus and middle frontal gyrus) and subcortical regions (e.g., cerebellum and thalamus). The DMN consists of overlapping posterior cingulate cortex/precuneus, anterior cingulate cortex, frontal, parietal, and temporal regions (Greicius et al., 2003; Laird et al., 2009). Although we did not directly stimulate nodes of the DMN, the posterior cingulate cortex/precuneus also showed modified rsFC to regions outside the DMN post-rTMS, e.g., basal ganglia and cerebellum (Table 5.3). Increasing evidence suggests that specific cerebellar regions are integral to the DMN (Brissenden, Levin, Osher, Halko, & Somers, 2016; Buckner et al., 2011). The cerebellum is rarely reported as a node of the DMN as many studies do not acquire whole-brain data or acquisition/analysis methods may be insensitive. Identification of subcortical effects in the present study may be attributed to ME-ICA sensitivity. These subcortical effects are reported to be unobservable with single-echo rsfMRI at the current sample size and with alternative denoising techniques where effects are obscured by greater amounts of non-BOLD noise, e.g., low functional contrast-to-noise due to cerebral spinal fluid and blood flow pulsatility (Kundu et al., 2012; Lombardo et al., 2016).

Notably, for both seed ROIs, effects of single session rTMS did not emerge until 1 hr post-rTMS. The delayed changes in rsFC suggest that either effects are too diffuse and weak immediately post-rTMS to be detected, or that there is greater inter-individual variability immediately post-rTMS, and therefore rsFC changes were not significant. We tested the former by using a less conservative voxel-level threshold ($p < .01$) to investigate weaker effects, yet we continued to observe no significant changes in rsFC between pre-rTMS and immediate post-rTMS visits. Exploring individual-level rsFC maps revealed little change in connectivity values for either seed ROI between pre-rTMS and immediately post-rTMS visits. The continued

absence of rsFC changes immediately post-rTMS suggests that the latter may be more likely, or perhaps a combination of the two has occurred.

Further, it is interesting that rsFC changes following a single session of rTMS outlast those measured by other neurotechniques that have recorded shorter aftereffects. Our knowledge of rTMS aftereffects has relied heavily on EEG recordings. In the case of low-frequency rTMS to the visual cortex, EEG recordings following 10–20 min of 1 Hz rTMS have established aftereffects lasting in the range of 10–40 min (for a review see, Thut & Pasucal-Leone, 2010). Accordingly, we did not expect rsFC changes to persist at 1 hr post-rTMS following a single rTMS session and certainly not that these effects would only be reliable at 1 hr post-rTMS. This finding critically highlights that our understanding of noninvasive brain stimulation is highly dependent on and limited by the tool of measure; specifically, rsfMRI aftereffects persist longer than those measured by EEG. In line with our results, Nettekoven and colleagues (2014) previously demonstrate that accelerated TBS causes changes in excitability (as measured by motor evoked potentials) that are unrelated to changes in motor network rsFC. These findings suggest that rsfMRI may not be as sensitive as EEG to immediate post-rTMS effects, but instead shows delayed network changes. Alternatively, aftereffects observed using electrophysiological measures compared to functional connectivity likely occur via different mechanisms and/or dissimilar timeframes. In addition, ME-ICA is considered to be more sensitive to slower emerging changes with TMS than previous conventional methods; therefore, we may be unlikely to capture these effects using single-echo rsfMRI and alternative denoising techniques (e.g., band-pass filtering) (Evans et al., 2015), and perhaps even with EEG.

We observed a rather unexpected finding of null effects following five accelerated 20 min sessions of rTMS on rsFC. We expected either an inversion of effects compared to single

rTMS, as had been previously observed with longer trains of stimulation (e.g., Gamboa et al., 2010), or a strengthening of effects (e.g., Nettekoven et al., 2014). One possible explanation for this null finding is the presence of larger inter-individual variability in TMS response (Ridding & Ziemann, 2010; Stewart et al., 2001b), which would likely intensify with concentrated doses of rTMS such as accelerated sessions. However, investigation of individual-level connectivity values following accelerated rTMS showed very little change in rsFC between seed ROIs and correlated regions compared with pre-rTMS. Again, to test for weaker effects, we repeated analyses with a less conservative uncorrected voxel-level threshold ($p < .01$) and did in fact observe weak and diffuse differences in rsFC following accelerated rTMS (Tables 5.4–5.5). These diffuse changes encompassed a large number of brain regions (clusters > 1000 voxels) that were detected only at 24 hr post-rTMS for effects associated with the stimulation site, and were only observed at 1-week post-rTMS for the posterior cingulate cortex/precuneus seed. The continued absence of immediate post-rTMS effects suggests subtle accelerated rTMS effects do not become stable and/or arise until at least 24 h, yet these subtle effects persist for at least 1-week.

A consideration for accelerated rTMS effects relates to metaplasticity induced by TMS and the ability of functional cortical networks to maintain neuronal activity within a dynamic range (Bocci et al., 2014; Lang et al., 2004). It could be, at least in terms of rsFC, that the brain becomes resistant to change and the dose-dependent effects of accelerated rTMS throughout the day are due to metaplasticity as a compensatory measure to maintain homeostasis in healthy control individuals. Support for the presence of this resistant effect comes from the strong observed changes in rsFC following just a single session of rTMS that are not seen with subsequent stimulation. Gamboa and colleagues (2011, 2010) observe suppression of aftereffects

following two accelerated TBS sessions within one day that were dependent on the TBS protocol and the timing of the break interval in between sessions. A commonly proposed description of these aftereffects with multiple rTMS sessions is the Bienenstock-Cooper-Munro theory (Bienenstock, Cooper, & Munro, 1982). Hebbian synaptic plasticity would enable a continuous unidirectional change in network excitability following stimulation that would essentially destabilise a neural system (Bocci et al., 2014). According to the Bienenstock-Cooper-Munro theory, LTP effects induced after stimulation favour the induction of LTD with subsequent stimulation, thereby preventing an excessive buildup of LTP or LTD. This mechanism regulates intrinsic excitability and ensures stable neuronal activity through dynamic modification of LTP and LTD thresholds. Therefore, an increased LTD response will occur following enhanced postsynaptic activity from saturation of LTP-induced mechanisms and vice versa. Conversely, a strengthened effect is recorded with multiple/accelerated stimulation protocols in patient populations (for a review, see Goldsworthy et al., 2014; Rafique et al., 2016) and in healthy controls (Bastani & Jaberzadeh, 2014; Kettekoven et al., 2014). The contradictory findings between studies across research groups likely pertains to differences in stimulation protocols, intervals between multiple stimulation sessions, site of stimulation, and the neurotechnique employed to measure aftereffects. We have previously observed a reduction in MRS measured GABA+ at the visual cortex with this accelerated rTMS protocol (Chapter 4), suggesting that restorative effects with our protocol may only be at the functional network connectivity level. If we consider the influence of GABA+/Glx concentration on rsFC changes following accelerated rTMS, we observe significant widespread changes to networks associated with both seed ROIs (Tables 5.8–5.9). This contrasting finding in rsFC when taking into consideration GABA+ and Glx concentrations with accelerated rTMS may indicate that the influence of GABA+ and Glx is

greater with accelerated sessions, and these rsFC changes become apparent because much of the unexplained variance is accounted for. At least in terms of GABA+ and Glx involvement, we can be confident post-accelerated rTMS effects are occurring, and other mechanisms must be concerned beyond involvement of these neurotransmitters to produce a restorative effect in rsFC. The interaction between GABAergic and glutamatergic systems may be a more appropriate indicator of TMS effects since these systems are critical in LTD and LTP.

Influence of GABA+ and Glx on Intrinsic Visual Cortex Functional Connectivity

Our previous study investigating changes in GABA+ and Glx concentration at the stimulation site using identical rTMS protocols found no significant change in metabolites with a single session, and a significant reduction in GABA+ concentration for up to 24 hr following accelerated rTMS (Chapter 4). Yet, when we investigate the influence of these GABA+ and Glx concentrations on rsFC, we see these metabolite changes influence rsFC immediately after rTMS ceased for both stimulation protocols (Tables 5.6–5.9). In addition, these rsFC changes persist until at least the last follow-up visits for both protocols. Our distinct findings highlight technique sensitivity, namely MRS versus rsfMRI. Functional connectivity is influenced by cortical network oscillations in the gamma frequency range (Cabral, Hugues, Sporns, & Deco, 2011), and the interaction with GABA-mediated responses (Muthukumaraswamy, Edden, Jones, Swettenham, & Singh, 2009). In the visual cortex, gamma frequency oscillations are positively related with MRS measured GABA and inversely correlated with the magnitude of BOLD response (Muthukumaraswamy et al., 2009). Synchronised neural oscillations in cortical networks are particularly mediated by postsynaptic $GABA_A$ receptors (for a review, see Gonzalez-Burgos & Lewis, 2008). Conversely, MRS is considered insensitive to synaptic activity, but instead measures the total concentration of $GABA_A$ and $GABA_B$ within the MRS

voxel, reflecting extrasynaptic GABAergic tone (Stagg et al., 2011c). Lastly, spontaneous neurotransmitter release at synapses occurs in the absence of neuronal spikes or action potentials (for a review, see Kavalali, 2015). Taken together, the findings suggest that spontaneous neurotransmitter release may reflect an important component of spontaneous fluctuations, and it may be that measuring rsFC is an indirect measure that is more sensitive to changes in GABA+ and Glx than measuring GABA+ and Glx directly with MRS.

In these analyses, we observed stronger widespread activity following accelerated rTMS than with a single session, which is consistent with our previous finding of a greater effect of accelerated rTMS on MRS measured GABA+ (Chapter 4). Differential effects between single session and accelerated rTMS were observed for Glx influence on rsFC with the DMN node posterior cingulate gyrus/precuneus. Glx concentration was not associated with rsFC changes in regions interconnected with the posterior cingulate gyrus/precuneus following a single session of rTMS (Table 5.7). However, following accelerated rTMS, both GABA+ and Glx influenced rsFC with the posterior cingulate gyrus/precuneus (Table 5.9). Indeed, prior work suggests that glutamate and GABA are significantly associated with DMN activity (Hu, Chen, Gu, & Yang, 2013; Kapogiannis, Reiter, Willette, & Mattson, 2013). In contrast, both GABA+ and Glx concentration influenced rsFC associated with the stimulation site following single and accelerated rTMS sessions. These findings imply that Glx is not sufficiently altered at the visual cortex following a single session of 1 Hz rTMS to influence rsFC between the posterior cingulate gyrus/precuneus and interconnected regions. Nonetheless, changes in GABA+ and Glx as measured from the stimulation site (V1) were otherwise sufficient to influence direct and indirect local and distal changes in rsFC.

Implications on Intrinsic Functional Connectivity in Visual-Related Disorders

Our findings have important implications for understanding the underlying effects of low-frequency rTMS to the visual cortex, and for developing therapeutic applications for visual-related disorders. We do not intend to predict effects in pathophysiology coexisting with impaired functional state and altered responsiveness to rTMS (e.g., Antal et al., 2008). We know from patient populations that accelerated rTMS has a stronger cumulative effect than conventional single sessions applied over consecutive days (for a review, see Goldsworthy et al., 2015). It is highly plausible that these promising results obtained in patient populations are owed to impaired systems (e.g., inability to maintain homeostasis, impaired metaplasticity), and the magnitude and direction of neuromodulated effects induced by rTMS will differ considerably from healthy subjects. Our intention was to provide a baseline framework for under-investigated effects of 1 Hz rTMS to the visual cortex. We nonetheless consider it necessary to investigate the response in the absence of pathophysiology in order to develop therapeutic techniques in terms of the most efficient protocol that combines optimal effects with minimal stimulation time (e.g., stimulation over days rather than weeks to improve patient compliance, etc.). Moreover, differences in responses between healthy controls and patient populations can highlight potential biomarkers.

Although effects were widespread and dependent on the rTMS protocol, it is not within the scope of the paper to describe the implication and function of each region functionally associated with the seed ROIs in this study. However, the regions implicated must be taken into consideration in therapeutic applications, and future studies should probe more detailed relationships using ROI-to-ROI analyses. For example, in lesion location mapping, recent studies suggest stimulating nodes functionally connected to the lesion since it will propagate to the

lesion site (Boes et al., 2015). Therefore, regions displaying aberrant activity close to the lesion are not only targeted, but remote nodes interconnected to the damaged tissue are (e.g., Boes et al., 2015), thus targeting multiple nodes at once. Alternatively, to target a network region that lies outside the stimulation depth parameters of rTMS, one can indirectly target distal nodes that are within reach and interconnected to the ROI implicated in specific disorders. Importantly, the direction of effect (correlated or anticorrelated) is vital when considering desired stimulation effects given that a rTMS protocol may worsen an already aberrant connection between the visual cortex and distal nodes. For example, abnormalities in correlated and anticorrelated networks are observed in a number of neuropsychiatric disorders (Greicius, 2008; Mulders, van Eijndhoven, Schene, Beckmann, & Tendolkar 2015; Whitfield-Gabrieli & Ford, 2012). Developing protocols in these instances requires comparative data in healthy controls to understand the normal connectivity response to rTMS so as not to worsen the pathology. The frequent inverse change from correlated to anticorrelated rsFC post-rTMS in this study is likely owed to the inhibitory effect of low-frequency rTMS and should be taken into consideration in future clinical applications. In some interconnected regions, we observed a switch from anticorrelated to correlated rsFC, possibly to maintain a somewhat dynamic functionally organised system.

When considering the clinical application of accelerated rTMS in greater doses (e.g., across consecutive days), it is crucial to consider inadvertently induced perceptual, neurobiochemical and behavioural adverse effects. Insight into rTMS effects on resting-state networks provides one such tool. Although we observe significant connectivity changes following our protocols of lower rTMS doses compared with those used in patient populations, these changes did not cause significant measurable or perceptual deficits in at least visual or

cognitive function, nor did participants report significant adverse effects (Chapter 4, pp. 111–112, 129). Given the widespread effects following our rTMS protocols, and involvement of numerous nodes, there is greater potential of adverse effects with greater stimulation doses in patients. This area remains to be investigated, despite the frequent therapeutic use of noninvasive stimulation in pathology. For example, the DMN is involved in cognitive function associated with intrinsic processing and external inputs (Fox et al., 2005) and may become impaired with greater rTMS doses. Other regions affected by rTMS in our study are implicated in attention (e.g., middle temporal and prefrontal regions; Fox et al., 2005; Laufs et al., 2003), auditory function (e.g., planum polare and insular cortex) and executive control (e.g., prefrontal and cingulate cortices) (for a review, see Beckman et al., 2005).

Limitations

Although a smaller sample size was employed due to high neuroimaging costs with repeated visits, we used conservative statistical thresholds and employed non-parametric methods to limit false positive findings. Additionally, we used a within-subject design to decrease inter-individual variability of rTMS effects and to increase statistical power. Despite the small sample size, we observed strong effects with a single session of rTMS and for both rTMS protocols when considering the influence of GABA+/Glx concentrations. Lastly, ME-ICA is considered to substantially improve effect size estimates and statistical power with traditional sample sizes in fMRI studies by specifically addressing problems related to non-BOLD artefact variability (Lombardo et al., 2016), while remaining conservative in the cut-off for retaining BOLD signal components (Evans et al., 2015).

Our understanding of 1 Hz rTMS aftereffects on rsFC is limited by our follow-up visit time intervals. We observed changes that likely continue well past our last time points and

requires further investigation to determine when rsFC starts to stabilise and/or return to baseline following rTMS, but is beyond the scope of the present study. In addition, to accurately determine whether accelerated rTMS induces a restorative change (i.e., a relatively homeostatic response) in rsFC in healthy controls, rsfMRI would need to be repeated following each consecutive session. Moreover, our findings are limited to effects produced by 1 Hz rTMS at 100% PT to the visual cortex. Previous studies demonstrate that the magnitude and direction of effects is highly dependent on the intensity of stimulation (i.e., sub- and supra-PT/MT; Di Lazzaro et al., 1998; Ziemann, Rothwell, & Ridding, 1996).

Changes in metabolite concentrations were obtained from the stimulation site in the visual cortex. Therefore, metabolite changes associated with change in rsFC of the posterior cingulate cortex/precuneus seed ROI are in reference to those obtained from the stimulation site. Given that the stimulation site shows significant correlation to the precuneus and other nodes in the DMN, it is expected that metabolite changes would relay to interconnected nodes including the posterior cingulate cortex/precuneus. This indirect measure of metabolite influence when considering network effects associated with the posterior cingulate cortex/precuneus is key in making inferences. We acknowledge that metabolite concentration changes at the posterior cingulate cortex/precuneus seed will indeed be different; however, we can only obtain single voxel MRS acquisition. We can of course obtain direct measures in a separate analysis, which would require repeating the full experiment with all follow-up visits using an MRS voxel at the posterior cingulate cortex/precuneus seed that would add considerable MRI costs. This would have the added limitation that the functional state of the individual might be different.

For participants who underwent accelerated rTMS, rsfMRI was acquired in the same session as MRS (counterbalanced) since this only required an additional 10 min of data

acquisition. In the single rTMS group, due to known shorter aftereffects, rsfMRI and MRS were acquired on different days (with an otherwise identical experimental protocol) separated by an interval of at least 1-week (to prevent residual aftereffects of rTMS between sessions) and no more than a month. Therefore, in the accelerated rTMS group, we assessed the association between metabolite levels and functional connectivity at the same functional state, but not for the single rTMS group.

Conclusion

Based on connectivity changes with the seed ROIs, findings from the present study suggest that the spatial topography of the visual network and DMN is altered following low-frequency (1 Hz) rTMS to the visual cortex. These results extend our understanding of how focal disruption to early visual cortex using rTMS affects network communication. Accelerated rTMS within a single day resulted in a resistant effect, while a single session of rTMS induced widespread rsFC changes compared with pre-rTMS. These results have important implications in developing therapeutic protocols for visual-related disorders in that a single session of 1 Hz rTMS to the visual cortex may be more effective than accelerated rTMS in targeting interconnected networks. ME resting-state analysis provides an important tool to investigate longer lasting and slower emerging TMS-induced aftereffects across multiple networks over conventional methods such as EEG that demonstrate shorter duration aftereffects.

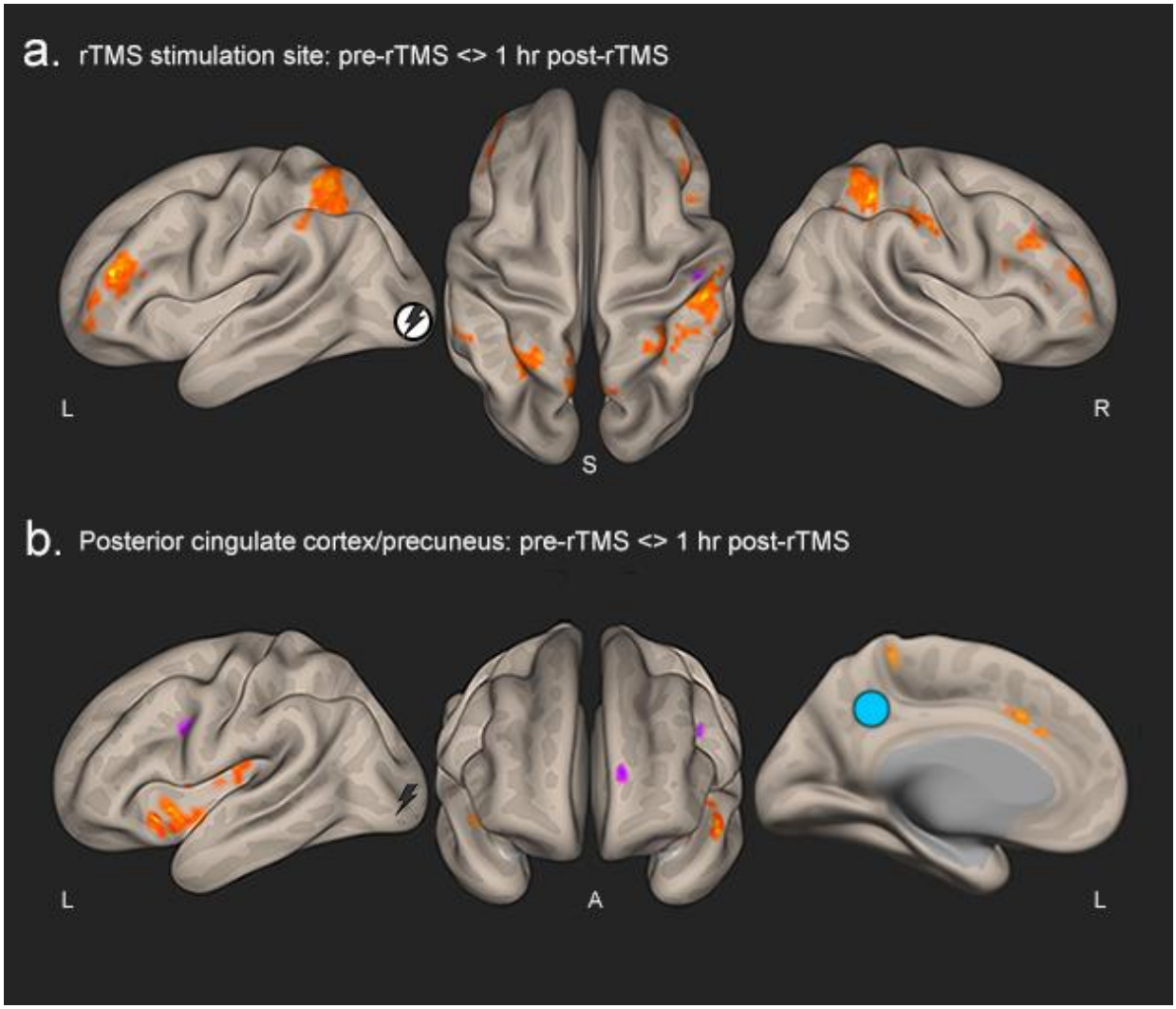

Figure 5.1. Resting-state maps of average change in functional connectivity with seeds of interest following a single session of 1 Hz rTMS. (a) Regions showing significant change in connectivity with the stimulation site seed (white circle). (b) Regions showing significant change in connectivity with the posterior cingulate cortex/precuneus seed (light blue circle). Orange/yellow regions show a positive change in correlation with the seed (decrease in connectivity at 1 hr post-rTMS), while pink/purple regions show a negative change in correlation with the seed (increase in connectivity at 1 hr post-rTMS). Lightning bolt indicates the stimulation site at the visual cortex. L = left; R = right; S = superior; A = anterior.

Table 5.1.

Individual MNI Coordinates for the Stimulation Site at the Visual Cortex

	MNI coordinates		
Participant #	x	y	z
Single rTMS group			
1	1	-83	13
2	1	-79	18
3	0	-84	16
4	0	-84	7
5	0	-83	8
6	-1	-84	11
7	1	-75	23
8	4	-82	13
Accelerated rTMS group			
9	-5	-83	9
10	2	-79	15
11	2	-82	12
12	-1	-83	15
13	1	-80	20
14	1	-76	19
15	1	-78	20
16	1	-85	14

Note. The columns list (from left to right) each participant (identified numerically) and their associated rTMS group, and peak MNI coordinates where 10 mm radius sphere seed ROIs were centred.

Table 5.2.

Average Change in Functional Connectivity Between the Visual Cortex (Stimulation Site) and Correlated Regions Following a Single rTMS Session

Contrast/ Region	Brodmann area	MNI coordinates x	y	z	Voxels	Effect size
Pre-rTMS < > immediate post-rTMS						
N.S.						
Pre-rTMS < > 1 hr post-rTMS						
R superior parietal lobule	7	29	-46	50	628	.28[b]
L superior parietal lobule	7	-34	-60	53	465	.25[b]
R anterior supramarginal gyrus	40	48	-30	39	183	.25[b]
R posterior supramarginal gyrus	40	59	-46	45	36	.17[b]
L posterior supramarginal gyrus	40	-53	-49	15	54	.14[a,b]
R postcentral gyrus	2	51	-19	37	105	.19[b]
R postcentral gyrus	2	51	-14	50	99	- .18[a]
Precuneus	7	2	-66	48	489	.23
R middle frontal gyrus	9	48	16	31	389	.24[b]
R frontal Pole	46	51	43	18	239	.29[b]
L frontal Pole	46	-44	38	12	303	.23[b]
Brainstem		-9	-33	-10	129	- .23[a]
L posterior inferior temporal gyrus	20	-50	-19	-29	111	- .13[a]
R thalamus		7	-27	15	81	- .17[a]
R cerebellum crus 1		40	-76	-23	66	- .22[a]
L fusiform gyrus	19	-31	-74	-7	54	- .18

Note. The columns list (from left to right) regions showing significant differences in rsFC with the stimulation site between pre- and post-rTMS visits (uncorrected $p < .001$; cluster-mass $p < .05$ FDR corrected), the associated Brodmann area, peak MNI coordinates of the cluster, cluster voxel size (≥ 25 voxels), and effect size. Effect sizes represent the average difference in Fisher-transformed correlation coefficients between visits (pre-TMS minus the post-rTMS visit) for the stimulation site (seed) and the correlated region. A positive effect size indicates a decrease in rsFC at the post-rTMS visit, while a negative effect size indicates an increase in rsFC at the post-rTMS visit. N.S. = no significant difference; R = right; L = left. [a]anticorrelated pre-rTMS; [b]anticorrelated post-rTMS.

Table 5.3.

Average Change in Functional Connectivity Between the Posterior Cingulate Cortex/Precuneus and Correlated Regions Following a Single rTMS Session

Contrast/ Region	Brodmann area	MNI coordinates x	y	z	Voxels	Effect size
Pre-rTMS < > immediate post-rTMS						
N.S.						
Pre-rTMS < > 1 hr post-rTMS						
L insular cortex	13	-42	11	-4	633	.26[b]
R frontal pole	10	-1	65	7	34	- .22[a]
L frontal pole	10	-14	65	9	254	- .25
R cerebellum crus 2		37	-74	-45	54	- .27[a]
L cerebellum crus 2		-42	-63	-42	36	- .22[a]
L cerebellum 8		-14	-68	-37	39	.12[b]
L cerebellum 7b		-6	-79	-40	57	.17[b]
L cerebellum 6		-28	-49	-37	81	.19[b]
R putamen		24	13	-10	117	.19[a]
L putamen		-34	-6	1	156	.17[b]
L pallidum		-20	0	-7	81	.24[b]
R accumbens		10	11	-10	45	.20[b]
R posterior superior temporal gyrus	22	51	-11	-10	135	.18[b]
R inferior temporal gyrus	20	65	-22	-29	30	- .20[a]
L planum polare	13	-47	-8	-1	60	.31[b]
L precentral gyrus	6	-39	0	26	120	- .20[a]
L paracingulate gyrus	32	-12	16	34	102	.28[b]
L central opercular cortex	13	-42	-8	12	90	.17[b]

Note. The columns list (from left to right) regions showing significant differences in rsFC with the posterior cingulate cortex/precuneus between pre- and post-rTMS visits (uncorrected $p < .001$; cluster-mass $p < .05$ FDR corrected), the associated Brodmann area, peak MNI coordinates of the cluster, cluster voxel size (≥ 25 voxels), and effect size. Effect sizes represent the average difference in Fisher-transformed correlation coefficients between visits (pre-TMS minus the post-rTMS visit) for the posterior cingulate cortex/precuneus (seed) and the correlated region. A positive effect size indicates a decrease in rsFC at the post-rTMS visit, while a negative effect size indicates an increase in rsFC at the post-rTMS visit. N.S. = no significant difference; R = right; L = left. [a]anticorrelated pre-rTMS. [b]anticorrelated post-rTMS.

Table 5.4.

Subtle Diffuse Changes in Functional Connectivity Between the Visual Cortex (Stimulation Site) and Correlated Regions Following Accelerated rTMS Sessions

Contrast/ Region	MNI coordinates x	y	z	Voxels	Effect size
Pre-rTMS < > immediate post-rTMS					
N.S.					
Pre-rTMS < > 24 hr post-rTMS					
Cluster 1	-12	-63	67	3511	.20[b]
Precuneus				1727	
L superior parietal lobule				491	
R superior lateral occipital cortex				12	
L superior lateral occipital cortex				430	
R postcentral gyrus				10	
L postcentral gyrus				184	
Pre-rTMS < > 1-week post-rTMS					
N.S.					

Note. The columns list (from left to right) regions within the cluster showing significant differences in average rsFC with the stimulation site between pre- and post-rTMS visits (uncorrected $p < .01$; cluster-mass $p < .05$ FDR corrected), peak MNI coordinates of the cluster, cluster voxel size (≥ 10 voxels), and effect size of the cluster. Effect sizes represent the average difference in Fisher-transformed correlation coefficients between visits (pre-TMS minus the post-rTMS visit) for the stimulation site (seed) and the correlated region. A positive effect size indicates a decrease in rsFC at the post-rTMS visit. N.S. = no significant difference; R = right; L = left. [b]anticorrelated post-rTMS.

Table 5.5.

Subtle Diffuse Changes in Functional Connectivity Between the Posterior Cingulate Cortex/Precuneus and Correlated Regions Following Accelerated rTMS Sessions

Contrast/ Region	MNI coordinates x	y	z	Voxels	Effect size
Pre-rTMS < > immediate post-rTMS					
N.S.					
Pre-rTMS < > 24 hr post-rTMS					
N.S.					
Pre-rTMS < > 1-week post-rTMS					
Cluster 1	54	-41	1	4364	.20
R middle temporo-occipital				1597	
R posterior middle temporal gyrus				159	
R posterior superior temporal gyrus				136	
R angular gyrus				715	
R posterior supramarginal gyrus				207	
R temporal fusiform cortex				32	
R superior lateral occipital cortex				15	
R inferior lateral occipital cortex				10	

Note. The columns list (from left to right) regions within the cluster showing significant differences in average rsFC with the posterior cingulate cortex/precuneus between pre- and post-rTMS visits (uncorrected $p < .01$; cluster-mass $p < .05$ FDR corrected), peak MNI coordinates of the cluster, cluster voxel size (≥ 10 voxels), and effect size of the cluster. Effect sizes represent the average difference in Fisher-transformed correlation coefficients between visits (pre-TMS minus the post-rTMS visit) for the posterior cingulate cortex/precuneus (seed) and the correlated region. A positive effect size indicates a decrease in rsFC at the post-rTMS visit. N.S. = no significant difference; R = right; L = left.

[b]anticorrelated post-rTMS.

Table 5.6.

Average Change in Functional Connectivity Between the Visual Cortex (Stimulation Site) and Regions Correlated With GABA+ and Glx Following a Single rTMS Session

Metabolite/ Contrast/ Region	Brodmann area	MNI coordinates			Voxels	Effect size
		x	y	z		
GABA+						
Pre-rTMS < > immediate post-rTMS						
N.S.						
Pre-rTMS < > 1 hr post-rTMS						
R precentral gyrus	4	21	-14	50	147	- .74
L precentral gyrus	6	-50	-3	37	36	.74
R lingual gyrus	17	18	-96	4	117	1.02
L inferior occipital gyrus	18	-30	-99	-3	112	1.21
Precuneus		21	-60	26	45	- .74
R middle frontal gyrus	6	45	13	48	45	.62
R cerebellum 9		13	-46	-59	68	- .68
R cerebellum 7b		29	-76	-53	48	- .58
Glx						
Pre-rTMS < > immediate post-rTMS						
N.S.						
Pre-rTMS < > 1 hr post-rTMS						
L superior frontal gyrus	6	-12	41	53	102	.28
R cerebellum 8		18	-44	-56	72	- .21
Precuneus	7	10	-71	48	45	- .23
R precentral gyrus		26	-17	75	42	.26

Note. The columns list (from left to right) regions showing significant differences in rsFC with the stimulation site associated with GABA+/Glx concentrations between pre- and post-rTMS visits (uncorrected $p < .001$; cluster-mass $p < .05$ FDR corrected), the associated Brodmann area, peak MNI coordinates of the cluster, cluster voxel size, and effect size. Effect sizes represent Fisher-transformed regression coefficients as a ratio of change in rsFC between the stimulation site (seed) and the correlated region per unit change in metabolite concentration. A positive effect size indicates a decrease in rsFC at the post-rTMS visit, while a negative effect size indicates an increase in rsFC at the post-rTMS visit. Average change in GABA+ concentration between pre-rTMS and: immediate post-rTMS = -0.176 i.u.; 1 hr post-rTMS = -0.057 i.u. Average change in Glx concentration between pre-rTMS and: immediate post-rTMS = -0.039 i.u.; 1 hr post-rTMS = 0.109 i.u. N.S. = no significant difference; R = right; L = left.

Table 5.7.

Average Change in Functional Connectivity Between the posterior cingulate cortex/precuneus and Regions Correlated With GABA+ Following a Single rTMS Session

Contrast/ Region	Brodmann area	MNI coordinates x	y	z	Voxels	Effect size
Pre-rTMS < > immediate post-rTMS						
R superior frontal gyrus	6	18	3	69	126	- .31
L superior frontal gyrus	6	-1	8	67	374	- .38
R pars opercularis	44/45	56	13	4	90	- .38
L inferior frontal gyrus	45	-47	22	7	93	- .30
R middle frontal gyrus	8	29	24	34	72	- .34
R frontal pole	68	35	38	45	68	- .28
L orbitofrontal cortex	47	-20	19	-26	27	.10
R caudate		15	16	15	207	.32
R precentral gyrus	6	45	5	34	135	- .45
R parietal operculum cortex	13	59	-30	23	117	.30
R thalamus		18	-25	12	81	.23
L cerebellum 9		-20	-52	-45	81	- .22
L cerebellum 8		-20	-66	-42	36	- .12
L cerebellum 6		-31	-63	-26	27	- .21
R cerebellum crus 2		5	-82	-26	45	- .24
R cerebellum crus 1		56	-46	-31	50	- .21
L cerebellum crus 1		-39	-82	-29	27	- .23
L superior lateral occipital cortex		-44	-71	23	63	- .47
L inferior lateral occipital cortex		-47	-66	-7	27	- .16
Anterior cingulate gyrus	24	-6	3	29	50	- .25
R temporal pole		21	8	-48	41	.23
L inferior temporal gyrus	37	-47	-55	-15	27	- .11
R central opercular cortex	13	43	8	4	30	- .26
L central opercular cortex	43	-58	-6	7	36	- .34
L cuneus	18	-4	-98	15	30	- .24
L insular Cortex	13	-42	0	-4	27	- .22
R fusiform gyrus	19	26	-79	-15	27	.09
Pre-rTMS < > 1 hr post-rTMS						
R temporal pole	22	56	11	10	229	.84
R cerebellum crus 2		51	-63	-45	68	- .86
R cerebellum 8		29	-57	-59	30	- .60
L cerebellum 8		-20	-52	-59	219	.84
L frontal pole	10	-6	68	-1	99	- .96
R middle frontal gyrus	8	35	27	34	36	-1.25
R anterior superior temporal gyrus	22	65	-6	-1	98	1.21
R posterior middle temporal gyrus		59	-14	-23	54	- .61
L posterior supramarginal gyrus	40	-50	-46	42	63	- .83
L superior parietal lobule	7	-34	-44	67	39	.83
Posterior cingulate gyrus	31	-4	-33	39	45	- .77

Table 5.7. (continued)

Note. The columns list (from left to right) regions showing significant differences in rsFC with the posterior cingulate cortex/precuneus associated with GABA+ concentrations between pre- and post-rTMS visits (uncorrected $p < .001$; cluster-mass $p < .05$ FDR corrected), the associated Brodmann area, peak MNI coordinates of the cluster, cluster voxel size (≥ 25 voxels), and effect size. Effect sizes represent Fisher-transformed regression coefficients as a ratio of change in rsFC between the posterior cingulate cortex/precuneus (seed) and the correlated region per unit change in GABA+ concentration. A positive effect size indicates a decrease in rsFC at the post-rTMS visit, while a negative effect size indicates an increase in rsFC at the post-rTMS visit. Average change in GABA+ concentration between pre-rTMS and: immediate post-rTMS = -0.176 i.u.; 1 hr post-rTMS = -0.057 i.u. There were no significant differences in rsFC in regions associated with Glx concentrations. R = right; L = left.

Table 5.8.

Average Change in Functional Connectivity Between the Visual Cortex (Stimulation Site) and Regions Correlated With GABA+ and Glx Following Accelerated rTMS Sessions

Metabolite/ Contrast/ Region	Brodmann area	MNI coordinates x	y	z	Voxels	Effect size
GABA+						
Pre-rTMS < > immediate post-rTMS						
R superior frontal gyrus	8	24	38	48	486	.63
L pars opercularis	44	-55	13	15	273	- .63
L pars triangularis	45	-50	27	4	27	- .60
R middle frontal gyrus	9	45	24	34	99	.53
Frontal medial cortex	11	-1	41	-37	50	- .45
R middle temporal gyrus	21/22	56	-22	-7	72	- .59
L lingual gyrus	19	-25	-74	4	141	.52
L superior lateral occipital cortex	7	-31	-63	50	27	.56
L precentral gyrus	6	-53	0	39	81	.63
L postcentral gyrus	40	-53	-30	53	27	.32
L angular gyrus	39	-42	-57	39	30	.40
R caudate		10	19	4	39	.37
Subcallosal cortex	25	-4	19	-23	27	- .34
Pre-rTMS < > 24 hr post-rTMS						
L putamen		-28	8	4	135	.4
R cerebellum crus 1		35	-66	-37	123	.78
R cerebellum crus 6		24	-57	-31	38	.78
R superior lateral occipital cortex		32	-82	20	27	- .69
L superior lateral occipital cortex	19	-31	-79	20	81	- .46
L superior frontal gyrus	10	-36	57	12	66	.54
L frontal medial cortex	10	-6	60	-12	59	- .82
L orbitofrontal cortex	47	-17	13	-23	27	.44
L anterior middle temporal gyrus	21	-58	-11	-20	56	- .56
R precentral gyrus	6	37	-11	67	36	.50
R angular gyrus	40	62	-52	37	28	- .39
R superior parietal lobule	7	21	-55	53	27	- .39
Anterior cingulate	24	-4	-6	34	27	.44
Pre-rTMS < > 1-week post-rTMS						
L orbitofrontal cortex	47	-39	16	-10	210	- .43
L superior frontal gyrus	6	-25	27	50	61	.47
R pars opercularis	9	45	16	23	27	- .19
R superior lateral occipital cortex	19	35	-82	34	36	- .31
L superior lateral occipital cortex	19	-36	-82	29	111	.33
L angular gyrus	40	-55	-49	23	90	- .32
R posterior supramarginal gyrus		45	-44	18	63	- .42
L postcentral gyrus	7	-17	-44	56	27	.32
L parietal operculum cortex	40	-50	-33	23	27	.34
R posterior middle temporal gyrus	21/22	62	-22	-7	54	- .30

Table 5.8. (continued)

Metabolite/ Contrast/ Region	Brodmann area	MNI coordinates x	y	z	Voxels	Effect size
Glx						
Pre-rTMS < > immediate post-rTMS						
R angular gyrus	22	62	-57	20	210	.22
L cerebellum crus 1		-20	-66	-34	117	- .15
L cerebellum 6		-34	-36	-37	54	- .16
R superior frontal gyrus	8	18	30	42	108	.22
R middle frontal gyrus		45	38	-10	27	- .11
L middle frontal gyrus	6	-39	8	61	53	.19
R posterior inferior frontal gyrus		43	-25	-26	36	- .13
R precentral gyrus	9	54	08	18	93	.20
L postcentral gyrus	40	-53	-33	56	67	.15
Precuneus	31	15	-63	34	81	.19
L superior lateral occipital cortex	19	-14	-87	45	86	- .21
L superior lateral occipital cortex	19	-44	-74	45	67	.24
R insular cortex	13	29	24	04	63	.17
R posterior middle temporal gyrus	21	70	-38	-15	62	.22
R posterior middle temporal gyrus	21	59	-25	-10	27	- .20
R posterior inferior temporal gyrus	20	62	-25	-26	27	- .09
R thalamus		10	-30	9	27	- .14
Pre-rTMS < > 24 hr post-rTMS						
R inferior lateral occipital cortex	19	51	-66	-4	338	- .30
L inferior lateral occipital cortex	19	-47	-82	9	258	- .36
L superior lateral occipital cortex		-47	-71	26	27	- .27
L middle temporo-occipital	21	-64	-52	7	256	- .35
R posterior middle temporal gyrus		51	-33	-10	108	- .27
L posterior middle temporal gyrus	21	-61	-14	-10	225	- .40
R fusiform gyrus	19	29	-85	-12	156	- .46
L fusiform gyrus	19	-39	-74	-10	72	- .38
R temporal fusiform cortex		29	-52	-20	54	- .40
L temporal fusiform cortex	37	-36	-60	-15	45	- .31
R superior parietal lobule	7	24	-57	59	149	- .37
L superior parietal lobule	7	-20	-57	64	72	- .16
L orbitofrontal cortex		-25	22	-15	99	.34
L superior frontal gyrus	8	-4	54	34	27	- .25
L middle frontal gyrus	6	-39	5	42	27	- .13
R cerebellum 4–5		7	-46	-10	57	- .21
R amygdala		18	-3	-15	54	.18
R postcentral gyrus	2	40	-22	39	27	.18
L postcentral gyrus	7	-14	-41	59	42	.20
R thalamus		2	-3	4	27	.24
Pre-rTMS < > 1-week post-rTMS						
L cerebellum 9		-17	-55	-45	156	- .39
R temporal fusiform cortex	19/37	26	-55	-10	111	- .40

Table 5.8. (continued)

Note. The columns list (from left to right) regions showing significant differences in rsFC with the stimulation site associated with GABA+/Glx concentrations between pre- and post-rTMS visits (uncorrected $p < .001$; cluster-mass $p < .05$ FDR corrected), the associated Brodmann area, peak MNI coordinates of the cluster, cluster voxel size (≥ 25 voxels), and effect size. Effect sizes represent Fisher-transformed regression coefficients as a ratio of change in rsFC between the stimulation site (seed) and the correlated region per unit change in metabolite concentration. A positive effect size indicates a decrease in rsFC at the post-rTMS visit, while a negative effect size indicates an increase in rsFC at the post-rTMS visit. Average change in GABA+ concentration between pre-rTMS and: immediate post-rTMS = 0.285 i.u.; 24 hr post-rTMS = 0.229 i.u.; 1-week post-rTMS = -0.1775 i.u. Average change in Glx concentration between pre-rTMS and: immediate post-rTMS = 0.294 i.u.; 24 hr post-rTMS = 0.114 i.u.; 1-week post-rTMS = -0.165 i.u. R = right; L = left.

Table 5.9.

Average Change in Functional Connectivity Between the Posterior Cingulate Cortex/Precuneus and Regions Correlated With GABA+ and Glx Following Accelerated rTMS Sessions

Metabolite/ Contrast/ Region	Brodmann area	MNI coordinates			Voxels	Effect size
		x	y	z		
GABA+						
Pre-rTMS < > immediate post-rTMS						
R superior frontal gyrus	6	26	0	64	237	- .86
L orbitofrontal cortex	47	-44	24	-10	30	.67
R superior lateral occipital cortex	7	15	-68	59	168	- .74
L cerebellum crus 1		-50	-52	-40	108	- .68
L cerebellum crus 2		-25	-68	-40	104	- .44
R paracingulate gyrus	8	7	24	42	72	- .81
L paracingulate gyrus	9	-9	46	18	66	.70
L posterior middle temporal gyrus	21	-66	-33	-7	45	.63
Pre-rTMS < > 24 hr post-rTMS						
R posterior middle temporal gyrus	21	62	-22	-7	27	.42
L posterior middle temporal gyrus	21	-66	-22	-10	90	.78
R superior temporal gyrus	22	48	-25	-1	30	.38
L superior temporal gyrus	38	-50	19	-23	27	- .53
L cerebellum crus 1		-47	-49	-29	69	- .80
R frontal operculum cortex	13	48	16	-1	48	.72
Brainstem		-1	-38	-40	36	- .41
R precentral gyrus	6	45	0	45	27	.51
L precentral gyrus	6	-36	-8	64	32	- .46
L thalamus		-9	-33	4	27	.34
Pre-rTMS < > 1-week post-rTMS						
R cerebellum crus 2		40	-52	-40	54	- .42
L cerebellum crus 2		-50	-52	-48	51	- .33
L hippocampus	30	-12	-41	1	45	.39
R superior frontal gyrus	6	10	24	56	27	- .21
L thalamus		-4	-22	9	27	.41
R lingual gyrus	30	21	-44	-7	27	- .36
Glx						
Pre-rTMS < > immediate post-rTMS						
R paracingulate gyrus	8	5	27	45	680	- .28
L paracingulate gyrus	9	-9	49	18	36	.23
R postcingulate gyrus	5	2	-41	72	27	- .15
R anterior cingulate gyrus	24	-6	5	29	66	- .21
R posterior supramarginal gyrus	40	43	-46	42	105	- .26
L precentral gyrus	6	-47	-11	31	27	.09
R angular gyrus		40	-55	34	105	- .28
R occipital pole	18	24	-96	20	135	.21
R inferior lateral occipital cortex	18	32	-87	-7	63	.19

Table 5.9. (continued)

Metabolite/ Contrast/ Region	Brodmann area	MNI coordinates x	y	z	Voxels	Effect size
Glx (continued)						
Pre-rTMS < > immediate post-rTMS						
R superior lateral occipital cortex	7	32	-71	56	38	- .22
L superior lateral occipital cortex		-44	-68	26	57	- .21
R orbitofrontal cortex	45	51	33	-7	60	.25
L cerebellum crus 2		-28	-68	-40	36	- .18
Pre-rTMS < > 24 hr post-rTMS						
R fusiform gyrus		18	-79	-18	144	- .35
R paracingulate gyrus	32	10	11	39	48	.35
L paracingulate gyrus	32	-4	27	34	99	.25
R planum polare	13	51	3	-4	87	.31
L planum polare	22	-58	-3	-1	36	.32
R superior lateral occipital cortex	7	18	-68	59	66	- .17
L superior parietal lobule	7	-28	-46	56	63	- .29
R superior temporal gyrus	22	51	13	-10	45	.32
R inferior temporal gyrus	37	56	-52	-18	27	- .14
R posterior middle temporal gyrus	22	62	-22	-4	57	.19
Subcallosal cortex		2	13	-4	27	- .17
Pre-rTMS < > 1-week post-rTMS						
R accumbens		10	13	-10	108	.43
L cerebellum crus 1 & 2		-47	-49	-40	90	- .42
R superior lateral occipital cortex	7	35	-66	59	72	- .39
R lingual gyrus	18	10	-90	-10	54	.21
R inferior temporo-occipital	37	62	-52	-18	54	- .22
R anterior supramarginal gyrus	2	59	-22	31	54	- .37
L frontal pole	10	-17	63	-18	28	- .31
L middle frontal gyrus	8	-42	35	34	27	.40
Anterior cingulate gyrus	32	2	38	15	27	.14
L fusiform gyrus		-31	-66	-15	27	- .27

Note. The columns list (from left to right) regions showing significant differences in rsFC with the posterior cingulate cortex/precuneus associated with GABA+/Glx concentrations between pre- and post-rTMS visits (uncorrected $p < .001$; cluster-mass $p < .05$ FDR corrected), the associated Brodmann area, peak MNI coordinates of the cluster, cluster voxel size (≥ 25 voxels), and effect size. Effect sizes represent Fisher-transformed regression coefficients as a ratio of change in rsFC between the posterior cingulate cortex/precuneus (seed) and the correlated region per unit change in metabolite concentration. A positive effect size indicates a decrease in rsFC at the post-rTMS visit, while a negative effect size indicates an increase in rsFC at the post-rTMS visit. Average change in GABA+ concentration between

pre-rTMS and: immediate post-rTMS = 0.285 i.u.; 24 hr post-rTMS = 0.229 i.u.; 1-week post-rTMS = -0.1775 i.u. Average change in Glx concentration between pre-rTMS and: immediate post-rTMS = 0.294 i.u.; 24 hr post-rTMS = 0.114 i.u.; 1-week post-rTMS = -0.165 i.u. R = right; L = left.

CHAPTER 6

GENERAL DISCUSSION

Summary

In Chapter 2, I investigated the efficacy of 1 Hz rTMS in mitigating visual hallucinations that are prevalent following visual pathway damage. Multiday rTMS of 30 min sessions was applied to the visual cortex in a patient who experienced disruptive and continuous phosphene hallucinations for more than 2 years following occipital stroke. rTMS significantly attenuated the perception of hallucinations and the effect outlasted stimulation. However, despite repeated doses, the therapeutic effect of rTMS only persisted for a few days following rTMS cessation. In the only other study that has investigated rTMS to alleviate visual hallucinations in visual pathway damage, a single 30 min session of rTMS was sufficient to cease intermittent hallucinations for two weeks (Merabet et al., 2003). Further, in another sensory domain, 1 Hz rTMS has shown promise in alleviating auditory hallucinations (Lee et al., 2005; Vercammen et al., 2010). Although rTMS substantially redistributed the imbalanced and aberrant functional activity in our patient to more closely resemble that of controls, and this attempt at "renormalisation" was reflected in the attenuation of hallucinations, I sought to determine why the positive impact of rTMS had not been as enduring in this patient as it is in other cases. Therefore, in Chapter 3, I investigated white matter structural connectivity to determine whether more persistent changes in connectivity that are not as malleable to neuromodulation may provide insight. I observed that more permanent and maladaptive structural changes had indeed occurred. Diffusion imaging showed regeneration of optic radiations that deviated from their regular pathway, as well as a combination of greater and reduced structural tracts between the visual cortices and frontal, temporal, and parietal regions. The extent of structural changes likely offer explanation as to why the patient was not as responsive as expected. In the presence of longer-term structural reorganisation, transient neuromodulation effects on functional activity are

insufficient to overcome more permanent aberrant structural changes with sustained effects. However, it is promising that despite these extensive structural changes, we were nonetheless able to modify functional activity and significantly decrease the perception of hallucinations providing substantial relief for the patient, even if it was only for a week. rTMS still holds promise, and longer repeated application of rTMS will have a more sustained response. Longer-term functional changes may in turn lead to longer-term structural changes and better functional outcome. The combination of fMRI and DTI is invaluable as it provides insight into neural mechanisms underlying pathophysiology (e.g., in this case visual hallucinations) and changes with rTMS, as well as information on barriers for better prognosis (e.g., significant structural changes).

In Chapter 2, I also observed that despite the significant reduction in perception of visual hallucinations with rTMS and the corresponding rebalance of functional activity across hemispheres post-rTMS in the patient, the stimulation site showed an overall increase in functional activity with a 1 Hz rTMS "inhibitory" paradigm. As discussed previously, numerous studies suggest that low-frequency "inhibitory" effects depend on numerous factors including stimulation intensity relative to cortical excitability thresholds. We nonetheless had predicted a reduction in functional activity at the stimulation site. This expectation was based on the view that visual hallucinations are thought to arise from dysfunctional persistent neuronal firing in peri-infarct regions (De Haan et al., 2007; Kasten et al., 1998; Manford & Andermann, 1998; Rijntjes et al., 1994); therefore, one would expect that if rTMS decreases the perception of hallucinations, it also decreases the increased neuronal firing (i.e., BOLD signal) around the lesion (rTMS target site). This unexpected finding suggested that either the rTMS response deviated from the typical response because of pathophysiology in the patient, or that we simply

do not know enough about multiday 1 Hz rTMS effects in the visual cortex, and accordingly, cannot predict changes in BOLD signal post-rTMS. The unexpected finding of increased functional activity at the stimulation target site (lesion) also suggested that the alleviation of symptoms (perception of hallucinations) occurred via mechanisms of which BOLD signal may be a poor indicator. It could also be that the alleviation of symptoms occurred via alterations in BOLD signal downstream from the rTMS target site as well as a rebalancing of BOLD signal at the target site. For these reasons, it was clear that I had to investigate rTMS effects in healthy control participants and determine the expected response in the absence of pathophysiology in order to guide development of therapeutic protocols. Investigation in the absence of dysfunction would highlight which mechanisms rTMS can target and is capable of altering, and therefore, which visual disorders it would be suitable for. Furthermore, obtaining more complete representation of neural substrates of rTMS can prevent inadvertently induced adverse effects in patient populations. Lastly, knowledge of rTMS effects in healthy controls and deviation from these effects in patients can highlight mechanisms underlying pathophysiology and offer insight into the pathology that we may not already know.

To address limitations of the patient study and gain insight into neural mechanisms of 1 Hz rTMS to the visual cortex, in Chapter 4 I investigated rTMS effects on GABA and glutamate neurotransmitters that are key in plasticity. In addition, in Chapter 5, I investigated the effects of rTMS on intrinsic functional connectivity between the visual cortex and remote regions. To refine parameters and find the most efficient rTMS protocol for clinical application, I also compared single session and accelerated rTMS regimes, two alternative approaches that are used in clinical applications in non-visual disorders (Goldsworthy et al., 2015). I observed that 1 Hz rTMS targets MRS measured GABA but not Glx activity in the visual cortex, and that overall

GABA concentration (consisting of inhibitory $GABA_A$ and excitatory $GABA_B$ concentrations) decreased with accelerated 1 Hz rTMS sessions but not with a single session. On the other hand, single session rTMS induced strong diffuse widespread changes in rsFC, whereas accelerated rTMS produced weak subtle changes. Moreover, rsFC changes were associated with changes in GABA and Glx activity. These findings highlight that the choice of regimen would largely be based on the mechanism you wish to alter. Specifically, single session rTMS may have a better response on altering dysfunctional connectivity between nodes, whereas accelerated rTMS may be better suited to modulating GABA concentrations at the visual cortex.

Collectively, these studies were intended to advance our knowledge of low-frequency rTMS on the visual cortex, with a specific interesting in developing therapeutic protocols relevant to visual disorders.

Limitations

Limitations associated with each of the experimental studies are discussed within the appropriate chapters. Other general limitations are discussed here.

With regards to experimental design, in hindsight, rsfMRI and MRS in our patient pre- and post-rTMS would have been extremely valuable. Unfortunately, due to limited availability of the patient because she resides in a different country, refinement of parameters and further investigation have not been possible. In Chapters 4–5, inconsistent follow-up time points were used between single session and accelerated rTMS regimes. We chose these time points based on previous research on known rTMS aftereffect durations (for a review, see Thut & Pasucal-Leone, 2010) to minimise high MRI costs and fatigue effects in individuals who underwent a rather long protocol with accelerated rTMS (4–5 hr session). However, based on the present findings on rsfMRI that indicate aftereffects persist for much longer than the chosen timepoints, it would be

important to continue follow-up visits for longer periods that are consistent across regimes for better comparison and for a fuller determination of the duration of rTMS effects.

A difficulty arises with TMS coil orientation when stimulating visual areas depending on individual anatomy such as the proximity of the target stimulation site with external anatomy such as the neck. The bulk of the coil and coil cable can result in restricted positioning depending on the curvature of the back of the head and location of the neck and shoulders. The main concern is that the TMS coil is tangential to the target stimulation site to ensure minimal coil-to-target stimulation distance (Ulmer & Jansen, 2010) as dictated by image-guided stereotaxy. Therefore, if needed, the coil may be rotated in order to obtain the optimal position, which may not be a consistent orientation across individuals. The direction of the current in the TMS coil is opposite to the direction of the induced current immediately underneath the coil. The direction of the induced current can significantly influence mechanisms of neuronal activation, including the type of neurons recruited (e.g., interneuron versus pyramidal) and the site of the neuronal depolarisation (e.g., soma versus axon hillock) (Fox et al., 2004; Thielscher, Opitz, & Windhoff, 2011; Wagner et al., 2004). The effect of coil orientation on TMS induced effects has primarily been examined in the motor cortex. For instance, posterior–anterior, anterior–posterior, and lateral–medial induced currents in the brain produce different patterns of corticospinal volleys (Di Lazzaro et al., 2012). Therefore, coil rotation with occipital stimulation may have had a large impact on stimulation effects across individuals, but without investigation of TMS coil orientation on the visual cortex, it is difficult to ascertain. Moreover, inter-individual variability in TMS-induced responses may be partly related to differences in the coil-to-cortex distance and physiological variability. The coil-to-cortex distance is not homogenous across cortical and subcortical layers nor across individuals. Layers of neural tissue located underneath the TMS

coil, e.g., skull, cerebrospinal fluid, grey and white matter, all have distinct electrical properties. The inconsistency in tissue leads to an inhomogeneous dispersion of the electrical field in each layer and a buildup of electrostatic charge at the boundaries (Rotenberg et al., 2014), and these physiological-specific differences are further influenced by coil orientation (Opitz et al., 2013). Moreover, there are individual state-dependency effects of underlying neuronal activity that affect the TMS response (Pasley et al., 2009; Perini et al., 2012).

There are limitations associated with interpretation of TMS-induced changes. TMS stimulates neuronal tissue externally and artificially, thus, changes revealed by TMS may be different from those following physiological processes. Remote changes observed in response to TMS with neuroimaging may reflect other factors besides propagation of activity along cortical connections and TMS-induced plasticity, consequently complicating interpretation. These confounds include effects induced from the tapping or clicking sensation from the coil, e.g., intensity of tapping sensation, coil clicking noise, or muscle twitching to stimulation, all of which increase with greater stimulation intensity. There are also behavioural or cognitive consequences of TMS leading to changes in neuronal activity, or neuronal adaptation to the TMS perturbation. These confounds are accounted for to some extent in a repeated measures design (as employed in the present studies). A placebo rTMS condition (e.g., sham rTMS or rTMS to the vertex) was not employed in Chapters 4–5 in addition to the baseline/no rTMS condition due to the already extremely high MRI costs. There are also issues associated with these rTMS control conditions. rTMS to the vertex induces significant network changes across the brain (e.g., via DMN), and sham stimulation can induce changes in neural activity via clicking noises or the tapping sensation (Duecker & Sack, 2015; Jung, Bungert, Bowtell, & Jackson, 2016). Additionally, with sham rTMS, participants are usually aware the stimulation sensation and

clicking noise is different to real stimulation. No single control condition can satisfy the potential confounds induced by rTMS unless we account for them all, which was financially not possible.

We are also limited by the noninvasive techniques available to determine underlying neural mechanisms in humans, including limitations of spatial and temporal resolution. We can obtain indirect measures, e.g., fMRI BOLD signal, rather than directly measuring neuronal activity to infer changes (Logothetis & Wandell, 2004). It is not possible in the human brain to noninvasively investigate at the level of individual neurons and synapses, or at the level of neuronal groups and populations, but we can obtain information on neural networks using rsFC. We also cannot measure precise neurotransmitter receptor activity, but only measure overall concentrations extrasynaptically using MRS. Despite these limitations, we can obtain vast knowledge using a combination of techniques to gain as much understanding as possible.

Future Directions – What Next?

The work in this dissertation barely scratches the surface in determining effects of rTMS to the visual cortex and translation to therapeutic intervention. A considerable amount of research on rTMS still needs to be conducted to determine a complete representation of underlying neural substrates, longer-term effects, adverse effects with repeated application, and determining the most efficient stimulation protocols. I will begin by mentioning some immediate future areas of work that can contribute valuably to the field. These future directions are not exhaustive. There are, of course, undoubtedly many future areas of research with regards to developing therapeutic noninvasive brain stimulation techniques for visual disorders that are yet to be investigated.

First, a variety of stimulation parameters need to be investigated. This includes testing the effects of high-frequency rTMS to the visual cortex, but also exploring different low-frequency

protocols, e.g., 1 Hz versus 3 Hz, to determine the most efficient protocol and to create a wide array of parameters suitable for a range of disorders. Moreover, other rTMS parameters also need to be manipulated including sub-PT versus supra-PT intensity. A different response is expected with sub- and supra-PT rTMS (e.g., Di Lazzaro et al., 1998; Ziemann et al., 1996) that can target different mechanisms compared with rTMS applied at PT intensity. The interval time between accelerated sessions, as well the length of a session, are important factors to consider that may substantially affect results. It is important to identify intervals that are optimal for inducing long-lasting and stable neuroplastic change, and these will likely change for different cortical targets. Although this has been done to a greater extent for tDCS and the motor cortex, it is very unlikely that the same spacing interval will be optimal for all noninvasive brain stimulation techniques (Goldsworthy et al., 2015). The relevance of intervals during conventional rTMS impacts the direction of aftereffects irrespective of the frequency (i.e., low- versus high-frequency) (Monte-Silva et al., 2010; Rothkegel, Sommer, & Paulus, 2010). It has also been shown that simply prolonging stimulation duration for enhancing the efficacy of a TBS protocol without spaced intervals results in a reversal of aftereffects on cortical excitability (Gamboa et al., 2010). We have previously observed different effects on object and scene processing with 20 min compared with 30 min of 1 Hz rTMS to occipital regions (Mullin & Steeves, 2013; Rafique et al., 2015). Ultimately, it will be important to ascertain the minimal stimulation time that produces the most efficient sustained response. And then, most importantly, we must consider how these results with different parameters translate to different clinical populations.

There is also the essential consideration of other noninvasive brain stimulation techniques. TBS allows for much shorter application time and longer-lasting cortical excitability effects than conventional rTMS (Chistyakov, Rubicsek, Kaplan, Zaaroor, & Klein, 2010; Huang

et al., 2009; Ishikawa et al., 2007). Can we then replicate findings of low- and high-frequency rTMS with TBS and significantly shorter application times? Or, will TBS parameters produce vastly different effects and therefore be better suited to different visual disorders than those suited to rTMS? How do effects change with a variety of TBS parameters to the visual cortex? Varying effects on GABA/glutamate concentrations are observed depending on the type of noninvasive brain stimulation. Continuous TBS to motor cortex increases MRS measured GABA (Stagg et al., 2009b) consistent with the known inhibitory neurophysiological effects of continuous TBS. However, pharmacological studies have shown that the aftereffects of continuous TBS are mediated to an extent by glutamatergic mechanisms (Huang, Chen, Rothwell, & Wen, 2007) to which MRS may not be sensitive. Anodal (facilitatory) tDCS to motor cortex decreases GABA (Stagg et al., 2009a), while increasing Glx in the parietal lobe (Clark, Coffman, Trumbo, & Gasparovic, 2011). Cathodal (inhibitory) tDCS leads to a significant decrease in Glx and a correlated decrease in GABA in the motor cortex (Stagg et al., 2009b). Continuous TBS and cathodal tDCS have very similar neurophysiological effects, yet have markedly different effects on neurotransmitters (Stagg, 2014). The LTP-like and LTD-like effects of rTMS rely on NMDA receptor-mediated glutamatergic and GABAergic function, and rTMS is capable of inducing action potentials in nearby stimulated neuronal tissue. tDCS on the other hand is considered to induce a modulatory effect via biasing cortical excitability (Nitsche & Paulus, 2000). More specifically, animal studies have established that anodal tDCS increases neuronal excitability and spontaneous firing rate by depolarising resting membrane potentials, whereas cathodal tDCS hyperpolarises membrane potentials, leading to decreased neuronal firing rate and excitability (for a review, see Dayan et al., 2013). Different stimulation techniques may therefore also stimulate populations of neurons to different extents that has important

implications for the therapeutic use of stimulation paradigms where it may be clinically beneficial to preferentially stimulate one group of neurons. Accordingly, one paradigm may be more effective than another.

While rTMS does alter functional connectivity, it appears to do so in unpredictable ways across individuals, and between unexpected regions. If the goal is to selectively increase or decrease connectivity between specific brain regions in a controlled manner, advances in our understanding of rTMS or alternative approaches is needed. One alternative approach that may help address this issue is to precondition the stimulation and modify connectivity in a more controlled manner. Preconditioning with a session of tDCS can be used to shape the conditioning effect of subsequent rTMS (Siebner et al., 2004). “Facilitatory” preconditioning with anodal tDCS followed by subsequent 1 Hz rTMS reduces corticospinal excitability to below baseline levels for more than 20 min. Conversely, “inhibitory” preconditioning with cathodal tDCS followed by subsequent 1 Hz rTMS increases corticospinal excitability for at least 20 min. This preconditioning pattern is interpreted in the context of homeostatic plasticity. Although activity-dependent synaptic plasticity is required for modification of network properties, homeostatic mechanisms ensure that plastic changes only occur within a physiologically useful range and allow for network stability (Turrigiano & Nelson, 2004). The variable aftereffects may be due to different excitability levels in participants at the time of rTMS conditioning (i.e., state-dependency; Pasley et al., 2009). Therefore, the preconditioning approach might be effective in enhancing the therapeutic efficacy of rTMS in patients and may produce more consistent aftereffects as well as limit inter-individual variability.

There are a variety of other noninvasive techniques that can be used to determine the effects of stimulation on other neurophysiological parameters in the visual cortex, e.g., PET, or

assessing changes on other neurometabolites. A valuable measure would be to assess BDNF concentration. BDNF regulates cell growth, survival, proliferation, and protects against oxidative stressors (Müller et al., 2000; Post et al., 1999). BDNF also modulates LTP and LTD mechanisms (Figurov, Pozzo-Miller, Olafsson, Wang, & Lu, 1996; Gottman, Mittmann, & Lessmann, 2009; Woo et al., 2005). With regards to the visual cortex, acceleration of BDNF promotes visual cortical development and plasticity (Berardi, Pizzorusso, Ratto, & Maffei, 2003; Huang et al., 1999; McAllister, Katz, & Lo, 1999). Notably, rTMS is shown to upregulate BDNF and improve aberrant visual cortical topography (Makowiecki, Harvey, Sherrard, & Rodger, 2014). Modulation of BDNF with noninvasive brain stimulation is therefore ideal in clinical applications. Furthermore, individuals expressing polymorphism in BDNF show impaired responses to noninvasive brain stimulation (Antal et al., 2010; Cheeran et al., 2008). This has critical value in clinical applications as it can determine the efficacy of treatment with regards to plasticity and resistance to treatment. Suitably, BDNF quantification has been suggested as a biological marker to characterise rTMS effects (Brunoni, Boggio, & Fregni, 2008). In humans, BDNF can be quantified noninvasively using salivary or blood samples (Saruta, Fujino, To, & Tsukinoki, 2012; Trajkovska et al., 2007; Vrijen, Schenk, Hartman, & Oldehinkel, 2017).

The diffusion tensor is only capable of representing a single fibre orientation per voxel. Therefore, in circumstances of complex fibre architecture (e.g., bending, crossing and kissing fibres, contamination between adjacent fibre populations), the diffusion tensor is a poor representation of the underlying structure that can lead to errors in the estimation of fibre orientations and associated errors in the reconstruction of fibre pathways (Smith, Tournier, Calamante, & Connelly, 2012). More sophisticated diffusion imaging techniques and analyses have been proposed. For example, high angular resolution diffusion imaging (HARDI) has better

angular and spatial resolution, demonstrating greater detection of crossing fibres in cases where DTI is inaccurate (Jansons & Alexander, 2003). Accordingly, HARDI has better discrimination of pathways and produces more fibres; therefore, it demonstrates better detection in disease states affecting white mater structure (Berman, Lanza, Blaskey, Edgar, & Roberts, 2013; Wang et al., 2016). A novel combination of processing, reconstruction, and tractography methods termed high definition fibre tracking (HDFT) have been developed using a high angular resolution-based approach (Fernández-Miranda et al., 2012). HDFT leverages high directional sampling of diffusion imaging space to get better resolution of underlying white matter geometry for tractography (Yeh, Wedeen, & Tseng, 2010). Studies demonstrate that HDFT provides accurate replication of complex known neuroanatomical features where DTI fails (Fernández-Miranda et al., 2015; Wang et al., 2013; Wu, Sun, Wang, Wang, & Ou, 2016). Furthermore, HDFT is proven to allow tracing from one cortical region to other cortical or subcortical regions through complex crossings areas, providing detailed evidence of the cortical site of origin or termination of fibres without the need for approximation as with DTI (Fernández-Miranda et al., 2015; Wu et al., 2016).

The information from a seed-based rsFC map is limited to the functional connections of the selected seed region, making it difficult to examine functional connectivity patterns on a whole-brain scale. Model-free methods exist to examine whole-brain connectivity patterns without the need of defining an a priori seed region. In contrast to seed-based methods, model-free methods look for general patterns of (unique) connectivity across brain regions. ICA-based methods are perhaps the most popular and powerful model-free technique (Beckmann et al., 2005; Calhoun, Adali, Pearlson, & Pekar, 2001; De Luca, Beckmann, De Stefano, Matthews, & Smith, 2006; van de Ven, Formisano, Prvulovic, Roeder, & Linden, 2004) and show a high level

of consistency (Damoiseaux et al., 2006). ICA methods search for a mixture of underlying sources that can explain resting-state patterns and look for the presence of spatial sources of resting-state signals that are maximally independent from each other. A possible disadvantage of ICA methods is that the ICs are often perceived as more difficult to understand than traditional seed-based rsFC maps since they contain a more complex representation of the data. ICA data may therefore complicate the translation of between-group results to clinical relevance (Fox & Raichle, 2007). Lastly, there are important limitations to measuring connectivity with rsfMRI. Because participants are not performing a specific task, there is no clear measure of performance or mental state. In this case, task-based fMRI can provide valuable information where rsfMRI fails. Moreover, rsfMRI is a correlational measure only, and not a causal measure, limiting the conclusions that can be drawn. Further research in patient populations would also benefit from effective connectivity models to investigate the causal influence of implicated regions on interconnected regions (Friston, 1994). For example, in the case of visual hallucinations in our patient, the causal influence of peri-infarct regions at the lingual gyrus (considered the main source of hallucinations) on interconnected regions with aberrant activity can confirm/refute which regions are the cause and which are involved as a secondary effect to the hallucinations.

In the pathological brain, restoring a normal pattern of activity within a given neural network may not be the most effective way to suppress symptoms and encourage rehabilitation. Instead, it may be more beneficial to induce changes that prove behaviourally more adaptive. Because increasing cortical excitability can facilitate learning, adjunct therapies or online stimulation protocols may have a greater impact in restorative neurology and rehabilitation (e.g., stimulation combined with visual tasks or vision restoration therapy). In this respect, findings from the learning literature suggest that the optimal interval spacing between training sessions is

influenced by numerous key factors, including the nature of the task being learned (for a review, see Donovan & Radosevich, 1999). The same principles may apply with different forms of noninvasive brain stimulation in addition to the spacing of intervals between stimulation sessions and the length of stimulation.

Shorter schedules of rTMS application were used in healthy controls and in our patient due to limited knowledge of aftereffects on the visual cortex (e.g., adverse effects) and associated ethical considerations. The repeated consecutive application of rTMS was well tolerated by controls and the patient. One would likely observe different results with prolonged application over consecutive weeks, as would be used in clinical applications, and this warrants further investigation now that I have established a safe starting point. With longer applications of stimulation, the likelihood of adverse effects increases. Although longitudinal studies are difficult to achieve due to high attrition rates and high financial costs, longer-term investigation over periods of months is necessary to rule out long-term side effects of rTMS. At present, longitudinal noninvasive brain stimulation studies are significantly lacking, particularly with follow-ups using neuroimaging. Current studies that have investigated long-term effects have done so using subjective or behavioural measures only (e.g., Dunner et al., 2014; Liepert et al., 2000a). Along with long-term follow-up with neuroimaging, more clinical trials in visual disorders are needed, and with much larger sample sizes. Longitudinal studies are particularly critical, as individual differences in brain plasticity are quite large (Maeda et al., 2000), and understanding factors that condition individual differences will offer unique and novel targets to promote individual brain recovery and restoration long-term with minimal adverse effects. Important factors to consider that likely contribute to differences in mechanisms of plasticity across individuals include genetic mechanisms (e.g., polymorphisms, genetic expression),

hormonal factors (e.g., gender, menstrual cycle), impact of systemic conditions (e.g. diabetes, cancer, or infections), and general day-to-day factors influencing health (e.g., exposure to toxins, stress, sleep deprivation, substance abuse, poor nutrition, etc.).

Relevance to Non-Visual Disorders

Visual hallucinations can be provoked by a variety pathophysiological processes, including cell death (e.g., visual pathway damage), psychological disorders (e.g., schizophrenia), drug substances, or neurodegenerative conditions (e.g., dementia with Lewy bodies, Parkinson's disease, Alzheimer's disease) (for a review, see Onofrj et al., 2015). The prevalence of visual hallucinations in Parkinson's disease for example is relatively high (Barnes, Boubert, Harris, Lee, & David, 2003; Williams & Lees, 2005). In Parkinson's disease, visual hallucinations can be accompanied by paranoia and, in comparison with other consequences such as motor disability and dementia, hallucinations are more important as a risk factor for nursing home placement and its associated mortality. The frequency and morbidity associated with visual hallucinations in Parkinson's disease underscores the need for understanding their pathophysiology and treatment (Diederich, Goetz, & Stebbins, 2005). The present work is not only relevant to visual hallucinations, but to general visual disorders and non-visual disorders that present with secondary visual complications. For instance, patients with Parkinson's disease also have impairments in contrast sensitivity, and rTMS has previously been shown to improve contrast sensitivity (Clavagnier et al., 2013; Thompson et al., 2008). In addition to visual hallucinations, patients with Alzheimer's and Parkinson's disease present with impaired object and face perception (Barnes et al., 2003; Tippet, Blackwood, & Farah, 2003). From previous research, we know that TMS can influence the processing of faces and objects (Mullin & Steeves, 2013; Rafique et al., 2015; Solomon-Harris et al., 2016). Therefore, noninvasive brain

stimulation to visual areas holds tremendous promise in improving visual-related symptoms in a variety of pathophysiology, and is applicable to any condition with impaired mechanisms that we know rTMS can target. It is then quite surprising that the application of noninvasive brain stimulation to visual cortices has received considerably less interest in developing relevant therapeutic protocols.

Final Thoughts

There are substantially more questions and areas that remain to be investigated. Although time-consuming and costly, it is vital that we explore effects of different noninvasive brain stimulation techniques and stimulation parameters to create optimal protocols with therapeutic relevance. A variety of optimal parameters will enable targeting of a diverse range of pathologies and neural mechanisms in visual-related disorders. The use of consecutive brain stimulation and neuroimaging techniques that are differentially sensitive to neural mechanisms, and thus complementary, is imperative. Effects of stimulation should continue to be explored in healthy controls as well as patient populations to gain valuable insight into neural mechanisms underlying rTMS and disease processes.

References

Aarsland, D., Ballard, C., Walker, Z., Bostrom, F., Alves, G., Kossakowski, K., et al. (2009). Memantine in patients with Parkinson's disease dementia or dementia with Lewy bodies: a double-blind, placebo-controlled, multicentre trial. *The Lancet Neurology*, *8*(7), 613–618.

Adachi, N., Watanabe, T., Matsuda, H., & Onuma, T. (2000). Hyperperfusion in the lateral temporal cortex, the striatum and the thalamus during complex visual hallucinations: single photon emission computed tomography findings in patients with Charles Bonnet syndrome. *Psychiatry and Clinical Neurosciences*, *54*(2), 157–162.

Aertsen, A. M., Gerstein, G. L., Habib, M. K., & Palm, G. (1989). Dynamics of neuronal firing correlation: modulation of "effective connectivity". *Journal of Neurophysiology*, *61*(5), 900–917.

Ajina, S., & Kennard, C. (2012). Rehabilitation of damage to the visual brain. *Revue Neurologique*, *168*(10), 754–761.

Alber, R., Cardoso, A. M. G., & Nafee, T. (2015). Effects of noninvasive brain stimulation in cerebral stroke related vision loss. *Principles and Practice of Clinical Research*, *1*(2), 15–21.

Alber, R., Moser, H., Gall, C., & Sabel, B. A. (2017). Combined transcranial direct current stimulation and vision restoration training in subacute stroke rehabilitation: a pilot study. *PM&R*, *9*(8), 787–794.

Allen, E. A., Pasley, B. N., Duong, T., & Freeman, R. D. (2007). Transcranial magnetic stimulation elicits coupled neural and hemodynamic consequences. *Science*, *317*(5846), 1918–1921.

Amassian, V. E., Eberle, L., Maccabee, P. J., & Cracco, R. Q. (1992). Modelling magnetic coil excitation of human cerebral cortex with a peripheral nerve immersed in a brain-shaped volume conductor: the significance of fiber bending in excitation. *Electroencephalography and Clinical Neurophysiology/Evoked Potentials Section*, *85*(5), 291–301.

Amedi, A., Malach, R., & Pascual-Leone, A. (2005). Negative BOLD differentiates visual imagery and perception. *Neuron*, *48*(5), 859–872.

Ames III, A. (2000). CNS energy metabolism as related to function. *Brain Research Reviews*, *34*(1–2), 42–68.

Anderson, S. W., & Rizzo, M. (1994). Hallucinations following occipital lobe damage: the pathological activation of visual representations. *Journal of Clinical and Experimental Neuropsychology*, *16*(5), 651–663.

Andersson, J. L., Jenkinson, M., & Smith, S. (2007). Non-linear registration, aka Spatial normalisation FMRIB technical report TR07JA2. *FMRIB Analysis Group of the University of Oxford*, *2*, 1–21.

Andersson, J. L., & Sotiropoulos, S. N. (2016). An integrated approach to correction for off-resonance effects and subject movement in diffusion MR imaging. *Neuroimage*, *125*, 1063–1078.

Antal, A., Chaieb, L., Moliadze, V., Monte-Silva, K., Poreisz, C., Thirugnanasambandam, N., W., et al. (2010). Brain-derived neurotrophic factor (BDNF) gene polymorphisms shape cortical plasticity in humans. *Brain Stimulation: Basic, Translational, and Clinical Research in Neuromodulation*, *3*(4), 230–237.

Antal, A., Lang, N., Boros, K., Nitsche, M., Siebner, H. R., & Paulus, W. (2008). Homeostatic metaplasticity of the motor cortex is altered during headache-free intervals in migraine with aura. *Cerebral Cortex*, *18*(11), 2701–2705.

Antal, A., Paulus, W., & Nitsche, M. A. (2011). Electrical stimulation and visual network plasticity. *Restorative Neurology and Neuroscience*, *29*(6), 365–374.

Arfanakis, K., Haughton, V. M., Carew, J. D., Rogers, B. P., Dempsey, R. J., & Meyerand, M. E. (2002). Diffusion tensor MR imaging in diffuse axonal injury. *American Journal of Neuroradiology*, *23*(5), 794–802.

Ashtari, M., Cottone, J., Ardekani, B. A., Cervellione, K., Szeszko, P. R., Wu, J., et al. (2007). Disruption of white matter integrity in the inferior longitudinal fasciculus in adolescents with schizophrenia as revealed by fiber tractography. *Archives of General Psychiatry, 64*(11), 1270–1280.

Attwell, D., & Laughlin, S. B. (2001). An energy budget for signaling in the grey matter of the brain. *Journal of Cerebral Blood Flow & Metabolism*, *21*(10), 1133–1145.

Aufhaus, E., Weber-Fahr, W., Sack, M., Tunc-Skarka, N., Oberthuer, G., Hoerst, M., et al. (2013). Absence of changes in GABA concentrations with age and gender in the human anterior cingulate cortex: A MEGA-PRESS study with symmetric editing pulse frequencies for macromolecule suppression. *Magnetic Resonance in Medicine*, *69*(2), 317–320.

Avery, D. H., Holtzheimer, P. E., Fawaz, W., Russo, J., Neumaier, J., Dunner, D. L., et al. (2006). A controlled study of repetitive transcranial magnetic stimulation in medication-resistant major depression. *Biological Psychiatry*, *59*(2), 187–194.

Aydin-Abidin, S., Moliadze, V., Eysel, U. T., & Funke, K. (2006). Effects of repetitive TMS on visually evoked potentials and EEG in the anaesthetized cat: dependence on stimulus frequency and train duration. *The Journal of Physiology*, *574*(2), 443–455.

Bäckström, T., Andersson, A., Andreé, L., Birzniece, V., Bixo, M., Björn, I., et al. (2003). Pathogenesis in menstrual cycle-linked CNS disorders. *Annals of the New York Academy of Sciences*, *1007*(1), 42–53.

Baier, B., De Haan, B., Mueller, N., Thoemke, F., Birklein, F., Dieterich, M., & Karnath, H. O. (2010). Anatomical correlate of positive spontaneous visual phenomena A voxelwise lesion study. *Neurology*, *74*(3), 218–222.

Bak, L. K., Schousboe, A., & Waagepetersen, H. S. (2006). The glutamate/GABA-glutamine cycle: aspects of transport, neurotransmitter homeostasis and ammonia transfer. *Journal of Neurochemistry*, *98*(3), 641–653.

Bammer, R. (2003). Basic principles of diffusion-weighted imaging. *European Journal of Radiology*, *45*(3), 169–184.

Barker, A. T., Jalinous, R., & Freeston, I. L. (1985). Non-invasive magnetic stimulation of human motor cortex. *The Lancet*, *325*(8437), 1106–1107.

Barnes, J., Boubert, L., Harris, J., Lee, A., & David, A. S. (2003). Reality monitoring and visual hallucinations in Parkinson's disease. *Neuropsychologia*, *41*(5), 565–574.

Bastani, A., & Jaberzadeh, S. (2014). Within-session repeated a-tDCS: the effects of repetition rate and inter-stimulus interval on corticospinal excitability and motor performance. *Clinical Neurophysiology*, *125*(9), 1809–1818.

Bäumer, T., Bock, F., Koch, G., Lange, R., Rothwell, J. C., Siebner, H. R., et al. (2006). Magnetic stimulation of human premotor or motor cortex produces interhemispheric facilitation through distinct pathways. *The Journal of Physiology*, *572*(3), 857–868.

Bäumer, T., Lange, R., Liepert, J., Weiller, C., Siebner, H. R., Rothwell, J. C., & Münchau, A. (2003). Repeated premotor rTMS leads to cumulative plastic changes of motor cortex excitability in humans. *Neuroimage*, *20*(1), 550–560.

Bear, M. F., & Kirkwood, A. (1993). Neocortical long-term potentiation. *Current Opinion in Neurobiology*, *3*(2), 197–202.

Bear, M. F., & Malenka, R. C. (1994). Synaptic plasticity: LTP and LTD. *Current Opinion in Neurobiology*, *4*(3), 389–399.

Beaulieu, C. (2002). The basis of anisotropic water diffusion in the nervous system – a technical review. *NMR in Biomedicine*, *15*(7-8), 435–455.

Beckmann, C. F., DeLuca, M., Devlin, J. T., & Smith, S. M. (2005). Investigations into resting-state connectivity using independent component analysis. *Philosophical Transactions of the Royal Society B: Biological Sciences*, *360*(1457), 1001–1013.

Behar, K. L., Rothman, D. L., Spencer, D. D., & Petroff, O. A. (1994). Analysis of macromolecule resonances in ^{1}H NMR spectra of human brain. *Magnetic Resonance in Medicine*, *32*(3), 294–302.

Behrendt, R. P. (2003). Hallucinations: Synchronisation of thalamocortical γ oscillations underconstrained by sensory input. *Consciousness and Cognition*, *12*(3), 413–451.

Behrendt, R. P. (2006). Dysregulation of thalamic sensory ‘transmission’in schizophrenia: neurochemical vulnerability to hallucinations. *Journal of Psychopharmacology*, *20*(3), 356–372.

Behrens, T. E., Woolrich, M. W., Jenkinson, M., Johansen-Berg, H., Nunes, R. G., Clare, S., et al. (2003). Characterization and propagation of uncertainty in diffusion-weighted MR imaging. *Magnetic Resonance in Medicine, 50*(5), 1077–1088.

Behrens, T. E. J., Berg, H. J., Jbabdi, S., Rushworth, M. F. S., & Woolrich, M. W. (2007). Probabilistic diffusion tractography with multiple fibre orientations: What can we gain? *Neuroimage, 34*(1), 144–155.

Behzadi, Y., Restom, K., Liau, J., & Liu, T. T. (2007). A component based noise correction method (CompCor) for BOLD and perfusion based fMRI. *Neuroimage, 37*(1), 90–101.

Benjamin, E. J., Blaha, M. J., Chiuve, S. E., Cushman, M., Das, S. R., Deo, R., et al. (2017). Heart disease and stroke statistics–2017 update: a report from the American Heart Association. *Circulation, 135*(10), e146–e603.

Ben-Shachar, D., Belmaker, R. H., Grisaru, N., & Klein, E. (1997). Transcranial magnetic stimulation induces alterations in brain monoamines. *Journal of Neural Transmission, 104*(2–3), 191–197.

Ben-Shachar, D., Gazawi, H., Riboyad-Levin, J., & Klein, E. (1999). Chronic repetitive transcranial magnetic stimulation alters β-adrenergic and 5-HT_2 receptor characteristics in rat brain. *Brain Research, 816*(1), 78–83.

Berardi, N., Pizzorusso, T., Ratto, G. M., & Maffei, L. (2003). Molecular basis of plasticity in the visual cortex. *Trends in Neurosciences, 26*(7), 369–378.

Berman, J. I., Lanza, M. R., Blaskey, L., Edgar, J. C., & Roberts, T. P. (2013). High angular resolution diffusion imaging probabilistic tractography of the auditory radiation. *American Journal of Neuroradiology, 34*(8), 1573–1578.

Bienenstock, E. L., Cooper, L. N., & Munro, P. W. (1982). Theory for the development of neuron selectivity: orientation specificity and binocular interaction in visual cortex. *Journal of Neuroscience*, *2*(1), 32–48.

Biswal, B., Zerrin Yetkin, F., Haughton, V. M., & Hyde, J. S. (1995). Functional connectivity in the motor cortex of resting human brain using echo-planar MRI. *Magnetic Resonance in Medicine*, *34*(4), 537–541.

Biswal, B. B., Kylen, J. V., & Hyde, J. S. (1997). Simultaneous assessment of flow and BOLD signals in resting-state functional connectivity maps. *NMR in Biomedicine*, *10*(4-5), 165–170.

Bocci, T., Caleo, M., Tognazzi, S., Francini, N., Briscese, L., Maffei, L., et al. (2014). Evidence for metaplasticity in the human visual cortex. *Journal of Neural Transmission*, *121*(3), 221–231.

Boes, A. D., Prasad, S., Liu, H., Liu, Q., Pascual-Leone, A., Caviness Jr, V. S., & Fox, M. D. (2015). Network localization of neurological symptoms from focal brain lesions. *Brain*, *138*(10), 3061–3075.

Bohning, D., Shastri, A., McConnell, K., Nahas, Z., Lorberbaum, J., Roberts, D., et al. (1999). A combined TMS/fMRI study of intensity-dependent TMS over motor cortex. *Biological Psychiatry*, *45*(4), 385–394.

Bohotin, V., Fumal, A., Vandenheede, M., Gerard, P., Bohotin, C., de Noordhout, A. M., et al. (2002). Effects of repetitive transcranial magnetic stimulation on visual evoked potentials in migraine. *Brain*, *125*(4), 912–922.

Böker, K. B., Hijman, R., Kahn, R. S., & Haan, E. H. (2000). Perception, mental imagery and reality discrimination in hallucinating and non-hallucinating schizophrenic patients. *British Journal of Clinical Psychology, 39*(4), 397–406.

Boroojerdi, B., Bushara, K. O., Corwell, B., Immisch, I., Battaglia, F., Muellbacher, W., & Cohen, L. G. (2000a). Enhanced excitability of the human visual cortex induced by short-term light deprivation. *Cerebral Cortex, 10*(5), 529–534.

Boroojerdi, B., Prager, A., Muellbacher, W., & Cohen, L. G. (2000b). Reduction of human visual cortex excitability using 1-Hz transcranial magnetic stimulation. *Neurology, 54*(7), 1529–1531.

Bortolomasi, M., Minelli, A., Fuggetta, G., Perini, M., Comencini, S., Fiaschi, A., & Manganotti, P. (2007). Long-lasting effects of high frequency repetitive transcranial magnetic stimulation in major depressed patients. *Psychiatry Research, 150*(2), 181–186.

Brandt, T., Thie, A., Caplan, L. R., & Hacke, W. (1995). Infarcts in the brain areas supplied by the posterior cerebral artery. Clinical aspects, pathogenesis and prognosis. *Der Nervenarzt, 66*(4), 267–274.

Braun, C. M., Dumont, M., Duval, J., Hamel-Hébert, I., & Godbout, L. (2003). Brain modules of hallucination: an analysis of multiple patients with brain lesions. *Journal of Psychiatry and Neuroscience, 28*(6), 432–449.

Brissenden, J. A., Levin, E. J., Osher, D. E., Halko, M. A., & Somers, D. C. (2016). Functional evidence for a cerebellar node of the dorsal attention network. *Journal of Neuroscience, 36*(22), 6083–6096.

Brodeur, M. B., Dionne-Dostie, E., Montreuil, T., & Lepage, M. (2010). The Bank of Standardized Stimuli (BOSS), a new set of 480 normative photos of objects to be used as visual stimuli in cognitive research. *PloS One, 5*(5), e10773.

Brodmann, K. (1909). *Vergleichende Lokalisationslehre der Grosshirnrinde in ihren Prinzipien dargestellt auf Grund des Zellenbaues.* Leipzig, Germany: Johann Ambrosius Barth.

Brodmann, K. (1910). Finer anatomy of the cerebrum. In *Handbook of Neurology* (pp. 206–307). Berlin, Germany: Springer.

Brown, C. E., Aminoltejari, K., Erb, H., Winship, I. R., & Murphy, T. H. (2009). In vivo Voltage-sensitive dye imaging in adult mice reveals that somatosensory maps lost to stroke are replaced over weeks by new structural and functional circuits with prolonged modes of activation within both the peri-infarct zone and distant sites. *The Journal of Neuroscience*, *29*(6), 1719–1734.

Brückner, S., Kiefer, M., & Kammer, T. (2013). Comparing the after-effects of continuous theta burst stimulation and conventional 1 Hz rTMS on semantic processing. *Neuroscience*, *233*, 64–71.

Brunoni, A. R., Boggio, P. S., & Fregni, F. (2008). Can the 'yin and yang' BDNF hypothesis be used to predict the effects of rTMS treatment in neuropsychiatry? *Medical Hypotheses*, *71*(2), 279–282.

Buchkremer-Ratzmann, I., & Witte, O. W. (1997). Extended brain disinhibition following small photothrombotic lesions in rat frontal cortex. *Neuroreport*, *8*(2), 519–522.

Buckner, R.L., Krienen, F.M., Castellanos, A., Diaz, J.C., & Yeo, B.T. (2011). The organization of the human cerebellum estimated by intrinsic functional connectivity. *Journal of Neurophysiology*, *106*, 2322–2345.

Bullmore, E., & Sporns, O. (2009). Complex brain networks: graph theoretical analysis of structural and functional systems. *Nature Reviews Neuroscience, 10*(3), 186–198.

Burke, W. (2002). The neural basis of Charles Bonnet hallucinations: a hypothesis. *Journal of Neurology, Neurosurgery & Psychiatry*, *73*(5), 535–541.

Cabral, J., Hugues, E., Sporns, O., & Deco, G. (2011). Role of local network oscillations in resting-state functional connectivity. *Neuroimage*, *57*(1), 130–139.

Calhoun, V. D., Adali, T., Pearlson, G. D., & Pekar, J. J. (2001). A method for making group inferences from functional MRI data using independent component analysis. *Human Brain Mapping*, *14*(3), 140–151.

Caparelli, E. C., Backus, W., Telang, F., Wang, G. J., Maloney, T., Goldstein, R. Z., et al. (2010). Simultaneous TMS-fMRI of the visual cortex reveals functional network, even in absence of phosphene sensation. *The Open Neuroimaging Journal*, *4*, 100–110.

Carmichael, S. T. (2003). Plasticity of cortical projections after stroke. *The Neuroscientist*, *9*(1), 64–75.

Cassidy, J. M., Gillick, B. T., & Carey, J. R. (2014). Priming the brain to capitalize on metaplasticity in stroke rehabilitation. *Physical Therapy*, *94*(1), 139–150.

Catani, M., Howard, R. J., Pajevic, S., & Jones, D. K. (2002). Virtual in vivo interactive dissection of white matter fasciculi in the human brain. *Neuroimage*, *17*(1), 77–94.

Catani, M., Jones, D. K., & Donato, R. (2003). Occipito-temporal connections in the human brain. *Brain*, *126*(9), 2093–2107.

Cazzoli, D., Müri, R. M., Schumacher, R., von Arx, S., Chaves, S., Gutbrod, K., et al. (2012). Theta burst stimulation reduces disability during the activities of daily living in spatial neglect. *Brain*, *135*(11), 3426–3439.

Çelebisoy, M., Çelebisoy, N., Bayam, E., & Köse, T. (2010). Recovery of visual-field defects after occipital lobe infarction: a perimetric study. *Journal of Neurology, Neurosurgery & Psychiatry, 82*, 695–702.

Chai, X. J., Castañón, A. N., Öngür, D., & Whitfield-Gabrieli, S. (2012). Anticorrelations in resting state networks without global signal regression. *Neuroimage, 59*(2), 1420–1428.

Chalifoux, J. R., & Carter, A. G. (2011). GABA B receptor modulation of synaptic function. *Current Opinion in Neurobiology, 21*(2), 339–344.

Chao, L. L., Haxby, J. V., & Martin, A. (1999). Attribute-based neural substrates in temporal cortex for perceiving and knowing about objects. *Nature Neuroscience, 2*(10), 913–919.

Cheeran, B., Talelli, P., Mori, F., Koch, G., Suppa, A., Edwards, M., et al. (2008). A common polymorphism in the brain-derived neurotrophic factor gene (BDNF) modulates human cortical plasticity and the response to rTMS. *The Journal of Physiology*, *586*(23), 5717–5725.

Chen, R., Classen, J., Gerloff, C., Celnik, P., Wassermann, E. M., Hallett, M., & Cohen, L. G. (1997). Depression of motor cortex excitability by low-frequency transcranial magnetic stimulation. *Neurology*, *48*(5), 1398–1403.

Chen, R., Cros, D., Curra, A., Di Lazzaro, V., Lefaucheur, J. P., Magistris, M. R., et al. (2008). The clinical diagnostic utility of transcranial magnetic stimulation: report of an IFCN committee. *Clinical Neurophysiology*, *119*(3), 504–532.

Chenevert, T. L., Brunberg, J. A., & Pipe, J. G. (1990). Anisotropic diffusion in human white matter: demonstration with MR techniques in vivo. *Radiology, 177*(2), 401–405.

Chistyakov, A. V., Rubicsek, O., Kaplan, B., Zaaroor, M., & Klein, E. (2010). Safety, tolerability and preliminary evidence for antidepressant efficacy of theta-burst transcranial magnetic stimulation in patients with major depression. *International Journal of Neuropsychopharmacology*, *13*(3), 387–393.

Ciccarelli, O., Catani, M., Johansen-Berg, H., Clark, C., & Thompson, A. (2008). Diffusion-based tractography in neurological disorders: concepts, applications, and future developments. *The Lancet Neurology*, *7*(8), 715–727.

Clark, V. P., Coffman, B. A., Trumbo, M. C., & Gasparovic, C. (2011). Transcranial direct current stimulation (tDCS) produces localized and specific alterations in neurochemistry: a 1H magnetic resonance spectroscopy study. *Neuroscience Letters*, *500*(1), 67–71.

Clarkson, A. N., Huang, B. S., MacIsaac, S. E., Mody, I., & Carmichael, S. T. (2010). Reducing excessive GABA-mediated tonic inhibition promotes functional recovery after stroke. *Nature*, *468*(7321), 305–309.

Classen, J., & Stefan, K. (2008). Changes in TMS measures induced by repetitive TMS. In E. M. Wassermann, C. M. Epstein, U. Ziemann, V. Walsh, T. Paus, S. Lisanby (Eds.), *The Oxford Handbook of Transcranial Stimulation* (pp. 185–200). New York, NY: Oxford University Press Inc.

Clavagnier, S., Thompson, B., & Hess, R. F. (2013). Long lasting effects of daily theta burst rTMS sessions in the human amblyopic cortex. *Brain Stimulation: Basic, Translational, and Clinical Research in Neuromodulation*, *6*(6), 860–867.

Cogan, D. G. (1973). Visual hallucinations as release phenomena. *Albrecht von Graefes Archiv Für Klinische und Experimentelle Ophthalmologie*, *188*(2), 139–150.

Corthout, E., Barker, A., & Cowey, A. (2001). Transcranial magnetic stimulation. *Experimental Brain Research*, *141*(1), 128–132.

Cowey, A. (1974). Atrophy of retinal ganglion cells after removal of striate cortex in a rhesus monkey. *Perception*, *3*(3), 257–260.

Cox, T. M. & ffytche, D. H. (2014). Negative outcome Charles Bonnet Syndrome. *British Journal of Ophthalmology*, *98*(9), 1236–1239.

Cramer, S. C. (2008). Repairing the human brain after stroke: I. Mechanisms of spontaneous recovery. *Annals of Neurology*, *63*(3), 272–287.

Crawford, J. R., & Garthwaite, P. H. (2002). Investigation of the single case in neuropsychology: Confidence limits on the abnormality of test scores and test score differences. *Neuropsychologia*, *40*(8), 1196–1208.

Crawford, J. R., Garthwaite, P. H., Azzalini, A., Howell, D. C., & Laws, K. R. (2006). Testing for a deficit in single-case studies: Effects of departures from normality. *Neuropsychologia*, *44*(4), 666–677.

Creutzfeldt, O. D., Fromm, G. H., & Kapp, H. (1962). Influence of transcortical d-c currents on cortical neuronal activity. *Experimental Neurology*, *5*(6), 436–452.

Ćurčić-Blake, B., Nanetti, L., van der Meer, L., Cerliani, L., Renken, R., Pijnenborg, G. H., & Aleman, A. (2015). Not on speaking terms: hallucinations and structural network disconnectivity in schizophrenia. *Brain Structure and Function*, *220*(1), 407–418.

Dai, H., Morelli, J. N., Ai, F., Yin, D., Hu, C., Xu, D., & Li, Y. (2013). Resting-state functional MRI: Functional connectivity analysis of the visual cortex in primary open-angle glaucoma patients. *Human Brain Mapping*, *34*(10), 2455–2463.

Damasio, A. R., Damasio, H., & Van Hoesen, G. W. (1982). Prosopagnosia: Anatomic basis and behavioral mechanisms. *Neurology*, *32*(4), 331–341.

Damasio, A., Yamada, T., Damasio, H., Corbett, J., & McKee, J. (1980). Central achromatopsia: Behavioral, anatomic, and physiologic aspects. *Neurology*, *Neurology*, *30*(10), 1064–1071.

Damoiseaux, J. S., Rombouts, S. A. R. B., Barkhof, F., Scheltens, P., Stam, C. J., Smith, S. M., & Beckmann, C. F. (2006). Consistent resting-state networks across healthy subjects. *Proceedings of the National Academy of Sciences*, *103*(37), 13848–13853.

Darian-Smith, C., & Gilbert, C. D. (1995). Topographic reorganization in the striate cortex of the adult cat and monkey is cortically mediated. *Journal of Neuroscience*, *15*(3), 1631–1647.

Davis, F. A., Bergen, D., Schauf, C., McDonald, I., & Deutsch, W (1976). Movement phosphenes in optic neuritis: a new clinical sign. *Neurology*, *26*, 1100–1104.

Day, B. L., Dressler, D., Maertens de Noordhout, A., Marsden, C. D., Nakashima, K., Rothwell, J. C., & Thompson, P. D. (1989). Electric and magnetic stimulation of human motor cortex: surface EMG and single motor unit responses. *The Journal of Physiology*, *412*(1), 449–473.

Day, B. L., Rothwell, J. C., Thompson, P. D., Dick, J. P. R., Cowan, J. M. A., Berardelli, A., & Marsden, C. D. (1987). Motor cortex stimulation in intact man: 2. Multiple descending volleys. *Brain*, *110*(5), 1191–1209.

Dayan, E., Censor, N., Buch, E. R., Sandrini, M., & Cohen, L. G. (2013). Noninvasive brain stimulation: from physiology to network dynamics and back. *Nature Neuroscience*, *16*(7), 838.

De Haan, E. H., Nys, G. M., van Zandvoort, M. J., & Ramsey, N. F. (2007). The physiological basis of visual hallucinations after damage to the primary visual cortex. *Neuroreport*, *18*(11), 1177–1180.

De Luca, M., Beckmann, C. F., De Stefano, N., Matthews, P. M., & Smith, S. M. (2006). fMRI resting state networks define distinct modes of long-distance interactions in the human brain. *Neuroimage*, *29*(4), 1359–1367.

Desikan, R. S., Ségonne, F., Fischl, B., Quinn, B. T., Dickerson, B. C., Blacker, D., et al. (2006). An automated labeling system for subdividing the human cerebral cortex on MRI scans into gyral based regions of interest. *Neuroimage*, *31*(3), 968–980.

Dickinson, W. C. (1950a). Dependence of the F^{19} nuclear resonance position on chemical compound. *Physical Review*, *77*(5), 736–737.

Dickinson, W. C. (1950b). Hartree computation of the internal diamagnetic field for atoms. *Physical Review*, *80*(4), 563–566.

Diederich, N. J., Goetz, C. G., & Stebbins, G. T. (2005). Repeated visual hallucinations in Parkinson's disease as disturbed external/internal perceptions: focused review and a new integrative model. *Movement Disorders*, *20*(2), 130–140.

Di Lazzaro, V., Profice, P., Ranieri, F., Capone, F., Dileone, M., Oliviero, A., & Pilato, F. (2012). I-wave origin and modulation. *Brain Stimulation: Basic, Translational, and Clinical Research in Neuromodulation*, *5*(4), 512–525.

Di Lazzaro, V., Restuccia, D., Oliviero, A., Profice, P., Ferrara, L., Insola, A., et al. (1998). Magnetic transcranial stimulation at intensities below active motor threshold activates intracortical inhibitory circuits. *Experimental Brain Research*, *119*(2), 265–268.

Donovan, J. J., & Radosevich, D. J. (1999). A meta-analytic review of the distribution of practice effect: Now you see it, now you don't. *Journal of Applied Psychology, 84*(5), 795–805.

Dudek, S. M., & Bear, M. F. (1992). Homosynaptic long-term depression in area CA1 of hippocampus and effects of *N*-methyl-D-aspartate receptor blockade. *Proceedings of the National Academy of Sciences, 89*(10), 4363–4367.

Duecker, F., & Sack, A. T. (2015). Rethinking the role of sham TMS. *Frontiers in Psychology, 6*, 210.

Dum, R. P., & Strick, P. L. (1991). The origin of corticospinal projections from the premotor areas in the frontal lobe. *The Journal of Neuroscience, 11*(3), 667–689.

Dunner, D. L., Aaronson, S. T., Sackeim, H. A., Janicak, P. G., Carpenter, L. L., Boyadjis, T., et al. (2014). A multisite, naturalistic, observational study of transcranial magnetic stimulation for patients with pharmacoresistant major depressive disorder: durability of benefit over a 1-year follow-up period. *The Journal of Clinical Psychiatry, 75*(12), 1394–1401.

Dyrby, T. B., Søgaard, L. V., Parker, G. J., Alexander, D. C., Lind, N. M., Baaré, W. F., et al. (2007). Validation of in vitro probabilistic tractography. *Neuroimage, 37*(4), 1267–1277.

Edden, R. A., Puts, N. A., Harris, A. D., Barker, P. B., & Evans, C. J. (2014). Gannet: A batch-processing tool for the quantitative analysis of gamma-aminobutyric acid-edited MR spectroscopy spectra. *Journal of Magnetic Resonance Imaging, 40*(6), 1445–1452.

Eklund, A., Nichols, T. E., & Knutsson, H. (2016). Cluster failure: why fMRI inferences for spatial extent have inflated false-positive rates. *Proceedings of the National Academy of Sciences, 113*(28), 7900–7905.

Elkin-Frankston, S., Fried, P. J., Pascual-Leone, A., Rushmore III, R. J., & Valero-Cabré, A. (2010). A novel approach for documenting phosphenes induced by transcranial magnetic stimulation. *Journal of visualized experiments: JoVE*, e1762.

Epperson, C. N., Haga, K., Mason, G. F., Sellers, E., Gueorguieva, R., Zhang, W., et al. (2002). Cortical γ-aminobutyric acid levels across the menstrual cycle in healthy women and those with premenstrual dysphoric disorder: a proton magnetic resonance spectroscopy study. *Archives of General Psychiatry*, *59*(9), 851–858.

Epperson, C. N., O'Malley, S., Czarkowski, K. A., Gueorguieva, R., Jatlow, P., Sanacora, G., et al. (2005). Sex, GABA, and nicotine: the impact of smoking on cortical GABA levels across the menstrual cycle as measured with proton magnetic resonance spectroscopy. *Biological Psychiatry*, *57*(1), 44–48.

Evans, C. J., McGonigle, D. J., & Edden, R. A. E. (2010). Diurnal stability of γ-aminobutyric acid concentration in visual and sensorimotor cortex. *Journal of Magnetic Resonance Imaging*, *31*(1), 204–209.

Evans, J. W., Kundu, P., Horovitz, S. G., & Bandettini, P. A. (2015). Separating slow BOLD from non-BOLD baseline drifts using multi-echo fMRI. *NeuroImage*, *105*, 189–197.

Ewbank, M. P., Schluppeck, D., & Andrews, T. J. (2005). fMR-adaptation reveals a distributed representation of inanimate objects and places in human visual cortex. *Neuroimage*, *28*(1), 268–279.

Eysel, U. T., Schweigart, G., Mittmann, T., Eyding, D., Qu, Y., Vandesande, F., et al. (1999). Reorganization in the visual cortex after retinal and cortical damage. *Restorative Neurology and Neuroscience*, *15*(2), 153–164.

Faraday, M. (1832). V. Experimental researches in electricity. *Philosophical Transactions of the Royal Society of London*, *122*, 125–162.

Feeney, D. M., & Baron, J. C. (1986). Diaschisis. *Stroke*, *17*(5), 817–830.

Felleman, D. J., & Van Essen, D. C. (1991). Distributed hierarchical processing in the primate cerebral cortex. *Cerebral Cortex*, *1*(1), 1–47.

Fernández-Miranda, J. C., Pathak, S., Engh, J., Jarbo, K., Verstynen, T., Yeh, F. C., et al. (2012). High-definition fiber tractography of the human brain: neuroanatomical validation and neurosurgical applications. *Neurosurgery*, *71*(2), 430–453.

Fernández-Miranda, J. C., Wang, Y., Pathak, S., Stefaneau, L., Verstynen, T., & Yeh, F. C. (2015). Asymmetry, connectivity, and segmentation of the arcuate fascicle in the human brain. *Brain Structure and Function*, *220*(3), 1665–1680.

ffytche, D. H. (2008). The hodology of hallucinations. *Cortex*, *44*(8), 1067–1083.

ffytche, D. H., & Howard, R. J. (1999). The perceptual consequences of visual loss: 'positive' pathologies of vision. *Brain*, *122*(7), 1247–1260.

ffytche, D. H., Howard, R. J., Brammer, M. J., David, A., Woodruff, P., & Williams, S. (1998). The anatomy of conscious vision: an fMRI study of visual hallucinations. *Nature Neuroscience*, *1*(8), 738–742.

Figurov, A., Pozzo-Miller, L. D., Olafsson, P., Wang, T., & Lu, B. (1996). Regulation of synaptic responses to high-frequency stimulation and LTP by neurotrophins in the hippocampus. *Nature*, *381*(6584), 706–709.

Fitzgerald, P. B., Brown, T. L., Marston, N. A., Daskalakis, Z. J., de Castella, A., & Kulkarni, J. (2003). Transcranial magnetic stimulation in the treatment of depression: a double-blind, placebo-controlled trial. *Archives of General Psychiatry*, *60*(10), 1002–1008.

Fitzgerald, P. B., Hoy, K., Daskalakis, Z. J., & Kulkarni, J. (2009). A randomized trial of the anti-depressant effects of low-and high-frequency transcranial magnetic stimulation in treatment-resistant depression. *Depression and Anxiety*, *26*(3), 229–234.

Fitzpatrick, D., Diamond, I. T., & Raczkowski, D. (1989). Cholinergic and monoaminergic innervation of the cat's thalamus: comparison of the lateral geniculate nucleus with other principal sensory nuclei. *Journal of Comparative Neurology*, *288*(4), 647–675.

Foerster, O. (1931). The cerebral cortex in man. *Lancet*, *2*, 309–312.

Fox, C. J., Iaria, G., & Barton, J. J. (2008). Disconnection in prosopagnosia and face processing. *Cortex*, *44*(8), 996–1009.

Fox, M. D., Buckner, R. L., Liu, H., Chakravarty, M. M., Lozano, A. M., & Pascual-Leone, A. (2014). Resting-state networks link invasive and noninvasive brain stimulation across diverse psychiatric and neurological diseases. *Proceedings of the National Academy of Sciences*, *111*(41), E4367–E4375.

Fox, M. D., & Greicius, M. (2010). Clinical applications of resting state functional connectivity. *Frontiers in Systems Neuroscience*, *4*, 19.

Fox, M. D., Halko, M. A., Eldaief, M. C., & Pascual-Leone, A. (2012). Measuring and manipulating brain connectivity with resting state functional connectivity magnetic resonance imaging (fcMRI) and transcranial magnetic stimulation (TMS). *Neuroimage*, *62*(4), 2232–2243.

Fox, M. D., & Raichle, M. E. (2007). Spontaneous fluctuations in brain activity observed with functional magnetic resonance imaging. *Nature Reviews Neuroscience*, *8*(9), 700–711.

Fox, M. D., Snyder, A. Z., Vincent, J. L., Corbetta, M., Van Essen, D. C., & Raichle, M. E. (2005). The human brain is intrinsically organized into dynamic, anticorrelated functional networks. *Proceedings of the National Academy of Sciences of the United States of America*, *102*(27), 9673–9678.

Fox, P., Ingham, R., George, M. S., Mayberg, H., Ingham, J., Roby, J., et al. (1997). Imaging human intra-cerebral connectivity by PET during TMS. *Neuroreport*, *8*(12), 2787–2791.

Fox, P. T., Narayana, S., Tandon, N., Sandoval, H., Fox, S. P., Kochunov, P., & Lancaster, J. L. (2004). Column-based model of electric field excitation of cerebral cortex. *Human Brain Mapping*, *22*(1), 1–14.

Fransson, P. (2005). Spontaneous low-frequency BOLD signal fluctuations: An fMRI investigation of the resting-state default mode of brain function hypothesis. *Human Brain Mapping*, *26*(1), 15–29.

Fregni, F., Boggio, P. S., Valle, A. C., Rocha, R. R., Duarte, J., Ferreira, M. J., et al. (2006). A sham-controlled trial of a 5-day course of repetitive transcranial magnetic stimulation of the unaffected hemisphere in stroke patients. *Stroke*, *37*(8), 2115–2122.

Fregni, F., & Pascual-Leone, A. (2007). Technology insight: noninvasive brain stimulation in neurology: perspectives on the therapeutic potential of rTMS and tDCS. *Nature Reviews Neurology*, *3*(7), 383–393.

Freitas, C., Fregni, F., & Pascual-Leone, A. (2009). Meta-analysis of the effects of repetitive transcranial magnetic stimulation (rTMS) on negative and positive symptoms in schizophrenia. *Schizophrenia Research*, *108*(1), 11–24.

Friston, K. J. (1994). Functional and effective connectivity in neuroimaging: a synthesis. *Human Brain Mapping*, *2*(1–2), 56–78.

Friston, K. J., Frith, C. D., Liddle, P. F., & Frackowiak, R. S. J. (1993). Functional connectivity: the principal-component analysis of large (PET) data sets. *Journal of Cerebral Blood Flow & Metabolism*, *13*(1), 5–14.

Friston, K. J., Jezzard, P., & Turner, R. (1994). Analysis of functional MRI time-series. *Human Brain Mapping*, *1*(2), 153–171.

Fujiki, M., & Steward, O. (1997). High frequency transcranial magnetic stimulation mimics the effects of ECS in upregulating astroglial gene expression in the murine CNS. *Molecular Brain Research*, *44*(2), 301–308.

Fumal, A., Bohotin, V., Vandenheede, M., Seidel, L., De Pasqua, V., de Noordhout, A. M., & Schoenen, J. (2003). Effects of repetitive transcranial magnetic stimulation on visual evoked potentials: new insights in healthy subjects. *Experimental Brain Research*, *150*(3), 332–340.

Fumal, A., Coppola, G., Bohotin, V., Gérardy, P. Y., Seidel, L., Donneau, A. F., et al. (2006). Induction of long-lasting changes of visual cortex excitability by five daily sessions of repetitive transcranial magnetic stimulation (rTMS) in healthy volunteers and migraine patients. *Cephalalgia*, *26*(2), 143–149.

Gall, C., Silvennoinen, K., Granata, G., de Rossi, F., Vecchio, F., Brösel, D., et al. (2015). Non-invasive electric current stimulation for restoration of vision after unilateral occipital stroke. *Contemporary Clinical Trials*, *43*, 231–236.

Gamboa, O. L., Antal, A., Laczo, B., Moliadze, V., Nitsche, M. A., & Paulus, W. (2011). Impact of repetitive theta burst stimulation on motor cortex excitability. *Brain Stimulation: Basic, Translational, and Clinical Research in Neuromodulation*, *4*(3), 145–151.

Gamboa, O. L., Antal, A., Moliadze, V., & Paulus, W. (2010). Simply longer is not better: reversal of theta burst after-effect with prolonged stimulation. *Experimental Brain Research*, *204*(2), 181–187.

Ganaden, R. E., Mullin, C. R., & Steeves, J. K. (2013). Transcranial magnetic stimulation to the transverse occipital sulcus affects scene but not object processing. *Journal of Cognitive Neuroscience*, *25*(6), 961–968.

Gauthier, I., Tarr, M. J., Anderson, A. W., Skudlarski, P., & Gore, J. C. (1999). Activation of the middle fusiform 'face area' increases with expertise in recognizing novel objects. *Nature Neuroscience*, *2*(6), 568–573.

George, M. S., Lisanby, S. H., & Sackeim, H. A. (1999). Transcranial magnetic stimulation: applications in neuropsychiatry. *Archives of General Psychiatry*, *56*(4), 300–311.

Gerschlager, W., Siebner, H. R., & Rothwell, J. C. (2001). Decreased corticospinal excitability after subthreshold 1 Hz rTMS over lateral premotor cortex. *Neurology*, *57*(3), 449–455.

Goldsworthy, M. R., Müller-Dahlhaus, F., Ridding, M. C., & Ziemann, U. (2014). Resistant against de-depression: LTD-like plasticity in the human motor cortex induced by spaced cTBS. *Cerebral Cortex*, *25*(7), 1724–1734.

Goldsworthy, M. R., Pitcher, J. B., & Ridding, M. C. (2015). Spaced noninvasive brain stimulation: prospects for inducing long-lasting human cortical plasticity. *Neurorehabilitation and Neural Repair*, *29*(8), 714–721.

Gonzalez-Burgos, G., & Lewis, D. A. (2008). GABA neurons and the mechanisms of network oscillations: implications for understanding cortical dysfunction in schizophrenia. *Schizophrenia Bulletin*, *34*(5), 944–961.

Gordon, K. D. (2016). Prevalence of visual hallucinations in a national low vision client population. *Canadian Journal of Ophthalmology*, *51*(1), 3–6.

Gottmann, K., Mittmann, T., & Lessmann, V. (2009). BDNF signaling in the formation, maturation and plasticity of glutamatergic and GABAergic synapses. *Experimental Brain Research*, *199*(3–4), 203–234.

Govindaraju, V., Young, K., & Maudsley, A. A. (2000). Proton NMR chemical shifts and coupling constants for brain metabolites. *NMR in Biomedicine*, *13*(3), 129–153.

Grealy, M. A., & Lee, D. N. (2011). An automatic-voluntary dissociation and mental imagery disturbance following a cerebellar lesion. *Neuropsychologia*, *49*(2), 271–275.

Grefkes, C., Nowak, D. A., Eickhoff, S. B., Dafotakis, M., Küst, J., Karbe, H., et al. (2008). Cortical connectivity after subcortical stroke assessed with functional magnetic resonance imaging. *Annals of Neurology*, *63*(2), 236–246.

Grefkes, C., Nowak, D. A., Wang, L. E., Dafotakis, M., Eickhoff, S. B., & Fink, G. R. (2010). Modulating cortical connectivity in stroke patients by rTMS assessed with fMRI and dynamic causal modeling. *Neuroimage*, *50*(1), 233–242.

Greicius, M. (2008). Resting-state functional connectivity in neuropsychiatric disorders. *Current Opinion in Neurology*, *21*(4), 424–430.

Greicius, M. D., Flores, B. H., Menon, V., Glover, G. H., Solvason, H. B., Kenna, H., et al. (2007). Resting-state functional connectivity in major depression: abnormally increased contributions from subgenual cingulate cortex and thalamus. *Biological Psychiatry*, *62*(5), 429–437.

Greicius, M. D., Krasnow, B., Reiss, A. L., & Menon, V. (2003). Functional connectivity in the resting brain: a network analysis of the default mode hypothesis. *Proceedings of the National Academy of Sciences*, *100*(1), 253–258.

Grill-Spector, K., Kushnir, T., Edelman, S., Avidan, G., Itzchak, Y., & Malach, R. (1999). Differential processing of objects under various viewing conditions in the human lateral occipital complex. *Neuron*, *24*(1), 187–203.

Gross, C. G. (1994). How inferior temporal cortex became a visual area. *Cerebral Cortex, 4*(5), 455–469.

Guo, X., Jin, Z., Feng, X., & Tong, S. (2014). Enhanced effective connectivity in mild occipital stroke patients with hemianopia. *IEEE Transactions on Neural Systems and Rehabilitation Engineering, 22*(6), 1210–1217.

Gusnard, D. A., Akbudak, E., Shulman, G. L., & Raichle, M. E. (2001). Medial prefrontal cortex and self-referential mental activity: relation to a default mode of brain function. *Proceedings of the National Academy of Sciences*, *98*(7), 4259–4264.

Hagmann, P., Cammoun, L., Gigandet, X., Meuli, R., Honey, C. J., Wedeen, V. J., & Sporns, O. (2008). Mapping the structural core of human cerebral cortex. *PLoS Biology*, *6*(7), e159.

Hagmann, P., Jonasson, L., Maeder, P., Thiran, J. P., Wedeen, V. J., & Meuli, R. (2006). Understanding diffusion MR imaging techniques: from scalar diffusion-weighted imaging to diffusion tensor imaging and beyond. *Radiographics*, *26*, S205–S223.

Halko, M. A., Datta, A., Plow, E. B., Scaturro, J., Bikson, M., & Merabet, L. B. (2011). Neuroplastic changes following rehabilitative training correlate with regional electrical field induced with tDCS. *Neuroimage*, *57*(3), 885–891.

Hallett, M. (2007). Transcranial magnetic stimulation: a primer. *Neuron*, *55*(2), 187–199.

Harada, M., Kubo, H., Nose, A., Nishitani, H., & Matsuda, T. (2011). Measurement of variation in the human cerebral GABA level by in vivo MEGA-editing proton MR spectroscopy using a clinical 3 T instrument and its dependence on brain region and the female menstrual cycle. *Human Brain Mapping*, *32*(5), 828–833.

Harris, A. D., Puts, N. A., & Edden, R. A. (2015). Tissue correction for GABA-edited MRS: Considerations of voxel composition, tissue segmentation, and tissue relaxations. *Journal of Magnetic Resonance Imaging*, *42*(5), 1431–1440.

Haxby, J. V., Gobbini, M. I., Furey, M. L., Ishai, A., Schouten, J. L., & Pietrini, P. (2001). Distributed and overlapping representations of faces and objects in ventral temporal cortex. *Science*, *293*(5539), 2425–2430.

Heeger, D. J., & Ress, D. (2002). What does fMRI tell us about neuronal activity? *Nature Reviews Neuroscience*, *3*(2), 142–151.

Henry, M. E., Lauriat, T. L., Shanahan, M., Renshaw, P. F., & Jensen, J. E. (2011). Accuracy and stability of measuring GABA, glutamate, and glutamine by proton magnetic resonance spectroscopy: a phantom study at 4 Tesla. *Journal of Magnetic Resonance*, *208*(2), 210–218.

Henry, P. G., Dautry, C., Hantraye, P., & Bloch, G. (2001). Brain GABA editing without macromolecule contamination. *Magnetic Resonance in Medicine*, *45*(3), 517–520.

Hofmann, L., Slotboom, J., Boesch, C., & Kreis, R. (2001). Characterization of the macromolecule baseline in localized ^{1}H-MR spectra of human brain. *Magnetic Resonance in Medicine*, *46*(5), 855–863.

Holtzheimer, P. E., McDonald, W. M., Mufti, M., Kelley, M. E., Quinn, S., Corso, G., & Epstein, C. M. (2010). Accelerated repetitive transcranial magnetic stimulation for treatment-resistant depression. *Depression and Anxiety*, *27*(10), 960–963.

Honey, C. J., Sporns, O., Cammoun, L., Gigandet, X., Thiran, J. P., Meuli, R., & Hagmann, P. (2009). Predicting human resting-state functional connectivity from structural connectivity. *Proceedings of the National Academy of Sciences*, *106*(6), 2035–2040.

Hoogendam, J. M., Ramakers, G. M., & Di Lazzaro, V. (2010). Physiology of repetitive transcranial magnetic stimulation of the human brain. *Brain Stimulation: Basic, Translational, and Clinical Research in Neuromodulation*, *3*(2), 95–118.

Horvath J.C., Najib U., Press D. (2014) Transcranial Magnetic Stimulation (TMS) Clinical Applications: Therapeutics. In: A. Rotenberg, J. Horvath, A. Pascual-Leone (Eds.), *Transcranial Magnetic Stimulation* (pp. 235–237). New York, NY: Humana Press.

Houdayer, E., Degardin, A., Cassim, F., Bocquillon, P., Derambure, P., & Devanne, H. (2008). The effects of low-and high-frequency repetitive TMS on the input/output properties of the human corticospinal pathway. *Experimental Brain Research*, *187*(2), 207–217.

Hu, Y., Chen, X., Gu, H., & Yang, Y. (2013). Resting-state glutamate and GABA concentrations predict task-induced deactivation in the default mode network. *Journal of Neuroscience*, *33*(47), 18566–18573.

Huang, Y. Z., Chen, R. S., Rothwell, J. C., & Wen, H. Y. (2007). The after-effect of human theta burst stimulation is NMDA receptor dependent. *Clinical Neurophysiology*, *118*(5), 1028–1032.

Huang, Y. Z., Edwards, M. J., Rounis, E., Bhatia, K. P., & Rothwell, J. C. (2005). Theta burst stimulation of the human motor cortex. *Neuron*, *45*(2), 201–206.

Huang, Y. Z., Rothwell, J. C., Lu, C. S., Wang, J., Weng, Y. H., Lai, S. C., et al. (2009). The effect of continuous theta burst stimulation over premotor cortex on circuits in primary motor cortex and spinal cord. *Clinical Neurophysiology, 120*(4), 796–801.

Huang, Z. J., Kirkwood, A., Pizzorusso, T., Porciatti, V., Morales, B., Bear, M. F., et al. (1999). BDNF regulates the maturation of inhibition and the critical period of plasticity in mouse visual cortex. *Cell*, *98*(6), 739–755.

Huettel, S. A., Song, A. W., & McCarthy, G. (2004). *Functional Magnetic Resonance Imaging.* Sunderland, MA: Sinauer Associates, Inc.

Hughes, D. F. (2013). Charles Bonnet syndrome: a literature review into diagnostic criteria, treatment and implications for nursing practice. *Journal of Psychiatric and Mental Health Nursing*, *20*(2), 169–175.

Hummel, F., Celnik, P., Giraux, P., Floel, A., Wu, W. H., Gerloff, C., & Cohen, L. G. (2005). Effects of non-invasive cortical stimulation on skilled motor function in chronic stroke. *Brain*, *128*(3), 490–499.

Hummel, F. C., & Cohen, L. G. (2006). Non-invasive brain stimulation: a new strategy to improve neurorehabilitation after stroke? *The Lancet Neurology*, *5*(8), 708–712.

Ikeda, T., Kurosawa, M., Uchikawa, C., Kitayama, S., & Nukina, N. (2005). Modulation of monoamine transporter expression and function by repetitive transcranial magnetic stimulation. *Biochemical and Biophysical Research Communications*, *327*(1), 218–224.

Inzitari, D., Pracucci, G., Poggesi, A., Carlucci, G., Barkhof, F., Chabriat, H., et al. (2009). Changes in white matter as determinant of global functional decline in older independent outpatients: three year follow-up of LADIS (leukoaraiosis and disability) study cohort. *BMJ*, *339*, b2477.

Ishai, A., & Sagi, D. (1995). Common mechanisms of visual imagery and perception. *Science*, *268*(5218), 1772–1774.

Ishikawa, S., Matsunaga, K., Nakanishi, R., Kawahira, K., Murayama, N., Tsuji, S., et al. (2007). Effect of theta burst stimulation over the human sensorimotor cortex on motor and somatosensory evoked potentials. *Clinical Neurophysiology*, *118*(5), 1033–1043.

Jansons, K. M., & Alexander, D. C. (2003). Persistent angular structure: new insights from diffusion magnetic resonance imaging data. *Inverse problems*, *19*(5), 1031–1046.

Jbabdi, S., Behrens, T. E., & Smith, S. M. (2010). Crossing fibres in tract-based spatial statistics. *Neuroimage*, *49*(1), 249–256.

Jenkinson, M., Bannister, P., Brady, M., & Smith, S. (2002). Improved optimization for the robust and accurate linear registration and motion correction of brain images. *Neuroimage*, *17*(2), 825–841.

Johnson, H., & Cowey, A. (2000). Transneuronal retrograde degeneration of retinal ganglion cells following restricted lesions of striate cortex in the monkey. *Experimental Brain Research*, *132*(2), 269–275.

Jones, D. K. (2010). Challenges and limitations of quantifying brain connectivity in vivo with diffusion MRI. *Imaging in Medicine*, *2*(3), 341–355.

Jones, D. K., Knösche, T. R., & Turner, R. (2013). White matter integrity, fiber count, and other fallacies: the do's and don'ts of diffusion MRI. *Neuroimage*, 73, 239–254.

Jones, D. K., Simmons, A., Williams, S. C., & Horsfield, M. A. (1999). Non-invasive assessment of axonal fiber connectivity in the human brain via diffusion tensor MRI. *Magnetic Resonance in Medicine*, *42*(1), 37–41.

Jones, D. K., Travis, A. R., Eden, G., Pierpaoli, C., & Basser, P. J. (2005). PASTA: pointwise assessment of streamline tractography attributes. *Magnetic Resonance in Medicine*, *53*(6), 1462–1467.

Jones, E. G., & Powell, T. P. S. (1970). An anatomical study of converging sensory pathways within the cerebral cortex of the monkey. *Brain*, *93*(4), 793–820.

Jueptner, M., & Weiller, C. (1995). Does measurement of regional cerebral blood flow reflect synaptic activity? Implications for PET and fMRI. *Neuroimage*, *2*(2), 148–156.

Jung, J., Bungert, A., Bowtell, R., & Jackson, S. R. (2016). Vertex stimulation as a control site for transcranial magnetic stimulation: A concurrent TMS/fMRI study. *Brain Stimulation: Basic, Translational, and Clinical Research in Neuromodulation*, *9*(1), 58–64.

Kantarci, K., Avula, R., Senjem, M. L., Samikoglu, A. R., Zhang, B., Weigand, S. D., et al. (2010). Dementia with Lewy bodies and Alzheimer disease: neurodegenerative patterns characterized by DTI. *Neurology*,*74*(22), 1814–1821.

Kanwisher, N. (2000). Domain specificity in face perception. *Nature Neuroscience*, *3*, 759–763.

Kaore, S. N., Langade, D. K., Yadav, V. K., Sharma, P., Thawani, V. R., & Sharma, R. (2012). Novel actions of progesterone: what we know today and what will be the scenario in the future? *Journal of Pharmacy and Pharmacology*, *64*(8), 1040–1062.

Kapogiannis, D., Reiter, D. A., Willette, A. A., & Mattson, M. P. (2013). Posteromedial cortex glutamate and GABA predict intrinsic functional connectivity of the default mode network. *Neuroimage*, *64*, 112–119.

Karnath, H. O., Rüter, J., Mandler, A., & Himmelbach, M. (2009). The anatomy of object recognition-visual form agnosia caused by medial occipitotemporal stroke. *The Journal of Neuroscience*, *29*(18), 5854–5862.

Kasten, E., Wüst, S., Behrens-Baumann, W., & Sabel, B. A. (1998). Computer-based training for the treatment of partial blindness. *Nature Medicine*, *4*(9), 1083–1087.

Kavalali, E. T. (2015). The mechanisms and functions of spontaneous neurotransmitter release. *Nature Reviews Neuroscience*, *16*(1), 5–16.

Keck, M. E., Welt, T., Müller, M. B., Erhardt, A., Ohl, F., Toschi, N., et al. (2002). Repetitive transcranial magnetic stimulation increases the release of dopamine in the mesolimbic and mesostriatal system. *Neuropharmacology*, *43*(1), 101–109.

Kellermann, T., Regenbogen, C., De Vos, M., Mößnang, C., Finkelmeyer, A., & Habel, U. (2012). Effective connectivity of the human cerebellum during visual attention. *The Journal of Neuroscience*, *32*(33), 11453–11460.

Kennedy, C., Des Rosiers, M. H., Jehle, J. W., Reivich, M., Sharpe, F., & Sokoloff, L. (1975). Mapping of functional neural pathways by autoradiographic survey of local metabolic rate with [^{14}C]deoxyglucose. *Science*, *187*(4179), 850–853.

Kenny, E. R., Blamire, A. M., Firbank, M. J., & O'Brien, J. T. (2012). Functional connectivity in cortical regions in dementia with Lewy bodies and Alzheimer's disease. *Brain*, *135*(2), 569–581.

Kier, E. L., Staib, L. H., Davis, L. M., & Bronen, R. A. (2004). MR imaging of the temporal stem: anatomic dissection tractography of the uncinate fasciculus, inferior occipitofrontal fasciculus, and Meyer’s loop of the optic radiation. *American Journal of Neuroradiology*, *25*(5), 677–691.

Kim, Y. H., You, S. H., Ko, M. H., Park, J. W., Lee, K. H., Jang, S. H., et al. (2006). Repetitive transcranial magnetic stimulation-induced corticomotor excitability and associated motor skill acquisition in chronic stroke. *Stroke*, *37*(6), 1471–1476.

Kirkwood, A., Dudek, S. M., Gold, J. T., Aizenman, C. D., & Bear, M. (1993). Common forms of synaptic plasticity in the hippocampus and neocortex in vitro. *Science, 260*, 1518–1520.

Kishi, T., Ishino, H., & Naganuma, R. (1998). Insight into phosphene: a case with occipital lobe damage. *General Hospital Psychiatry*, *20*(4), 260–261.

Ko, J. H., Monchi, O., Ptito, A., Bloomfield, P., Houle, S., & Strafella, A. P. (2008). Theta burst stimulation-induced inhibition of dorsolateral prefrontal cortex reveals hemispheric asymmetry in striatal dopamine release during a set-shifting task – a TMS–[^{11}C]raclopride PET study. *European Journal of Neuroscience*, *28*(10), 2147–2155.

Kobayashi, M., & Pascual-Leone, A. (2003). Transcranial magnetic stimulation in *The Lancet Neurology*, *2*(3), 145–156.

Koch, M. A., Norris, D. G., & Hund-Georgiadis, M. (2002). An investigation of functional and anatomical connectivity using magnetic resonance imaging. *Neuroimage*, *16*(1), 241–250.

Kölmel, H. W. (1984). Coloured patterns in hemianopic fields. *Brain*, *107*(1), 155–167.

Kölmel, H. W. (1985). Complex visual hallucinations in the hemianopic field. *Journal of Neurology, Neurosurgery & Psychiatry*, *48*(1), 29–38.

Komatsu, Y. U., Fujii, K., Maeda, J., Sakaguchi, H. I., & Toyama, K. E. (1988). Long-term potentiation of synaptic transmission in kitten visual cortex. *Journal of Neurophysiology*, *59*(1), 124–141.

Kosslyn, S. M., Pascual-Leone, A., Felician, O., Camposano, S., Keenan, J. P., Ganis, G., et al. (1999). The role of area 17 in visual imagery: convergent evidence from PET and rTMS. *Science*, *284*(5411), 167–170.

Kosslyn, S. M., Thompson, W. L., & Alpert, N. M. (1997). Neural systems shared by visual imagery and visual perception: A positron emission tomography study. *Neuroimage*, *6*(4), 320–334.

Kozel, F. A., Nahas, Z., Debrux, C., Molloy, M., Lorberbaum, J. P., Bohning, D., et al. (2000). How coil-cortex distance relates to age, motor threshold, and antidepressant response to repetitive transcranial magnetic stimulation. *The Journal of Neuropsychiatry and Clinical Neurosciences*, *12*(3), 376–384.

Kreis, R., Slotboom, J., Hofmann, L., & Boesch, C. (2005). Integrated data acquisition and processing to determine metabolite contents, relaxation times, and macromolecule baseline in single examinations of individual subjects. *Magnetic Resonance in Medicine*, *54*(4), 761–768.

Kundu, P., Benson, B. E., Baldwin, K. L., Rosen, D., Luh, W. M., Bandettini, P. A., et al. (2015). Robust resting state fMRI processing for studies on typical brain development based on multi-echo EPI acquisition. *Brain Imaging and Behavior*, *9*(1), 56–73.

Kundu, P., Brenowitz, N. D., Voon, V., Worbe, Y., Vértes, P. E., Inati, S. J., et al. (2013). Integrated strategy for improving functional connectivity mapping using multiecho fMRI. *Proceedings of the National Academy of Sciences*, *110*(40), 16187–16192.

Kundu, P., Inati, S. J., Evans, J. W., Luh, W. M., & Bandettini, P. A. (2012). Differentiating BOLD and non-BOLD signals in fMRI time series using multi-echo EPI. *Neuroimage*, *60*(3), 1759–1770.

Kundu, P., Voon, V., Balchandani, P., Lombardo, M. V., Poser, B. A., & Bandettini, P. A. (2017). Multi-echo fMRI: A review of applications in fMRI denoising and analysis of BOLD signals. *Neuroimage*, *154*, 59–80.

Kunimatsu, A., Aoki, S., Masutani, Y., Abe, O., Mori, H., & Ohtomo, K. (2003). Three-dimensional white matter tractography by diffusion tensor imaging in ischaemic stroke involving the corticospinal tract. *Neuroradiology, 45*(8), 532–535.

Laird, A. R., Eickhoff, S. B., Li, K., Robin, D. A., Glahn, D. C., & Fox, P. T. (2009). Investigating the functional heterogeneity of the default mode network using coordinate-based meta-analytic modeling. *The Journal of Neuroscience, 29*(46), 14496–14505

Lance, J. W. (1976). Simple formed hallucinations confined to the area of a specific visual field defect. *Brain: A Journal of Neurology, 99*(4), 719–734.

Lang, N., Siebner, H. R., Ernst, D., Nitsche, M. A., Paulus, W., Lemon, R. N., & Rothwell, J. C. (2004). Preconditioning with transcranial direct current stimulation sensitizes the motor cortex to rapid-rate transcranial magnetic stimulation and controls the direction of after-effects. *Biological Psychiatry, 56*(9), 634–639.

Laufs, H., Krakow, K., Sterzer, P., Eger, E., Beyerle, A., Salek-Haddadi, A., & Kleinschmidt, A. (2003). Electroencephalographic signatures of attentional and cognitive default modes in spontaneous brain activity fluctuations at rest. *Proceedings of the National Academy of Sciences, 100*(19), 11053–11058.

Launay, G., & Slade, P. (1981). The measurement of hallucinatory predisposition in male and female prisoners. *Personality and Individual Differences, 2*(3), 221–234.

Lawes, I. N. C., Barrick, T. R., Murugam, V., Spierings, N., Evans, D. R., Song, M., & Clark, C. A. (2008). Atlas-based segmentation of white matter tracts of the human brain using diffusion tensor tractography and comparison with classical dissection. *Neuroimage, 39*(1), 62–79.

Lee, H. W., Hong, S. B., Seo, D. W., Tae, W. S., & Hong, S. C. (2000). Mapping of functional organization in human visual cortex: electrical cortical stimulation. *Neurology*, *54*(4), 849–854.

Lee, L., Siebner, H. R., Rowe, J. B., Rizzo, V., Rothwell, J. C., Frackowiak, R. S., & Friston, K. J. (2003). Acute remapping within the motor system induced by low-frequency repetitive transcranial magnetic stimulation. *Journal of Neuroscience*, *23*(12), 5308–5318.

Lee, S. H., Kim, W., Chung, Y. C., Jung, K. H., Bahk, W. M., Jun, T. Y., et al. (2005). A double blind study showing that two weeks of daily repetitive TMS over the left or right temporoparietal cortex reduces symptoms in patients with schizophrenia who are having treatment-refractory auditory hallucinations. *Neuroscience Letters*, *376*(3), 177–181.

Lee, S., Ueno, M., & Yamashita, T. (2011). Axonal remodeling for motor recovery after traumatic brain injury requires downregulation of γ-aminobutyric acid signaling. *Cell Death & Disease*, *2*(3), e133.

Lepore, F. E. (1990). Spontaneous visual phenomena with visual loss 104 patients with lesions of retinal and neural afferent pathways. *Neurology*, *40*(3 Part 1), 444-447.

Lewis, S. J., Shine, J. M., Brooks, D., & Halliday, G. M. (2014). Hallucinogenic mechanisms: pathological and pharmacological insights. In D. Collerton, U. P. Mosimann, & E. Perry (Eds.), *The Neuroscience of Visual Hallucinations* (pp. 119–149). West Sussex, UK: John Wiley & Sons, Ltd.

Li, S. J., Li, Z., Wu, G., Zhang, M. J., Franczak, M., & Antuono, P. G. (2002). Alzheimer disease: evaluation of a functional MR imaging index as a marker. *Radiology*, *225*(1), 253–259.

Liang, M., Zhou, Y., Jiang, T., Liu, Z., Tian, L., Liu, H., & Hao, Y. (2006). Widespread functional disconnectivity in schizophrenia with resting-state functional magnetic resonance imaging. *Neuroreport*, *17*(2), 209–213.

Liebetanz, D., Fauser, S., Michaelis, T., Czeh, B., Watanabe, T., Paulus, W., et al. (2003). Safety aspects of chronic low-frequency transcranial magnetic stimulation based on localized proton magnetic resonance spectroscopy and histology of the rat brain. *Journal of Psychiatric Research*, *37*(4), 277–286.

Liepert, J., Bauder, H., Miltner, W. H., Taub, E., & Weiller, C. (2000a). Treatment-induced cortical reorganization after stroke in humans. *Stroke*, *31*(6), 1210–1216.

Liepert, J., Hamzei, F., & Weiller, C. (2000b). Motor cortex disinhibition of the unaffected hemisphere after acute stroke. *Muscle & Nerve*, *23*(11), 1761–1763.

Liu, Y., Yu, C., Liang, M., Li, J., Tian, L., Zhou, Y., et al. (2007). Whole brain functional connectivity in the early blind. *Brain*, *130*(8), 2085–2096.

Lobo, I. A., & Harris, R. A. (2008). GABA A receptors and alcohol. *Pharmacology Biochemistry and Behavior*, *90*(1), 90–94.

Logothetis, N. K. (2003). The underpinnings of the BOLD functional magnetic resonance imaging signal. *Journal of Neuroscience*, *23*(10), 3963–3971.

Logothetis, N. K. (2008). What we can do and what we cannot do with fMRI. *Nature*, *453*, 869–878.

Logothetis, N. K., & Wandell, B. A. (2004). Interpreting the BOLD signal. *Annual Review of Physiology*, *66*, 735–769.

Lomarev, M. P., Kanchana, S., Bara-Jimenez, W., Iyer, M., Wassermann, E. M., & Hallett, M. (2006). Placebo-controlled study of rTMS for the treatment of Parkinson's disease. *Movement Disorders*, *21*(3), 325–331.

Lombardo, M. V., Auyeung, B., Holt, R. J., Waldman, J., Ruigrok, A. N., Mooney, N., et al. (2016). Improving effect size estimation and statistical power with multi-echo fMRI and its impact on understanding the neural systems supporting mentalizing. *Neuroimage*, *142*, 55–66.

Lowe, M. J., Dzemidzic, M., Lurito, J. T., Mathews, V. P., & Phillips, M. D. (2000). Correlations in low-frequency BOLD fluctuations reflect cortico-cortical connection. *Neuroimage*, *12*(5), 582–587.

Luke, L. M., Allred, R. P., & Jones, T. A. (2004). Unilateral ischemic sensorimotor cortical damage induces contralesional synaptogenesis and enhances skilled reaching with the ipsilateral forelimb in adult male rats. *Synapse*, *54*(4), 187–199.

Luo, B., Wang, H. T., Su, Y. Y., Wu, S. H., & Chen, L. (2011). Activation of presynaptic $GABA_B$ receptors modulates GABAergic and glutamatergic inputs to the medial geniculate body. *Hearing Research*, *280*(1–2), 157–165.

Lüscher, C., & Malenka, R. C. (2012). NMDA receptor-dependent long-term potentiation and long-term depression (LTP/LTD). *Cold Spring Harbor Perspectives in Biology*, *4*(6), 1–15.

Mader, I., Seeger, U., Karitzky, J., Erb, M., Schick, F., & Klose, U. (2002). Proton magnetic resonance spectroscopy with metabolite nulling reveals regional differences of macromolecules in normal human brain. *Journal of Magnetic Resonance Imaging*, *16*(5), 538–546

Maeda, F., Keenan, J. P., Tormos, J. M., Topka, H., & Pascual-Leone, A. (2000). Interindividual variability of the modulatory effects of repetitive transcranial magnetic stimulation on cortical excitability. *Experimental Brain Research*, *133*(4), 425–430.

Magistretti, P. J., & Pellerin, L. (1999). Cellular mechanisms of brain energy metabolism and their relevance to functional brain imaging. *Philosophical Transactions of the Royal Society B: Biological Sciences*, *354*(1387), 1155–1163.

Makowiecki, K., Harvey, A. R., Sherrard, R. M., & Rodger, J. (2014). Low-intensity repetitive transcranial magnetic stimulation improves abnormal visual cortical circuit topography and upregulates BDNF in mice. *Journal of Neuroscience*, *34*(32), 10780–10792.

Manes, F., Jorge, R., Morcuende, M., Yamada, T., Paradiso, S., & Robinson, R. G. (2001). A controlled study of repetitive transcranial magnetic stimulation as a treatment of depression in the elderly. *International Psychogeriatrics*, *13*(2), 225–231.

Manford, M. & Andermann, F. (1998). Complex visual hallucinations. Clinical and neurobiological insights. *Brain*, *121*(10), 1819–1840.

Mansur, C. G., Fregni, F., Boggio, P. S., Riberto, M., Gallucci-Neto, J., Santos, C. M., et al. (2005). A sham stimulation-controlled trial of rTMS of the unaffected hemisphere in stroke patients. *Neurology*, *64*(10), 1802–1804.

Marg, E., & Rudiak, D. (1994). Phosphenes induced by magnetic stimulation over the occipital brain: description and probable site of stimulation. *Optometry and Vision Science*, *71*(5), 301–311.

Margulies, D. S., Vincent, J. L., Kelly, C., Lohmann, G., Uddin, L. Q., Biswal, B. B., et al. (2009). Precuneus shares intrinsic functional architecture in humans and monkeys. *Proceedings of the National Academy of Sciences*, *106*(47), 20069–20074.

Marinković, S. V., Milisavljević, M. M., Lolić-Draganić, V., & Kovacević, M. S. (1987). Distribution of the occipital branches of the posterior cerebral artery. Correlation with occipital lobe infarcts. *Stroke*, *18*(4), 728–732.

Marks, D. F. (1973). Visual imagery differences in the recall of pictures. *British Journal of Psychology*, *64*(1), 17–24.

Martino, J., Brogna, C., Robles, S. G., Vergani, F., & Duffau, H. (2010). Anatomic dissection of the inferior fronto-occipital fasciculus revisited in the lights of brain stimulation data. *Cortex*, *46*(5), 691–699.

McAllister, A. K., Katz, L. C., & Lo, D. C. (1999). Neurotrophins and synaptic plasticity. *Annual Review of Neuroscience*, *22*(1), 295–318.

Merabet, L. B., Kobayashi, M., Barton, J., & Pascual-Leone, A. (2003). Suppression of complex visual hallucinatory experiences by occipital transcranial magnetic stimulation: a case report. *Neurocase*, *9*(5), 436–440.

Mescher, M., Merkle, H., Kirsch, J., Garwood, M., & Gruetter, R. (1998). Simultaneous in vivo spectral editing and water suppression. *NMR in Biomedicine*, *11*, 266–272.

Meyer, B. U., Röricht, S., Von Einsiedel, H. G., Kruggel, F., & Weindl, A. (1995). Inhibitory and excitatory interhemispheric transfers between motor cortical areas in normal humans and patients with abnormalities of the corpus callosum. *Brain*, *118*(2), 429–440.

Michael, N., Gösling, M., Reutemann, M., Kersting, A., Heindel, W., Arolt, V., & Pfleiderer, B. (2003). Metabolic changes after repetitive transcranial magnetic stimulation (rTMS) of the left prefrontal cortex: a sham-controlled proton magnetic resonance spectroscopy (^{1}H MRS) study of healthy brain. *European Journal of Neuroscience*, 17(11), 2462–2468.

Mikl, M., Mareček, R., Hluštík, P., Pavlicová, M., Drastich, A., Chlebus, P., et al. (2008). Effects of spatial smoothing on fMRI group inferences. *Magnetic Resonance Imaging*, *26*(4), 490–503.

Miniussi, C., Bonato, C., Bignotti, S., Gazzoli, A., Gennarelli, M., Pasqualetti, P., et al. (2005). Repetitive transcranial magnetic stimulation (rTMS) at high and low frequency: an efficacious therapy for major drug-resistant depression? *Clinical Neurophysiology*, *116*(5), 1062–1071.

Mintz, S., & Alpert, M. (1972). Imagery vividness, reality testing, and schizophrenic hallucinations. *Journal of Abnormal Psychology*, *79*(3), 310–316.

Missimer, J. H., Seitz, R. J., & Kleiser, R. (2010). Data-driven analyses of an fMRI study of a subject experiencing phosphenes. *Journal of Magnetic Resonance Imaging*, *31*(4), 821–828.

Monte-Silva, K., Kuo, M. F., Hessenthaler, S., Fresnoza, S., Liebetanz, D., Paulus, W., & Nitsche, M. A. (2013). Induction of late LTP-like plasticity in the human motor cortex by repeated non-invasive brain stimulation. *Brain Stimulation: Basic, Translational, and Clinical Research in Neuromodulation*, *6*(3), 424–432.

Monte-Silva, K., Kuo, M. F., Liebetanz, D., Paulus, W., & Nitsche, M. A. (2010). Shaping the optimal repetition interval for cathodal transcranial direct current stimulation (tDCS). *Journal of Neurophysiology*, *103*(4), 1735–1740.

Mori, S., & Zhang, J. (2006). Principles of diffusion tensor imaging and its applications to basic neuroscience research. *Neuron*, *51*(5), 527–539.

Morrison, A. P., Wells, A., & Nothard, S. (2000). Cognitive factors in predisposition to auditory and visual hallucinations. *British Journal of Clinical Psychology*, *39*(1), 67–78.

Moseley, M. E., Cohen, Y., Kucharczyk, J., Mintorovitch, J., Asgari, H. S., Wendland, M. F., et al. (1990). Diffusion-weighted MR imaging of anisotropic water diffusion in cat central nervous system. *Radiology*, *176*(2), 439–445.

Mulders, P. C., van Eijndhoven, P. F., Schene, A. H., Beckmann, C. F., & Tendolkar, I. (2015). Resting-state functional connectivity in major depressive disorder: a review. *Neuroscience & Biobehavioral Reviews*, *56*, 330–344.

Mulkey, R. M., & Malenka, R. C. (1992). Mechanisms underlying induction of homosynaptic long-term depression in area CA1 of the hippocampus. *Neuron*, *9*(5), 967–975.

Mulleners, W. M., Chronicle, E. P., Vredeveld, J. W., & Koehler, P. J. (2002). Visual cortex excitability in migraine before and after valproate prophylaxis: a pilot study using TMS. *European Journal of Neurology*, *9*(1), 35–40.

Müller, M. B., Toschi, N., Kresse, A. E., Post, A., & Keck, M. E. (2000). Long-term repetitive transcranial magnetic stimulation increases the expression of brain-derived neurotrophic factor and cholecystokinin mRNA, but not neuropeptide tyrosine mRNA in specific areas of rat brain. *Neuropsychopharmacology*, *23*(2), 205–215.

Mullin, C. R., & Steeves, J. K. (2011). TMS to the lateral occipital cortex disrupts object processing but facilitates scene processing. *Journal of Cognitive Neuroscience*, *23*(12), 4174–4184.

Mullin, C. R., & Steeves, J. K. (2013). Consecutive TMS-fMRI reveals an inverse relationship in BOLD signal between object and scene processing. *Journal of Neuroscience*, *33*(49), 19243–19249.

Mullins, P. G., McGonigle, D. J., O'gorman, R. L., Puts, N. A., Vidyasagar, R., Evans, C. J., & Edden, R. A. (2014). Current practice in the use of MEGA-PRESS spectroscopy for the detection of GABA. *Neuroimage*, *86*, 43–52.

Murase, N., Duque, J., Mazzocchio, R., & Cohen, L. G. (2004). Influence of interhemispheric interactions on motor function in chronic stroke. *Annals of Neurology*, *55*(3), 400–409.

Muthukumaraswamy, S. D., Edden, R. A., Jones, D. K., Swettenham, J. B., & Singh, K. D. (2009). Resting GABA concentration predicts peak gamma frequency and fMRI amplitude in response to visual stimulation in humans. *Proceedings of the National Academy of Sciences*, *106*(20), 8356–8361.

Nagarajan, S. S., Durand, D. M., & Warman, E. N. (1993). Effects of induced electric fields on finite neuronal structures: a simulation study. *IEEE Transactions on Biomedical Engineering*, *40*(11), 1175–1188.

Nahas, Z., Lomarev, M., Roberts, D. R., Shastri, A., Lorberbaum, J. P., Teneback, C., et al. (2001). Unilateral left prefrontal transcranial magnetic stimulation (TMS) produces intensity-dependent bilateral effects as measured by interleaved BOLD fMRI. *Biological Psychiatry*, *50*(9), 712–720.

Najib, U., & Horvath, J. C. (2014). Transcranial Magnetic Stimulation (TMS) Safety Considerations and Recommendations. In: A. Rotenberg, J. Horvath, A. Pascual-Leone (Eds.), *Transcranial Magnetic Stimulation* (pp. 15–30). New York, NY: Humana Press.

Nakamura, H., Kitagawa, H., Kawaguchi, Y., & Tsuji, H. (1997). Intracortical facilitation and inhibition after transcranial magnetic stimulation in conscious humans. *The Journal of Physiology*, *498*(3), 817–823.

Nasreddine, Z. S., Phillips, N. A., Bédirian, V., Charbonneau, S., Whitehead, V., Collin, I., et al. (2005). The Montreal Cognitive Assessment, MoCA: a brief screening tool for mild cognitive impairment. *Journal of the American Geriatrics Society*, *53*(4), 695–699.

Near, J., Ho, Y. C. L., Sandberg, K., Kumaragamage, C., & Blicher, J. U. (2014). Long-term reproducibility of GABA magnetic resonance spectroscopy. *Neuroimage*, *99*, 191–196.

Nettekoven, C., Volz, L. J., Kutscha, M., Pool, E. M., Rehme, A. K., Eickhoff, S. B., et al. (2014). Dose-dependent effects of theta burst rTMS on cortical excitability and resting-state connectivity of the human motor system. *Journal of Neuroscience*, *34*(20), 6849–6859.

Neumann-Haefelin, T., Hagemann, G., & Witte, O. W. (1995). Cellular correlates of neuronal hyperexcitability in the vicinity of photochemically induced cortical infarcts in rats in vitro. *Neuroscience Letters*, *193*(2), 101–104.

Nitsche, M. A., & Paulus, W. (2000). Excitability changes induced in the human motor cortex by weak transcranial direct current stimulation. *The Journal of physiology*, *527*(3), 633–639.

Nomura, E. M., Gratton, C., Visser, R. M., Kayser, A., Perez, F., & D'Esposito, M. (2010). Double dissociation of two cognitive control networks in patients with focal brain lesions. *Proceedings of the National Academy of Sciences*, *107*(26), 12017–12022.

Nyffeler, T., Cazzoli, D., Hess, C. W., & Müri, R. M. (2009). One session of repeated parietal theta burst stimulation trains induces long-lasting improvement of visual neglect. *Stroke*, *40*(8), 2791–2796.

O'Gorman, R. L., Michels, L., Edden, R. A., Murdoch, J. B., & Martin, E. (2011). In vivo detection of GABA and glutamate with MEGA-PRESS: reproducibility and gender effects. *Journal of Magnetic Resonance Imaging*, *33*(5), 1262–1267.

Oishi, N., Udaka, F., Kameyama, M., Sawamoto, N., Hashikawa, K., & Fukuyama, H. (2005). Regional cerebral blood flow in Parkinson disease with nonpsychotic visual hallucinations. *Neurology*, *65*(11), 1708–1715.

Onofrj, M., Thomas, A., Martinotti, G., Anzellotti, F., Di Giannantonio, M., Ciccocioppo, F., & Bonanni, L. (2015). The clinical associations of visual hallucinations. In D. Collerton, U. P. Mosimann, & E. Perry (Eds.), *The Neuroscience of Visual Hallucinations* (pp. 91–117). West Sussex, UK: John Wiley & Sons, Ltd.

Opitz, A., Legon, W., Rowlands, A., Bickel, W. K., Paulus, W., & Tyler, W. J. (2013). Physiological observations validate finite element models for estimating subject-specific electric field distributions induced by transcranial magnetic stimulation of the human motor cortex. *Neuroimage*, *81*, 253–264.

Opitz, A., Windhoff, M., Heidemann, R. M., Turner, R., & Thielscher, A. (2011). How the brain tissue shapes the electric field induced by transcranial magnetic stimulation. *Neuroimage*, *58*(3), 849–859.

O'Reardon, J. P., Solvason, H. B., Janicak, P. G., Sampson, S., Isenberg, K. E., Nahas, Z. et al. (2007). Efficacy and safety of transcranial magnetic stimulation in the acute treatment of major depression: a multisite randomized controlled trial. *Biological Psychiatry*, *62*(11), 1208–1216.

Palop, J. J., & Mucke, L. (2010). Amyloid-ß induced neuronal dysfunction in Alzheimer's disease: from synapses toward neural networks. *Nature Neuroscience*, *13*(7), 812–818.

Pambakian, A. L. M., & Kennard, C. (1997). Can visual function be restored in patients with homonymous hemianopia? *British Journal of Ophthalmology*, *81*(4), 324–328.

Pascual-Leone, A., Amedi, A., Fregni, F., & Merabet, L. B. (2005). The plastic human brain cortex. *Annual Review of Neuroscience*, *28*, 377–401.

Pascual-Leone, A., Tormos, J. M., Keenan, J., Tarazona, F., Cañete, C., & Catalá, M. D. (1998). Study and modulation of human cortical excitability with transcranial magnetic stimulation. *Journal of Clinical Neurophysiology*, *15*(4), 333–343.

Pascual-Leone, A., Valls-Solé, J., Wassermann, E. M., & Hallett, M. (1994). Responses to rapid-rate transcranial magnetic stimulation of the human motor cortex. *Brain*, *117*(4), 847–858.

Pasley, B. N., Allen, E. A., & Freeman, R. D. (2009). State-dependent variability of neuronal responses to transcranial magnetic stimulation of the visual cortex. *Neuron*, *62*(2), 291–303.

Patel, A. B., de Graaf, R. A., Mason, G. F., Kanamatsu, T., Rothman, D. L., Shulman, R. G., & Behar, K. L. (2004). Glutamatergic neurotransmission and neuronal glucose oxidation are coupled during intense neuronal activation. *Journal of Cerebral Blood Flow & Metabolism*, *24*(9), 972–985.

Paulig, M., & Mentrup, H. (2001). Charles Bonnet's syndrome: complete remission of complex visual hallucinations treated by gabapentin. *Journal of Neurology, Neurosurgery & Psychiatry*, *70*(6), 813–814.

Paus, T., Jech, R., Thompson, C. J., Comeau, R., Peters, T., & Evans, A. C. (1998). Dose-dependent reduction of cerebral blood flow during rapid-rate transcranial magnetic stimulation of the human sensorimotor cortex. *Journal of Neurophysiology*, *79*(2), 1102–1107.

Payne, B. R., & Lomber, S. G. (2001). Reconstructing functional systems after lesions of cerebral cortex. *Nature Reviews Neuroscience*, *2*(12), 911–919.

Peinemann, A., Reimer, B., Löer, C., Quartarone, A., Münchau, A., Conrad, B., & Siebner, H. R. (2004). Long-lasting increase in corticospinal excitability after 1800 pulses of subthreshold 5 Hz repetitive TMS to the primary motor cortex. *Clinical Neurophysiology*, *115*(7), 1519–1526.

Pekna, M., Pekny, M., & Nilsson, M. (2012). Modulation of neural plasticity as a basis for stroke rehabilitation. *Stroke*, *43*(10), 2819–2828.

Pell, G. S., Roth, Y., & Zangen, A. (2011). Modulation of cortical excitability induced by repetitive transcranial magnetic stimulation: influence of timing and geometrical parameters and underlying mechanisms. *Progress in Neurobiology*, *93*(1), 59–98.

Penfield, W., & Perot, P. (1963). The brain's record of auditory and visual experience. *Brain*, *86*(4), 595–696.

Perini, F., Cattaneo, L., Carrasco, M., & Schwarzbach, J. V. (2012). Occipital transcranial magnetic stimulation has an activity-dependent suppressive effect. *Journal of Neuroscience*, *32*(36), 12361–12365.

Pernet, C. R., Latinus, M., Nichols, T. E., & Rousselet, G. A. (2015). Cluster-based computational methods for mass univariate analyses of event-related brain potentials/fields: A simulation study. *Journal of Neuroscience Methods*, *250*, 85–93.

Pfeuffer, J., Tkáč, I., Provencher, S. W., & Gruetter, R. (1999). Toward an in vivo neurochemical profile: quantification of 18 metabolites in short-echo-time ^{1}H NMR spectra of the rat brain. *Journal of Magnetic Resonance*, *141*(1), 104–120.

Pierpaoli, C., & Basser, P. J. (1996). Toward a quantitative assessment of diffusion anisotropy. *Magnetic Resonance in Medicine*, *36*(6), 893–906.

Pierpaoli, C., Jezzard, P., Basser, P. J., Barnett, A., & Di Chiro, G. (1996). Diffusion tensor MR imaging of the human brain. *Radiology*, *201*(3), 637–648.

Pinter, M. M., & Brainin, M. (2013). Role of Repetitive Transcranial Magnetic Stimulation in in Stroke Rehabilitation. *Frontiers of Neurology and Neuroscience*, *32*, 112–121.

Plow, E. B., Obretenova, S. N., Halko, M. A., Kenkel, S., Jackson, M. L., Pascual-Leone, A., & Merabet, L. B. (2011). Combining visual rehabilitative training and noninvasive brain stimulation to enhance visual function in patients with hemianopia: a comparative case study. *PM&R*, *3*(9), 825–835.

Post, A., Müller, M. B., Engelmann, M., & Keck, M. E. (1999). Repetitive transcranial magnetic stimulation in rats: evidence for a neuroprotective effect in vitro and in vivo. *European Journal of Neuroscience*, *11*(9), 3247–3254.

Pridmore, S., Filho, J. A. F., Nahas, Z., Liberatos, C., & George, M. S. (1998). Motor threshold in transcranial magnetic stimulation: A comparison of a neurophysiological method and a visualization of movement method. *The Journal of ECT*, *14*(1), 25–27.

Prince, D. A., & Tseng, G. F. (1993). Epileptogenesis in chronically injured cortex: in vitro studies. *Journal of Neurophysiology*, *69*(4), 1276–1291.

Protor, W. G., & Yu, F. C. (1950). The dependence of nuclear magnetic resonance frequency upon chemical shift. *Physical Review*, *77*, 717.

Prout, A. J., & Eisen, A. A. (1994). The cortical silent period and amyotrophic lateral sclerosis. *Muscle & Nerve*, *17*(2), 217–223.

Puce, A., Allison, T., Asgari, M., Gore, J. C., & McCarthy, G. (1996). Differential sensitivity of human visual cortex to faces, letterstrings, and textures: a functional magnetic resonance imaging study. *The Journal of Neuroscience*, *16*, 5205–5215.

Puts, N. A., & Edden, R. A. (2012). In vivo magnetic resonance spectroscopy of GABA: a methodological review. *Progress in Nuclear Magnetic Resonance Spectroscopy*, *60*, 29–41.

Rae, C. D. (2014). A guide to the metabolic pathways and function of metabolites observed in human brain ^{1}H magnetic resonance spectra. *Neurochemical Research*, *39*(1), 1–36.

Rafique, S. A., Richards, J. R., & Steeves, J. K. (2016). rTMS reduces cortical imbalance associated with visual hallucinations after occipital stroke. *Neurology*, *87*(14), 1493–1500.

Rafique, S. A., Richards, J. R., & Steeves, J. K. (2018). Altered white matter connectivity associated with visual hallucinations following occipital stroke. *Brain and Behavior*, e01010.

Rafique, S. A., Solomon-Harris, L. M., & Steeves, J. K. (2015). TMS to object cortex affects both object and scene remote networks while TMS to scene cortex only affects scene networks. *Neuropsychologia*, *79*, 86–96.

Raichle, M. E., & Mintun, M. A. (2006). Brain work and brain imaging. *Annual Review of Neuroscience*, *29*, 449–476.

Ray, P. G., Meador, K. J., Epstein, C. M., Loring, D. W., & Day, L. J. (1998). Magnetic stimulation of visual cortex: factors influencing the perception of phosphenes. *Journal of Clinical Neurophysiology*, *15*(4), 351–357.

Redecker, C., Wang, W., Fritschy, J. M., & Witte, O. W. (2002). Widespread and long-lasting alterations in GABA(A)-receptor subtypes after focal cortical infarcts in rats: mediation by NMDA-dependent processes. *Journal of Cerebral Blood Flow & Metabolism*, *22*(12), 1463–1475.

Reithler, J., Peters, J. C., & Sack, A. T. (2011). Multimodal transcranial magnetic stimulation: using concurrent neuroimaging to reveal the neural network dynamics of noninvasive brain stimulation. *Progress in Neurobiology*, *94*(2), 149–165.

Restrepo, C. E., Manger, P. R., Spenger, C., & Innocenti, G. M. (2003). Immature cortex lesions alter retinotopic maps and interhemispheric connections. *Annals of Neurology*, *54*(1), 51–65.

Ridding, M. C., & Rothwell, J. C. (2007). Is there a future for therapeutic use of transcranial magnetic stimulation? *Nature Reviews Neuroscience*, *8*(7), 559–567.

Ridding, M. C., & Ziemann, U. (2010). Determinants of the induction of cortical plasticity by non-invasive brain stimulation in healthy subjects. *The Journal of Physiology*, *588*(13), 2291–2304.

Rijntjes, M., Weiller, C., Krams, M., Bauermann, T., Diener, H. C., & Faiss, J. H. (1994). Functional magnetic resonance imaging in recovery from motor stroke. *Stroke*, *25*(1), 256–256).

Rossi, S., Hallett, M., Rossini, P. M., & Pascual-Leone, A., & The Safety of TMS Consensus Group (2009). Safety, ethical considerations, and application guidelines for the use of transcranial magnetic stimulation in clinical practice and research. *Clinical Neurophysiology*, *120*(12), 2008–2039.

Rossi, S., & Rossini, P. M. (2004). TMS in cognitive plasticity and the potential for rehabilitation. *Trends in Cognitive Sciences, 8*(6), 273–279.

Rossini, P. M., Barker, A. T., Berardelli, A., Caramia, M. D., Caruso, G., Cracco, R. Q., et al. (1994). Non-invasive electrical and magnetic stimulation of the brain, spinal cord and roots: basic principles and procedures for routine clinical application. Report of an IFCN committee. *Electroencephalography and Clinical Neurophysiology*, *91*(2), 79–92.

Rotenberg, A., Horvath, J. C., Pascual-Leone, A. (2014). *Transcranial Magnetic Stimulation.* New York, NY: Humana Press.

Roth, Y., Amir, A., Levkovitz, Y., & Zangen, A. (2007). Three-dimensional distribution of the electric field induced in the brain by transcranial magnetic stimulation using figure-8 and deep H-coils. *Journal of Clinical Neurophysiology*, *24*(1), 31–38.

Rothkegel, H., Sommer, M., & Paulus, W. (2010). Breaks during 5 Hz rTMS are essential for facilitatory after effects. *Clinical Neurophysiology*, *121*(3), 426–430.

Rothman, D. L., Behar, K. L., Prichard, J. W., & Petroff, O. A. (1997). Homocarnosine and the measurement of neuronal pH in patients with epilepsy. *Magnetic Resonance in Medicine, 38*(6), 924–929.

Rothman, D. L., Petroff, O. A., Behar, K. L., & Mattson, R. H. (1993). Localized ^{1}H NMR measurements of gamma-aminobutyric acid in human brain in vivo. *Proceedings of the National Academy of Sciences, 90*(12), 5662–5666.

Rumi, D. O., Gattaz, W. F., Rigonatti, S. P., Rosa, M. A., Fregni, F., Rosa, M. O., et al. (2005). Transcranial magnetic stimulation accelerates the antidepressant effect of amitriptyline in severe depression: a double-blind placebo-controlled study. *Biological Psychiatry, 57*(2), 162–166.

Russo, L., Mariotti, P., Sangiorgi, E., Giordano, T., Ricci, I., Lupi, F., et al. (2005). A new susceptibility locus for migraine with aura in the 15q11-q13 genomic region containing three GABA-A receptor genes. *The American Journal of Human Genetics*, *76*(2), 327–333.

Sabel, B. A. (1997). Unrecognized Potential of Surviving Neurons: Within-systems Plasticity, Recovery of Function, and the Hypothesis of Minimal Residual Structure. *The Neuroscientist*, *3*(6), 366–370.

Sale, M. V., Ridding, M. C., & Nordstrom, M. A. (2007). Factors influencing the magnitude and reproducibility of corticomotor excitability changes induced by paired associative stimulation. *Experimental Brain Research*, *181*(4), 615–626.

Santhouse, A. M., Howard, R. J., & ffytche, D. H. (2000). Visual hallucinatory syndromes and the anatomy of the visual brain. *Brain*, *123*(10), 2055–2064.

Saruta, J., Fujino, K., To, M., & Tsukinoki, K. (2012). Expression and localization of brain-derived neurotrophic factor (BDNF) mRNA and protein in human submandibular gland. *Acta Histochemica et Cytochemica*, *45*(4), 211–218.

Schneider, R. C., Crosby, E. C., Bagchi, B. K., & Calhoun, H. D. (1961). Temporal or occipital lobe hallucinations triggered from frontal lobe lesions. *Neurology*, *11*(2), 172–179.

Schubert, F., Gallinat, J., Seifert, F., & Rinneberg, H. (2004). Glutamate concentrations in human brain using single voxel proton magnetic resonance spectroscopy at 3 Tesla. *Neuroimage*, *21*(4), 1762–1771.

Schutter, D. J. L. G. (2010). Quantitative review of the efficacy of slow-frequency magnetic brain stimulation in major depressive disorder. *Psychological Medicine*, *40*(11), 1789–1795.

Schutter, D. J., & van Honk, J. (2005). A framework for targeting alternative brain regions with repetitive transcranial magnetic stimulation in the treatment of depression. *Journal of Psychiatry & Neuroscience: JPN*, *30*(2), 91–97.

Seghier, M. L., Lazeyras, F., Zimine, S., Saudan-Frei, S., Safran, A. B., & Huppi, P. S. (2005). Visual recovery after perinatal stroke evidenced by functional and diffusion MRI: case report. *BMC Neurology*, *5*(17), 1–8.

Seguin, E. C. (1886). A Clinical Study of Lateral Hemianopsia.* *The Journal of Nervous and Mental Disease*, *13*(8), 445–454.

Seniów, J., Waldowski, K., Leśniak, M., Iwański, S., Czepiel, W., & Członkowska, A. (2013). Transcranial magnetic stimulation combined with speech and language training in early aphasia rehabilitation: a randomized double-blind controlled pilot study. *Topics in Stroke Rehabilitation*, *20*(3), 250–261.

Sergent, J., Ohta, S., & MacDonald, B. (1992). Functional neuroanatomy of face and object processing. *Brain*, *115*(1), 15–36.

Shih, L. Y., Chen, L. F., Kuo, W. J., Yeh, T. C., Wu, Y. T., Tzeng, O. J., et al. (2009). Sensory acquisition in the cerebellum: An fMRI study of cerebrocerebellar interaction during visual duration discrimination. *The Cerebellum*, *8*(2), 116–126.

Shipp, S. (2007). Structure and function of the cerebral cortex. *Current Biology*, *17*(12), R443–R449.

Shulman, R. G., Rothman, D. L., Behar, K. L., & Hyder, F. (2004). Energetic basis of brain activity: implications for neuroimaging. *Trends in Neurosciences*, *27*(8), 489–495.

Siebner, H. R., Auer, C., & Conrad, B. (1999a). Abnormal increase in the corticomotor output to the affected hand during repetitive transcranial magnetic stimulation of the primary motor cortex in patients with writer's cramp. *Neuroscience Letters*, *262*(2), 133–136.

Siebner, H. R., Lang, N., Rizzo, V., Nitsche, M. A., Paulus, W., Lemon, R. N., & Rothwell, J. C. (2004). Preconditioning of low-frequency repetitive transcranial magnetic stimulation with transcranial direct current stimulation: evidence for homeostatic plasticity in the human motor cortex. *Journal of Neuroscience*, *24*(13), 3379–3385.

Siebner, H. R., Peller, M., Bartenstein, P., Willoch, F., Rossmeier, C., Schwaiger, M., & Conrad, B. (2001). Activation of frontal premotor areas during suprathreshold transcranial magnetic stimulation of the left primary sensorimotor cortex: a glucose metabolic PET study. *Human Brain Mapping*, *12*(3), 157–167.

Siebner, H. R., Peller, M., Willoch, F., Minoshima, S., Boecker, H., Auer, C., et al. (2000a). Lasting cortical activation after repetitive TMS of the motor cortex A glucose metabolic study. *Neurology*, *54*(4), 956–963.

Siebner, H. R., Rossmeier, C., Mentschel, C., Peinemann, A., & Conrad, B. (2000b). Short-term motor improvement after sub-threshold 5-Hz repetitive transcranial magnetic stimulation of the primary motor hand area in Parkinson's disease. *Journal of the Neurological Sciences*, *178*(2), 91–94.

Siebner, H., & Rothwell, J. (2003). Transcranial magnetic stimulation: new insights into representational cortical plasticity. *Experimental Brain Research*, *148*(1), 1–16.

Siebner, H. R., Tormos, J. M., Ceballos-Baumann, A. O., Auer, C., Catala, M. D., Conrad, B., & Pascual-Leone, A. (1999b). Low-frequency repetitive transcranial magnetic stimulation of the motor cortex in writer's cramp. *Neurology*, *52*(3), 529–529.

Sillito, A. M., Cudeiro, J., & Jones, H. E. (2006). Always returning: feedback and sensory processing in visual cortex and thalamus. *Trends in Neurosciences*, *29*(6), 307–316.

Silva, S., Basser, P. J., & Miranda, P. C. (2008). Elucidating the mechanisms and loci of neuronal excitation by transcranial magnetic stimulation using a finite element model of a cortical sulcus. *Clinical Neurophysiology*, *119*(10), 2405–2413.

Silvanto, J., & Pascual-Leone, A. (2008). State-dependency of transcranial magnetic stimulation. *Brain Topography*, *21*(1), 1–10.

Smith, A. J., Blumenfeld, H., Behar, K. L., Rothman, D. L., Shulman, R. G., & Hyder, F. (2002a). Cerebral energetics and spiking frequency: the neurophysiological basis of fMRI. *Proceedings of the National Academy of Sciences*, *99*(16), 10765–10770.

Smith, M. J., Adams, L. F., Schmidt, P. J., Rubinow, D. R., & Wassermann, E. M. (2002b). Effects of ovarian hormones on human cortical excitability. *Annals of Neurology*, *51*(5), 599–603.

Smith, R. E., Tournier, J. D., Calamante, F., & Connelly, A. (2012). Anatomically-constrained tractography: improved diffusion MRI streamlines tractography through effective use of anatomical information. *Neuroimage*, *62*(3), 1924–1938.

Smith, S. M. (2002). Fast robust automated brain extraction. *Human Brain Mapping*, *17*(3), 143–155.

Smith, S. M., Jenkinson, M., Johansen-Berg, H., Rueckert, D., Nichols, T. E., Mackay, C. E., et al. (2006). Tract-based spatial statistics: voxelwise analysis of multi-subject diffusion data. *Neuroimage*, *31*(4), 1487–1505.

Smith, Y., Pare, D., Deschenes, M., Parent, A., & Steriade, M. (1988). Cholinergic and non-cholinergic projections from the upper brainstem core to the visual thalamus in the cat. *Experimental Brain Research, 70*(1), 166–180.

Soares, J., Marques, P., Alves, V., & Sousa, N. (2013). A hitchhiker's guide to diffusion tensor imaging. *Frontiers in Neuroscience, 7*, 31.

Solomon-Harris, L. M., Rafique, S. A., & Steeves, J. K. (2016). Consecutive TMS-fMRI reveals remote effects of neural noise to the "occipital face area". *Brain Research, 1650*, 134–141.

Song, S. K., Sun, S. W., Ramsbottom, M. J., Chang, C., Russell, J., & Cross, A. H. (2002). Dysmyelination revealed through MRI as increased radial (but unchanged axial) diffusion of water. *Neuroimage, 17*(3), 1429–1436.

Speer, A. M., Kimbrell, T. A., Wassermann, E. M., Repella, J. D., Willis, M. W., Herscovitch, P., & Post, R. M. (2000). Opposite effects of high and low frequency rTMS on regional brain activity in depressed patients. *Biological Psychiatry, 48*(12), 1133–1141.

Spiegel, D. P., Byblow, W. D., Hess, R. F., & Thompson, B. (2013). Anodal transcranial direct current stimulation transiently improves contrast sensitivity and normalizes visual cortex activation in individuals with amblyopia. *Neurorehabilitation and Neural Repair, 27*(8), 760–769.

Spronk, D., Arns, M., & Fitzgerald, P. B. (2011). Repetitive Transcranial Magnetic Stimulation in Depression: Protocols, Mechanisms, and New Developments. In *Neurofeedback and Neuromodulation Techniques and Applications* (pp. 257–291). San Diego, CA: Academic Press.

Stagg, C. J. (2014). Magnetic resonance spectroscopy as a tool to study the role of GABA in motor-cortical plasticity. *Neuroimage*, *86*, 19–27.

Stagg, C. J., Bachtiar, V., & Johansen-Berg, H. (2011a). The role of GABA in human motor learning. *Current Biology*, *21*(6), 480–484.

Stagg, C. J., Bachtiar, V., & Johansen-Berg, H. (2011b). What are we measuring with GABA magnetic resonance spectroscopy? *Communicative & Integrative Biology*, *4*(5), 573–575.

Stagg, C. J., Best, J. G., Stephenson, M. C., O'Shea, J., Wylezinska, M., Kincses, Z. T., et al. (2009a). Polarity-sensitive modulation of cortical neurotransmitters by transcranial stimulation. *Journal of Neuroscience*, *29*(16), 5202–5206.

Stagg, C. J., Bestmann, S., Constantinescu, A. O., Moreno Moreno, L., Allman, C., Mekle, R., et al. (2011c). Relationship between physiological measures of excitability and levels of glutamate and GABA in the human motor cortex. *The Journal of Physiology*, *589*(23), 5845–5855.

Stagg, C. J., & Nitsche, M. A. (2011). Physiological basis of transcranial direct current stimulation. *The Neuroscientist*, *17*(1), 37–53.

Stagg, C. J., Wylezinska, M., Matthews, P. M., Johansen-Berg, H., Jezzard, P., Rothwell, J. C., & Bestmann, S. (2009b). Neurochemical effects of theta burst stimulation as assessed by magnetic resonance spectroscopy. *Journal of Neurophysiology*, *101*(6), 2872–2877.

Stell, B. M., Brickley, S. G., Tang, C. Y., Farrant, M., & Mody, I. (2003). Neuroactive steroids reduce neuronal excitability by selectively enhancing tonic inhibition mediated by δ subunit-containing $GABA_A$ receptors. *Proceedings of the National Academy of Sciences*, *100*(24), 14439–14444.

Steward, O., Torre, E. R., Phillips, L. L., & Trimmer, P. A. (1990). The process of reinnervation in the dentate gyrus of adult rats: time course of increases in mRNA for glial fibrillary acidic protein. *Journal of Neuroscience, 10*(7), 2373–2384.

Stewart, L., Walsh, V., Frith, U., & Rothwell, J. C. (2001a). TMS produces two dissociable types of speech disruption. *Neuroimage, 13*(3), 472–478.

Stewart, L. M., Walsh, V., & Rothwell, J. C. (2001b). Motor and phosphene thresholds: a transcranial magnetic stimulation correlation study. *Neuropsychologia*, *39*(4), 415–419.

Strafella, A. P., Paus, T., Barrett, J., & Dagher, A. (2001). Repetitive transcranial magnetic stimulation of the human prefrontal cortex induces dopamine release in the caudate nucleus. *Journal of Neuroscience*, *21*(15), 1–4.

Strafella, A. P., Paus, T., Fraraccio, M., & Dagher, A. (2003). Striatal dopamine release induced by repetitive transcranial magnetic stimulation of the human motor cortex. *Brain*, *126*(12), 2609–2615.

Takeuchi, N., Tada, T., Toshima, M., Chuma, T., Matsuo, Y., & Ikoma, K. (2008). Inhibition of the unaffected motor cortex by 1 Hz repetitive transcranial magnetic stimulation enhances motor performance and training effect of the paretic hand in patients with chronic stroke. *Journal of Rehabilitation Medicine*, *40*(4), 298–303.

Talairach J, Tournoux P. 1988. *Co-Planar Stereotaxic Atlas of the Human Brain*. New York, NY: Thieme Medical Publishers.

Talelli, P., Greenwood, R. J., & Rothwell, J. C. (2007). Exploring Theta Burst Stimulation as an intervention to improve motor recovery in chronic stroke. *Clinical Neurophysiology, 118*(2), 333–342.

Terhune, D. B., Murray, E., Near, J., Stagg, C. J., Cowey, A., & Cohen Kadosh, R. (2015). Phosphene perception relates to visual cortex glutamate levels and covaries with atypical visuospatial awareness. *Cerebral Cortex*, *25*(11), 4341–4350.

Thickbroom, G. W. (2007). Transcranial magnetic stimulation and synaptic plasticity: experimental framework and human models. *Experimental Brain Research*, *180*(4), 583–593.

Thielscher, A., Opitz, A., & Windhoff, M. (2011). Impact of the gyral geometry on the electric field induced by transcranial magnetic stimulation. *Neuroimage*, *54*(1), 234–243.

Thompson, B., Mansouri, B., Koski, L., & Hess, R. F. (2008). Brain plasticity in the adult: modulation of function in amblyopia with rTMS. *Current Biology*, *18*(14), 1067–1071.

Thut, G., & Pascual–Leone, A. (2010). A review of combined TMS-EEG studies to characterize lasting effects of repetitive TMS and assess their usefulness in cognitive and clinical neuroscience. *Brain Topography*, *22*(4), 219-232.

Tiel And, K., & Kölmel, H. W. (1991). Patterns of recovery from homonymous hemianopia subsequent to infarction in the distribution of the posterior cerebral artery. *Neuro-Ophthalmology*, *11*(1), 33–39.

Tippett, L. J., Blackwood, K., & Farah, M. J. (2003). Visual object and face processing in mild-to-moderate Alzheimer's disease: from segmentation to imagination. *Neuropsychologia*, *41*(4), 453–468.

Tootell, R. B., Dale, A. M., Sereno, M. I., & Malach, R. (1996). New images from human visual cortex. *Trends in Neurosciences*, *19*(11), 481–489.

Touge, T., Gerschlager, W., Brown, P., & Rothwell, J. C. (2001). Are the after-effects of low-frequency rTMS on motor cortex excitability due to changes in the efficacy of cortical synapses? *Clinical Neurophysiology*, *112*(11), 2138–2145.

Trajkovska, V., Marcussen, A. B., Vinberg, M., Hartvig, P., Aznar, S., & Knudsen, G. M. (2007). Measurements of brain-derived neurotrophic factor: methodological aspects and demographical data. *Brain Research Bulletin*, *73*(1–3), 143–149.

Traversa, R., Cicinelli, P., Oliveri, M., Giuseppina Palmieri, M., Maddalena Filippi, M., Pasqualetti, P., et al. (2000). Neurophysiological follow-up of motor cortical output in stroke patients. *Clinical Neurophysiology*, *111*(9), 1695–1703.

Tremblay, S., Beaulé, V., Proulx, S., De Beaumont, L., Marjańska, M., Doyon, J., et al. (2012). Relationship between transcranial magnetic stimulation measures of intracortical inhibition and spectroscopy measures of GABA and glutamate+glutamine. *Journal of Neurophysiology*, *109*(5), 1343–1349.

Triggs, W. J., McCoy, K. J., Greer, R., Rossi, F., Bowers, D., Kortenkamp, S., et al. (1999). Effects of left frontal transcranial magnetic stimulation on depressed mood, cognition, and corticomotor threshold. *Biological Psychiatry*, *45*(11), 1440–1446.

Turrigiano, G. G., & Nelson, S. B. (2004). Homeostatic plasticity in the developing nervous system. *Nature Reviews Neuroscience*, *5*(2), 97–107.

Tzourio-Mazoyer, N., Landeau, B., Papathanassiou, D., Crivello, F., Etard, O., Delcroix, N., et al. (2002). Automated anatomical labeling of activations in SPM using a macroscopic anatomical parcellation of the MNI MRI single-subject brain. *Neuroimage*, *15*(1), 273–289.

Udupa, K., & Chen., R (2010). Paired pulse TMS. In *Encyclopedia of Movement Disorders* (pp. 354–358). Oxford, UK: Academic Press.

Ulmer, S., & Jansen, O. (2010). *fMRI: Basics and Clinical Applications*. Berlin, Germany: Springer-Verlag.

Valero-Cabré, A., Payne, B. R., & Pascual-Leone, A. (2007). Opposite impact on 14C-2-deoxyglucose brain metabolism following patterns of high and low frequency repetitive transcranial magnetic stimulation in the posterior parietal cortex. *Experimental Brain Research*, *176*(4), 603–615.

van den Heuvel, M., Mandl, R., & Hulshoff Pol, H. (2008). Normalized cut group clustering of resting-state fMRI data. *PloS One*, *3*(4), e2001.

van den Heuvel, M. P., & Hulshoff Pol, H. E. (2010). Exploring the brain network: a review on resting-state fMRI functional connectivity. *European Neuropsychopharmacology*, *20*(8), 519–534.

van den Heuvel, M. P., Mandl, R. C., Kahn, R. S., Hulshoff Pol, H., & Hilleke, E. (2009). Functionally linked resting-state networks reflect the underlying structural connectivity architecture of the human brain. *Human Brain Mapping*, *30*(10), 3127–3141.

van de Ven, V. G., Formisano, E., Prvulovic, D., Roeder, C. H., & Linden, D. E. (2004). Functional connectivity as revealed by spatial independent component analysis of fMRI measurements during rest. *Human Brain Mapping*, *22*(3), 165–178.

van der Werf, Y. D., Sanz-Arigita, E. J., Menning, S., & van den Heuvel, O. A. (2010). Modulating spontaneous brain activity using repetitive transcranial magnetic stimulation. *BMC Neuroscience*, *11*(1), 145.

van Lutterveld, R., Diederen, K. M., Koops, S., Begemann, M. J., & Sommer, I. E. (2013). The influence of stimulus detection on activation patterns during auditory hallucinations. *Schizophrenia Research*, *145*(1), 27–32.

Vaphiades, M. S., Celesia, G. G., & Brigell, M. G. (1996). Positive spontaneous visual phenomena limited to the hemianopic field in lesions of central visual pathways. *Neurology*, *47*(2), 408–417.

Vercammen, A., Knegtering, H., Liemburg, E. J., den Boer, J. A., & Aleman, A. (2010). Functional connectivity of the temporo-parietal region in schizophrenia: effects of rTMS treatment of auditory hallucinations. *Journal of Psychiatric Research*, *44*(11), 725–731.

Vetencourt, J. F. M., Sale, A., Viegi, A., Baroncelli, L., De Pasquale, R., O'leary, O. F., et al. (2008). The antidepressant fluoxetine restores plasticity in the adult visual cortex. *Science*, *320*(5874), 385–388.

Vignal, J. P., Chauvel, P., & Halgren, E. (2000). Localised face processing by the human prefrontal cortex: stimulation-evoked hallucinations of faces. *Cognitive Neuropsychology*, *17*(1–3), 281–291.

Vrijen, C., Schenk, H. M., Hartman, C. A., & Oldehinkel, A. J. (2017). Measuring BDNF in saliva using commercial ELISA: Results from a small pilot study. *Psychiatry Research*, *254*, 340–346.

Wagner, T., Gangitano, M., Romero, R., Théoret, H., Kobayashi, M., Anschel, D., et al. (2004). Intracranial measurement of current densities induced by transcranial magnetic stimulation in the human brain. *Neuroscience Letters*, *354*(2), 91–94.

Wagner, T., Rushmore, J., Eden, U., & Valero-Cabre, A. (2009). Biophysical foundations underlying TMS: setting the stage for an effective use of neurostimulation in the cognitive neurosciences. *Cortex*, *45*(9), 1025–1034.

Wagner, T., Valero–Cabre, A., & Pascual-Leone, A. (2007). Noninvasive human brain stimulation. *Annual Review of Biomedical Engineering.*, *9*, 527–565.

Wakana, S., Caprihan, A., Panzenboeck, M. M., Fallon, J. H., Perry, M., Gollub, R. L., et al. (2007). Reproducibility of quantitative tractography methods applied to cerebral white matter. *Neuroimage*, *36*(3), 630–644.

Wakana, S., Jiang, H., Nagae-Poetscher, L. M., van Zijl, P. C., & Mori, S. (2004). Fiber tract-based atlas of human white matter anatomy. *Radiology*, *230*(1), 77–87.

Wang, T., Li, Q., Guo, M., Peng, Y., Li, Q., Qin, W., & Yu, C. (2014). Abnormal functional connectivity density in children with anisometropic amblyopia at resting-state. *Brain Research*, *1563*, 41–51.

Wang, T., Shi, F., Jin, Y., Yap, P. T., Wee, C. Y., Zhang, J., et al. (2016). Multilevel deficiency of white matter connectivity networks in Alzheimer's disease: a diffusion MRI study with DTI and HARDI models. *Neural Plasticity*, 2016, 1–14.

Wang, Y., Fernández-Miranda, J. C., Verstynen, T., Pathak, S., Schneider, W., & Yeh, F. C. (2012). Rethinking the role of the middle longitudinal fascicle in language and auditory pathways. *Cerebral Cortex*, *23*(10), 2347–2356.

Ward, N. S., Brown, M. M., Thompson, A. J., & Frackowiak, R. S. J. (2003). Neural correlates of motor recovery after stroke: a longitudinal fMRI study. *Brain*, *126*(11), 2476–2496.

Ward, N. S., & Cohen, L. G. (2004). Mechanisms underlying recovery of motor function after stroke. *Archives of Neurology*, *61*(12), 1844–1848.

Wassermann, E. M. (1998). Risk and safety of repetitive transcranial magnetic stimulation: report and suggested guidelines from the International Workshop on the Safety of Repetitive Transcranial Magnetic Stimulation, June 5–7, 1996. *Electroencephalography and Clinical Neurophysiology/Evoked Potentials Section*, *108*(1), 1–16.

Wassermann, E. M. (2002). Variation in the response to transcranial magnetic brain stimulation in the general population. *Clinical Neurophysiology*, *113*(7), 1165–1171.

Wassermann, E. M., & Lisanby, S. H. (2001). Therapeutic application of repetitive transcranial magnetic stimulation: a review. *Clinical Neurophysiology*, *112*(8), 1367–1377.

Watanabe, T., Hanajima, R., Shirota, Y., Ohminami, S., Tsutsumi, R., Terao, Y., et al. (2014). Bidirectional effects on interhemispheric resting-state functional connectivity induced by excitatory and inhibitory repetitive transcranial magnetic stimulation. *Human Brain Mapping*, *35*(5), 1896–1905.

Weinberger, L. M., & Grant, F. C. (1940). Visual hallucinations and their neuro-optical correlates. *Archives of Ophthalmology*, *23*(1), 166–199.

Whitfield-Gabrieli, S., & Ford, J. M. (2012). Default mode network activity and connectivity in psychopathology. *Annual Review of Clinical Psychology*, *8*, 49–76.

Whitfield-Gabrieli, S., & Nieto-Castanon, A. (2012). Conn: a functional connectivity toolbox for correlated and anticorrelated brain networks. *Brain Connectivity*, *2*(3), 125–141.

Williams, D. R., & Lees, A. J. (2005). Visual hallucinations in the diagnosis of idiopathic Parkinson's disease: a retrospective autopsy study. *The Lancet Neurology*, *4*(10), 605–610.

Wilson, J. R. (1993). Circuitry of the dorsal lateral geniculate nucleus in the cat and monkey. *Cells Tissues Organs*, *147*(1), 1–13.

Woods, A. J., Antal, A., Bikson, M., Boggio, P. S., Brunoni, A. R., Celnik, P., et al. (2016). A technical guide to tDCS, and related non-invasive brain stimulation tools. *Clinical Neurophysiology*, *127*(2), 1031–1048.

Wong, N. A., Rafique, S. A., Kelly, K. R., Moro, S. S., Gallie, B. L., & Steeves, J. K. (2018). Altered white matter structure in the visual system following early monocular enucleation. *Human Brain Mapping*, *39*(1), 133–144.

Woo, N. H., Teng, H. K., Siao, C. J., Chiaruttini, C., Pang, P. T., Milner, T. A., et al. (2005). Activation of $p75^{NTR}$ by proBDNF facilitates hippocampal long-term depression. *Nature Neuroscience*, *8*(8), 1069-1077.

Wu, Y., Sun, D., Wang, Y., Wang, Y., & Ou, S. (2016). Segmentation of the cingulum bundle in the human brain: a new perspective based on DSI tractography and fiber dissection study. *Frontiers in Neuroanatomy*, *10*, 84.

Yeh, F. C., Wedeen, V. J., & Tseng, W. Y. I. (2010). Generalized *q*-Sampling Imaging. *IEEE Transactions on Medical Imaging*, *29*(9), 1626–1635.

Yeo, B. T., Krienen, F. M., Sepulcre, J., Sabuncu, M. R., Lashkari, D., Hollinshead, M., et al. (2011). The organization of the human cerebral cortex estimated by intrinsic functional connectivity. *Journal of Neurophysiology*, *106*(3), 1125–1165.

Yonelinas, A. P., Hopfinger, J. B., Buonocore, M. H., Kroll, N. E. A., & Baynes, K. (2001). Hippocampal, parahippocampal and occipital-temporal contributions to associative and item recognition memory: an fMRI study. *Neuroreport*, *12*(2), 359–363.

Yoon, J. H., Maddock, R. J., Rokem, A., Silver, M. A., Minzenberg, M. J., Ragland, J. D., et al. (2010). GABA concentration is reduced in visual cortex in schizophrenia and correlates with orientation-specific surround suppression. *The Journal of Neuroscience*, *30*(10), 3777–3781.

Yu, C., Liu, Y., Li, J., Zhou, Y., Wang, K., Tian, L., et al. (2008). Altered functional connectivity of primary visual cortex in early blindness. *Human Brain Mapping*, *29*(5), 533–543.

Yu, C., Shu, N., Li, J., Qin, W., Jiang, T., & Li, K. (2007). Plasticity of the corticospinal tract in early blindness revealed by quantitative analysis of fractional anisotropy based on diffusion tensor tractography. *Neuroimage*, *36*(2), 411–417.

Yue, L., Xiao-Lin, H., & Tao, S. (2009). The effects of chronic repetitive transcranial magnetic stimulation on glutamate and gamma-aminobutyric acid in rat brain. *Brain Research*, *1260*, 94–99.

Zangen, A., Roth, Y., Voller, B., & Hallett, M. (2005). Transcranial magnetic stimulation of deep brain regions: evidence for efficacy of the H-coil. *Clinical Neurophysiology*, *116*(4), 775–779.

Zhang, X., Kedar, S., Lynn, M. J., Newman, N. J., & Biousse, V. (2006). Natural history of homonymous hemianopia. *Neurology*, *66*(6), 901–905.

Ziemann, U. L. F., Rothwell, J. C., & Ridding, M. C. (1996). Interaction between intracortical inhibition and facilitation in human motor cortex. *The Journal of Physiology*, *496*(3), 873–881.

Appendix A: Probabilistic Tractography for Controls

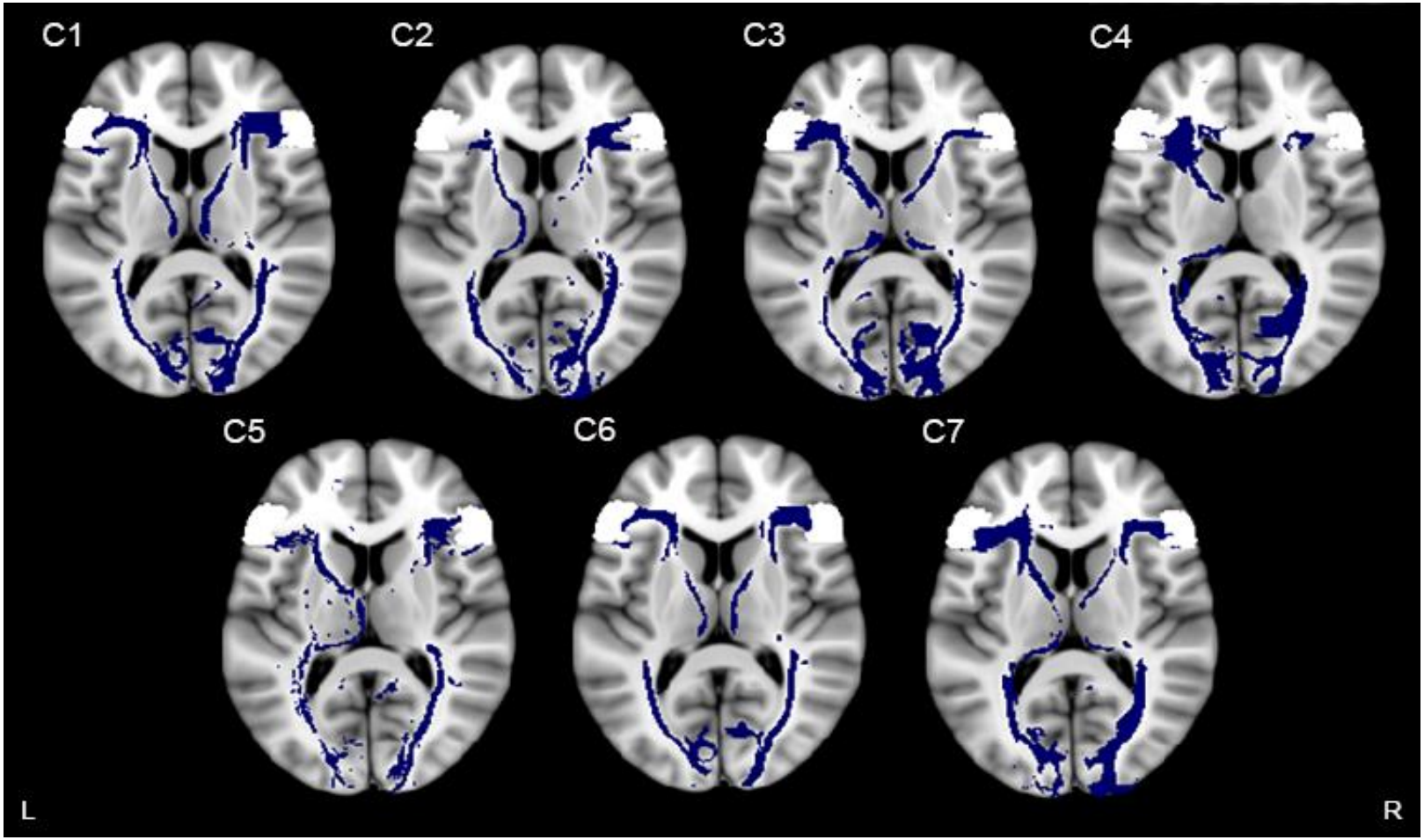

Figure A1. Probabilistic fibre tractography for intrahemispheric tracts seeded from the visual cortex to the inferior frontal gyrus (white mask) for all control participants (C1–C7). Results for C1 are also presented in Figure 3.2a (Chapter 3) as a representative comparison to the patient's probabilistic fibre tractography. L = left; R = right.

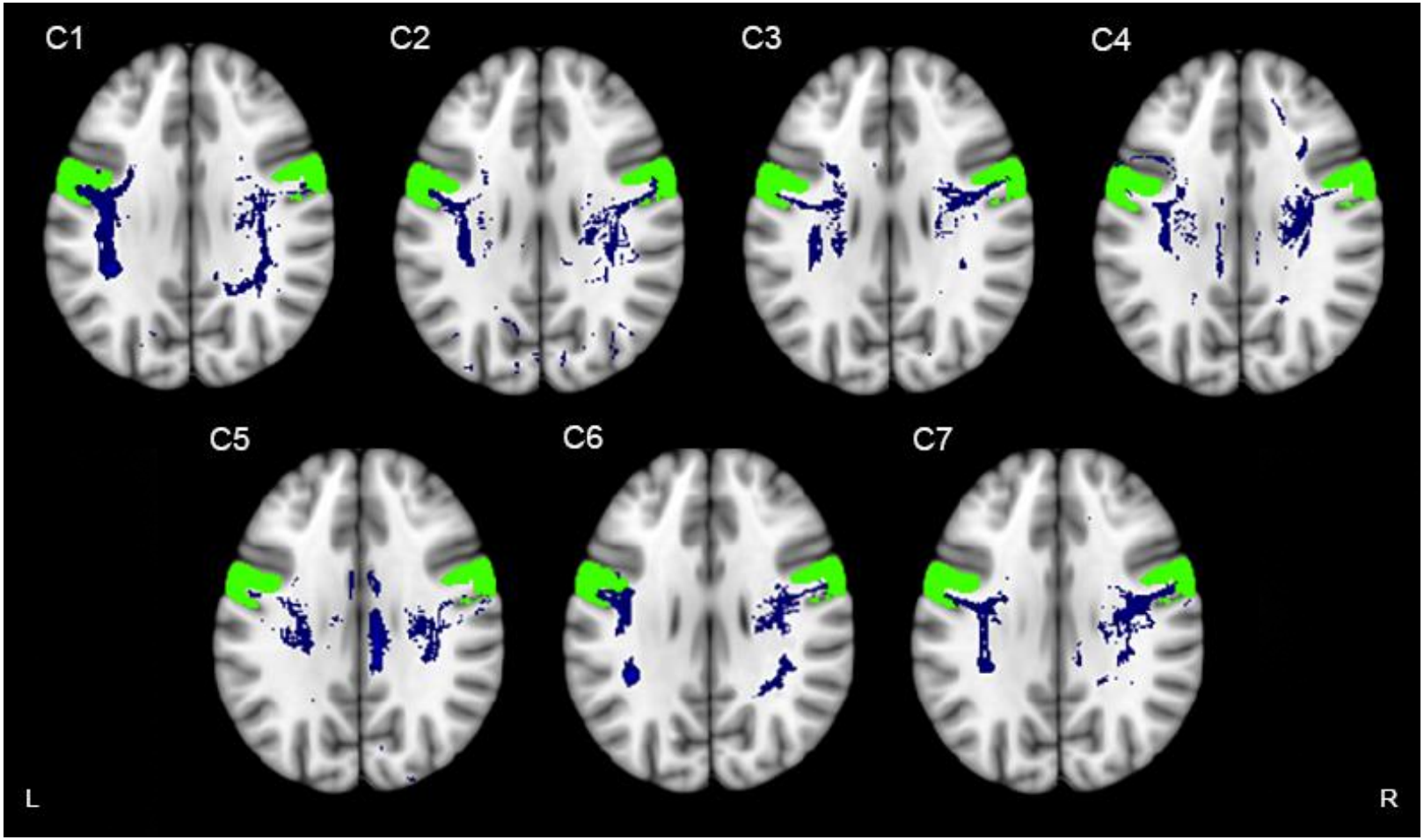

Figure A2. Probabilistic fibre tractography for intrahemispheric tracts seeded from the visual cortex to the precentral gyrus (lime green mask) for all control participants (C1–C7). Results for C1 are also presented in Figure 3.2b (Chapter 3) as a representative comparison to the patient's probabilistic fibre tractography. L = left; R = right.

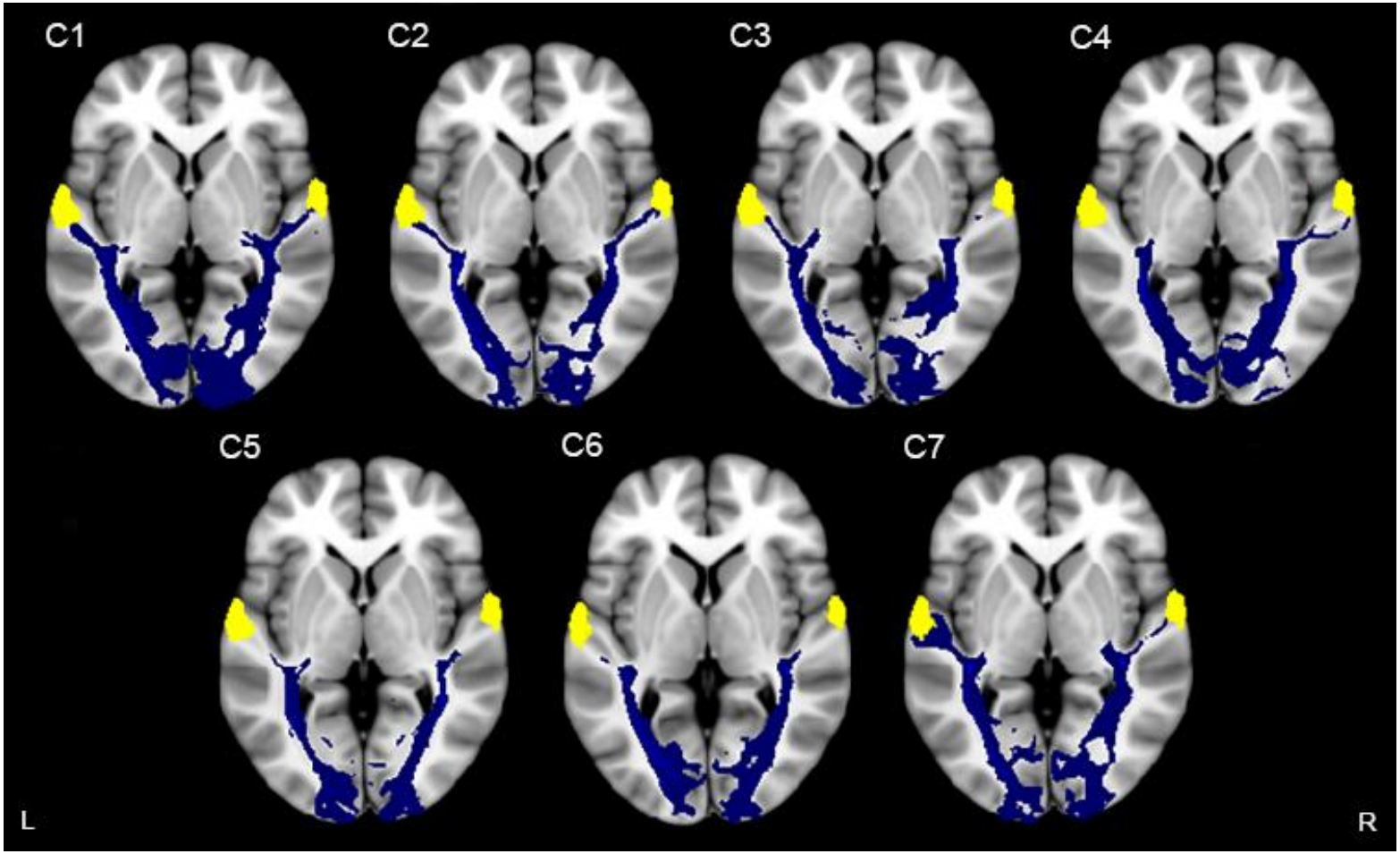

Figure A3. Probabilistic fibre tractography for intrahemispheric tracts seeded from the visual cortex to the superior temporal gyrus (yellow mask) for all control participants (C1–C7). Results for C1 are also presented in Figure 3.3a (Chapter 3) as a representative comparison to the patient's probabilistic fibre tractography. L = left; R = right.

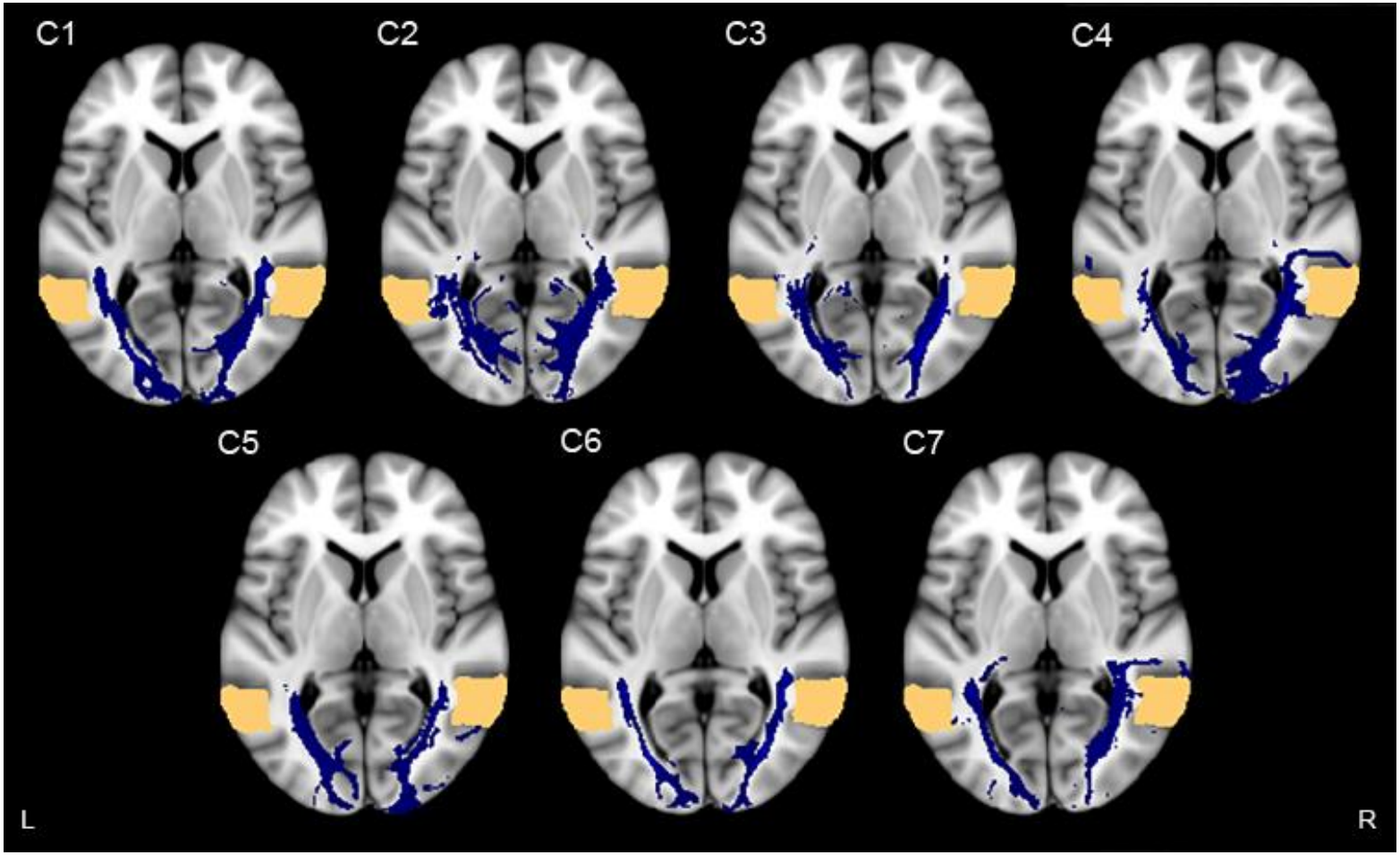

Figure A4. Probabilistic fibre tractography for intrahemispheric tracts seeded from the visual cortex to the middle temporo-occipital gyrus (peach mask) for all control participants (C1–C7). Results for C1 are also presented in Figure 3.3b (Chapter 3) as a representative comparison to the patient's probabilistic fibre tractography. L = left; R = right.

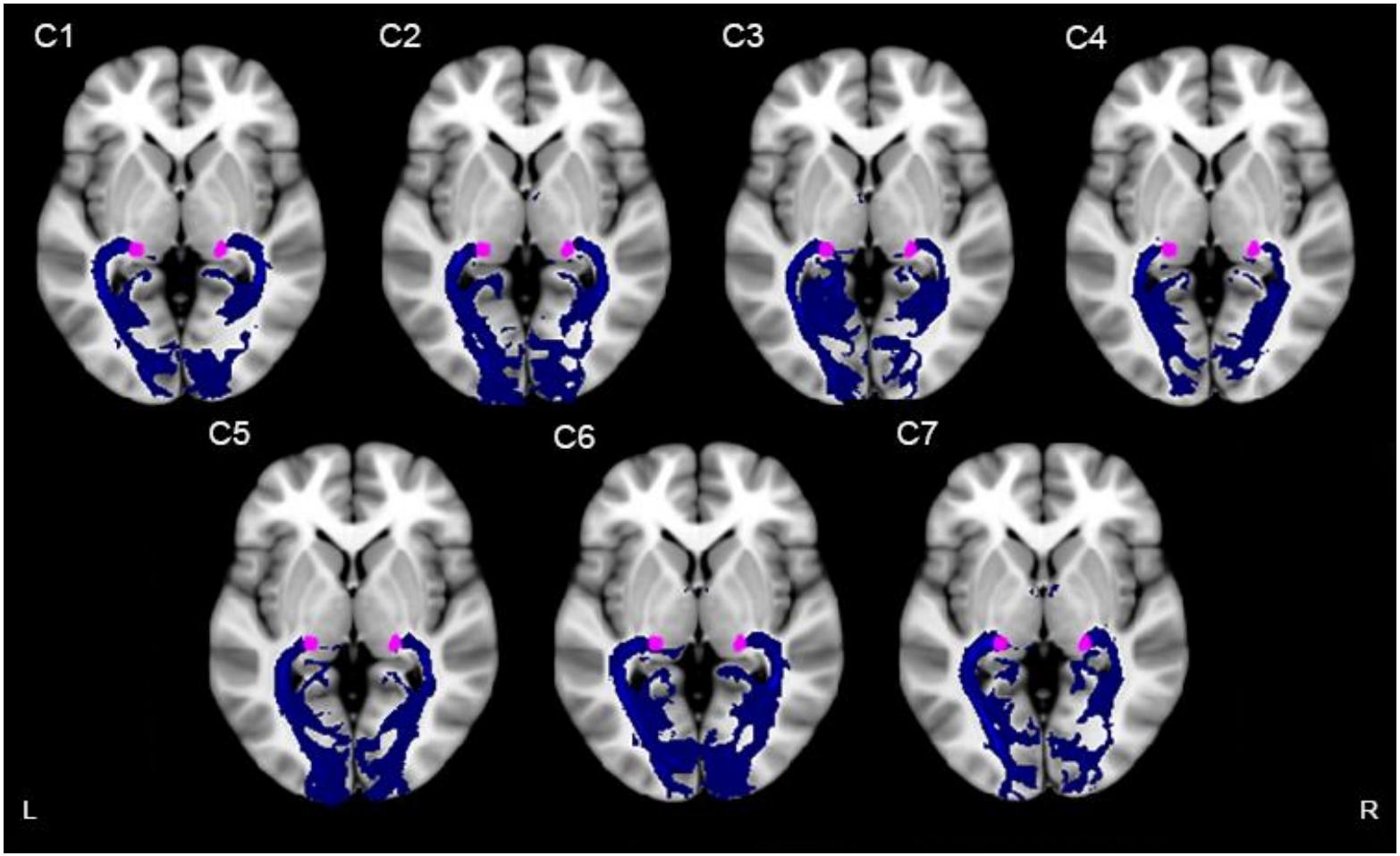

Figure A5. Probabilistic fibre tractography for intrahemispheric tracts seeded from the visual cortex to the lateral geniculate body (pink mask) for all control participants (C1–C7). Results for C1 are also presented in Figure 3.3c (Chapter 3) as a representative comparison to the patient's probabilistic fibre tractography. L = left; R = right.

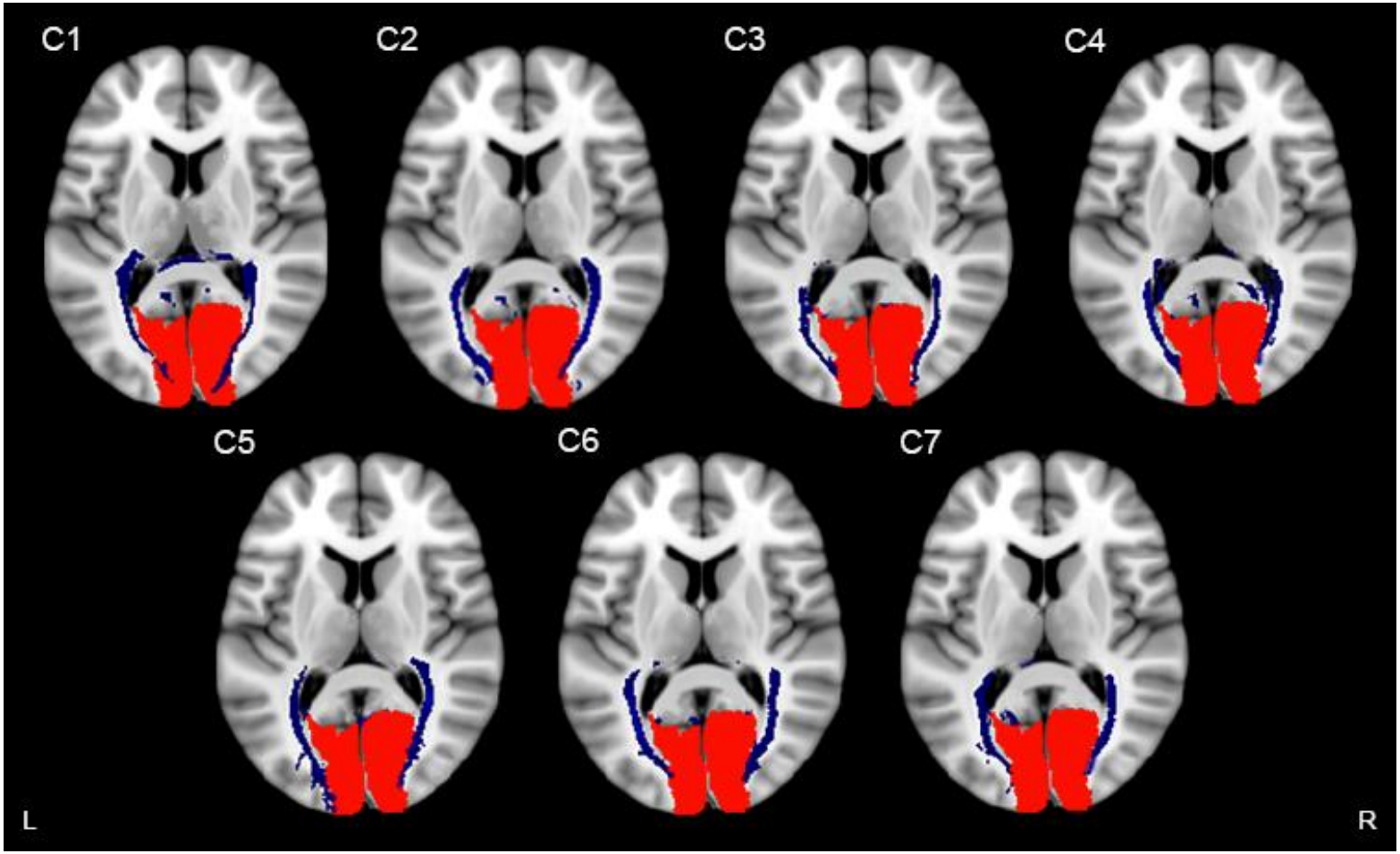

Figure A6. Probabilistic fibre tractography for intrahemispheric tracts seeded from the lateral geniculate body to the visual cortex (red mask) for all control participants (C1–C7). Results for C1 are also presented in Figure 3.4 (Chapter 3) as a representative comparison to the patient's probabilistic fibre tractography. L = left; R = right.

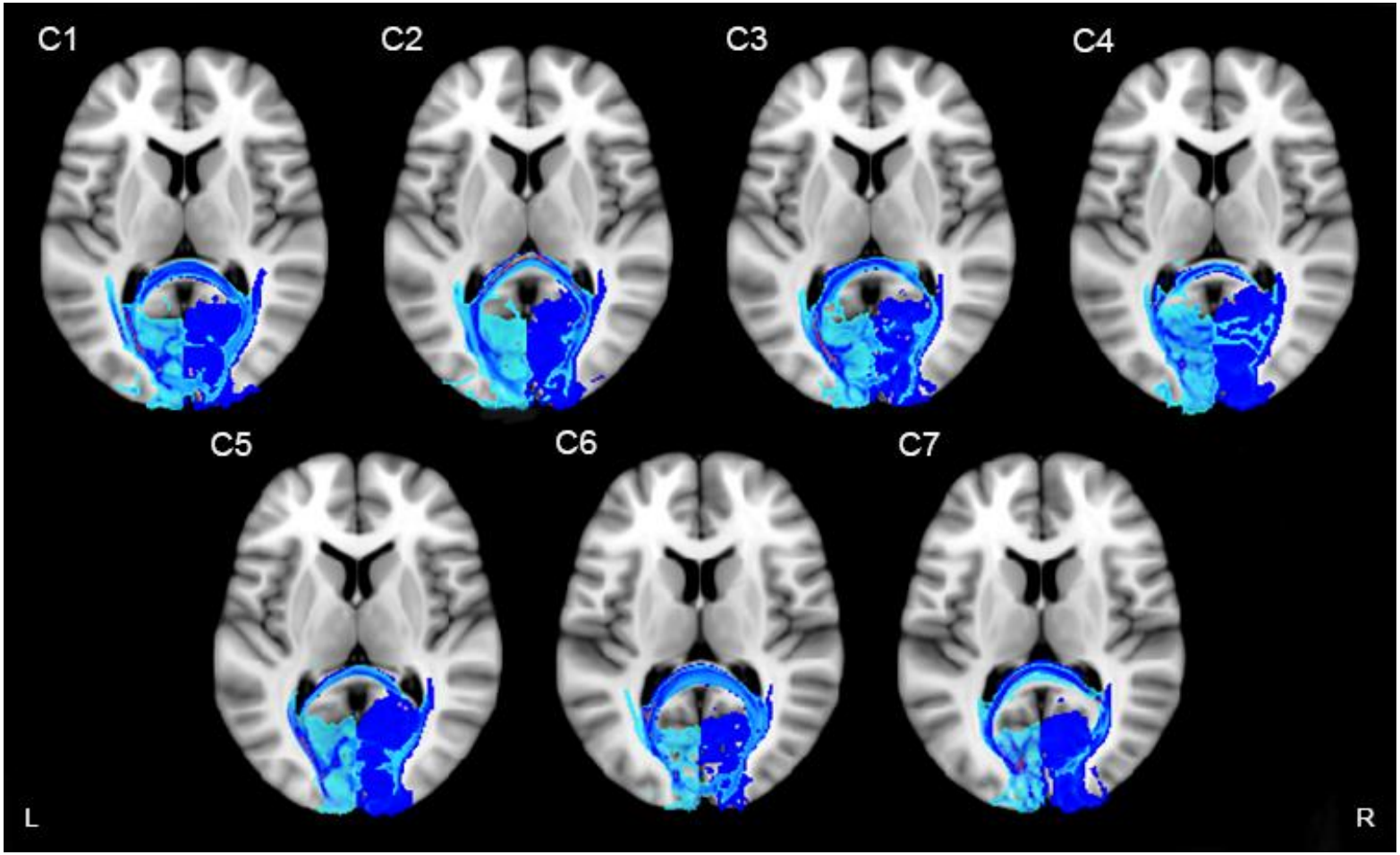

Figure A7. Probabilistic fibre tractography of interhemispheric tracts between visual cortices for all control participants (C1–C7). Results for C1 are also presented in Figure 3.5 (Chapter 3) as a representative comparison to the patient's probabilistic fibre tractography. L = left; R = right.

Appendix B: Example of Montreal Cognitive Assessment

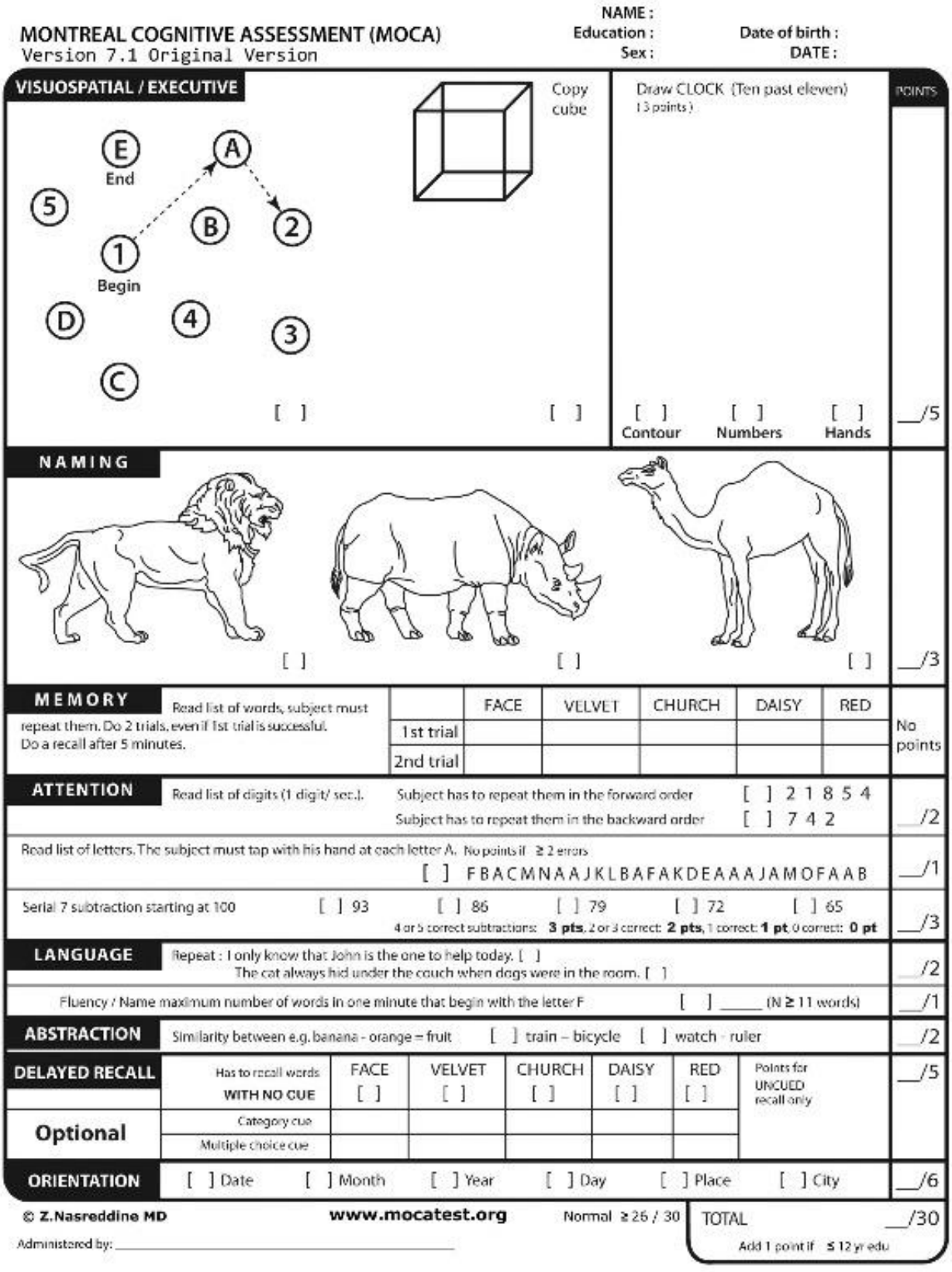

MONTREAL COGNITIVE ASSESSMENT (MOCA)
Version 7.1 Original Version

NAME :
Education :
Sex :
Date of birth :
DATE :

VISUOSPATIAL / EXECUTIVE — POINTS

Copy cube [ ]

Draw CLOCK (Ten past eleven) (3 points) [ ] Contour [ ] Numbers [ ] Hands

__/5

NAMING

[ ] [ ] [ ]

__/3

MEMORY Read list of words, subject must repeat them. Do 2 trials, even if 1st trial is successful. Do a recall after 5 minutes.

	FACE	VELVET	CHURCH	DAISY	RED
1st trial					
2nd trial					

No points

ATTENTION Read list of digits (1 digit/ sec.).

Subject has to repeat them in the forward order [ ] 2 1 8 5 4

Subject has to repeat them in the backward order [ ] 7 4 2

__/2

Read list of letters. The subject must tap with his hand at each letter A. No points if ≥ 2 errors

[ ] F B A C M N A A J K L B A F A K D E A A A J A M O F A A B

__/1

Serial 7 subtraction starting at 100 [ ] 93 [ ] 86 [ ] 79 [ ] 72 [ ] 65

4 or 5 correct subtractions: **3 pts**, 2 or 3 correct: **2 pts**, 1 correct: **1 pt**, 0 correct: **0 pt**

__/3

LANGUAGE Repeat : I only know that John is the one to help today. [ ]

The cat always hid under the couch when dogs were in the room. [ ]

__/2

Fluency / Name maximum number of words in one minute that begin with the letter F [ ] _____ (N ≥ 11 words)

__/1

ABSTRACTION Similarity between e.g. banana - orange = fruit [ ] train – bicycle [ ] watch - ruler

__/2

DELAYED RECALL

	FACE	VELVET	CHURCH	DAISY	RED	Points for UNCUED recall only
Has to recall words WITH NO CUE	[ ]	[ ]	[ ]	[ ]	[ ]	
Optional Category cue						
Optional Multiple choice cue						

__/5

ORIENTATION [ ] Date [ ] Month [ ] Year [ ] Day [ ] Place [ ] City

__/6

www.mocatest.org

Normal ≥ 26 / 30

TOTAL __/30

Add 1 point if ≤ 12 yr edu

Administered by: _____

Appendix C: Vividness of Visual Imagery Questionnaire

Visual imagery refers to the ability to visualise, that is, the ability to form mental pictures, or to "see in the mind's eye". Marked individual differences have been found in the strength and clarity of reported visual imagery and these differences are of considerable psychological interest.

The aim of this test is to determine the vividness of your visual imagery. The items of the test will possibly bring certain images to your mind. You are asked to rate the vividness of each image by reference to the 5-point scale given below. For example, if your image is "vague and dim" then give it a rating of 2. After each item write the appropriate number in the sheet provided. The first sheet is for images obtained with your eyes open and the second sheet is for images obtained with your eyes closed. Before you turn to the items on the next page, familiarise yourself with the different categories on the rating scale. Throughout the test, refer to the rating scale when judging the vividness of each image. Try to do each item separately, independent of how you may have done other items.

Complete all items for images obtained with the eyes open and then return to the beginning of the questionnaire and rate the image obtained for each item with your eyes closed. Try and give your "eyes closed" rating independently of the "eyes open" rating. The two ratings for a given item may not in all cases be the same. ***Use the same images for eyes open and closed.***

RATING SCALE

The image aroused by an item might be:

No image at all, you only "know" that you are thinking of an object	**rating 1**
Vague and dim	**rating 2**
Moderately clear and vivid	**rating 3**
Clear and reasonably vivid	**rating 4**
Perfectly clear and as vivid as normal vision	**rating 5**

……

In answering items 1 to 4, think of some relative or friend whom you frequently see (but who is not with you at present) and consider carefully the picture that comes before your mind's eye.

1 The exact contour of face, head, shoulders and body.

2 Characteristic poses of head, attitudes of body, etc.

3 The precise carriage, length of step, etc., in walking.

4 The different colours worn in some familiar clothes.

……

Visualise the rising sun. Consider carefully the picture that comes before your mind's eye.

5 The sun is rising above the horizon into a hazy sky.

6 The sky clears and surrounds the sun with blueness.

7 Clouds. A storm blows up, with flashes of lightening.

8 A rainbow appears.

……

Think of the front of a shop which you often go to. Consider the picture that comes before your mind's eye.

9 The overall appearance of the shop from the opposite side of the road.

10 A window display including colours, shape and details of individual items for sale.

11 You are near the entrance. The colour, shape and details of the door.

12 You enter the shop and go to the counter. The counter assistant serves you. Money changes hands.

……

Finally, think of a country scene which involves trees, mountains and a lake. Consider the picture that comes before your mind's eye.

13 The contours of the landscape.

14 The colour and shape of the trees.

15 The colour and shape of the lake.

16 A strong wind blows on the tree and on the lake causing waves.

……

Appendix D: Revised Launay-Slade Hallucination Scale

Rating scale:
1 = never, 2 = sometimes, 3 = often, 4 = almost always

Questions:
1. A passing thought will seem so real that it frightens me
2. My thoughts seem as real as actual events in my life
3. No matter how much I try to concentrate on my work unrelated thoughts always creep into my mind.
4. I have had the experience of hearing a person's voice and then found that there was no one there.
5. The sounds I hear in my daydreams are generally clear and distinct.
6. The people in my daydreams seem so true to life that I think they are real.
7. In my daydreams I can hear the sound of a tune almost as clearly as if I were actually listening to it.
8. I hear a voice speaking my thoughts aloud.
9. I have been troubled by hearing voices in my head.
10. I have seen a person's face in front of me when no one was there.
11. I have heard the voice of God speaking to me.
12. When I look at things they appear strange to me.
13. I see shadows and shapes when there is nothing there.
14. When I look at things they look unreal to me.
15. When I look at myself in the mirror I look different.